EXTENDED END-PLATE BEAM-COLUMN JOINTS IN SEISMIC MOMENT RESISTING FRAMES

by

ASHRAF M. GAMAL EL DIN OSMAN

A Thesis

Submitted to the School of Graduate Studies

in Partial Fulfilment of the Requirements

for the Degree

Doctor of Philosophy

McMaster University

May 1991

EXTENDED END-PLATE BEAM-COLUMN JOINTS IN SEISMIC MOMENT RESISTING FRAMES

DOCTOR OF PHILOSOPHY (1991) McMASTER UNIVERSITY
(Civil Engineering and Engineering Mechanics) Hamilton, Ontario

TITLE: Extended end-plate beam-column joints in seismic moment resisting frames

AUTHOR: Ashraf M. Gamal El din Osman, B.Sc. (Cairo University)
M.Sc. (Cairo University)

SUPERVISOR: Professor A. Ghobarah
Professor R.M. Korol

NUMBER OF PAGES: xxiv, 306

ABSTRACT

Although moment resisting frames (MRFs) are the most widely used structural system for seismic-resistant steel buildings, several important aspects of their behaviour under real earthquake excitation are not well understood. One of these issues that needs to be further studied is the seismic performance of beam-to-column joints. During severe earthquakes, joints can undergo severe inelastic deformations affecting the strength, stiffness and inelastic action distribution throughout the frames.

Therefore, the objectives of this study are to investigate the behaviour of beam-to-column joints, to assess the effect of the joints' response on the frame's overall behaviour and to provide guidelines and design rules for detailing the joints. In this thesis, attention was focused on studying the behaviour of bolted extended end-plate joints. This was achieved through an experimental-analytical research program.

The experimental work carried out involved two phases. First, cyclic tests on full scale beam-to-column connections was done to examine the behaviour of such a connection type, together with the response of its individual components. Second, cyclic tests on full scale subassemblages were done to study the response of panel zones of this joint type.

Based on the observation and results of the experimental program, analytical models to predict the behaviour of both the connection and the panel zone were developed. The sensitivity of these models was checked by comparing their predictions with the experimental results. The models were then incorporated into Drain-2D computer program to be used in analyzing MRFs.

Analytical research on the dynamic behaviour of MRFs designed to allow active yielding of panel zone joints and to permit connection deformation was performed. Several steel MRF designs for an eight-storey and twenty-storey office

buildings were analyzed using various ground acceleration records. Finally, design criteria for detailing the joints, i.e the connection and the panel zone, and code recommendations to improve the performance of MRFs subjected to severe earthquakes were introduced.

ACKNOWLEDGEMENTS

I wish to express my sincere appreciation to my research supervisors, Dr. A. Ghobarah and Dr. R.M. Korol for their guidance and encouragement throughout the course of this study. I am gratefull to their dedication and the number of hours that they spent with me on this research.

I am indebted to my supervisor committee members, Dr. M. Dokainish, and Dr. W.K. Tso for their valuable comments and suggestions on my research and also their time in reviewing this thesis.

The help of the ADL technicians, Dave Parrett who assisted me in the experiments and Ross McAndrew who fabricated the testing fixtures is appreciated.

Financial support from McMaster University is gratefully acknowledged. Much appreciation is extended to Marshall steel, Ltd. of Mississuga, Ontario for supplying and fabricating the steel for some of the test specimens.

Finally, I would like to thank my parents for their encouragement, support and patience during the course of this study.

To my dear parents

TABLE OF CONTENTS

Table of Contents (cont'd)

Table of Contents (cont'd)

Table of Contents (cont'd)

Table of Contents (cont'd)

List of Figures

List of Figures (cont'd)

List of Figures (cont'd)

List of Figures (cont'd)

List of Figures (cont'd)

List of Figures (cont'd)

List of Figures (cont'd)

List of Figures (cont'd)

List of Figures (cont'd)

List of Figures (cont'd)

List of Figures (cont'd)

List of Tables

List of Tables (cont'd)

LIST OF SYMBOLS

A_b = Nominal area of the bolt

A_f = Cross-sectional area of the column flange

A_s = Effective shear area of the end-plate

B_{cf} = Column flange width excluding the column web thickness

B_{ep} = End-plate width

C = Rate of decay parameter

c = Vertical distance between the centres of the two bolts in the tension side in the connection

c_f = Column axial force

D = Bolt hole diameter

D^* = Plate flexural rigidity

d_b = The beam depth

d_c = The column depth

E = Young's modulus

E_{st} = Strain hardening modulus of elasticity

F = Foundation factor

F_c = Column web compression capacity

F_{mf} = Maximum force can be supported by unstiffened column flange

F_{ms} = Maximum force can be supported by stiffened column flange

F_{mt} = Overstrength tension force component in the beam flange

F_u = Specified minimum tensile strength

G = Steel shear modulus

G_{st} = Steel shear modulus at strain hardening

H_c = Column shear

List of Symbols (cont'd)

h_i = The height of the ith storey

I = Importance factor

I_c = Column section moment of inertia

I_{ep} = End-plate section moment of inertia

K = The column "K" distance

K_e = Panel zone elastic stiffness

K_i = Connection initial stiffness

K_{in} = Connection initial stiffness at the nth cycle

K_p = Connection post elastic stiffness

K_s = Panel zone stiffness at strain hardening

K_T = Panel zone stiffness during transition range

L_c = Column height

M_{bi} = Bending moment of the ith beam

M_p = Beam plastic moment

M_{pc} = Connection plastic moment

M_{pfi} = Plastic moment of the ith column flange

M_{pn} = Panel zone moment

M_{pn1} = Panel zone plastic moment

M_{pn2} = Panel zone moment at strain hardening

M_{max} = Connection ultimate strength

m = The horizontal distance from the bolt centre to the web toe of fillet of I-shaped section

N = Number of storeys

n = The horizontal distance from the web centre to the tip of the column flange

List of Symbols (cont'd)

n_b = Number of bolts in tension

P = Beam flange force

P_y = Column axial force at yield

Q = Panel shear force

Q_p = Panel zone plastic shear capacity

R = Force modification factor

R_u = Ultimate rotation capacity of the beam

r = Nodal displacement

$\dot{r}$ = Nodal velocity

$\ddot{r}$ = Nodal acceleration

s = Seismic response factor

T = Structure natural period

t_{bf} = Beam flange thickness

t_{bw} = Beam web thickness

t_{cf} = Column flange thickness

t_{cw} = Column web thickness

t_{ep} = End-plate thickness

t_{se} = End-plate stiffener thickness

t_s = Column flange stiffener thickness

t_{wf} = Size of the weld joining the beam flange to the end-plate

t_{ww} = Size of the weld joining the beam web to the end-plate

W = Building weight

W_b = Panel zone deformation due to pure bending

W_s = Panel zone deformation due to pure shear

List of Symbols (cont'd)

W_T = Panel zone total deformation

V = Building base shear

V_{des} = Panel zone design shear

V_{cap} = Panel zone shear capacity

x = Vertical distance between bolt centre and the toe of the weld joining the beam flange to the end-plate

Z = Plastic modulus of the I-section

Z_b = Beam plastic section modulus

Z_f = Plastic modulus of the column flange

β = Parameter determined experimentally to express the deterioration in the connection stiffness with loading progression

β_o = Damping coefficient proportional to the original elastic stiffness matrix

γ = Panel zone average shear strain

γ_T = Panel zone shear strain at the start of strain hardening range

γ_y = Panel zone shear strain at yield

Δ_{cf} = Column flange deformation

Δ_{cw} = Column web compression deformation

Δ_{ep} = End-plate deformation

Δ_T = Connection total deformation

Δt = Time step

ζ = Damping coefficient proportional to the tangent stiffness matrix

η = Damping coefficient proportional to the mass matrix

θ = Connection rotation

θ_m = Beam plastic rotation corresponding to the point where the maximum moment is attained

List of Symbols (cont'd)

θ_p = Maximum beam plastic rotation before failure occurs or moment capacity is exhausted, measured from zero rotation

θ_{p^*} = Beam plastic rotation measured from zero load intercept to the same point as defined in θ_p

θ_{pl} = The hypothetical beam plastic rotation , $M_pL/3EI$

θ_y = Connection rotation at yield

θ_{max} = The connection maximum rotation

λ = Proportional of critical damping

μ_θ = Beam rotation ductility

μ_p = Panel zone rotation ductility

ν = Possion's ratio

σ_{yb} = Beam yield stress

σ_{yc} = Column yield stress

σ_{ye} = End-plate yield stress

τ_y = Shear stress at yield

τ_y' = Reduced shear stress at yield

$[C_T]$ = Tangent viscous damping matrix

$[k_o]$ = Original elastic stiffness matrix

$[K_T]$ = Tangent stiffness matrix

$[M]$ = Mass matrix

CHAPTER 1

INTRODUCTION

1.1 General

In the analysis and design of moment resisting frames (MRFs), the beam-to-column joint constitutes a particularly critical region which can significantly affect their static and dynamic characteristics. Research conducted to investigate the effect the joints' behaviour on a frame's response has shown that, under static loads, the improper design of the joints can lead to a significant drop in frame stiffness. In the case of dynamic loads such as earthquakes, the situation may be further complicated. An inappropriate design of the joints will not only lead to a drop in frame stiffness, but may also negatively affect the energy dissipation capacity of the frame.

As a result, the design and detailing of seismic moment-resisting joints are very important since, the joints must be able to dissipate the earthquake input energy with a minimal loss of stiffness or strength. In other words, the joints are not only required to provide sufficient stiffness and strength, but also possess adequate ductility (Popov and Pinkney, 1969 and Popov, 1983).

In the early sixties, seismic design philosophy was first introduced and required two premises to be satisfied:

A) During a small or moderate earthquake, a building frame must provide the necessary stiffness and strength to prevent damage and to remain serviceable after the event.

B) During a major earthquake, a building frame must provide the necessary strength and ductility such that the structure will not collapse, i.e the frame must be able to dissipate the seismic energy.

Consequently, the behaviour of the different elements in MRFs and especially, the behaviour of the joints under earthquake loading, received considerable attention. Several studies were performed to investigate the response

of different joint types comprised of the connections themselves and the panel zones. The joints were subjected to severe cyclic loading conditions (Krawinkler el al, 1971; Popov et al, 1985 and Popov and Tsai, 1989).

Several attempts were also made to model a joint's behaviour and to incorporate such a model into the frame analysis. The purpose was to study the effect of joint deformation on the overall behaviour of the frame (Vasquez et al, 1969; Krawinkler and Mohasseb, 1987 and Tsai and Popov, 1990c). As a result of these studies, it was concluded that proper control of deformation in beam-to-column joints can help to achieve stable hysteretic behaviour for the frames. In addition, design criteria for detailing a joint's components such as the panel zones have been proposed and adopted by different codes (UBC, 1988 and CAN3-S16.1-M89, 1989)

However, previous research work essentially focused on the study of the behaviour of joints utilizing either beams fully welded to column flanges (Fig. 1.1(a)) or beams with flanges welded and web bolted to the column flanges (Fig. 1.1(b)). The extension of these recommendations and conclusions to code provisions that involve other connecting media, such as extended end-plate joints is questionable.

1.2 Bolted Extended End-plate Joints

Recently, the steel fabricating industry has opted for the use of field bolted joints. A moment resisting joint that is gaining popularity is the bolted extended end-plate joint. In this type of joining, the beam is shop welded to an end-plate, then the end-plate is field bolted to the column flange as shown in Fig. 1.2. This method of construction offers several advantages over other joint types (Griffiths, 1984 and Murray, 1988):

1) The joint is suitable for winter erection, since only field bolting is required.

2) All welding is performed in the shop thus eliminating any field welding associated problems and offering high quality control.

3) The number of bolts required for erection purposes is relatively small compared to other fully bolted joints, which makes the erection process relatively fast and efficient.

Although extensive research studies were carried out to investigate the behaviour of such a joint type to monotonic loadings (Krishnamurthy, 1978; Zoetemeijer, 1974 and Mann and Morris, 1979) there is still a dearth of knowledge about its response under severe cyclic loading conditions. Only limited work has been done in this regard. Johnstone and Walpole (1981 and 1982) tested four beam-to-column subassemblages utilizing bolted end-plate joints. In their tests, the beams sections were kept constant while the columns sections, the end-plate thicknesses, and the bolt diameters were varied. Two different detailing systems for stiffening the column flanges were adopted. The first is the common extended beam flange stiffener type that consists of plates fillet welded to both the column flanges and the column web. The second type has the plate stiffeners positioned parallel to the column web and welded to the column flange tips. Only minimal experimental results regarding the overall behaviour of the subassemblages and the associated modes of failure were recorded, however no data on the behaviour of the individual components of the subassemblages, such as the joint, the beam and the column, were obtained. Ballio et al (1986 and 1987) conducted research to investigate the cyclic behaviour of different beam-to-column joints. As part of this research, they tested four beam-to-column bolted extended end-plate joints. The major objective of this research was the development of a model that is able to simulate the joint behaviour. In the four tested specimens, unreasonably thick end-plates and column flanges were used. Only the overall hysteretic behaviour of the joints was recorded, i.e the behaviour of both the panel zone and the connection. In addition, the joints' ductilities, energy dissipation capacities and stiffness, were determined. Meanwhile, Tsai and Popov (1988, 1990a and 1990b) tested two specimens from which, they gathered information on the overall behaviour of the specimens and the variation of the pre-tensioned forces in four of the bolts.

It is evident from these earlier investigations that little attention was paid to the behaviour of the individual components in the joint. In almost all these tests, only the specimens' overall behaviour was recorded. Obviously, there remained a lack of understanding of the joint response, because in reality, the overall response is a

summation of the response of various components in the joint. Changing the strength of any of these individual components can significantly change the overall behaviour of the joint. Indeed, a lack of information about the response of individual elements has made the development of an analytical model that is capable of simulating the joint behaviour with adequate accuracy very difficult.

1.3 Objective and Scope:

To address the need for an understanding of the behaviour and to thereafter propose appropriate design criteria for extended end-plate joints, an experimental-analytical study was conducted (Fig.1.3). The experimental part consisted of two phases. The first involved investigating the cyclic behaviour of extended end-plate joints that possessed infinitely rigid panel zones. The scope of the experimental program in this phase consisted of the following aspects:

1) Assessing the cyclic performance of extended end-plate connections.

2) Examining the behaviour of the individual components comprising the connection such as the end-plate, the column flange and the bolts.

3) Recommending design criteria for detailing such a connection type to perform satisfactorily under severe earthquake excitation.

4) Developing an analytical model which is able to simulate the connection behaviour. The accuracy of it would need to be verified by comparing such results with experiments.

In the second phase of the experimental program, the behaviour of both the panel zone and the connection, were investigated with the column subjected to axial compression. The scope of the experimental program in this phase consisted of the following:

1) Investigating the behaviour of the joint with emphasis on the panel zone.

2) Checking the validity of the design criteria adopted by the current codes for the design and detailing of the panel zones.

3) Improving the design and detailing of such a joint type.

4) Developing an analytical model capable of predicting the behaviour of the panel

zone in such a joint type. The performance of this proposed model would be assessed by comparing the model's predicted response with the experimental results.

In addition to this experimental study, an analytical study was performed. In this analytical study, the previously developed models for the connection and the panel zone were incorporated into the **Drain-2D** computer program, after which a nonlinear-inelastic analysis for frames that takes into account the effect of connection and panel zone flexibilities was conducted. Several steel moment resisting frames (MRFs), that included realistic designs for eight and twenty-storey office buildings were analyzed using various ground acceleration records. In the design of these MRFs, the proposed joint design criteria were employed.

From the experimental and analytical research findings, a number of recently developed code provisions for the design of ductile steel MRF was examined. Finally, recommendations for the design and the detailing of bolted extended end-plate joint in seismic moment resisting frames are provided.

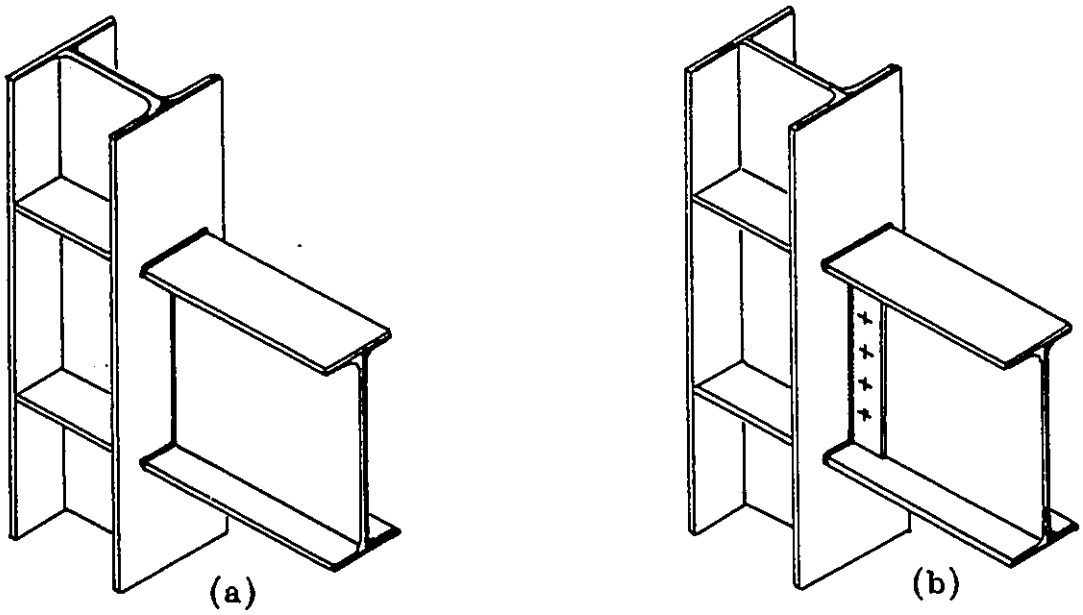

Fig. 1.1 Various beam–to–column moment joints.

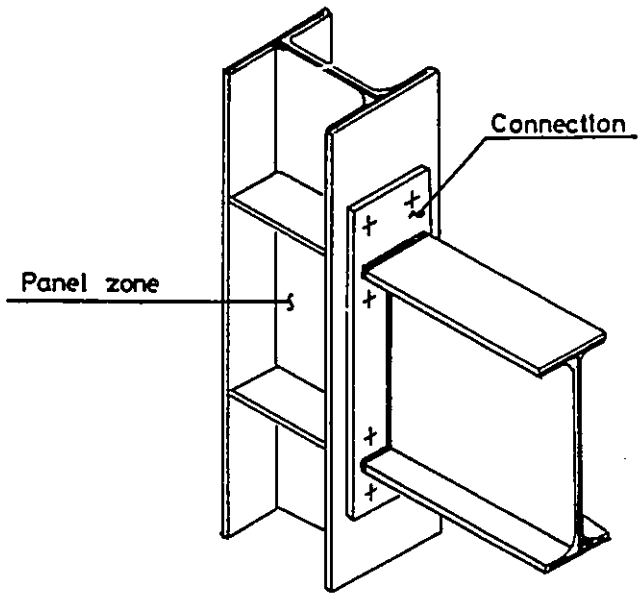

Fig. 1.2 Typical extended end–plate joint.

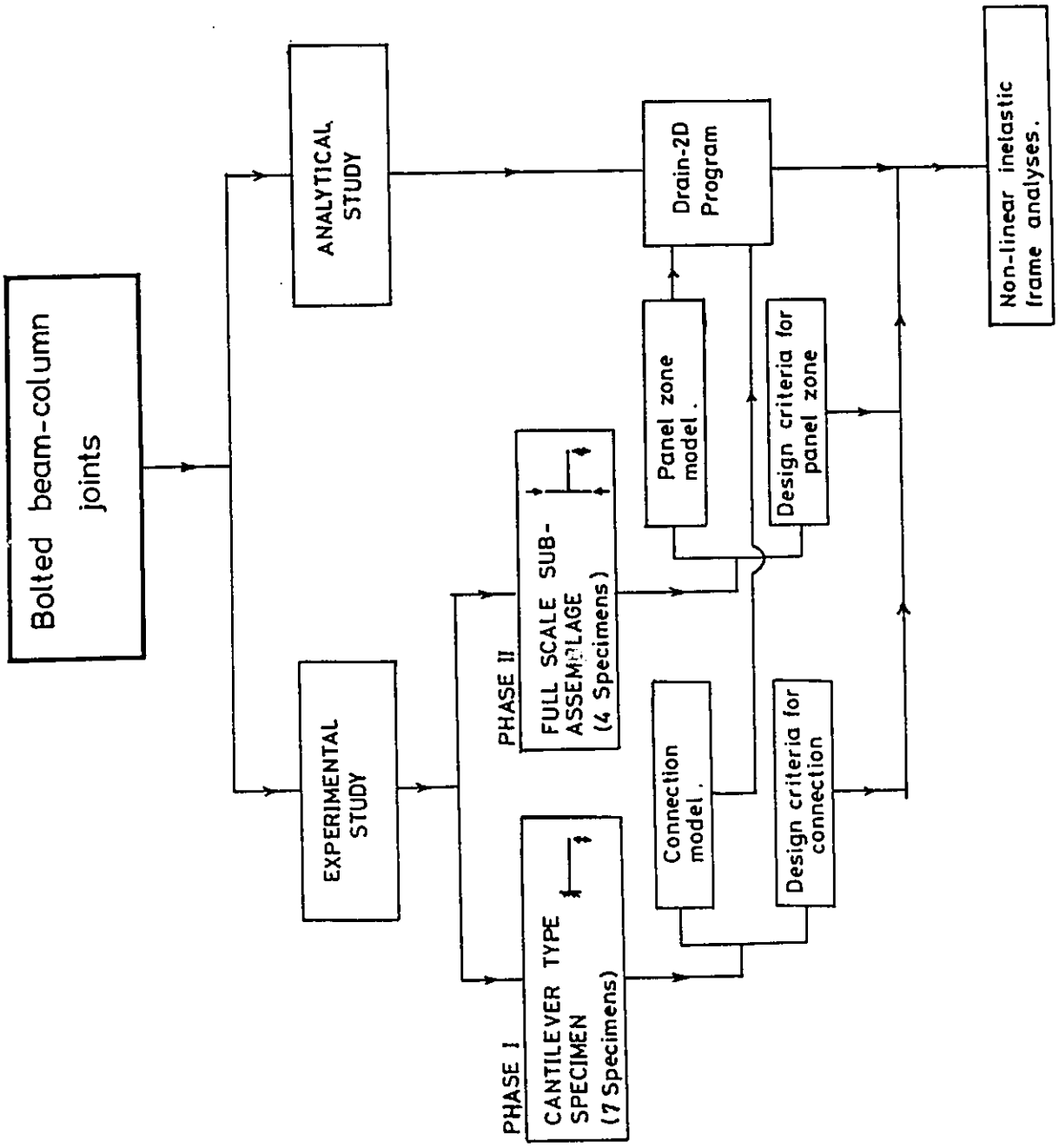

Fig. 1.3 Scope of the work.

CHAPTER 2

BEHAVIOUR OF EXTENDED END-PLATE CONNECTIONS UNDER CYCLIC LOAD

2.1 Selection of test specimens

The first phase of the experimental study focused on investigating the performance of extended end-plate connections when subjected to cyclic load. Seven full-scale extended end-plate beam-to-column connections were tested under a cyclic controlled displacement program. The tested specimens were of a simple cantilever type, in which a cantilever beam was connected to a column stub by an extended end-plate connection. A schematic illustration of a typical test specimen is shown in Fig.2.1. In this phase of testing, no attempt was made to simulate axial force in the column. Attention was principally confined to studying the behaviour of the connection itself.

The tested specimens were classified into two groups according to the section size used for the beam. Group A, which utilized a W360X45 (W14X30) section for the beam, included five specimens (A-1, A-2, A-3, A-4, and A-5). Group B employed a heavier section, W360X57 (W14X38), for two specimens (B-1 and B-2). For column stubs, two different sections were used W360X64 (W14X43) or W360X79 (W14X53).

2.2 Test setup

A special setup was constructed to accommodate the test specimens. The column stub was rigidly clamped to a rigid reaction frame by sixteen 25 mm diameter grade A490M bolts. The reaction frame was prestressed to a 600 mm thick floor slab of the laboratory by four 50 mm diameter rods. A hydraulic actuator of 600 kN capacity was used to apply the load at the beam tip in the vertical plane. The actuator was fixed to the floor by a pair of stiff angles prestressed to the floor slab by two 38 mm rods. The general arrangement of the setup is shown in Fig.2.2 and

Fig.2.3. As can be observed, the applied loads were delivered from the actuator to the beam-tip through a 50 mm diameter high-grade steel rod. At one of the rod ends a clevis was welded. This clevis was bolted to the beam end by a 50 mm diameter pin.

To prevent lateral buckling of the beams, a simple frame consisting of two angles was installed near the end of the beams to work as a guide. To simulate the effect of the floor deck which in actual practice provides lateral support to the top flange of the beam, a guide to prevent lateral displacement of the top flange was provided at the mid-span of the cantilever.

2.3 Description of test specimens

The material used for all seven test specimens including beams, columns, column flange stiffeners and end-plates was in accordance with GSA-G40.21-M300W steel (equivalent to 44 Ksi structural grade). Coupons from the beam and column sections were extracted to assess the members' physical properties. The test results are listed in Table 2.1.

Bolts used in all specimens were 25 mm diameter, grade ASTM A490M. The bolt holes were drilled 2 mm larger than the 25 mm nominal diameter of the bolt. Direct Tension Indicating Washers (DTI) were used underneath all bolt heads to check that the bolts were tightened to over 280 kN, which is the minimum bolt tension force recommended by the Canadian steel building code(CAN-S16.1-M89 ,1990) for 1-in A490 bolt.

All welds were made using compatible electrodes (CSA W48.1) and the welding design and practice was in accordance with CSA-W59. The welds were visually inspected and repaired if any defects were discovered. Details of the A group test specimens are shown in Fig.2.4 and are described below.

Specimen A-1

The specimen was fabricated by fillet welding a W360X45 beam section to a 25 mm thick end-plate. Then, the end-plate was bolted to a W360X64 column stub. Ten millimetres and 7 mm fillet welds for the flange and web, respectively, were used

to attach the beam to the end-plate. No continuity plates were provided at the levels of the beam flanges to stiffen the column flange.

Specimen A-2

This specimen was similar to specimen A-1, except that four 9 mm thick continuity plates were provided to stiffen the column flange. The continuity plates were welded to the column web and column flanges at the level of beam flanges using a 6 mm fillet weld.

Specimen A-3

The specimen was fabricated by welding a W360X45 beam section to a 19 mm thick end-plate. Two 9 mm thick small triangular plates were positioned and welded to both the end-plate and the beam flanges. These plates were provided to reduce the end-plate deformation and to investigate the effect of such a detail on reducing the end-plate thickness. In this specimen, a W360X79 section was used for the column stub. Again, 9 mm continuity plates were provided to stiffen the column flange.

Specimen A-4

The thickness of the end-plate was selected to be 19 mm for this specimen. A W360X79 section was used for the column and a W360X45 section was used for the beam. As in the case of specimen A-1, no continuity plates were provided to stiffen the column flange. During welding, a small degree of end-plate bending was observed. Tests conducted at both Vanderbilt University and at the University of Oklahoma (Griffiths, 1984) in which similar connections were tested under monotonic loading conditions, showed that such end-plate distortion did not decrease the overall connection capacity. However, the weld is subjected to high stresses during the field-tightening operation.

Specimen A-5

The specimen was made by welding a 16 mm thick end-plate to a W360X45 beam section. A W360X79 section was used for a column stub. Continuity plates were provided to stiffen the column flange. As in specimen A-3, two triangular plates were welded to the beam flanges and the end-plate to stiffen the end-plate.

Precautions were taken to minimize end-plate distortion by employing a proper sequence of welding.

The second group involved two specimens. The fabrication details of these specimens are shown in Fig.2.5.

Specimen B-1

This specimen was fabricated by fillet welding a 28.5 mm thick end-plate to a W360X57 beam section. For the column stub, a W360X64 section was used. Continuity plates for stiffening the column flanges were provided.

Specimen B-2

This specimen was similar to specimen B-1, except that a 22 mm thick end-plate with 10 mm triangular stiffeners were used.

In the design and detailing of all specimens, different aspects were considered and will be discussed in detail.

2.3.1 Ductility aspects

Since the beams in these specimens were expected to undergo severe inelastic deformations, the beam sections were chosen to meet the earthquake code requirements (CAN-S16.1-M89 ,1990 and LRFD ,1986) and hence were modelled after class 1; as such limitations were placed on the flange width-thickness and web depth-thickness ratios, and on the lateral unsupported length of the compression flange. It should be noted that the flange width-thickness ratio for group A specimens slightly exceeded the class 1 limit but in no case was it greater than 4%. Furthermore, the critical length of the upper flange was less than that of the lower flange, since the upper flange was braced laterally at mid span of the specimen to simulate the effect of a floor slab.

2.3.2 Strength aspects

According to the Canadian code (CAN-S16.1-M89 ,1990and Redwood et al, 1990), the beam to column connection must have adequate resistance to transmit a moment equal to the lesser of the beam flexural resistance and the moment that will

produce panel zone shearing forces equal to the joint resistance. In these specimens, the column stub was rigidly fixed to the reaction frame, i.e no deformation was allowed to occur in the panel zone. Therefore, it was decided that the connections be designed to sustain the beam strength. However, to investigate the possibility of connection participation in dissipating the input energy, some connections were detailed to sustain loads less than the beam strength. In other words, the connections in some cases were allowed to yield prior to beam yielding.

To help in the design and detailing of the connections, a review of the current design methods (Mann and Morris, 1979; Stark and Bijlaard, 1988; Packer and Morris, 1977; and AISC, 1980) was carried out . Although, such design methods are based on monotonic tests, it was felt that they could provide a guideline for designing the specimens. However, there were surprising discrepancies among the methods examined. Contrary to connections designed to carry static loads, these discrepancies can have deleterious effects on connections designed to sustain seismic loads. This can be explained by examining Table 2.2 which shows the yield strength of each component of the tested connections based on the actual measured yield stress and employing different connection design methods. These strengths were prescribed in terms of the corresponding loads applied to the beam-tip. Examining the table content shows that , for example in specimen A-4, if the AISC manual method were adopted for the design, it would be expected that the column flange of the specimen would yield first. However, if the method developed by Packer and Morris was adopted, the end-plate would be expected to yield first. Bearing in mind that the capacities of both elements to go into inelastic deformation are substantially different, the seriousness of these discrepancies on the connection seismic design can be understood.

The method developed by Packer and Morris (1977) based on yield line theories was adopted for detailing all the connections in this study. The bolts were overdesigned to avoid bolt failure.

2.3.3 Drift limitation

One of the important aspects that should be considered in the design and detailing of the specimens is interstorey drift (Park, 1989). The Canadian Code (NBCC, 1990) specified .005 as the limit for the specimen interstorey drift. In this study, the specimens' drifts were calculated by dividing the beam tip deflection at the instant of beam yielding by the beam cantilever length. In the absence of a method to assess the contribution of the connection rotation to a specimen's total deflection, the deflection was calculated at the point of the beam yielding assuming infinitely rigid connections. The resulting normalized deflection from this analysis is shown in Table 2.2. Obviously, these results are fairly high compared to the limit specified by the code, indicating that the specimens were flexible.

2.4 Instrumentation

To monitor the actuator load, a special built-up load cell was used. The cell consisted of eight strain gauges attached to the actuator rod(4 transversely and 4 longitudinally). The load cell was calibrated after each test in both tension and compression on a uniaxial Tinius machine. To measure the beam tip displacement, a cable type Linear Voltage Displacement Transducer (LVDT), was used. Dial gauges and LVDT's were used to measure the end plate rotation and the column flange rotation. Strain gauges were used to monitor the onset of beam flange local buckling and to determine initial yielding of the beam.

For the first two tests(A-1 and A-4), two bolts in each specimen were instrumented using strain gauges to monitor the fluctuation in the bolt pre-tension force. In subsequent tests, four bolts were strain gauged in each specimen. The bolt force was measured by the method developed by Surtees and Ibrahim (1980). In this method, the average strain in a rosette glued to the bolt head was calibrated against the force in the bolt. A special rig was fabricated to calibrate bolt forces prior to the test on a uniaxial Tinius testing machine.

All strain gauges and transducer data were scanned by a multichannel Autodata 9 Scanner System . The readings were recorded using a micro computer

system and were also punched onto a paper tape device to provide backup.

2.5 Loading sequence

To simulate seismic forces, the test specimens were subjected to a quasi-static cyclic loading. Although in practice the severe lateral loads are of a dynamic nature, it was believed that the rate of strain developed in the structural system was not sufficiently high to introduce significant variations in the so-called "static characteristics "of the material (Almalti and Hanson ,1973).

Before reaching the yield point, an individual specimen was subjected to four load cycles of half the expected yield value. The behaviour of the connection was therefore anticipated to be elastic. This pretest technique was employed to ensure proper connection set-up, welding, bolting and to check the data recording devices for proper functioning. The load was then increased until the initial beam yielding was recorded by the strain gages. Two cycles of reversed loads of this magnitude were then slowly applied. For subsequent loading cycles, the tip beam displacement was incrementally increased by half the yield displacement up to displacement ductility of four (Displacement ductility is defined as the ratio of beam tip displacement to the beam tip displacement at the first yield). If no failure was detected , two additional cycles one at five and another at six displacement ductility, were applied. Subsequently, the test was terminated since at this level a high ductility was achieved. In some cases the test was terminated before reaching displacement ductility of six due to severe lateral torsional buckling of the beam. A typical loading sequence for a test specimen consisted of ten inelastic cycles. During the test, the loading was temporarily stopped at each 5 mm displacement increment to allow for scanning the strain gages and transducers by the data acquisition system. A plot of such a routine is presented in Fig.2.6.

2.6 Experimental results

The data recorded during each test can be grouped into the following categories:

1) beam loading history represented by the relationship between the beam-tip load and the number of loading steps, the latter defined as the point at which the test temporarily stopped and the data scanned.

2) beam-tip load versus beam-tip deformation relationship. These hysteretic loops provide the basic data for determining the overall behaviour of the specimen.

3) beam moment versus connection rotation relationship. These hysteretic curves represent the connection behaviour, i.e the connection rotation due to end-plate and column flange deformations and bolt extension.

4) beam moment versus column flange rotation for unstiffened connections (specimens A-1 and A-4).

5) Variation of bolt pre-tension forces in several bolts.

In addition, strains at various locations such as the end-plate stiffeners and the beam flanges were recorded. Also, measurements were taken to determine the onset of beam buckling.

As noted, the test data were assembled under the various categories to illustrate certain aspects of the behaviour of a particular specimen. Also, these data allowed the determination of the influence of a particular variable on the overall behaviour of the subassembalge. At the same time, it was possible to isolate the behaviour of other components. As an example, the connection rotations were recorded for the tested specimens. Then, these rotations were multiplied by the cantilever length and subtracted from the overall beam-tip deformations. The resulting deformations are those due to elastic and inelastic beam rotation. Using elastic structural theory, the inelastic deformation of the beam can be separated.

In the following, the experimental results for each specimen will be described. More detailed description can be found in Osman et al. (1990b), Ghobarah et al.(1990) and Korol et al.(1990).

Specimen A-1

The applied loading history for specimen A-1 is shown in Fig.2.7. From this figure it can be noted that the maximum applied load attained during the test was about 147.7 kN at the thirteenth cycle. At this load, the corresponding measured

beam-tip deflection was 126 mm (upward). The resulting hysteretic loops of the beam-tip load versus beam-tip deflection for the specimen are shown in Fig.2.8. The loops consistently exhibited stable characteristics. The specimen responded essentially elastically up to a beam-tip load of 80 kN, at which point the column flange showed signs of yielding. This yielding was evident from examining Fig.2.9 which shows the beam-tip load versus beam-tip deflection due to column flange rotation only. The contribution of the column flange to the measured total beam-tip deflection as shown in Fig.2.9 was over 50%. In this test, the column flange was severely damaged with reversed buckling of the beam's top and bottom flanges and that of the web, as is evident from Fig.2.10. Rosettes glued to the bolts showed that gradual degradation in the bolts pre-tension forces were recorded throughout the test. It should be noted, that the column flange yield load was close to that predicted by Packer and Morris (1977) using the yield line theory (refer to Table 2.2).

Specimen A-2

The applied loading history of this specimen is shown in Fig.2.11. The maximum applied load monitored during the test was 154.5 kN and was attained during the tenth cycle (downward). The overall behaviour of the specimen represented by the beam-tip load versus beam-tip deflection hysteretic curves, is shown in Fig.2.12. As seen, well behaved hysteretic response can be observed up to the eleventh cycle at which point severe buckling to the beam flanges accompanied by beam web buckling was observed and resulted in a deterioration in its load carrying capacity. Specimen yielding was observed at a beam-tip load of 109 kN and was initiated in the column flange. This yielding was accurately predicted using the Packer and Morris (1977) yield line mechanisms. During this test, the variation of the bolt pre-tension forces in four bolts were monitored as plotted in Fig.2.13. As can be seen, degradation in the bolt pre-tension force occurred with the progression of loading. This degradation reached as much as 40% of the initial tightening force. The response of the connection which includes the column flange deformation, end-plate deformation and bolt extension during this test, was recorded as shown in Fig.2.14. Significant degradation in the connection stiffness with loading can be observed. The

inelastic rotation of the beam was isolated as shown in Fig.2.15. The test was terminated after pronounced ductility was reached. A photograph of the failed specimen is shown in Fig.2.16.It should be noted that specimens A-1 and A-2 were identical with the exception that in A-1 the column flange stiffeners were eliminated. Comparing the overall behaviour of the two specimens revealed the effect of the column flange stiffeners in improving the specimen's performance.

Specimen A-3

The loading history of specimen A-3 is shown in Fig. .17.The maximum load attained during this test was 156.4 kN during the ninth cycle (upward). The beam-tip load versus beam-tip deflection hysteretic behaviour is shown in Fig.2.18. The specimen responded elastically up to a beam-tip load of 115 kN, at which point the beam yielded. Similar to specimen A-2, the specimen behaved well up to the tenth cycle (upward) when deterioration in the load carrying capacity was detected. This strength deterioration was attributed to buckling of the beam's flanges as well as the beam web. Degradation in the pre-tension forces of the bolts was again monitored in all bolts. The presence of the end-plate stiffener in this specimen had the effect of shifting the plastic hinge location away from the face of the connection to the section where the triangular stiffeners terminate. The behaviour of the connection is shown in Fig.2.19, while that of the beam is indicated in Fig.2.20. Examining the latter figure shows that the beam exhibited unsymmetrical behaviour after the onset of beam web local buckling. As the cycles increased, the beam was able to attain a higher moment for the same rotation value in the positive direction (upward) than in the negative direction (downward). The reason for this behaviour is the development of lateral torsional buckling as noted in Fig.2.21.Since the upper flange was adequately braced laterally to simulate the slab effect compared to the lower one, the observation described can be explained. The test was terminated when high ductility was reached.

Specimen A-4

In this specimen, the end-plate was under-designed to examine the specimen behaviour when the end-plate in the connection constitutes the weakest element. The

specimen was subjected to the loading history shown in Fig.2.22. The maximum load reached during the test was 134.6 kN during the ninth cycle (downward). The resulting hysteretic behaviour of the specimen is shown in Fig.2.23. As can be seen, deterioration in both stiffness and strength was detected with the progression of load. This deterioration was attributed to the severe yielding of the column flange and the initiation of a cleavage crack at the toe of the weld between the end-plate and the beam flange. This crack was initiated during the fourth cycle and propagated in subsequent cycles through the end-plate thickness as shown in Fig.2.24. During the twelveth cycle, a fracture to the extended parts of the end-plate occurred resulting in a sudden drop in the load carrying capacity of the specimen. However, this fracture did not result in complete collapse of the connection, since the inside bolts were still able to sustain significant load. In general, no inelastic action was observed in the beam and the column flange was subjected to severe damage as evident from Fig.2.25.

Specimen A-5

The applied loading history of this specimen is shown in Fig.2.26. As can be observed, the maximum load was 158.9 kN, attained during the tenth cycle. Yielding of the specimen was observed at a beam-tip load of 121 kN and was initiated in the beam. The overall behaviour of the specimen, as recorded, is shown in Fig.2.27. As can be seen, the hysteretic behaviour was initially stable, up to the onset of local buckling, which was detected during the sixth cycle and became quite severe during the tenth cycle. This buckling resulted in significant strength deterioration. In fact, strain readings taken at the end-plate stiffeners show that they yielded in tension as recorded in Fig.2.28. Near the end of the test, crack initiation at the toe of the weld between the beam flange and the end-plate stiffener was observed. The location is identified by an arrow in Fig.2.29. In the specimen, the bolts showed a typical behaviour to those observed in previous specimens.

Specimen B-1

Similar to the previous specimens, specimen B-1 was subjected to a controlled cyclic displacement history. The resulting loading history is shown in

Fig.2.30. The maximum load attained during testing just exceeded 200 kN. The overall behaviour of the specimen was consistently stable as shown in Fig.2.31, while the connection response is given in Fig.2.32. Fig.2.33, indicates the well behaved behaviour of the beam throughout the test. Excellent performance of the beam in such a test was attributed to its stockier flanges that resulted in a delay of beam buckling. The test was terminated when high beam-tip displacement was reached. At the end of the test, cracks at the transition area between the column flange and the column web in the connection area were observed. These cracks were initiated as a result of subjecting the column flange to severe cyclic strain reversals. A photograph of the specimen after the test is shown in Fig.2.34.

Specimen B-2

Similar to specimen B-1, this specimen showed superior hysteretic behaviour throughout the test as can be concluded from examining Fig.2.35. However, near the end of the test, signs of strength deterioration due to beam flange buckling were detected. The behaviour of the connection in this specimen is shown in Fig.2.36. Yielding of the specimen was initiated in the column flange at a beam-tip load of 109 kN. Readings from strain gauges bonded to the end-plate stiffeners showed that they essentially yielded in tension. When subjected to excessive compression, they buckled locally as evident from Fig.2.37. The behaviour of the beam in this specimen is represented by the beam moment versus its inelastic rotation in Fig.2.38. The test was terminated at a high ductility level. At the end of the test, the specimen is shown in Fig.2.39.

2.7 Discussion of test results

2.7.1 Strength and stiffness of specimens

All specimens were able to sustain moments higher than the beam's nominal plastic moment capacity. In some specimens such as B-1 and B-2, superior hysteretic behaviour was observed. In others such as A-2, A-3 and A-5 strength degradation was noted with load progression. Specimens such as A-1 and A-4 showed poor hysteretic behaviour. From the test results, it was observed that the ability of the specimen to

maintain strength throughout the loading regime depends on two main factors. The first is the ability of the beam to undergo several inelastic strain reversals without severe local buckling or lateral torsional buckling. The second is the strength of the connection itself. In beams possessing small width-to-thickness ratios of flanges and webs and restrained adequately by lateral bracing, buckling can be delayed and satisfactory behaviour under cyclic loading can be achieved (De Buen 1980). This explains the improved behaviour of the group B specimens, whose sections were selected to have flange-to-thickness ratios ,b_{bf}/t_{bf} , equal to 6.6 and web depth-to-thickness ratio, h_{bw}/t_{bw}, equal to 41.5. In group A specimens, the b_{bf}/t_{bf} ratio was taken equal to 8.55 while h_{bw}/t_{bw} was equal to 47.4. The beam selection in group B specimens resulted in delaying the onset of beam local buckling, especially that of the web, which was the principal reason for the observed strength deterioration in the case of specimens A-2, A-3 and A-5. During these tests it was observed that the rotation capacity of the beams under cyclic loading is far less than that under monotonic loading conditions. As an example, in the study conducted by Mitani et al. (1977) to predict a beam's rotation capacity, sections W360X45 and W360X57 were calculated to have plastic rotational capacities, θ_p, of 0.095 and 0.1, respectively. These results can be compared with the rotational capacities and the ductility levels determined experimentally from this testing program as shown in Table 2.3. The shaded column shows that the rotation capacities of the tested beams were approximately half the predicted values. Apart from slenderness, buckling is a phenomena which depends mainly on the accumulated strains and under cyclic loading condition; a higher strain accumulation can occur at low rotation levels. As such, there is a discrepancy between the predicted rotational capacities under monotonic loading conditions and cyclic loading conditions.

The specimen strength is limited by the strengths of the connection components, i.e the end-plate, the column flange and the bolts. This is evident from examination of the cases of specimens A-1 and A-4 in which the connections constituted the weakest elements. In A-1, the column flange was able to sustain only 72% of the load required to yield the beam before the column flange itself formed

a mechanism. This early column flange yielding limited the load carrying capacity of the specimen and resulted in confining most of the inelastic action to the column flange which sustained severe damage. In the case of specimen A-4, the end-plate formed a mechanism at a load equal to about 62% of the load required to yield the beam. Severe damage to the end-plate in the form of brittle failure was observed. It should be noted that although in other specimens such as A-2, B-1 and B-2, the column flanges were also weak, good behaviour was observed. This was attributed to the presence of the column flange stiffeners. In unstiffened connections, once the column flange forms a mechanism, higher load carrying capacity can only be achieved through strain hardening. However, in stiffened connections, the column flange stiffener limits the flange deformation and participates in transmitting the loads allowing higher load carrying capacity. The effect of a column flange stiffener, can be noted by comparing the behaviour of both specimens A-1 and A-2. These specimens were identical except that in A-2 the column flange was stiffened. Its better behaviour is evident when compared with specimen A-1 as indicated in Figs. 2.8 and 2.12.

Concerning the specimens' stiffnesses, Table 2.4 shows the normalized beam-tip deflection at the initial yielding of the beam as measured from the tests. Comparing these results with the previously calculated ones in Table 2.2, shows that the connection significantly contributes to the specimen's overall behaviour. This contribution was relatively substantial in most of the specimens as a result of connections yielding prior to the yielding of the beam. The contribution of the connection to overall deflection in specimens A-2 and B-1 can be observed from examining Figs.2.40 and 2.41, respectively.

In view of the preceding discussion, it can be concluded that in selecting the beam section, special efforts should be made to prevent or at least delay the onset beam local and/or lateral torsional buckling. Connection components should be designed to sustain an overstrength of the beams and to limit the connection deformation. These restrictions apply to a lesser extent in the case of stiffened connections.

In addition, this study showed that the equations developed by Packer and Morris (1977) based on yield line theories were surprisingly accurate in predicting the yield load of the connections. Also, it showed the importance of incorporating the behaviour of the connections in the analysis of moment resisting frames.

2.7.3 Connection behaviour

The connection's rotation was the result of end-plate and column flange deformation and bolt extension. As can be observed from Figs. 2.15, 2.20, 2.33 and 2.38, all connections showed stable hysteretic behaviour up to either the onset of beam web buckling, or the occurrence of severe yielding to the column flange or the end-plate. Following web-buckling, the connection lost its ability to reproduce full loops and displayed unpredictable behaviour. This response is shown by dotted lines in the figures for clarity. In the case of column flange or end-plate yielding, significant degradation occurred in the connection strength after severe distortion and/or crack initiation.

As a general observation, all the connections experienced degradation in their stiffness with load cycling. Fig.2.42 shows this variation for several of the tested connections with the number of inelastic excursions. Analysis indicates that this stiffness degradation was due to both the loss of bolt pre-tension forces with loading cycles (see Fig.2.13) and the permanent deformations of the column flanges or the end-plates. Stiffness degradation can have a deleterious effect on the drift of moment resisting frames.

The tests indicate that a decrease of bolt pre-tension force is significant. These forces were reduced in some cases to the snug-tight condition. This severe deterioration was attributed to both inelastic strains developed in the threaded regions of the bolts and local yielding of column flange and/or the end-plate beneath the heads and the nuts. Indentations were observed during disassembly of the connection after testing which indicates substantial bearing strains from contact stresses. This behaviour can be improved by avoiding severe yielding to the column flange and end-plates.

Examining the hysteretic behaviour of the connections showed that the main parameters that can describe a connection's response are (1) the connection yield moment, M_{pc}, (2) the initial connection stiffness, K_i, (3) the connection ultimate strength, M_{max}, and (4) the connection rotation capacity (i.e ductility), θ_{max}. Table 2.5 shows these parameters for some of the tested specimens. From column 4 of Table 2.5, it is observed that large moments can only be sustained by large rotations developed through excessive yielding of the connections. Such deformations are undesirable and should be limited by avoiding excessive yielding of connections.

2.7.4 Energy dissipation

In seismic design, cyclic energy dissipation is of great importance, since it represents the ability of the members and their connections to dissipate earthquake input energy. Sufficient energy dissipation without substantial loss of strength and stiffness is desirable behaviour for beam-column subassemblages.

For the tested specimens and their individual components, the energy dissipated in each cycle can be assessed by calculating the area within the loop for that cycle. However, Popov et al (1973) suggested that the energy dissipation associated with inelastic load excursions (half cycles) is more meaningful to employ. Thus, the cumulative energy dissipated by each of the tested specimens was plotted against the number of inelastic excursions in Fig.2.43. This figure reveals the superiority of specimens A-2, A-3, A-5, B-1, B-2 compared to specimens A-1 and A-4, an improvement attributable to column flange stiffeners in the former group of specimens. As a result, the loading cycles forced the beam to yield and subsequently to participate in dissipating the input energy. Taking into account the good ductility characteristics of the beams and their ability to dissipate large amounts of energy, good performance was achieved. On the other hand, in the unstiffened connections A-1 and A-4, the main element to dissipate energy was the column flange with minimal participation from the beams. The result in these cases was poor connection behaviour. In addition, in specimen A-4, the end plate was designed to be relatively thin. Although it participated significantly in dissipating the input energy it

subsequently failed. As a result, it can be concluded that the end plate should not be allowed to participate in energy dissipation since this is expected to lead to a connection's demise.

During the tests, the energy dissipated by each element was calculated. Figs.2.44 through 2.48 show the accumulated energy dissipated by each element in specimens A-2, A-3, A-4, B-1 and B-2. Upon examining these figures, it was observed that:

1) In the case of specimen A-2 (Fig.2.44), a considerable amount of energy was dissipated by the beam (about 94% of the total dissipated energy) with only minimal participation from the connection.

2) In the case of specimen A-3 (Fig.2.45), the connection was strong enough to force most of the inelastic action to the beam (96% of the total dissipated energy).

3) In the case of specimen A-4 (Fig.2.46), the connection was weak and dissipated a considerable amount of energy. Of the total dissipated energy 46% and 33% were dissipated by the column flange and the end-plate, respectively.

4) In the case of specimen B-1 (Fig.2.47), 69% of the total energy was dissipated by the beam and the reminder by the connection, mainly by the column flange.

5) The beam in specimen B-2 dissipated 87% of the total dissipated energy as shown in Fig.2.48.

These observations support the contention that the weakest element in the specimen is subjected to the highest demand.

2.8 Proposed design method:

Based on the results of this experimental program, a quantitative procedure for detailing and designing the extended end-plate connections to sustain severe earthquake excitation can be proposed. The bases for such a method are:

1. The connection deformation should be limited to avoid excessive structural drift.
2. No inelastic action should take place in the end-plate to avoid a brittle failure as demonstrated by the failure of A-4.
3. In the case of unstiffened connections, elastic response for the column flanges is

desirable to avoid severe damage to the flange.

4. In the case of stiffened connections, inelastic action of column flanges is tolerable.

5. The equations developed by Packer and Morris (1977) based on the yield line theories are confirmed to be accurate from the tests. These equations can be used to predict the yielding of the connection components.

6. Beam moments due to strain hardening can reach up to 1.3 times the beam plastic moment.

7. Bolts lose their pre-tension forces significantly under cyclic loading conditions.

2.8.1 Design of bolts

In spite of bolt pre-tension forces deterioration, it is believed that the current design method (CSA-S16.1-M89) is satisfactory. In this method, the bolt force is determined as

$$F_b = M_p / n_b d_b \qquad (2.1)$$

where

M_p = the beam plastic moment.
d_b = the beam depth.
n_b = number of bolts in tension (in this case 4 bolts).

The bolt diameter can be selected so that, F_b, is less than ,T_b, which is the tensile resistance of the bolt and is given by

$$T_b = 0.75 \phi A_b F_u \qquad (2.2)$$

where

ϕ = 0.67
A_b = nominal area of the bolt.
F_u = specified minimum tensile strength.

Concerning the shear acting on the connection, it is usually small and is expected to be carried by the bolts on the compression side.

2.8.2 Design of end-plate

During testing of specimen A-4, the end-plate failed by the formation of a crack at the toe of the weld between the beam flange and the end-plate. This failure is believed to be the result of excessive deformation of the end-plate combined with the fact that this deformation took place in the heat affected zone which is brittle. Such a failure can be prevented by designing the end-plate to sustain the maximum strength of the beam. In other words, the end-plate should be designed to remain elastic. As such, the end-plate thickness, t_{ep}, is given by

$$t_{ep}=\left[\frac{M_p X}{B_{ep}\phi_{us}\sigma_{ye}(d_b-t_{bf})}\right]^{1/2} \tag{2.3}$$

where

M_p = beam plastic moment
ϕ_{us} = understrength factor and equal to 0.76.
σ_{ye} = end-plate yield stress.
d_b = depth of the beam.
t_{bf} = thickness of beam flange.
B_{ep} = end-plate width.
X = distance between bolt centre and the toe of the weld joining the end-plate and the beam flange.

This equation was formulated based on a yield line mechanism suggested by Packer and Morris (1977) and is shown in Fig.2.49(a). Applying this method will usually result in rather thick plates, especially in the case of beams with large sections. This problem can be overcome by welding small triangular plates such as the ones used with specimens A-3, A-5 and B-2 to stiffen the end-plate itself. In such a case the end-plate thickness can be drastically reduced. The end-plate thickness calculated using the yield line mechanism shown in Fig.2.49(b), is given as

$$t_{ep}=\left[\frac{M_p}{\frac{B_{ep}-t_{se}-D}{x}+\frac{B_{ep}-t_{bw}-D}{x_1}+\frac{p-t_{bf}-D+a+x}{x_2}(d_b-t_{bf})\phi_{us}\sigma_{ye}}\right]^{1/2} \tag{2.4}$$

Where,

p = $0.6(d_b - t_{bf})$,
t_{se} = thickness of the end-plate stiffener,
D = bolt hole diameter,
t_{bw} = beam web thickness, and
x, x_1, x_2 are shown in Fig.2.49(b).

2.8.3 Design of column flange

The tests have shown that unstiffened column flanges are more vulnerable to severe damage. This damage, observed in the form of excessive deformation, causes severe bending in the bolts and an increase in connection rotation. Therefore, it seems important to check the adequacy of the column flanges, especially in the tension region. The equation developed by Packer and Morris (1977) based on the yield line mechanism shown in Fig.2.50(b) can be used with a slight modification to account for the beam's overstrength. The maximum tension force component of the beam moment, F_{mt}, transmitted by the bolts to the column flange is given by

$$F_{mt} = \frac{M_p}{d_p} \tag{2.5}$$

which should be less than the maximum force, F_{mf}, that can be supported by the flange given by

$$F_{mf} = t_{cf}^2[\pi + (2n + c - D)/m]\phi_{us}\sigma_{yc} \tag{2.6}$$

where

t_{cf} = column flange thickness
σ_{yc} = yield stress of the column flange
n = distance from the bolt centre to the tip of the column flange.
c = the vertical distance between the centres of the two bolts in tension.
D = Diameter of the bolt hole.
m = distance between the bolt centre to the web toe of fillet of I-shaped section.

Satisfying this equation will ensure elastic response of the column flange under ultimate beam load.

In the case of unstiffened connections, the column web in the compression region should be checked. This can be done by ensuring that, F_c, the web compression capacity (Hendrick and Murray, 1984)

$$F_c = \sigma_{yc} t_{cw} (t_{bf} + 6K + 2t_{ep} + 2t_{wf}) \tag{2.7}$$

where

t_{cw} = thickness of column web.
t_{bf} = thickness of beam flange.
σ_{yc} = yield stress of column web
t_{wf} = weld size.
K = the column "k" distance.

is higher than ,F_{mt} given by Eq. 2.5.

If F_{mt} is higher than F_{mf} as calculated by Eq.2.6, the column flange has to be stiffened. It is prudent to check the column flanges for adequacy in tension to avoid excessive yielding and possible crack formation as was observed with specimens B-1 and B-2. The tension component of the beam, F_{mt}, transmitted by the tension bolts to the column flange should be less than the column flange resistance, F_{ms}, which is given based on the yield line mechanism shown in Fig.2.50(a) as follow

$$F_{ms} = 0.9 t_{cf}^2 \left\{ \frac{(2V + 2W - D)}{m} + \left(\frac{1}{V} + \frac{1}{W}\right)(2m + 2n - D) \right\} \sigma_{yc} \tag{2.8}$$

where

w = $[m(m+n-0.5D)]^{1/2}$
v = $(c - t_s - 2xt_{wf})/2$ and $> w$
t_s = thickness of the column flange stiffener.

In Eq.2.8, the coefficient 0.9 was used as the understrength factor instead of 0.76, since the stiffened column flanges showed capability to dissipate the input energy. Therefore, limited inelastic deformation is allowed to take place in the column flange in such a case. However, in all cases, the beam has to yield prior to the column flange.

2.9 Summary

Based on the reported experimental work and the analysis of the results the following remarks can be made:

1) In all the tests, the connections were able to sustain moments higher than the beam's nominal plastic moment capacity.

2) The connection's rotation is likely to contribute significantly to the interstorey drift of the structure.

3) Under cyclic loading conditions, all seven tested connections showed degradation in stiffness with load cycles due to diminished bolt pre-tension forces and inelastic deformation.

4) Excessive yielding of the column flange will make it more prone to low-cycle fatigue and may result in severe damage. Checking the adequacy of the column flange to resist the expected high-level forces is important.

5) Improved behaviour under seismic loading can be achieved by selecting beam sections with small width-to-thickness ratios for flanges and webs and by providing adequate lateral bracing.

6) Sufficient energy dissipation without substantial loss of strength and stiffness can be obtained by proper detailing of the connections.

7) Quantitative procedures for the design of seismic end-plate connections are proposed. It is believed that a connection proportioned according to these procedures will perform satisfactorily for moderate-to-severe earthquake loading.

Table 2.1 Mechanical properties of tensile coupons

Specimen No.	Coupon location	Yield stress (MPa)	Tensile stress (MPa)
A-1	Beam flange	310.9	500.0
	Beam web	315.7	480.7
	Column flange	310.1	492.2
A-2	Beam flange	316.1	503.3
	Beam web	322.1	480.6
	Column flange	310.1	492.2
A-3	Beam flange	310.9	500.0
	Beam web	315.7	480.7
	Column flange	269.8	450.5
A-4	Beam flange	310.9	500.0
	Beam web	315.7	480.7
	Column Flange	269.8	450.5
A-5	Beam flange	316.1	503.3
	Beam web	322.1	480.6
	Column flange	269.8	450.5
B-1	Beam flange	315.5	493.0
	Beam web	338.4	467.5
	Column flange	319.1	534.8
B-2	Beam flange	311.5	489.4
	Beam web	338.6	517.6
	Column flange	326.3	523.7

Table 2.2 Strength of specimen components based on measured yield stress

Specimens	A-1	A-2	A-3	A-4	A-5	B-1	B-2
Beam hinging	112.7	114.9	118.4	112.7	120.6	152.9	158
Column flange mechanism.							
Packer and Morris.	79.6	98.9	128.4	104.6	128.4	104.4	107
AISC manual.	59.2	141.6	160.8	78.2	160.8	163.0	161
End-plate mechanism.							
Packer and Morris.	125	125	-	70	-	164	-
AISC manual.	413	413	-	177	-	421	-
Mann and Morris.	209	209	-	117	-	286	-
Normalized tip deflection at yield.	1/158	1/155	1/174	1/158	1/174	1/164	1/182

All values are in (kN) except for the last row of entries (dimensionless).

Table 2.3 Rotational capacities of the beams

Specimen No.	θ_p X 10^{-2} (rad)		θ_p^* X 10^{-2} (rad)		θ_m X 10^{-2} (rad)		R_u	
	+ve	-ve	+ve	-ve	+ve	-ve	+ve	-ve
A-2	6.29	4.79	10.25	10.05	1.67	1.69	9.76	9.57
A-3	3.16	3.38	5.66	6.47	1.34	1.16	5.67	6.48
B-1	3.84	3.12	6.38	5.88	3.84	3.12	6.70	6.17
B-2	6.23	2.84	8.82	6.81	4.18	2.84	8.65	6.67

θ_p = maximum beam plastic rotation before failure occurs or moment capacity M_p is exhausted, measured from zero rotation.

θ_p^* = beam plastic rotation measured from zero load intercept to the same point as defined in θ_p.

θ_m = rotation corresponding to the point where the maximum moment is attained.

R_u = ultimate rotation capacity of the beam defined as θ_p^*/θ_{pl} (ductility).

θ_{pl} = the hypothetical plastic rotation defined as $M_pL/3EI$.

Table 2.4 Normalized beam-tip deflection at yield as measured.

Specimen No.	A-1	A-2	A-3	A-4	A-5	B-1	B-2
Normalized tip deflection	1/67	1/80	1/87	1/79	1/86	1/65	1/69

Table 2.5 Connection Characteristics

Specimen No.	M_{pc} (kN.m)	K_i (kN.m/rad)	M_{max} (kN.m)	θ_{max} (rad X 10^{-2})
A-2	200.7	63751	325.28	1.05
A-3	222.2	79370	333.00	0.99
B-1	202.0	74685	440.51	3.12
B-2	203.0	65924	422.00	2.34

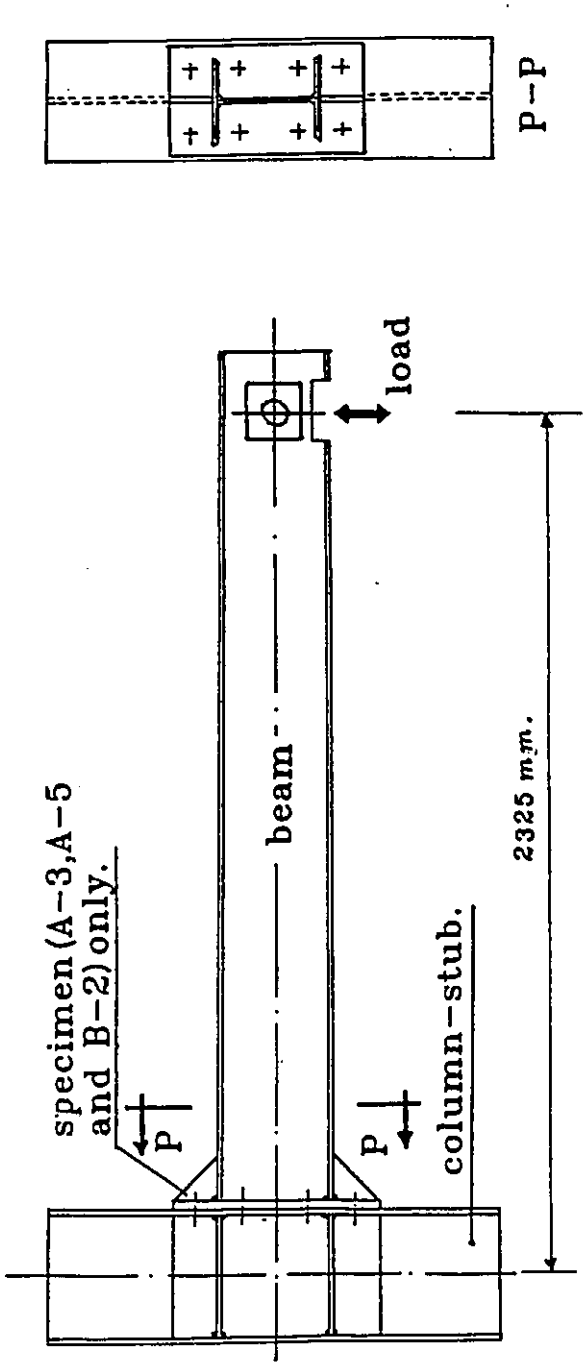

Fig. 2.1 Test specimen.

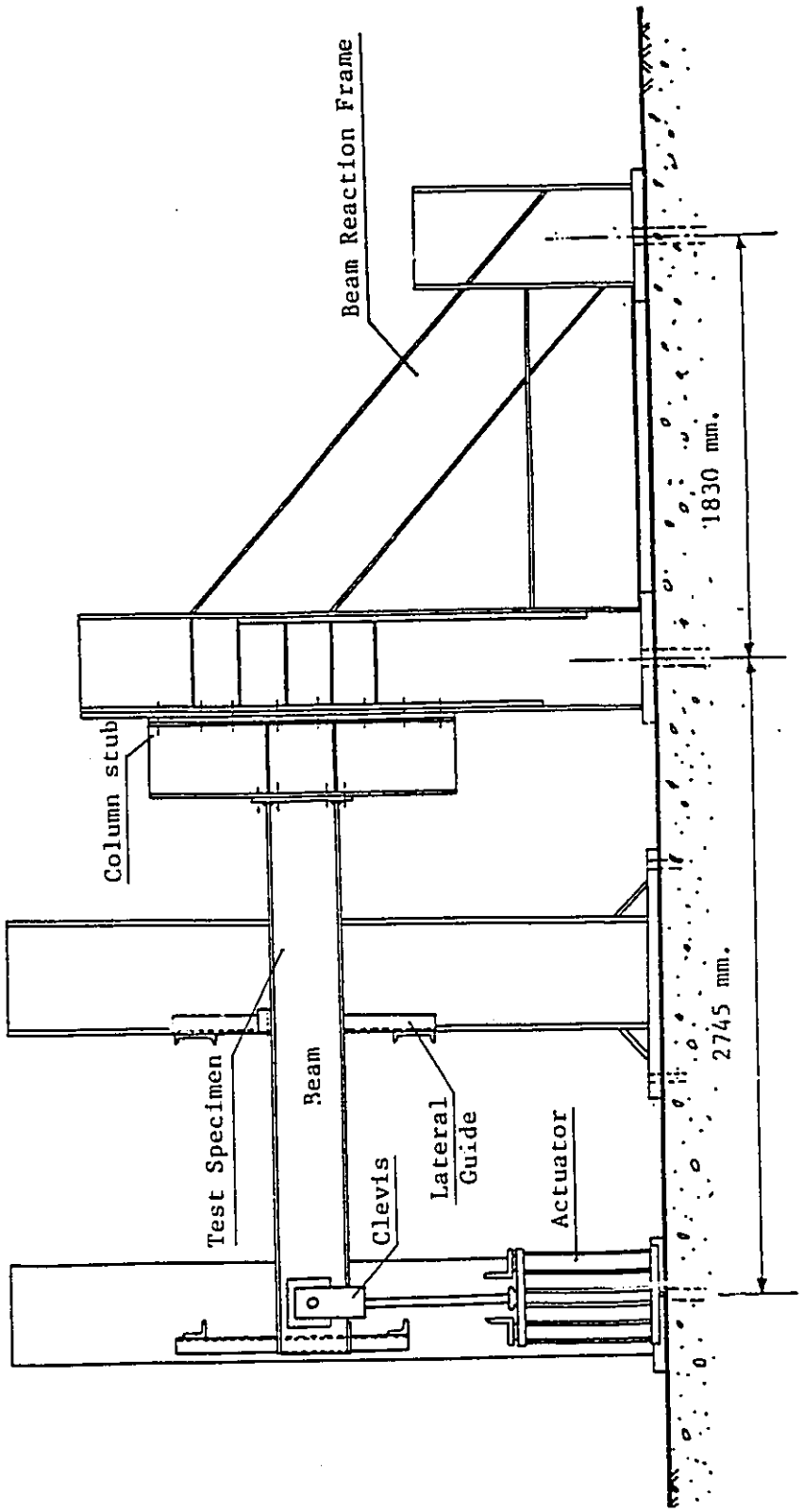

Fig. 2.2 Test setup.

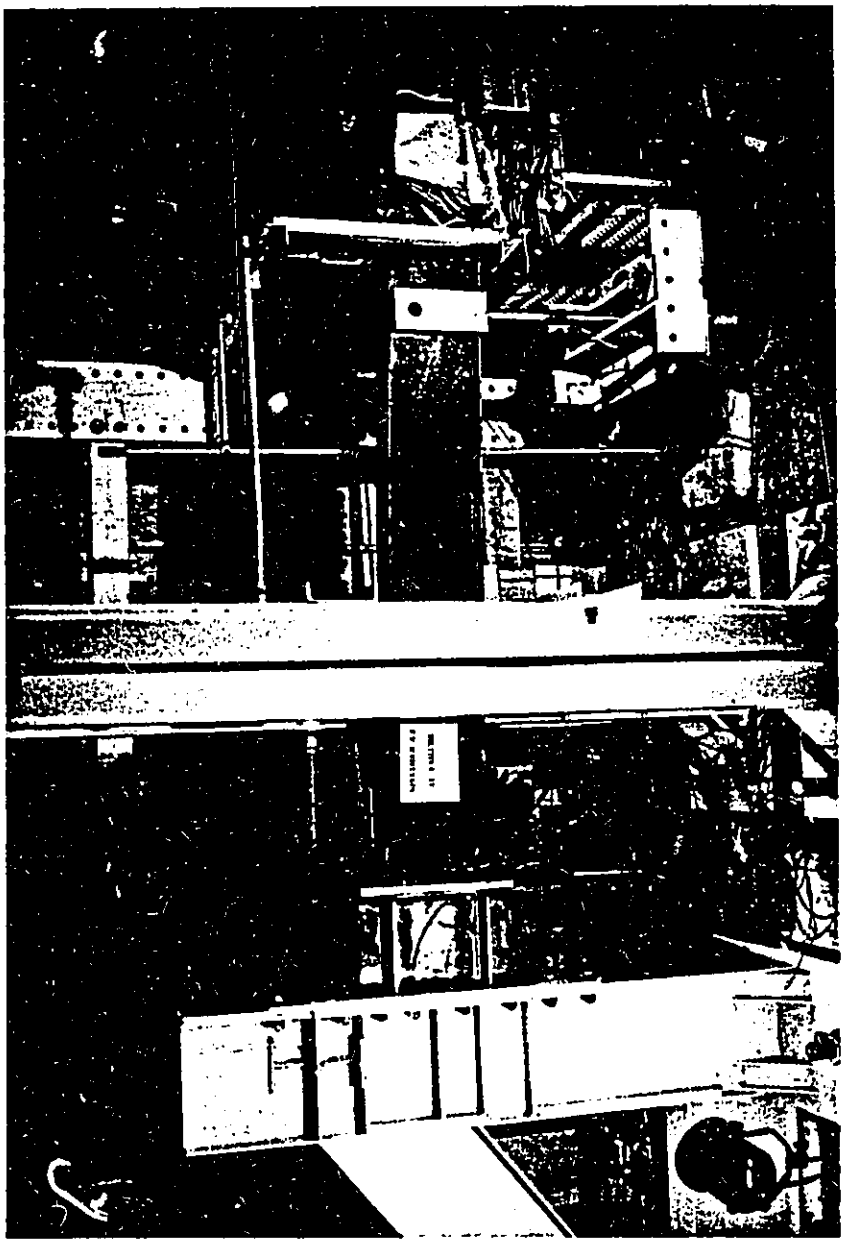

Fig. 2.3 View of test arrangement

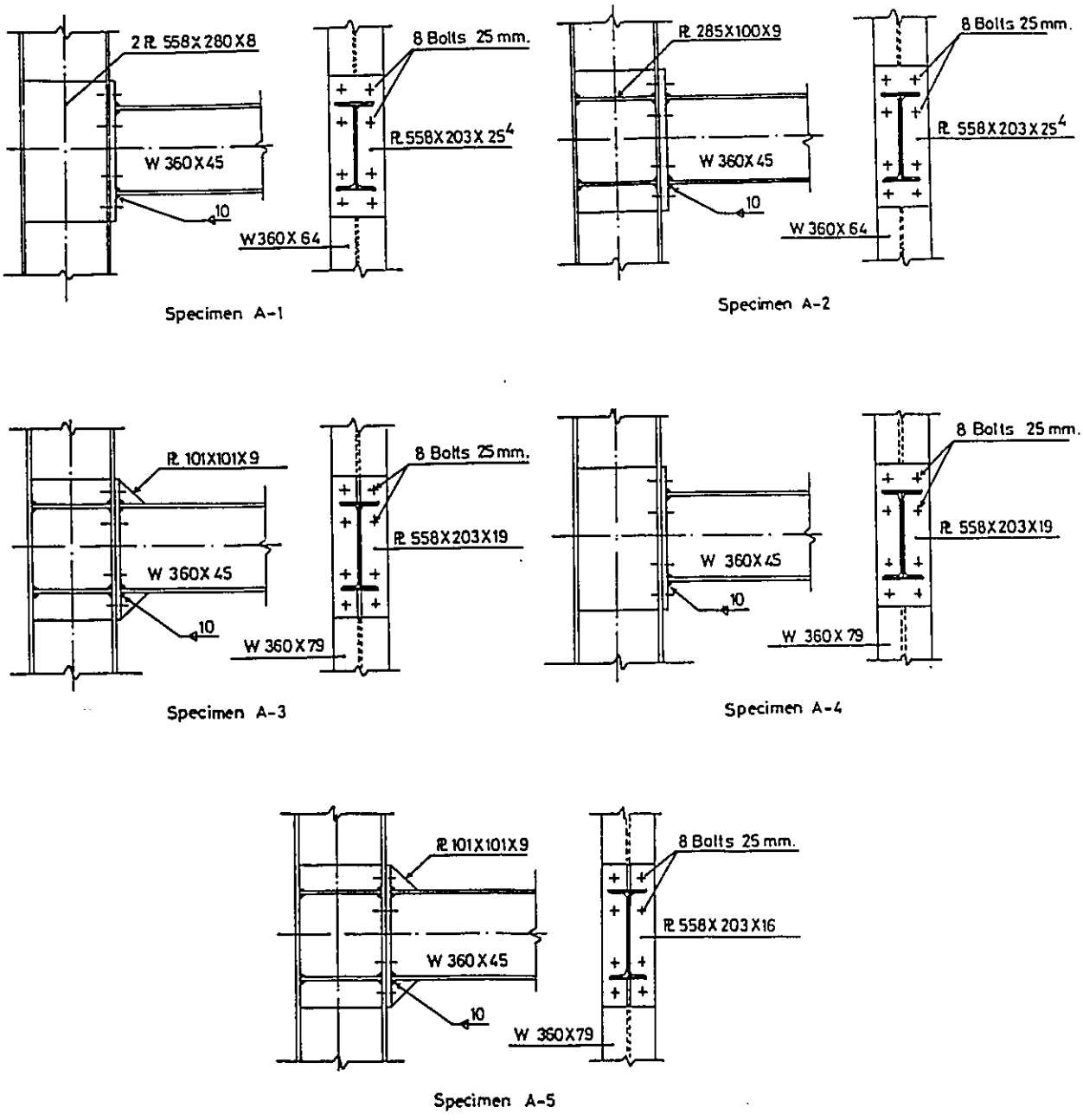

Fig. 2.4 Details of group A connections.

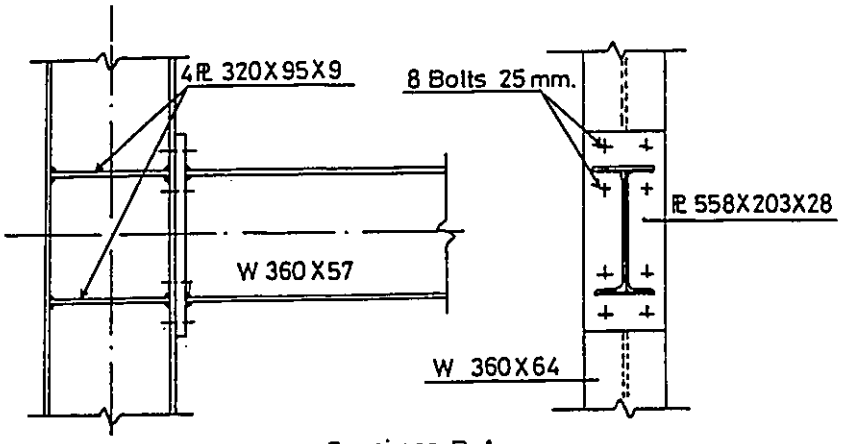

Specimen B-1

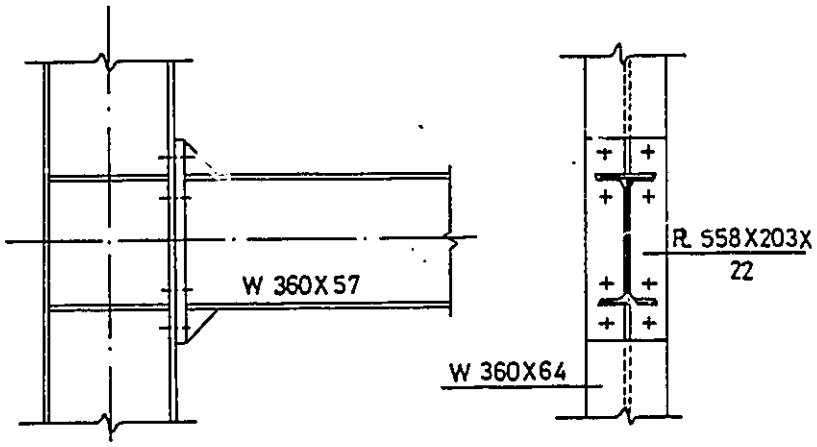

Specimen B-2

Fig. 2.5 Details of group B Connections.

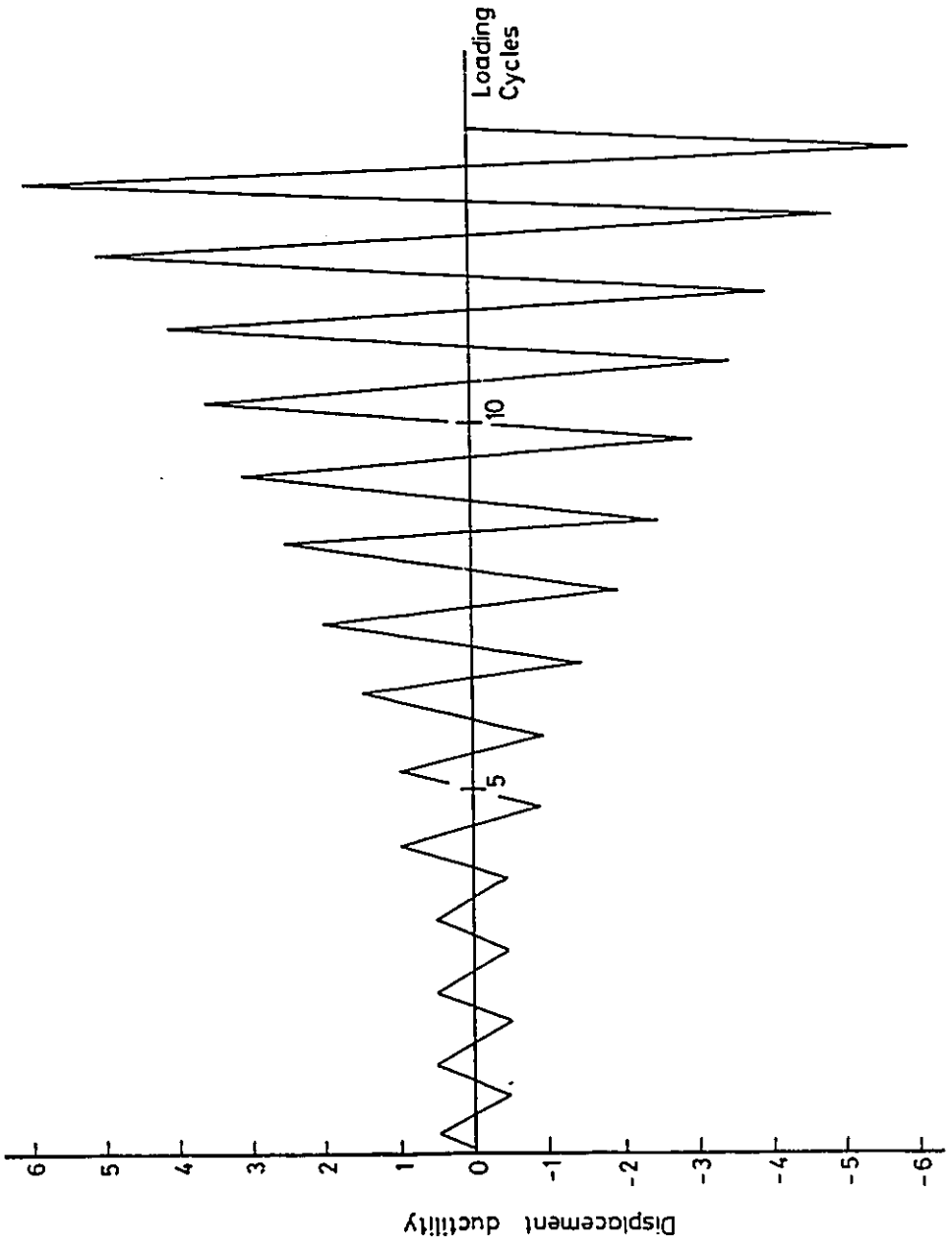

Fig. 2.6 Typical loading routine.

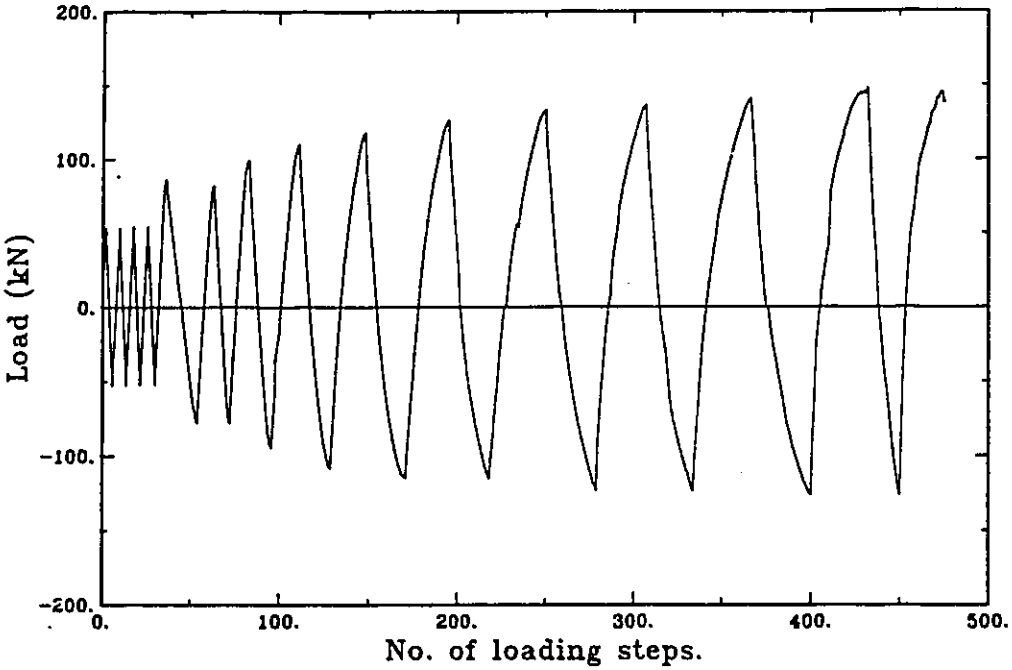

Fig. 2.7 Loading history for specimen A-1.

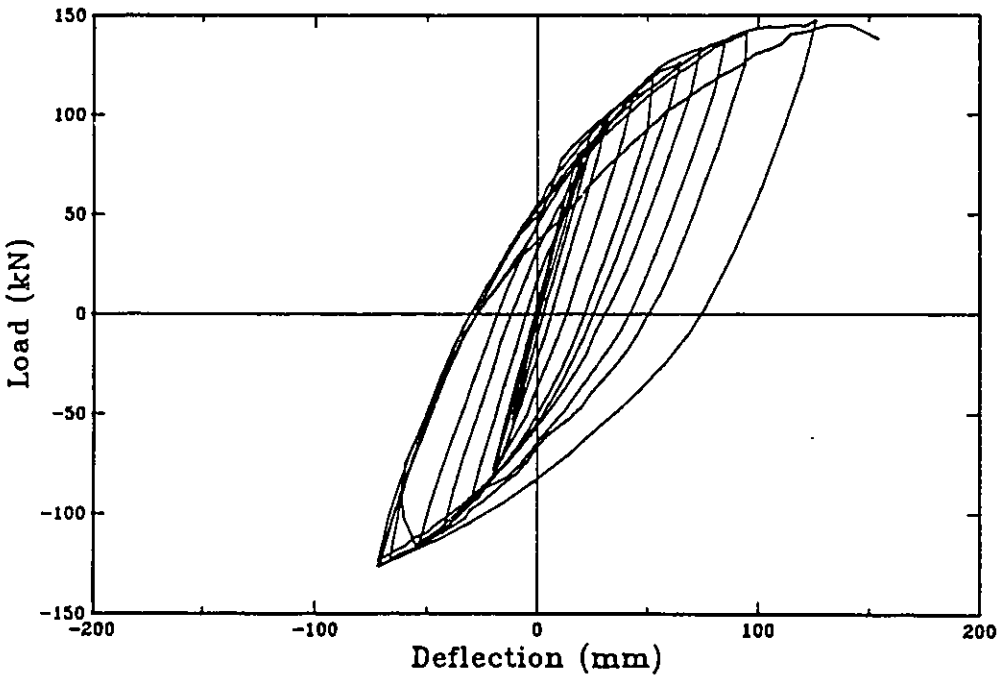

Fig. 2.8 Beam-tip load versus beam-tip deflection hysteretic curves for specimen A-1.

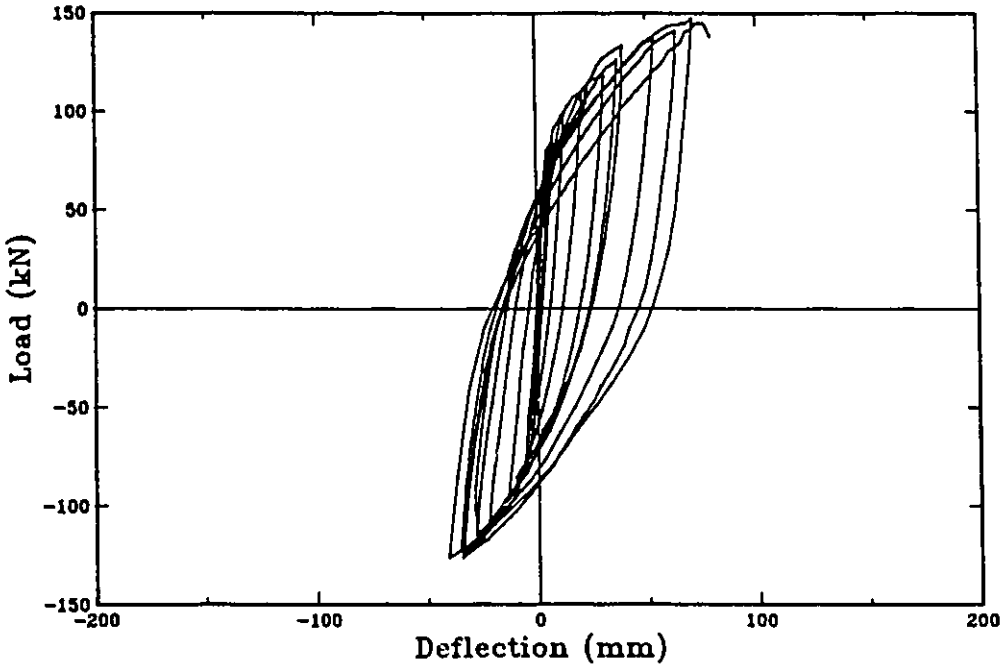

Fig. 2.9 Beam-tip load vs. beam-tip deflection due to column flange rotation for specimen A-1.

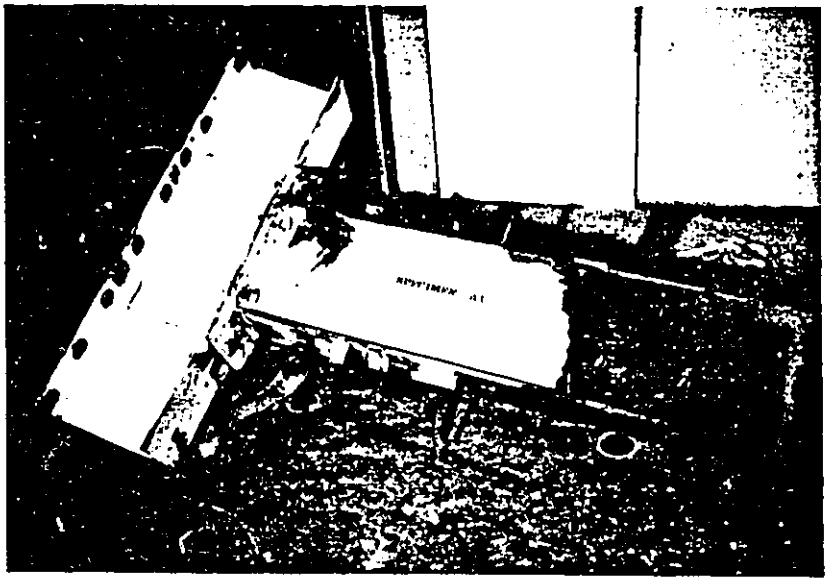

Fig. 2.10 Specimen A-1 at failure

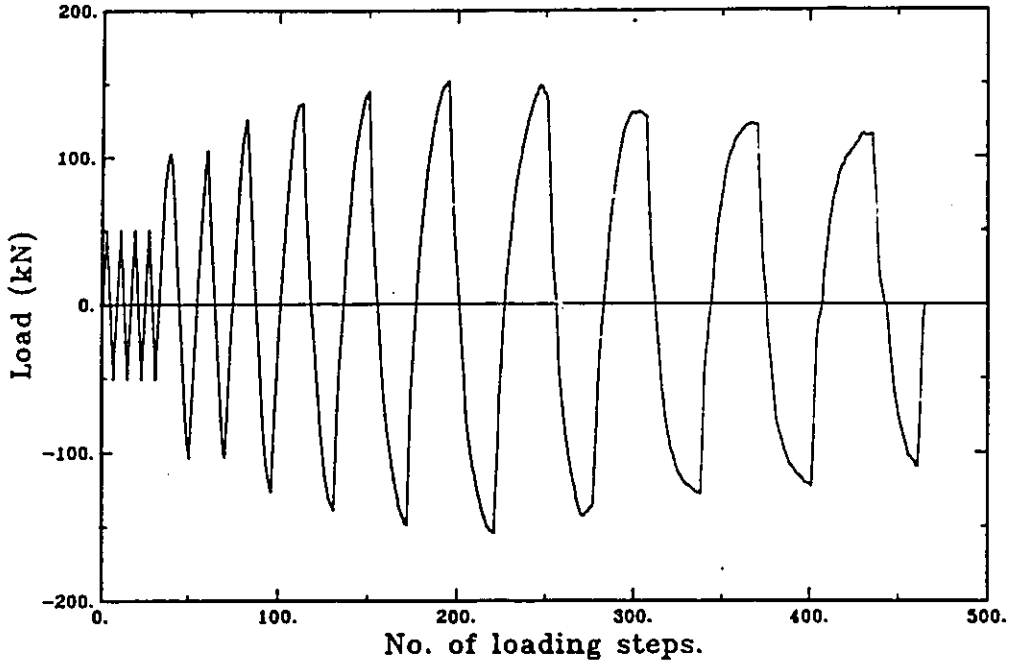

Fig. 2.11 Loading history for specimen A-2.

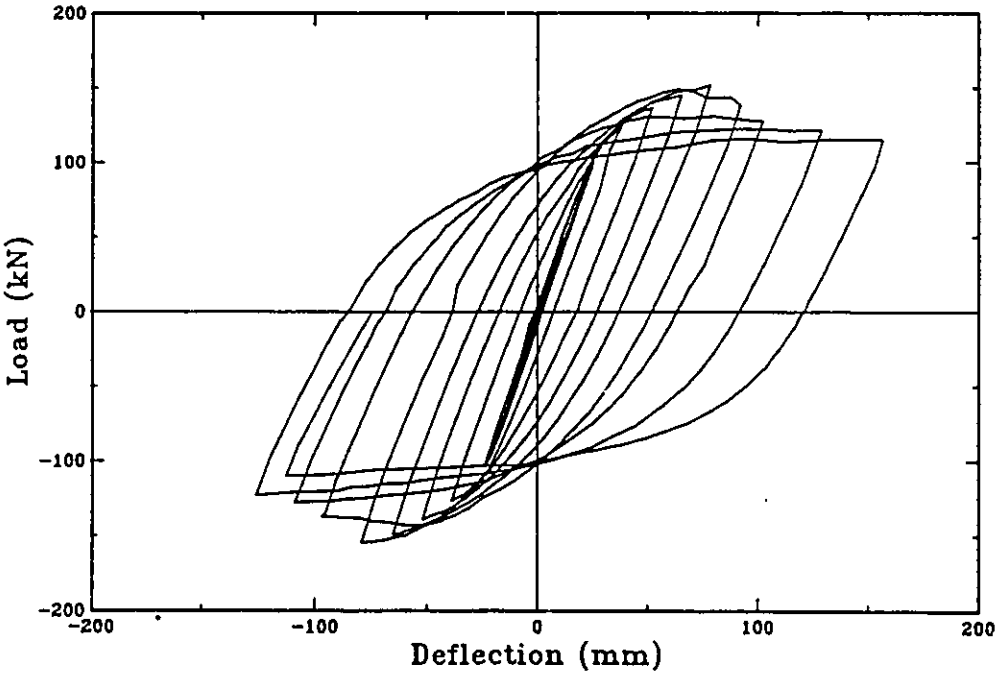

Fig. 2.12 Beam-tip load versus beam-tip deflection hysteretic curves for specimen A-2.

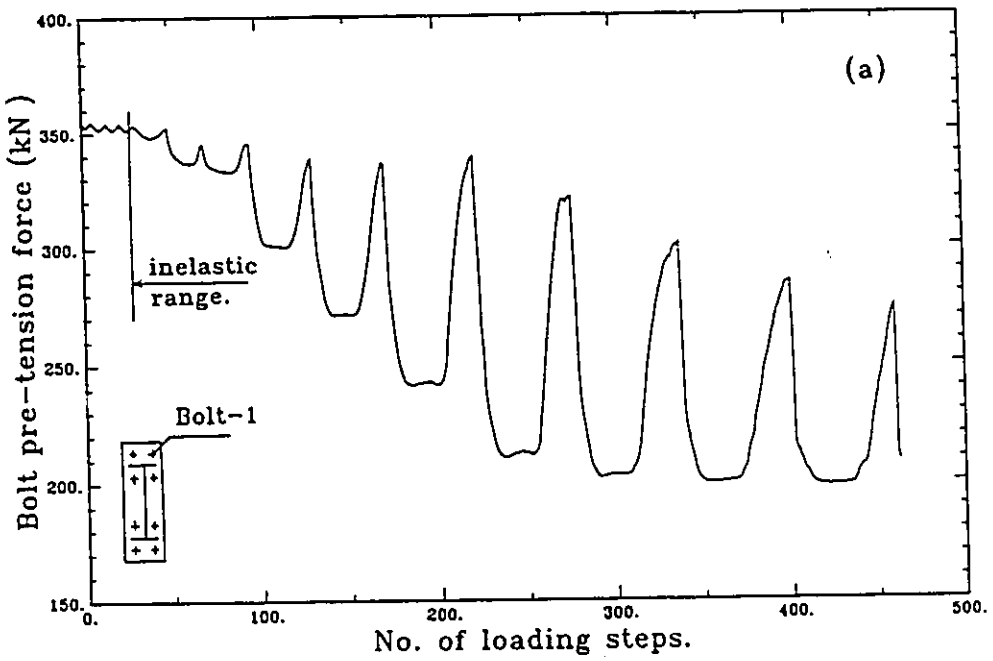
(a)
Bolt pre-tension force (kN)
400.
350.
300.
250.
200.
150.
0.
100.
200.
300.
400.
500.
inelastic
range.
Bolt-1
No. of loading steps.

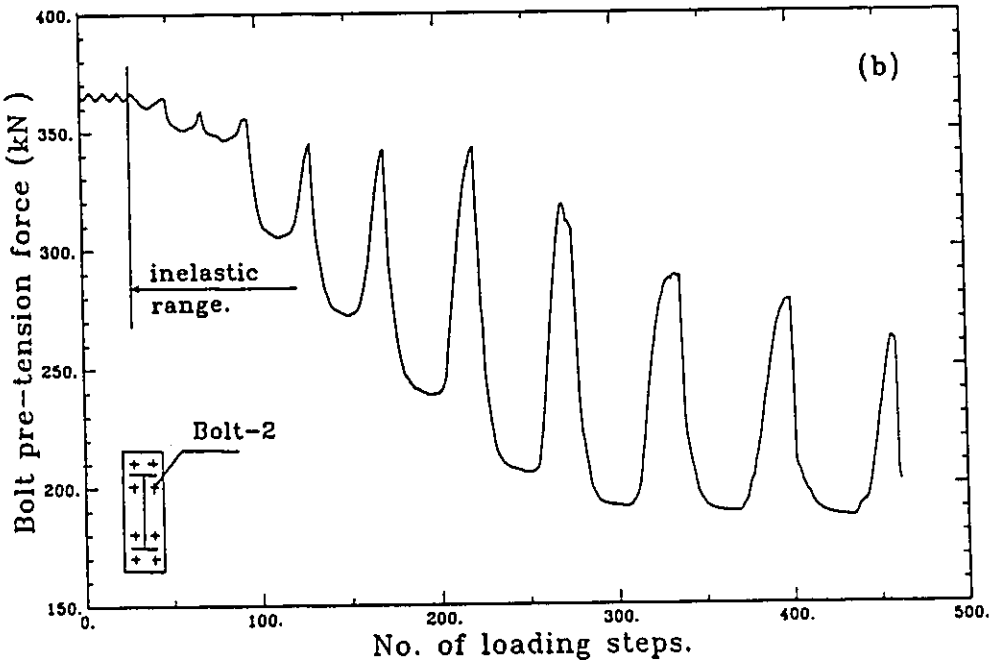
(b)
Bolt pre-tension force (kN)
400.
350.
300.
250.
200.
150.
0.
100.
200.
300.
400.
500.
inelastic
range.
Bolt-2
No. of loading steps.

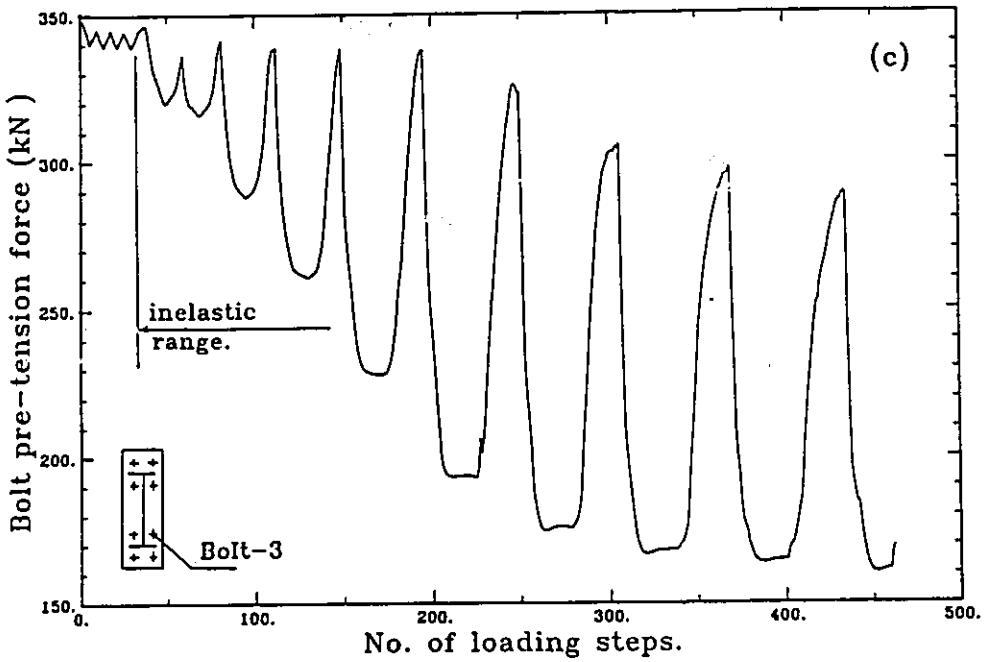

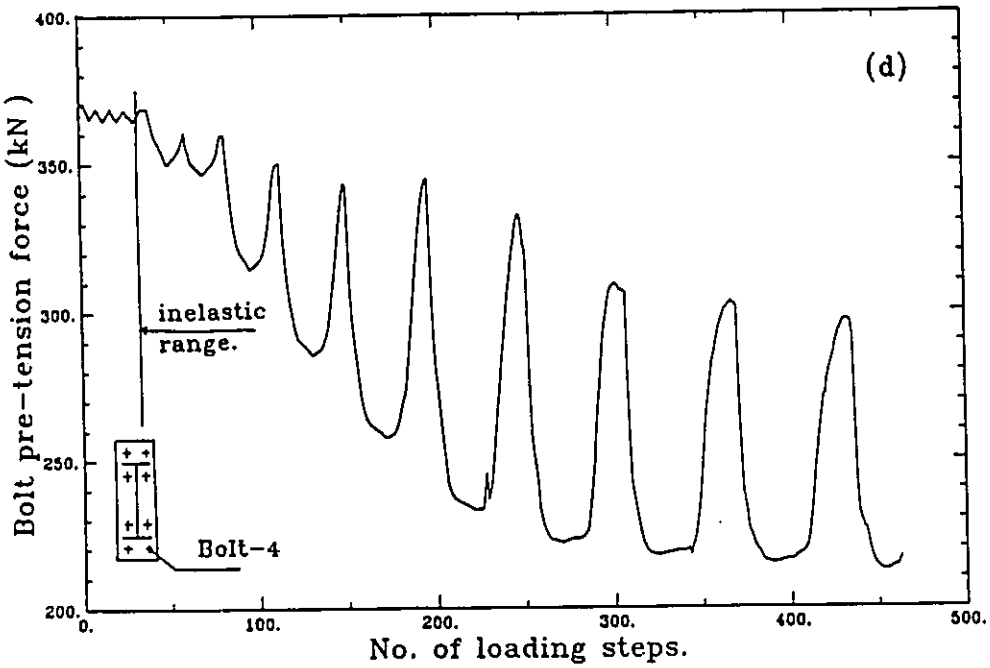

Fig. 2.13 Variation of bolts pre-tension forces with loading steps (specimen A-2).
(a) bolt No.1;(b) bolt No.2;(c) bolt No.3;(d) bolt No.4.

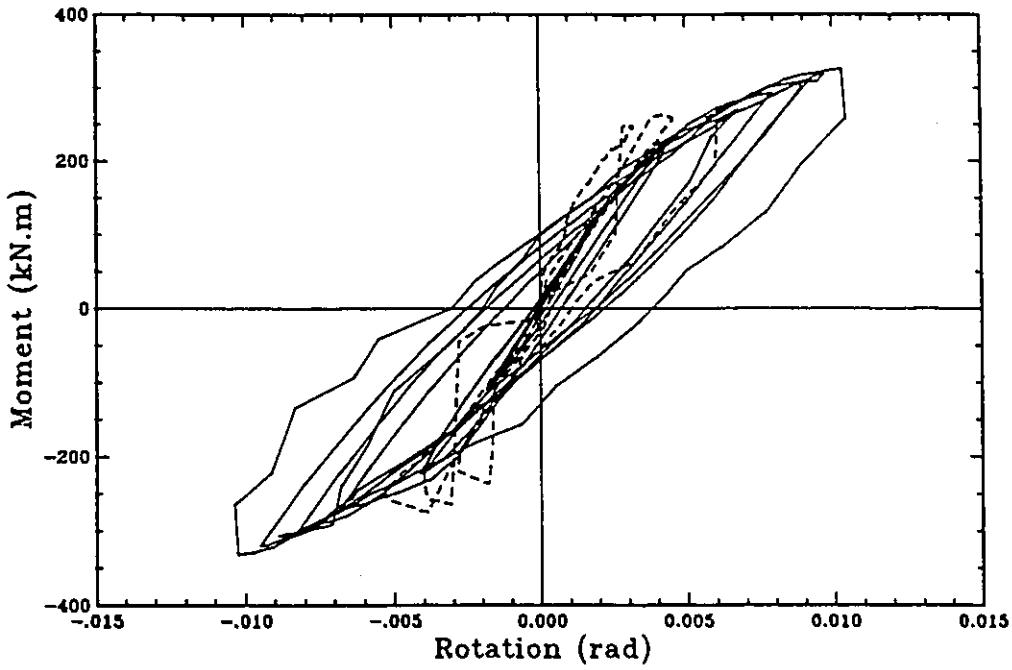

Fig. 2.14 Beam moment versus connection rotation hysteretic curves for specimen A-2.

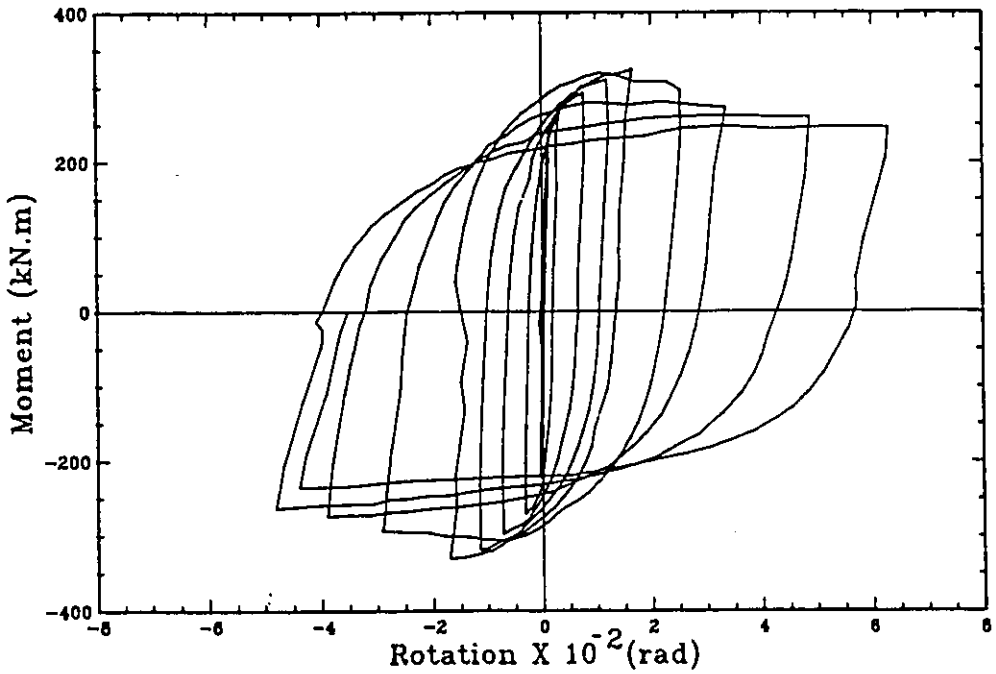

Fig. 2.15 Beam moment versus beam inelastic rotation hysteretic curves for specimen A-2.

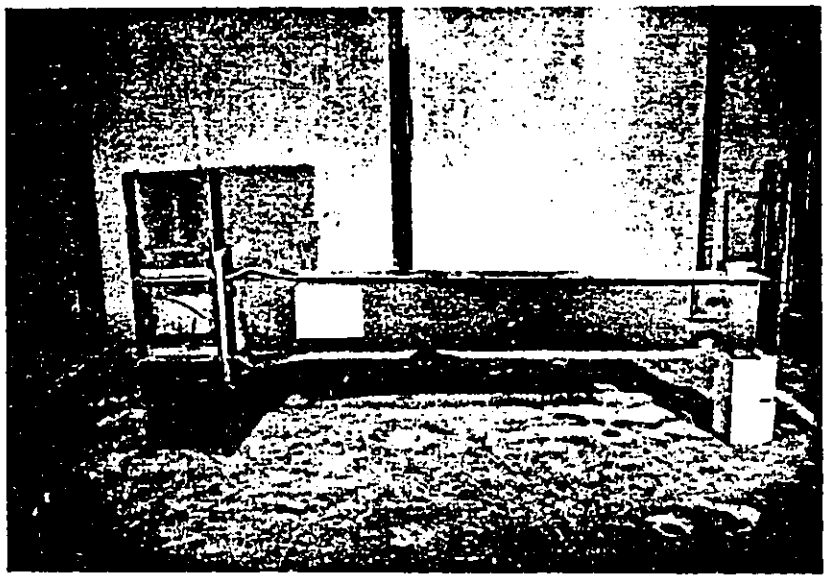

Fig. 2.16 Specimen A-2 after failure.

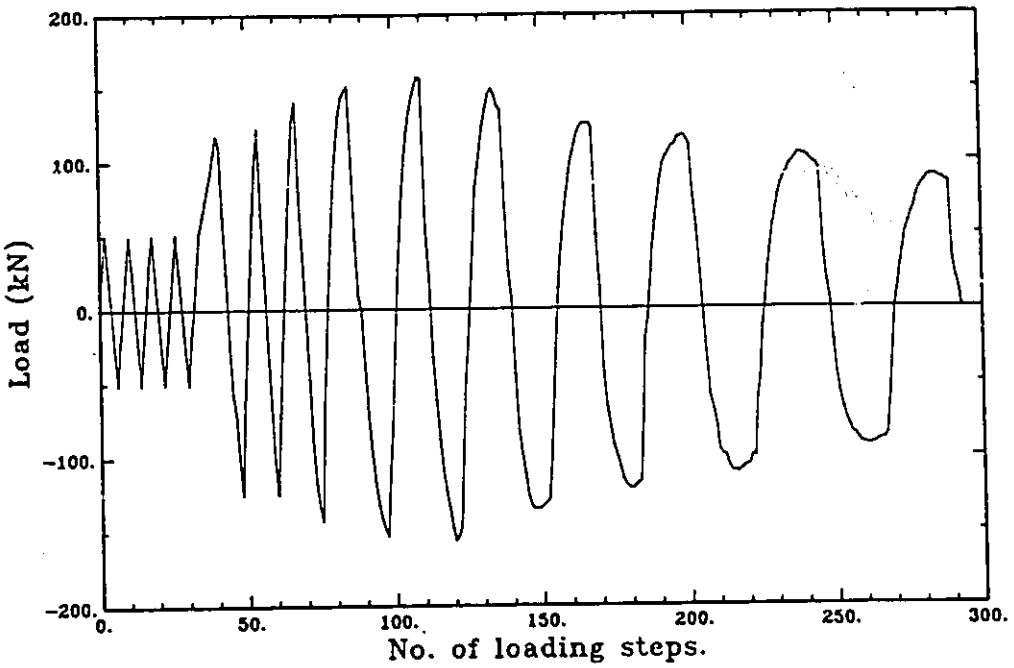

Fig. 2.17 Loading history for specimen A-3.

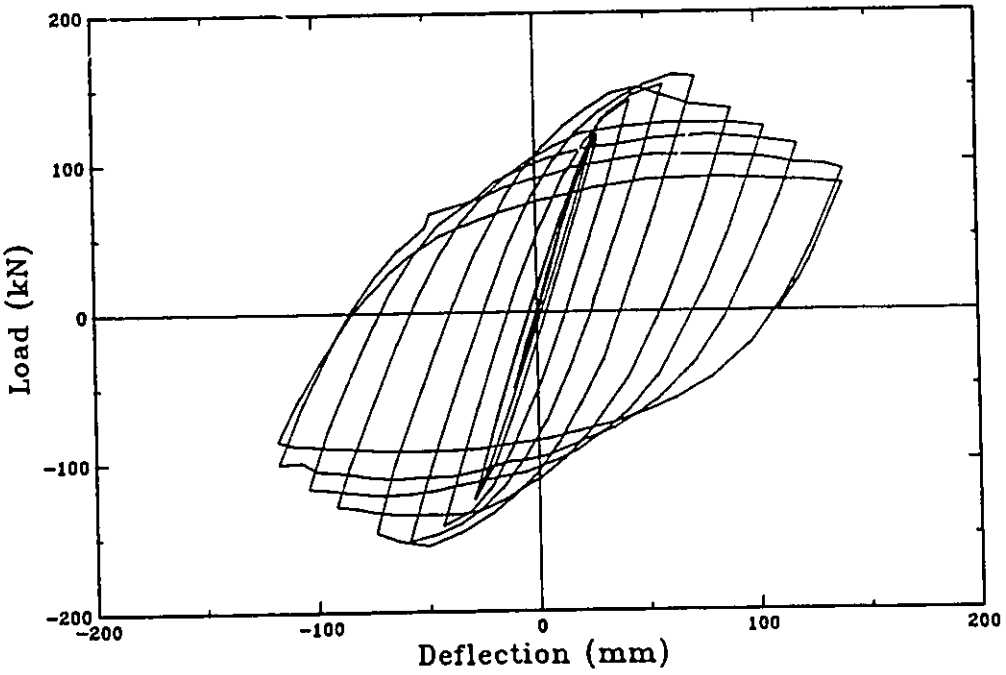

Fig. 2.18 Beam-tip load versus beam-tip deflection hysteretic curves for specimen A-3.

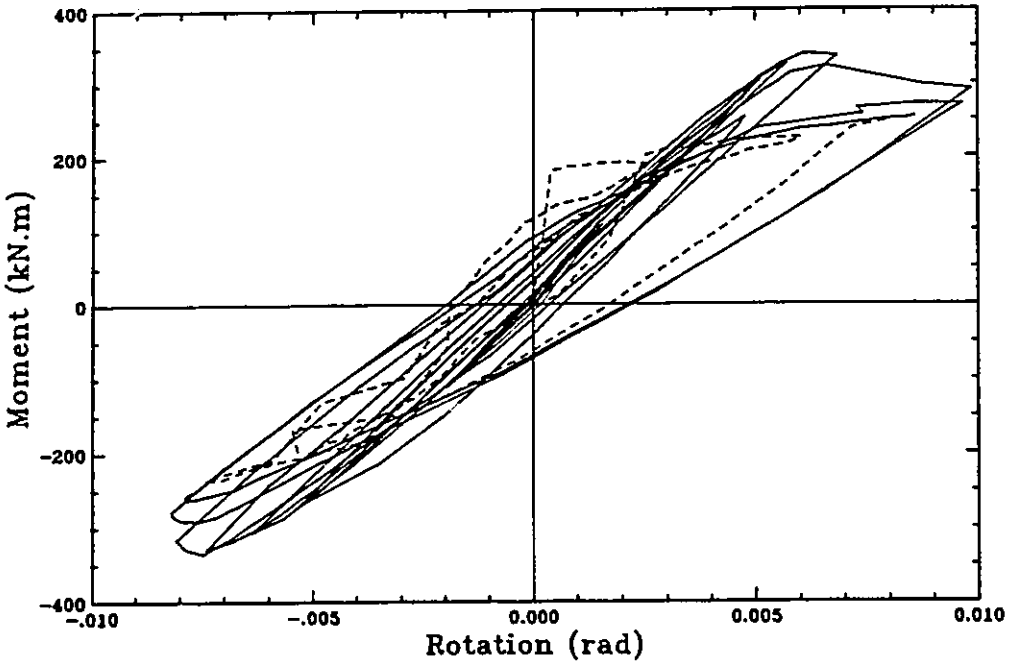

Fig. 2.19 Beam moment versus connection rotation hysteretic curves for specimen A-3.

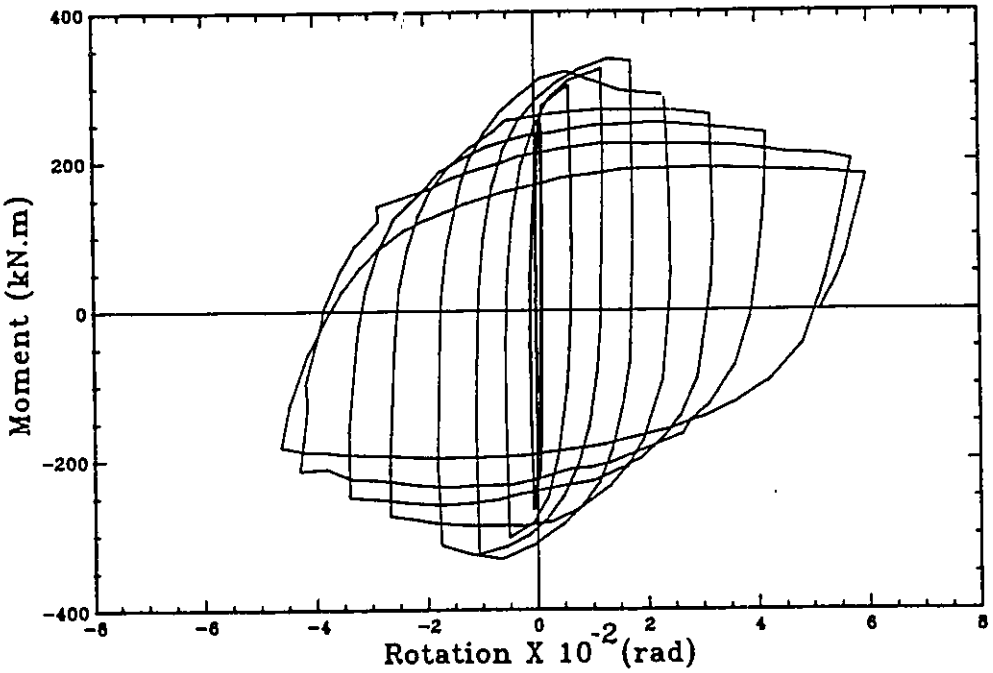

Fig. 2.20 Beam moment versus beam inelastic rotation hysteretic curves for specimen A-3.

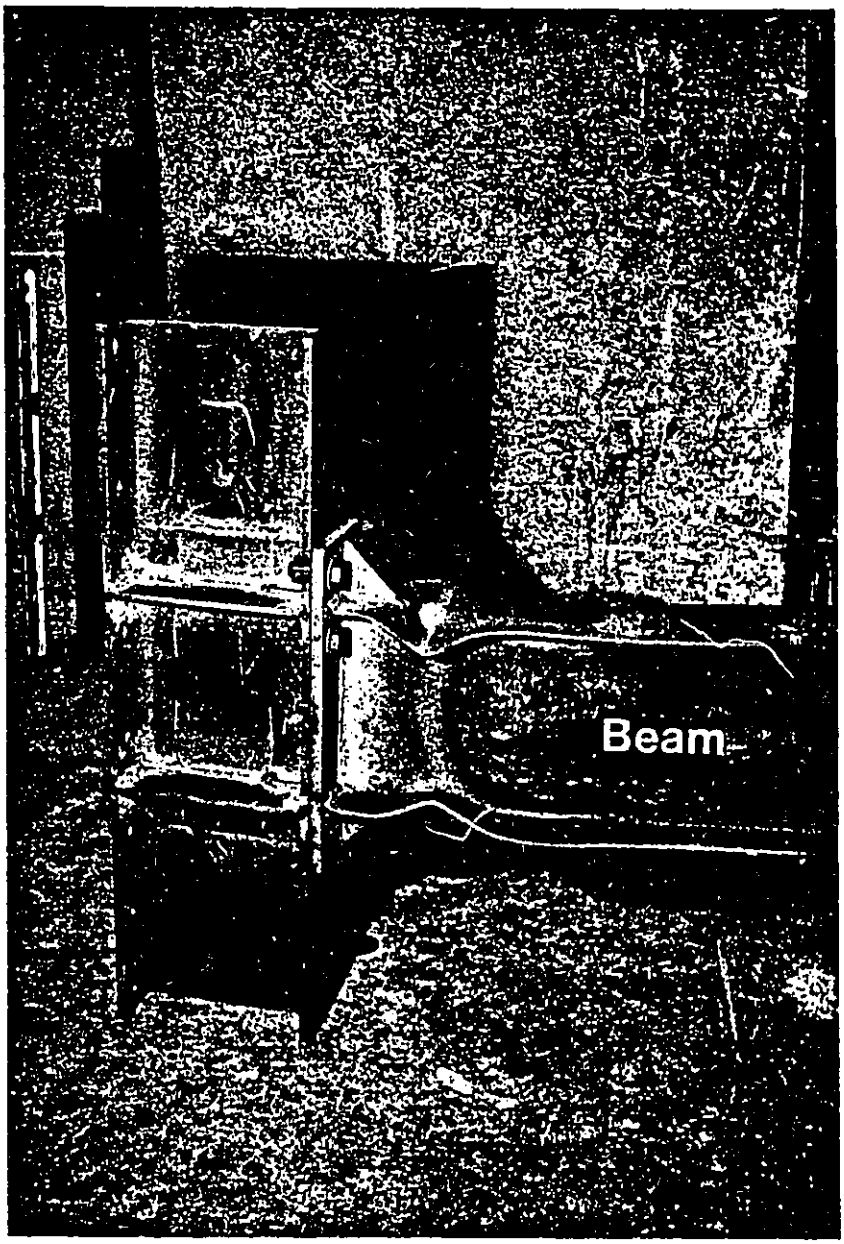

Fig. 2.21 Specimen A-3 after failure.

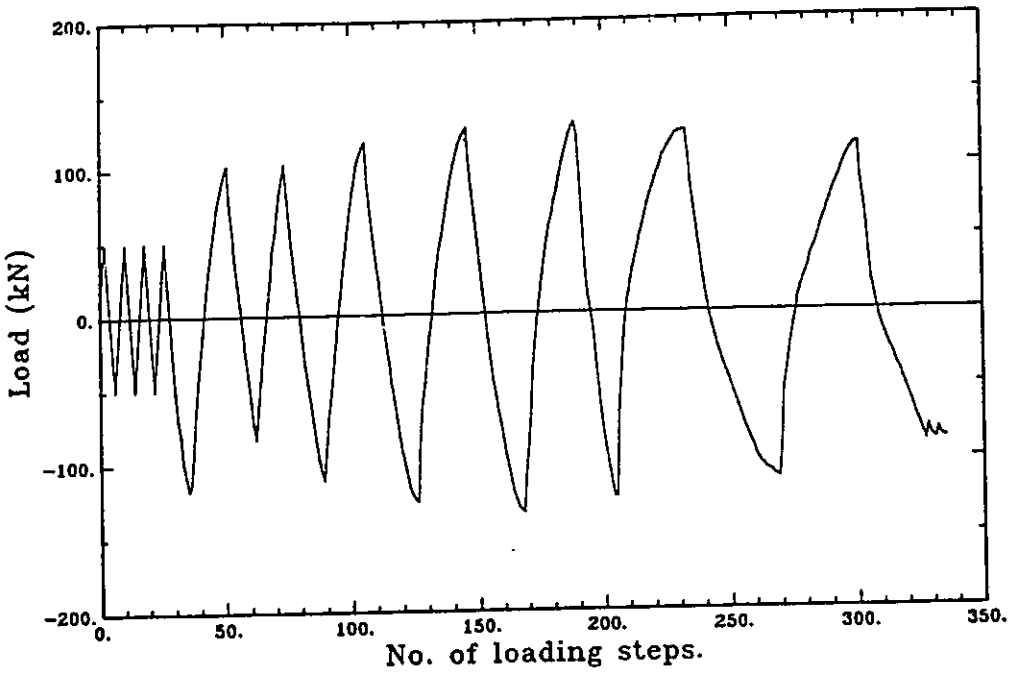

Fig. 2.22 Loading history for specimen A-4.

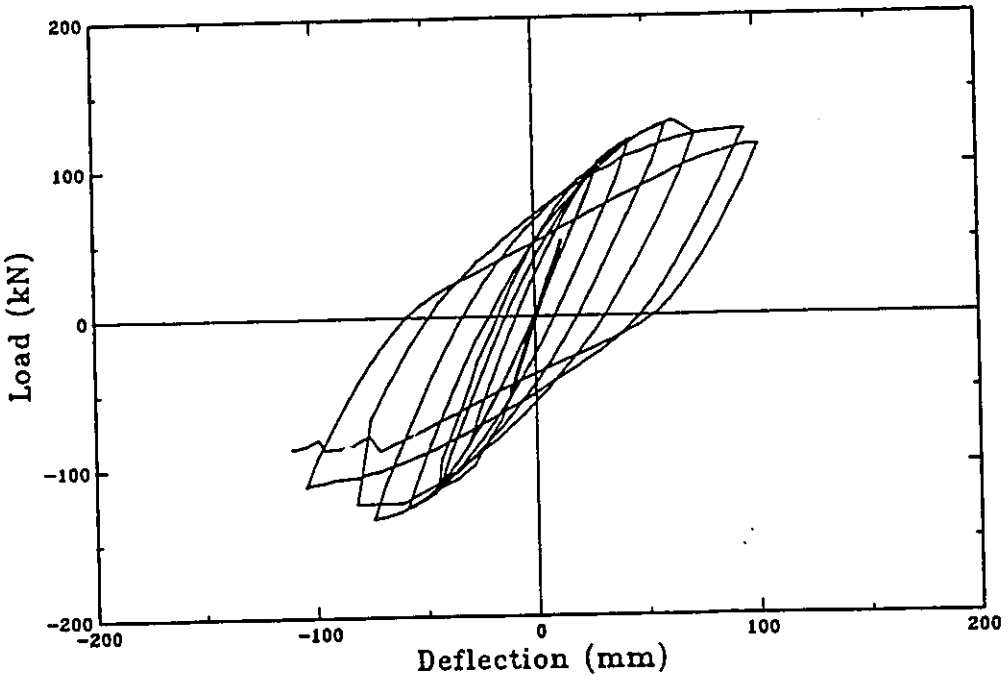

Fig. 2.23 Beam-tip load versus beam-tip deflection hysteretic curves for specimen A-4.

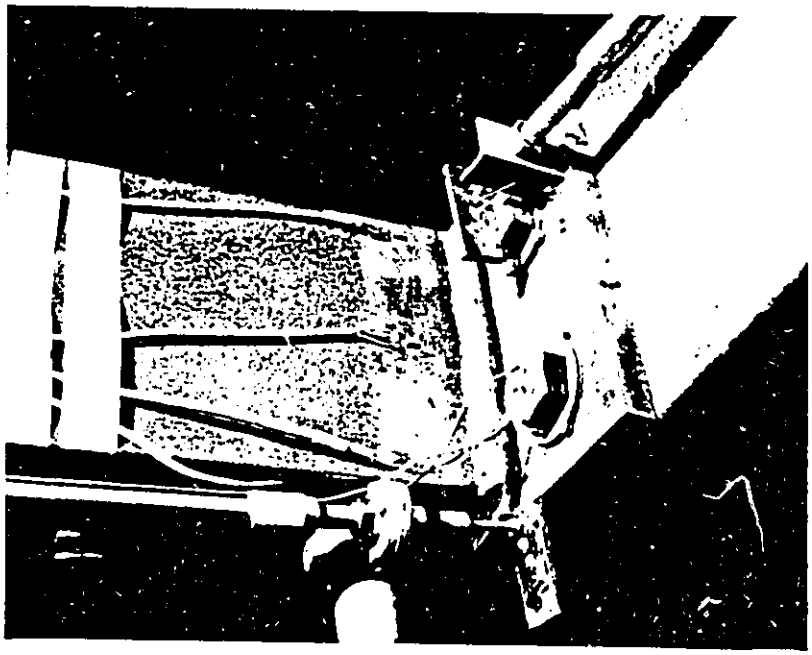

Fig. 2.24 Crack initiation in specimen A-4.

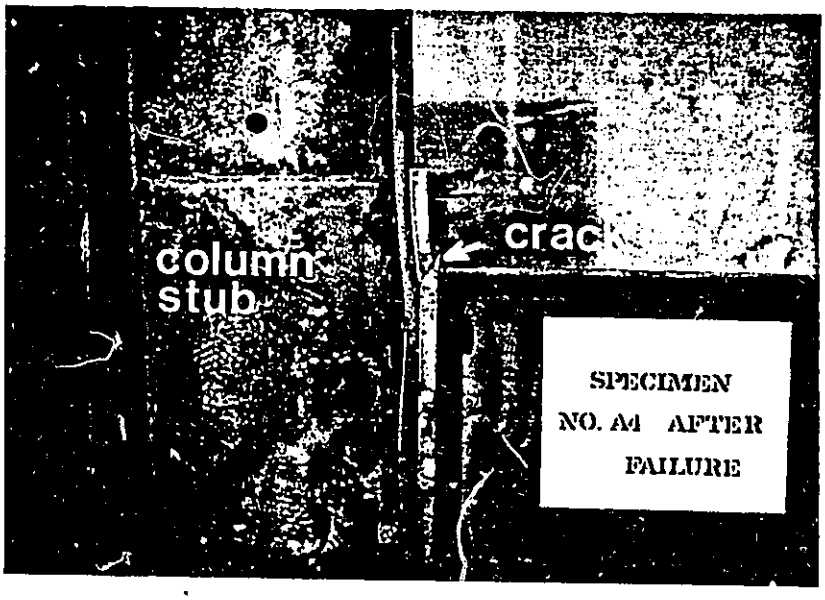

Fig. 2.25 Specimen A-4 at failure.

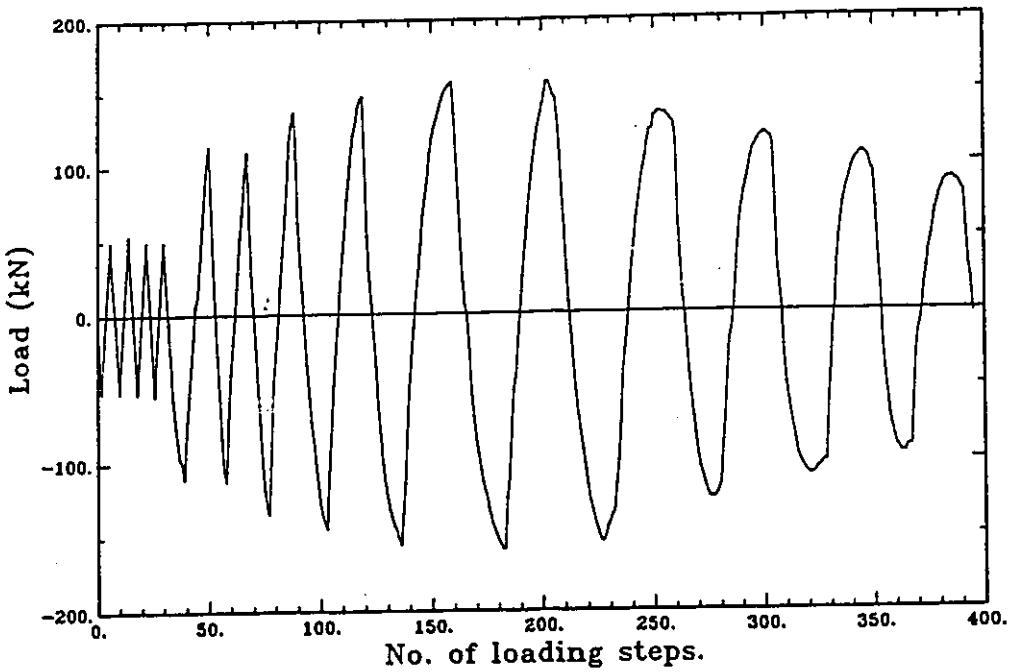

Fig. 2.26 Loading history for specimen A-5.

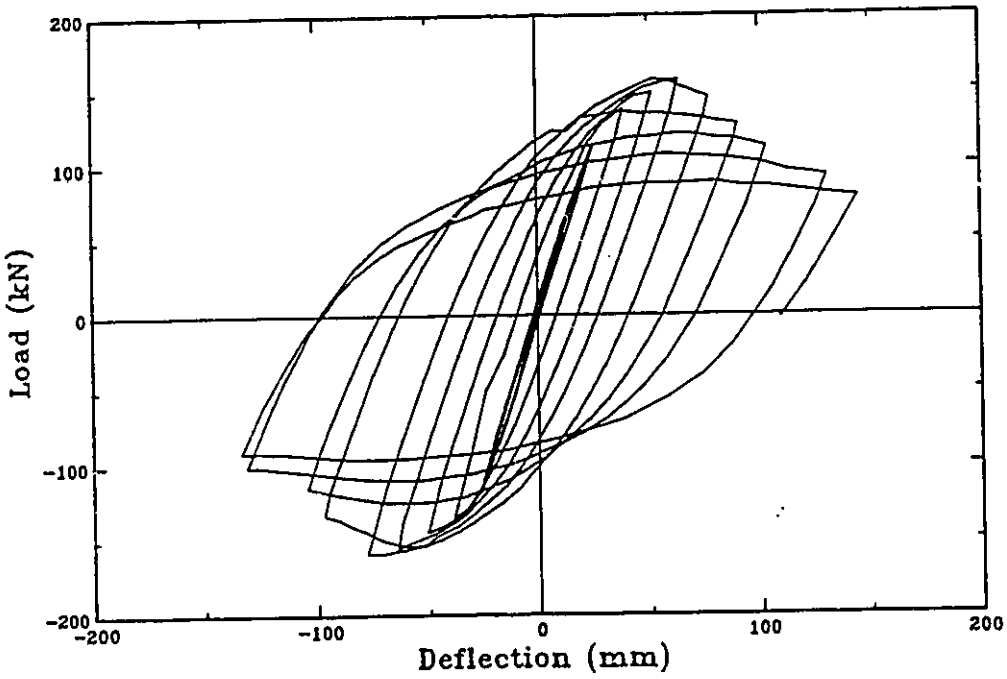

Fig. 2.27 Beam-tip load versus beam-tip deflection hysteretic curves for specimen A-5.

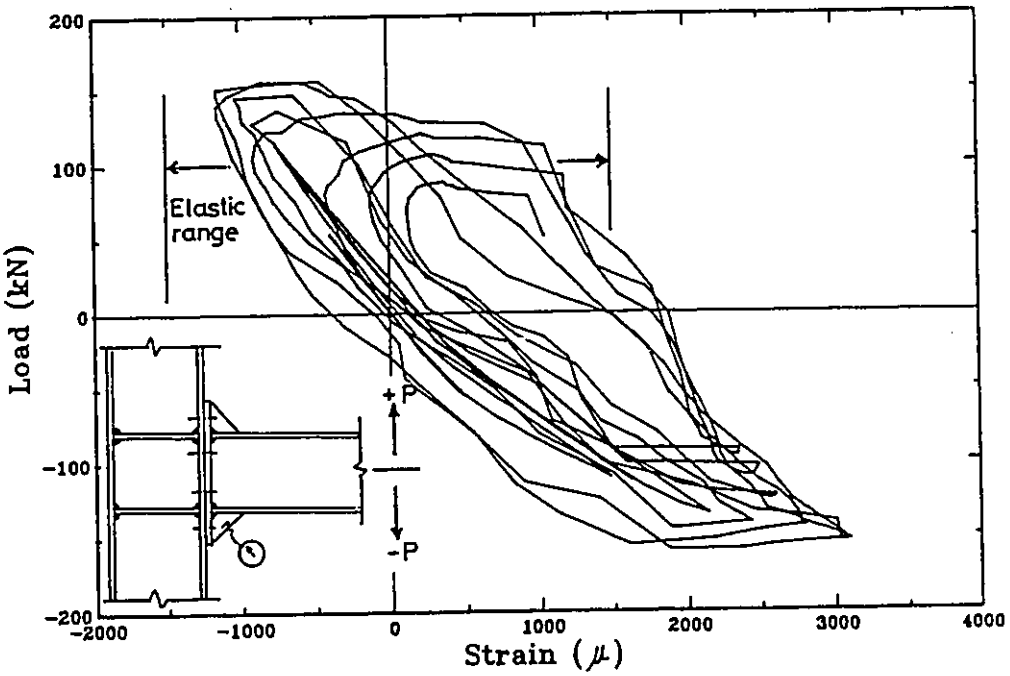

Fig. 2.28 Strain history versus beam load for the end-plate stiffeners (specimen A-5).

Fig. 2.29 Specimen A-5 after failure.

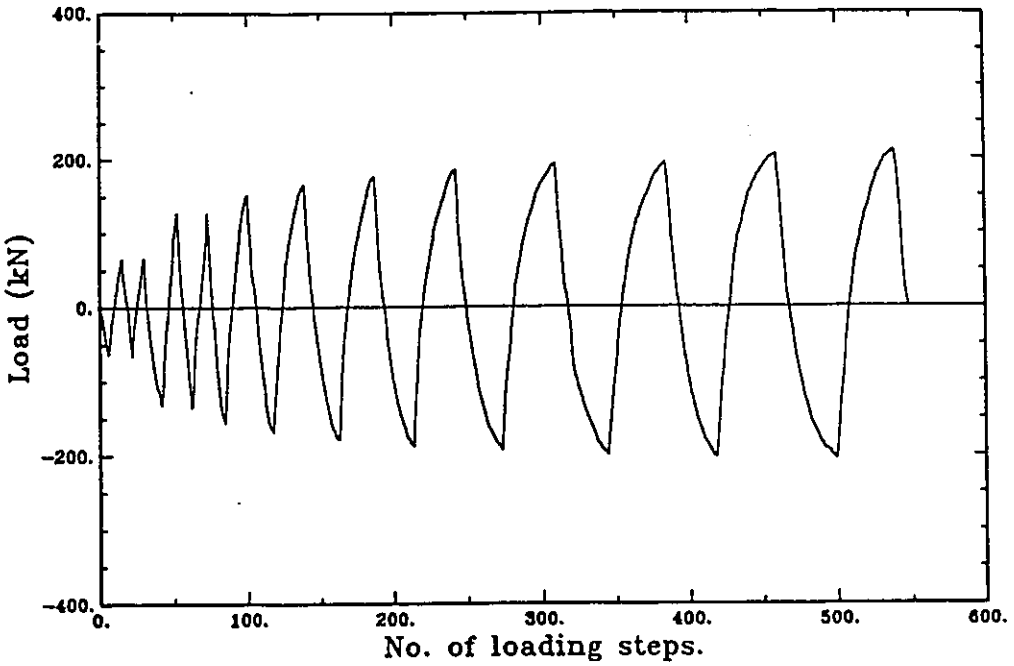

Fig. 2.30 Loading history for specimen B-1.

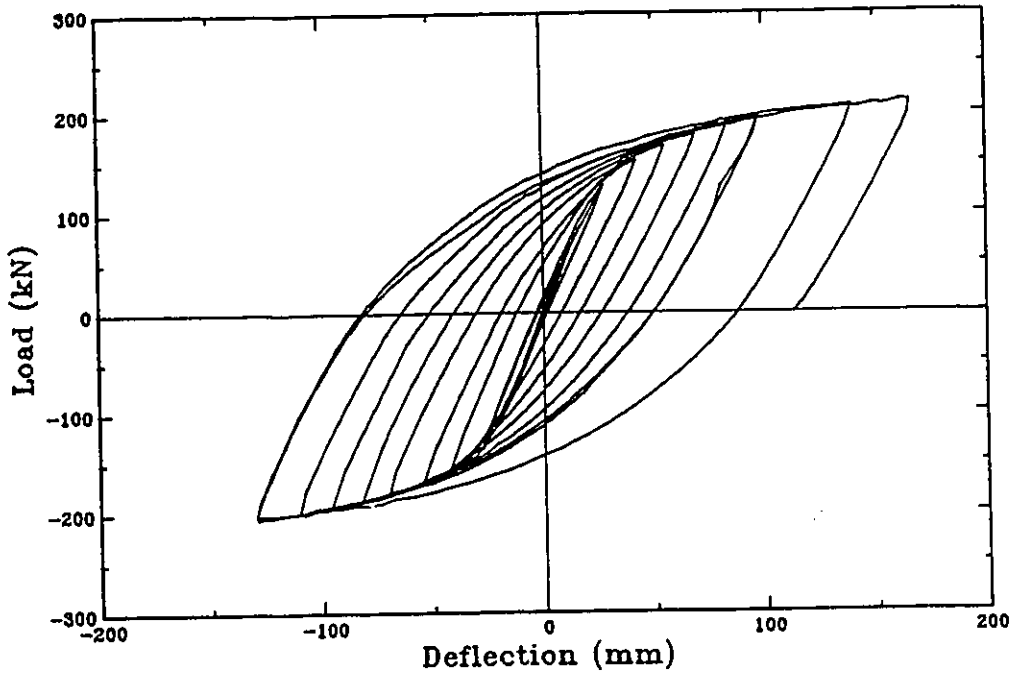

Fig. 2.31 Beam-tip load versus beam-tip deflection hysteretic curves for specimen B-1.

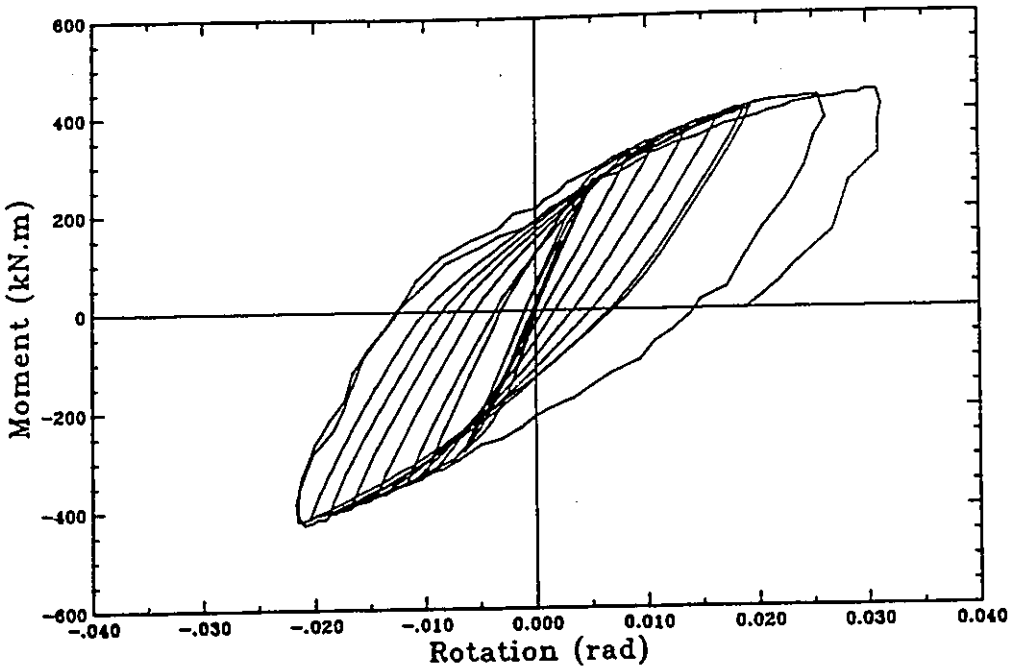

Fig. 2.32 Beam moment versus connection rotation hysteretic curves for specimen B-1.

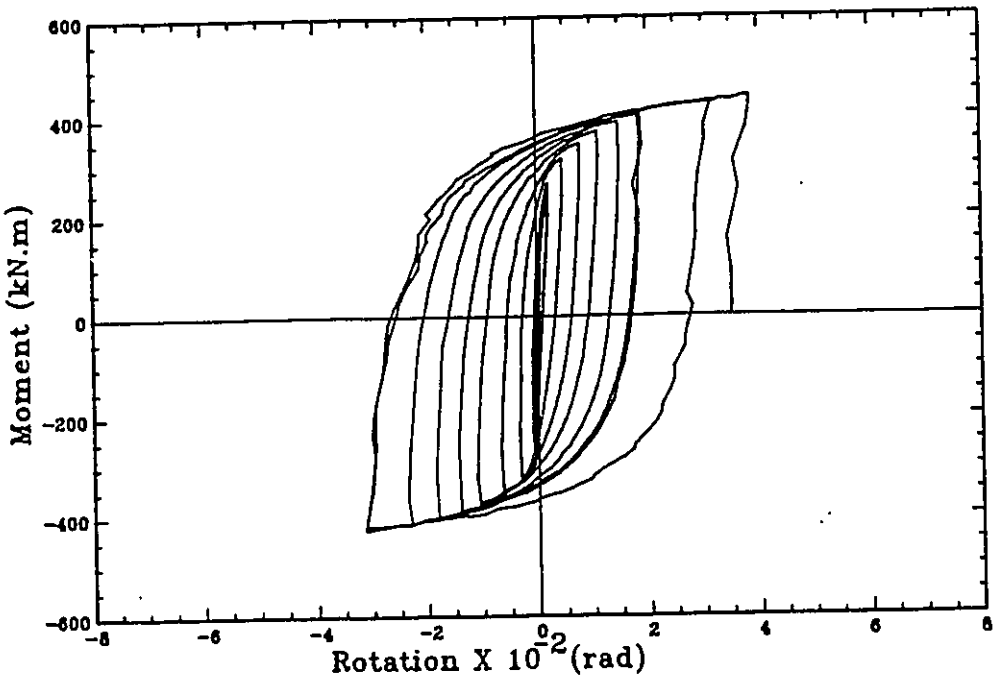

Fig. 2.33 Beam moment versus beam inelastic rotation hysteretic curves for specimen B-1.

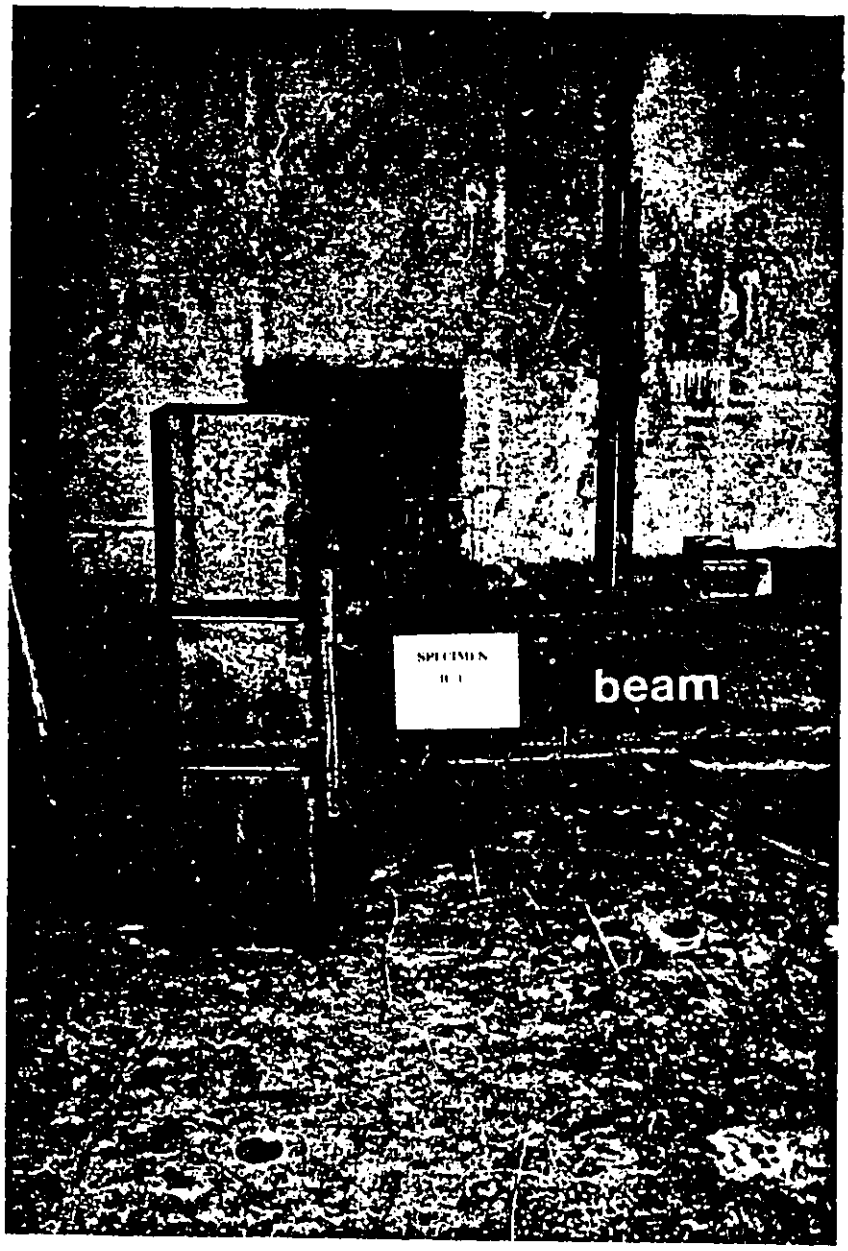

Fig. 2.34 Specimen B-1 after failure.

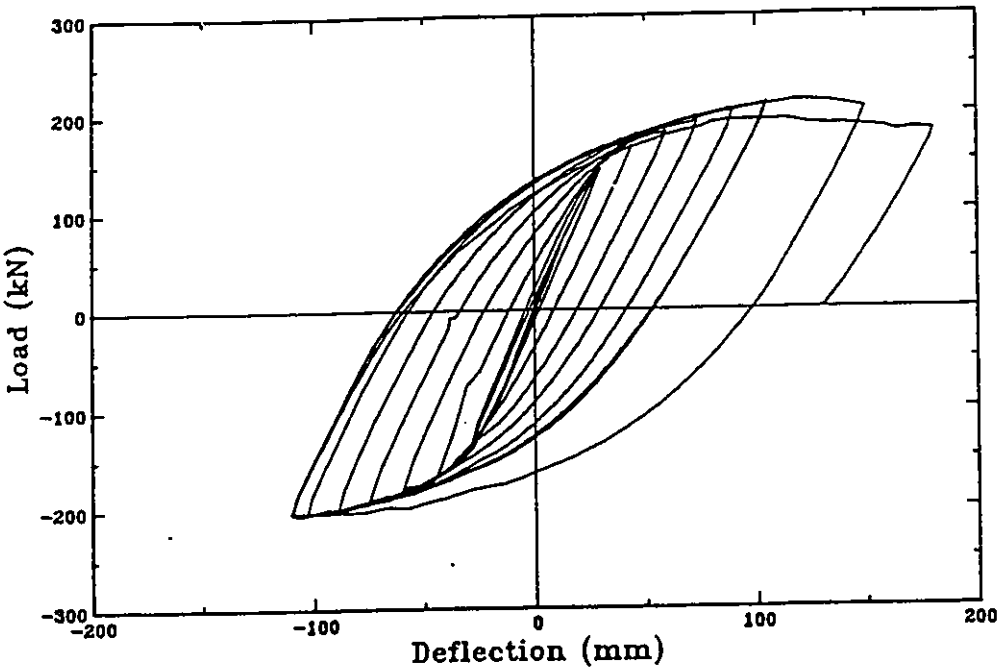

Fig. 2.35 Beam-tip load versus beam-tip deflection hysteretic curves for specimen B-2.

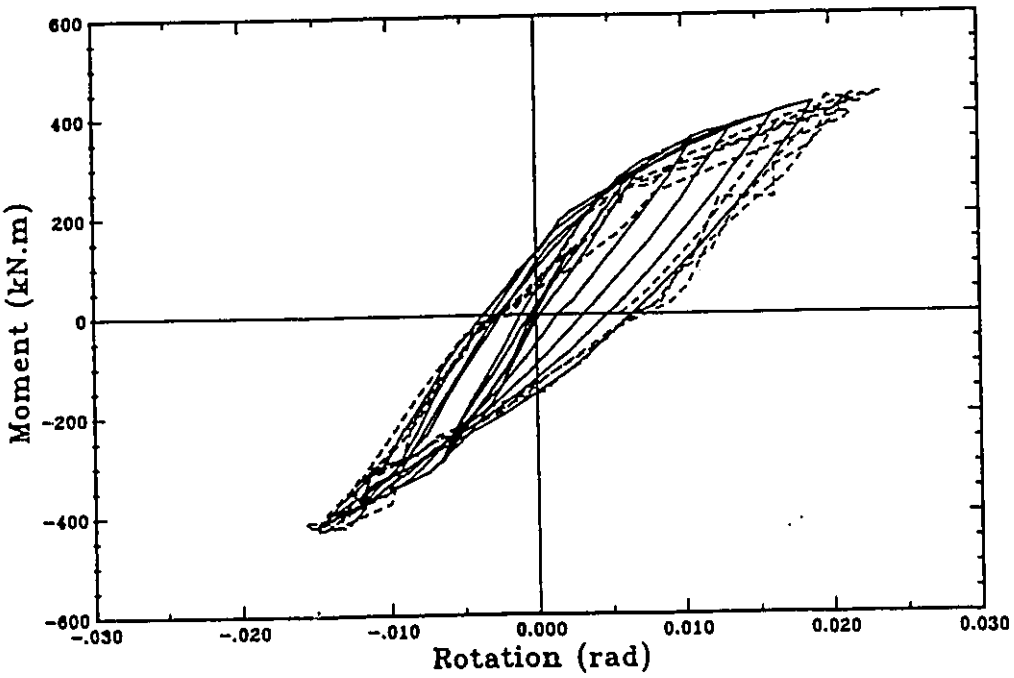

Fig. 2.36 Beam moment versus connection rotation hysteretic curves for specimen B-2.

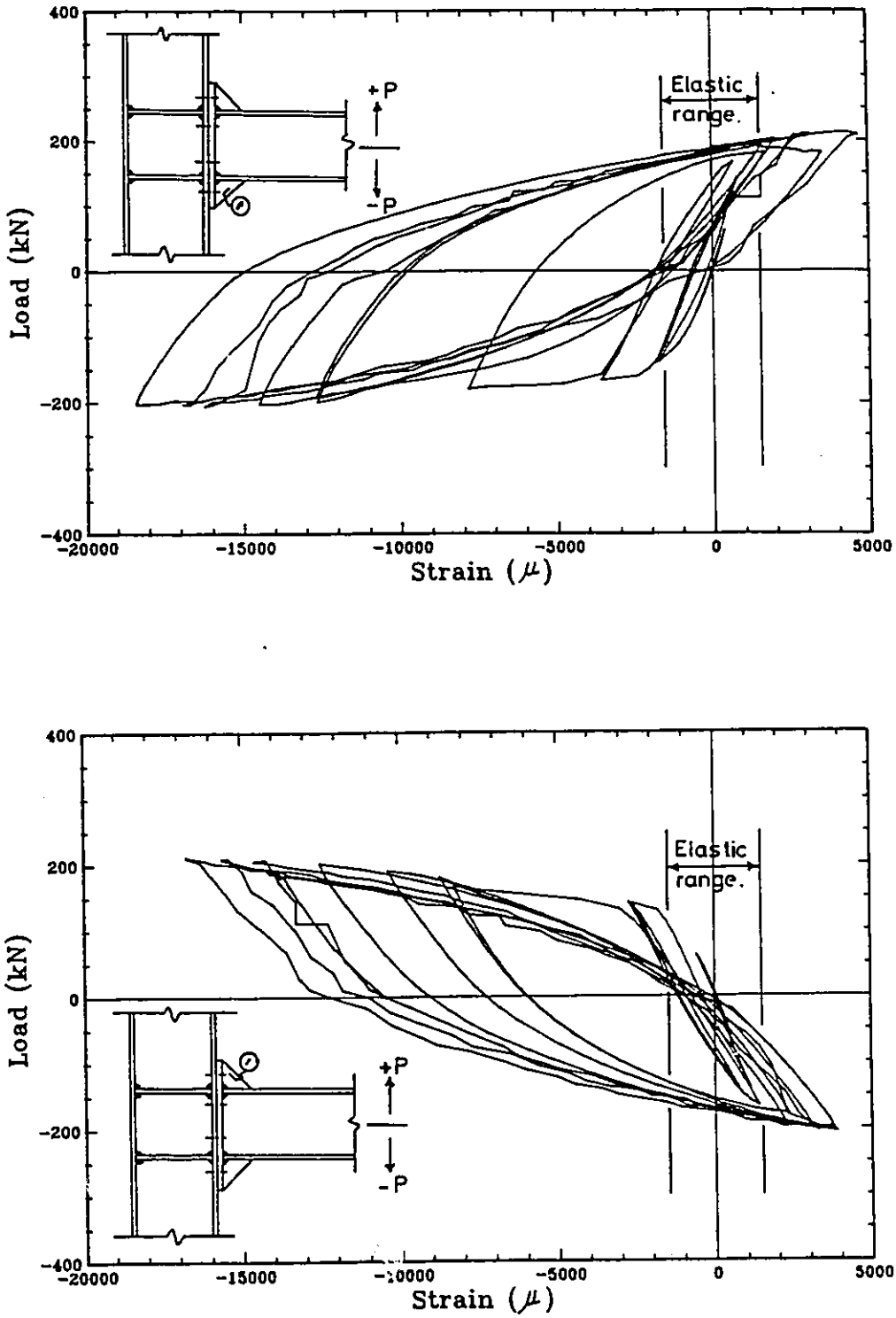

Fig. 2.37 Strain history versus beam load for the end-plate stiffeners (specimen B-2).

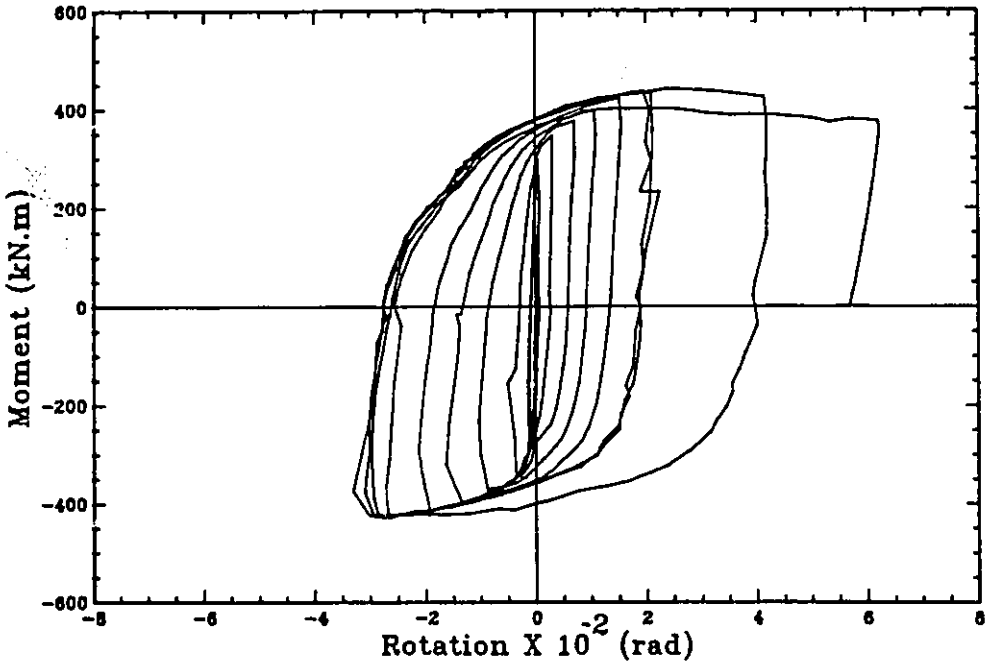

Fig. 2.38 Beam moment versus beam inelastic rotation hysteretic curves for specimen B-2.

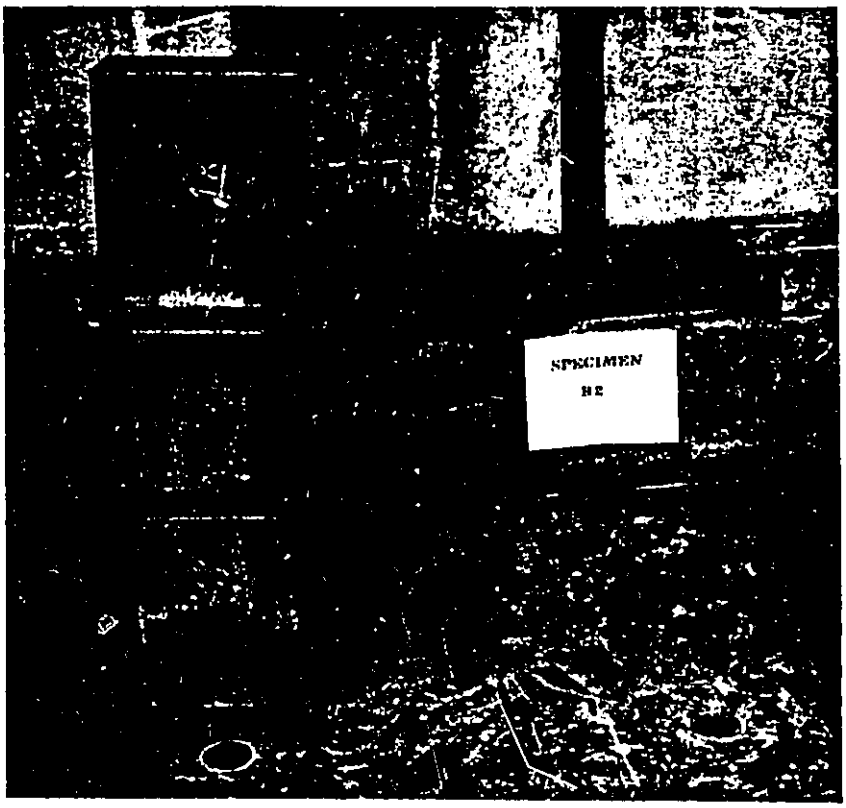

Fig. 2.39 Specimen B-2 after failure.

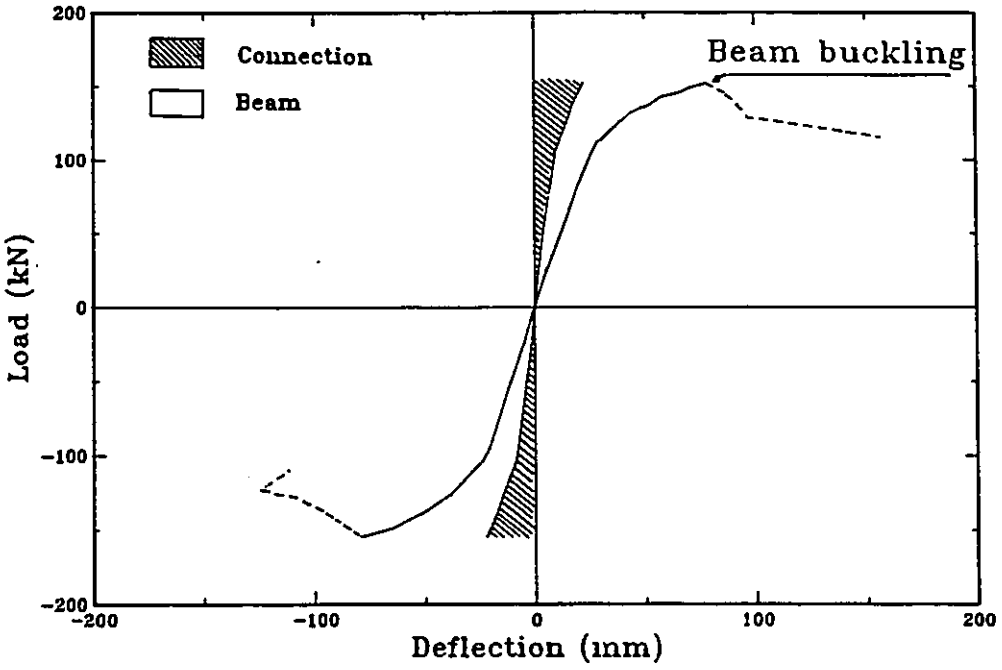

Fig. 2.40 Participation of each component in specimen A-2 to total deflection.

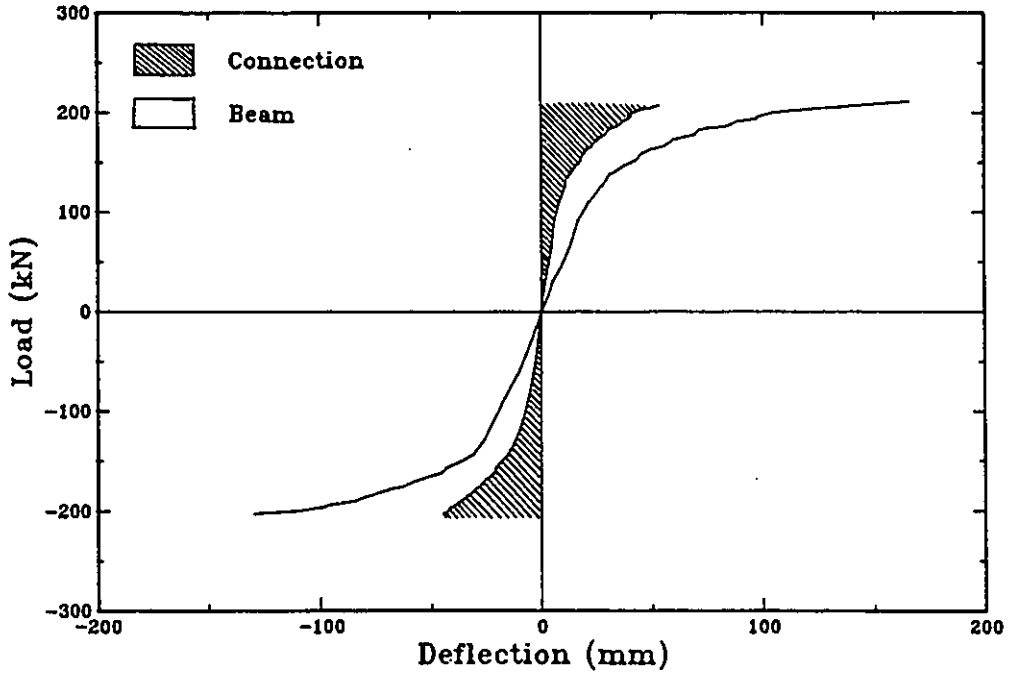

Fig. 2.41 Participation of each component in specimen B-1 to total deflection.

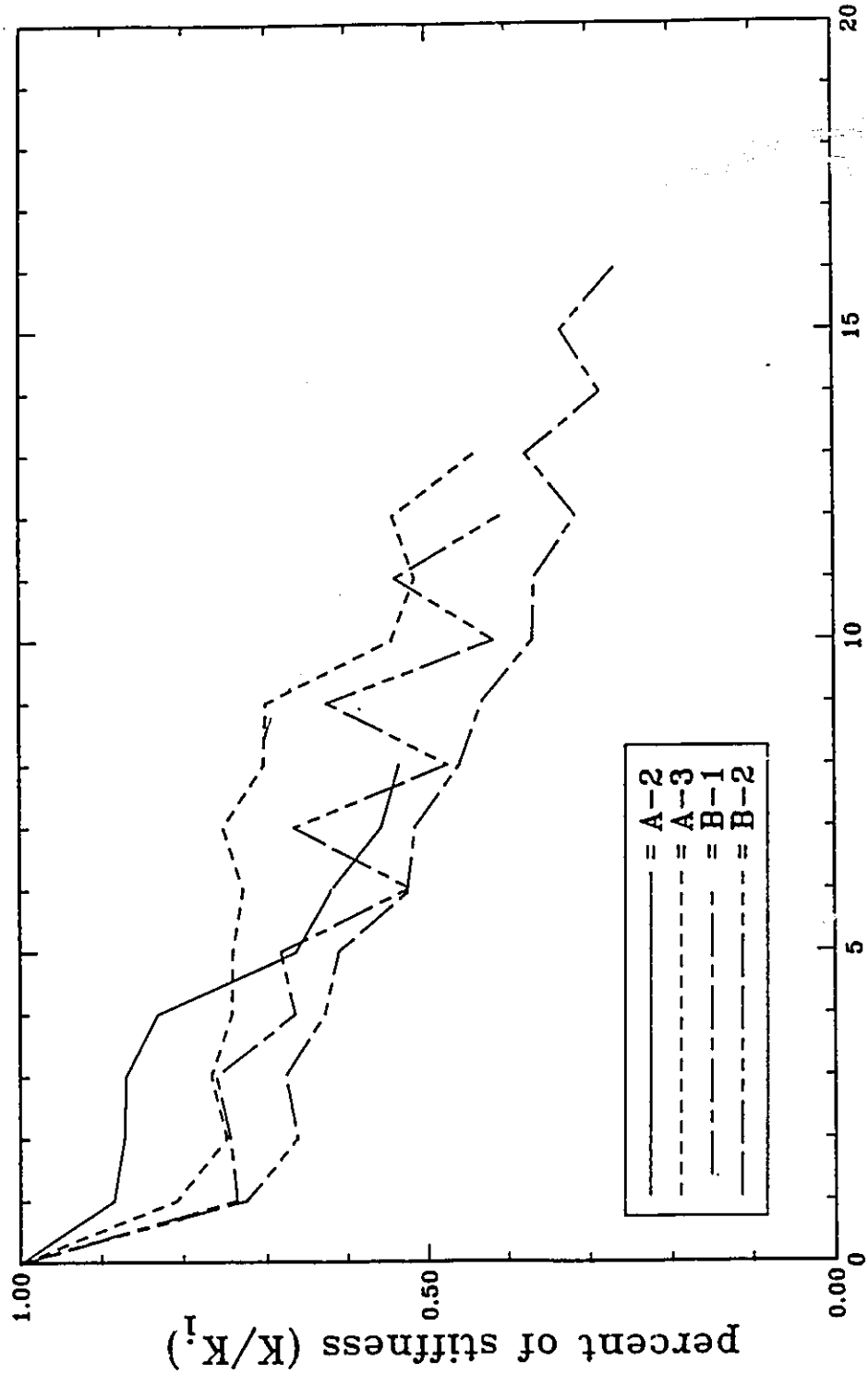

Fig. 2.42 Variation of connection stiffness as a percent of the initial stiffness

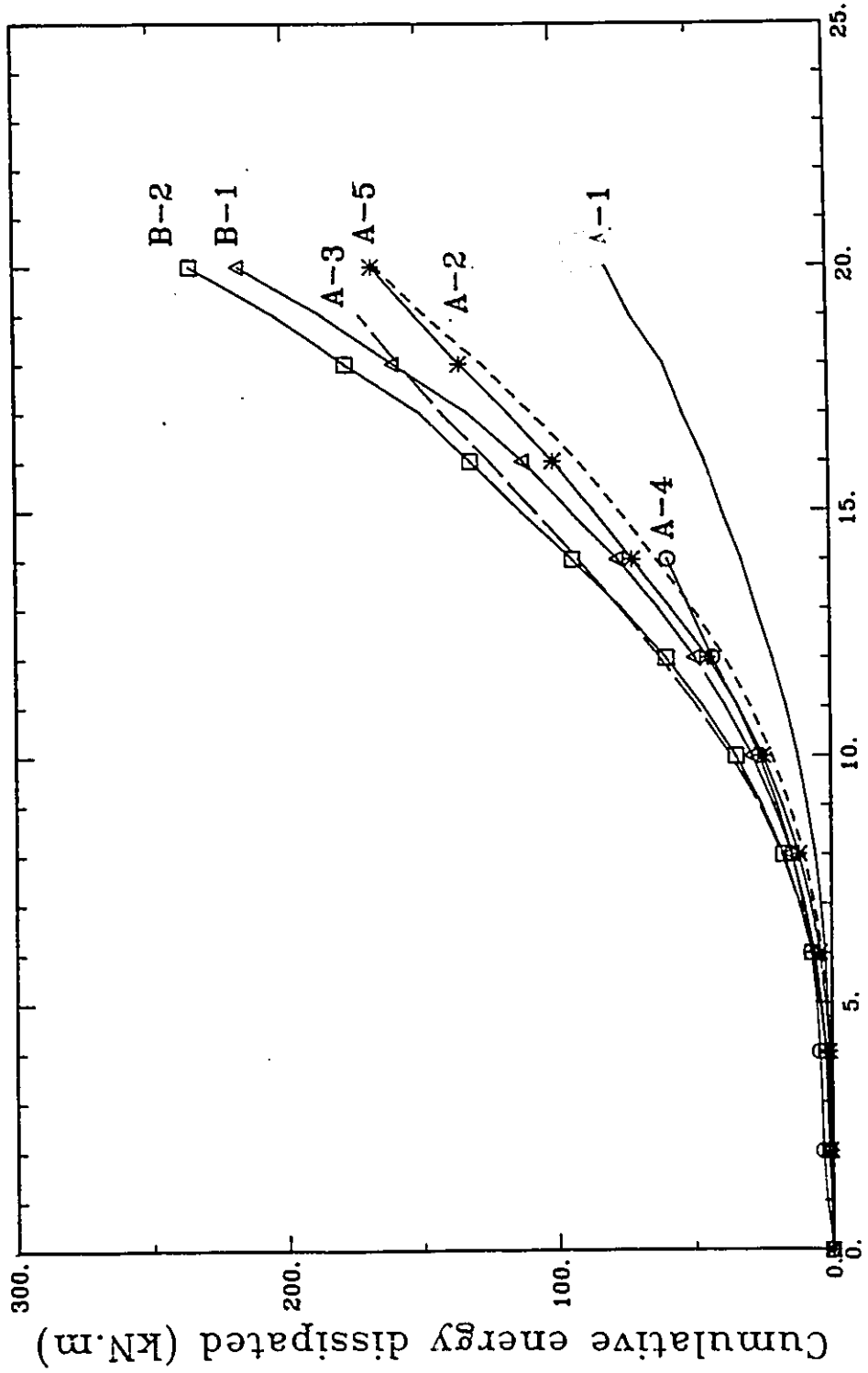

Fig. 2.43 Cumulative energy dissipated by each specimen versus number of inelastic excursions.

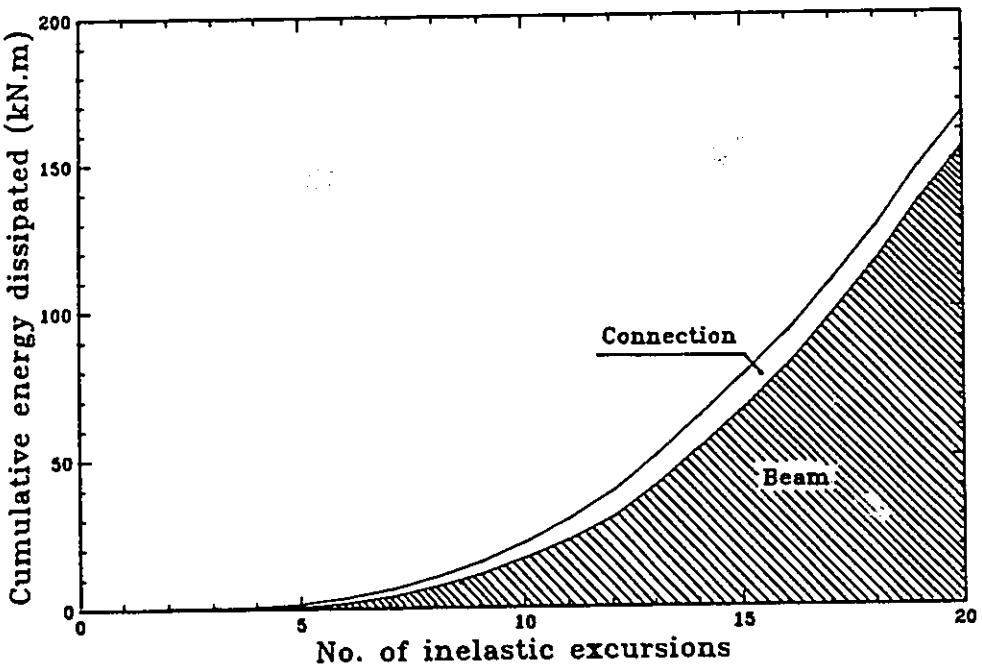

Fig. 2.44 Cumulative energy dissipated by each component in specmen A-2.

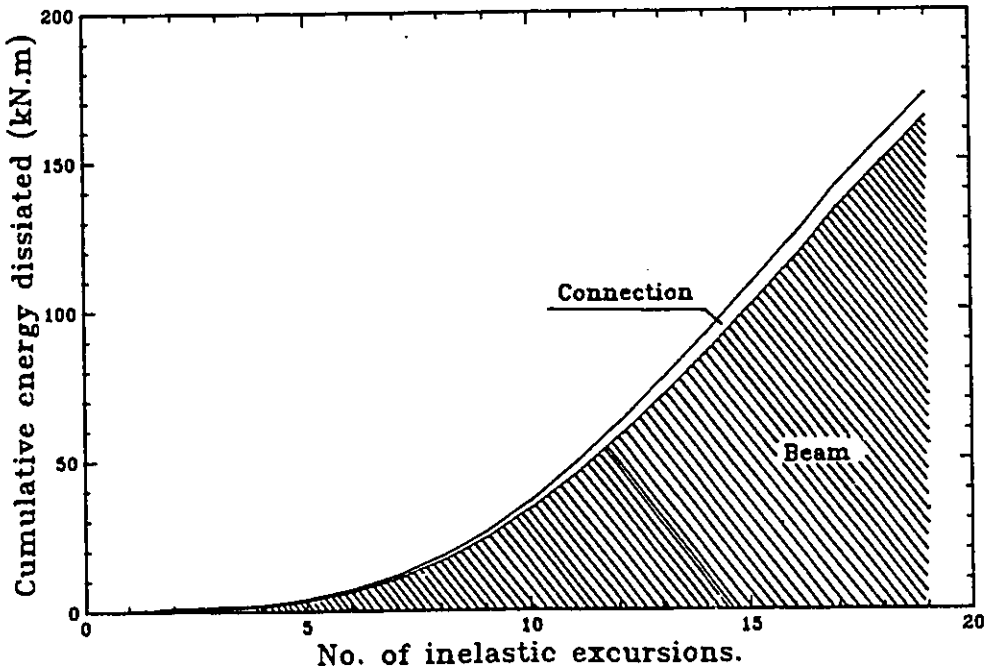

Fig. 2.45 Cumulative energy dissipated by each component in specimen A-3.

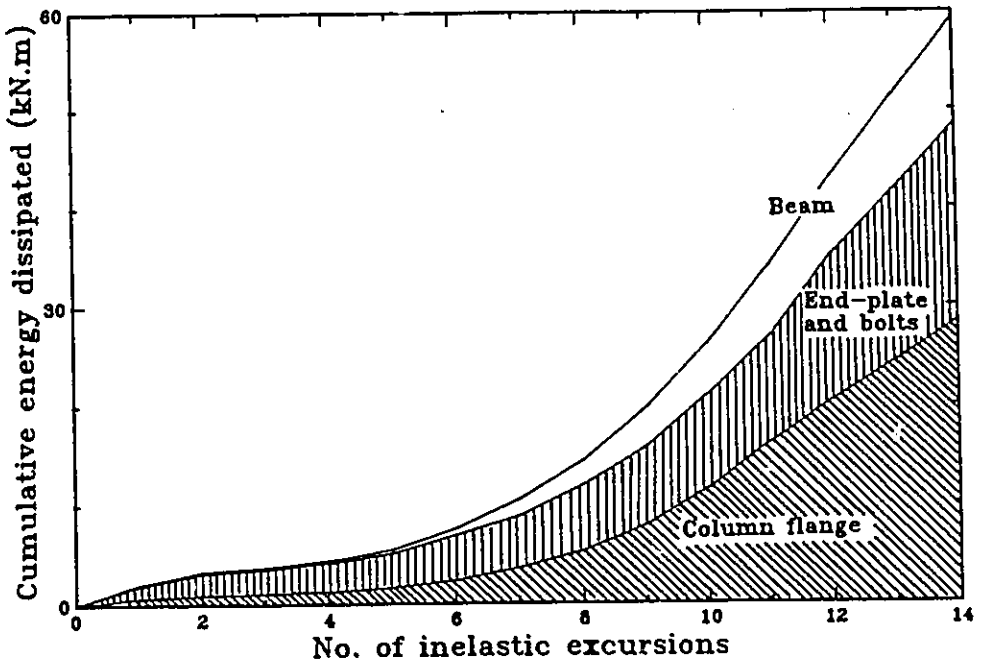

Fig. 2.46 Cumulative energy dissipated by each component in specimen A-4.

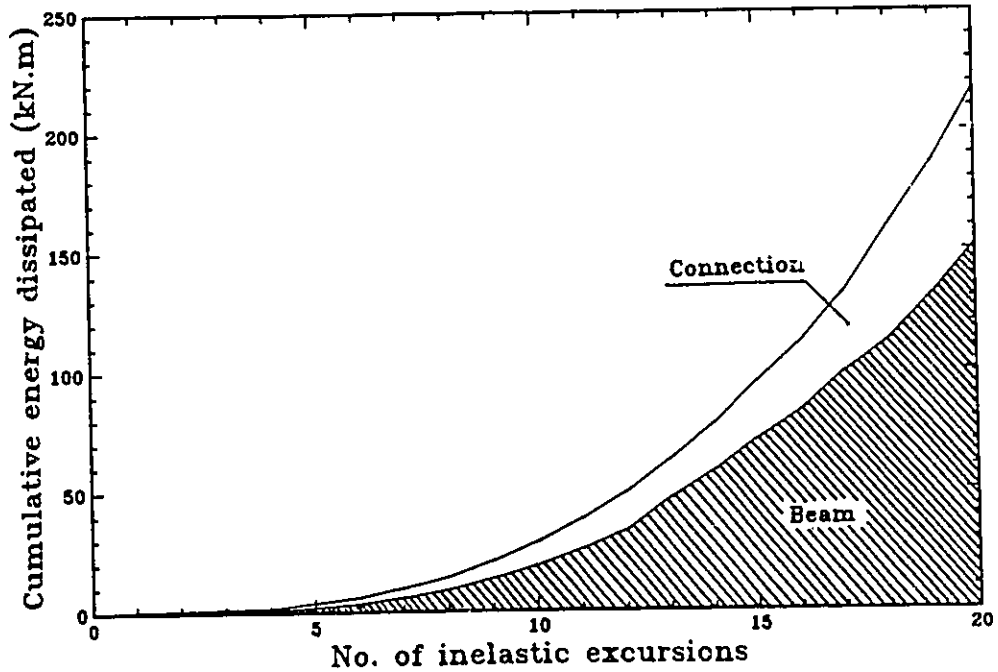

Fig. 2.47 Cumulative energy dissipated by each component in specimen B-1.

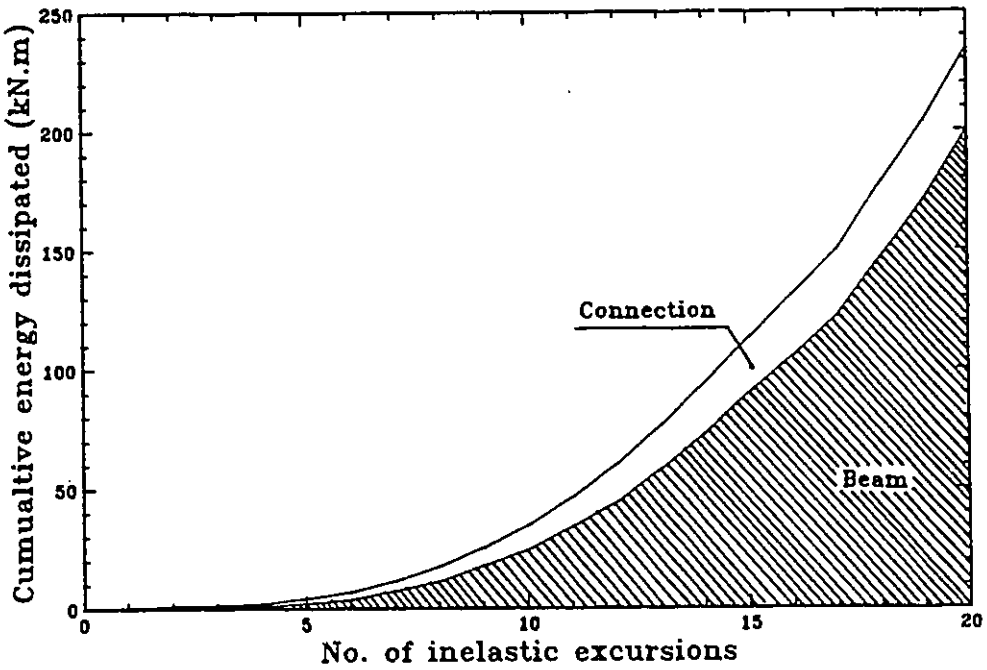

Fig. 2.48 Cumulative energy dissipated by each component in specimen B-2

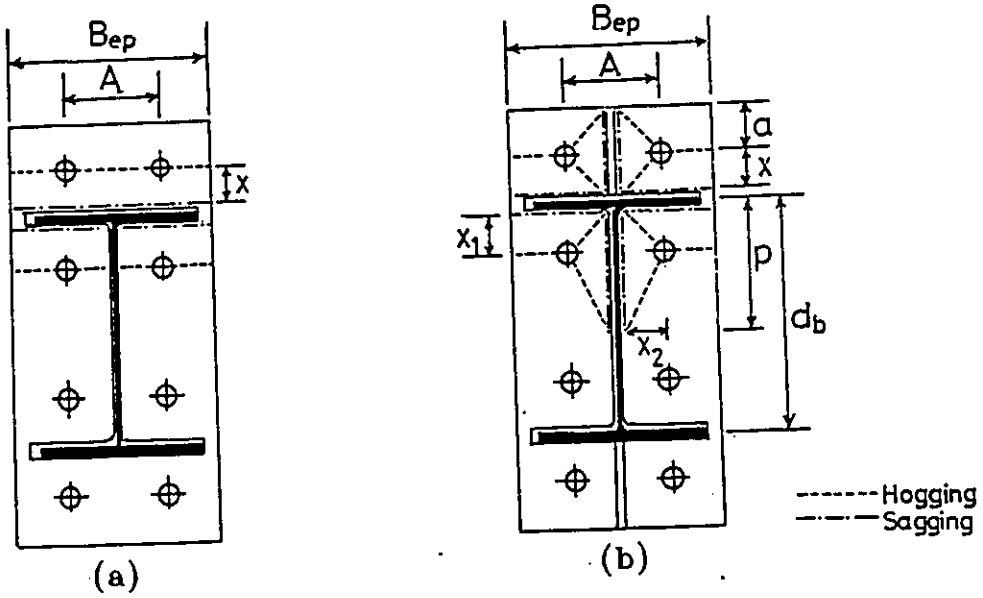

Fig. 2.49 End-plate yield line mechanisms.

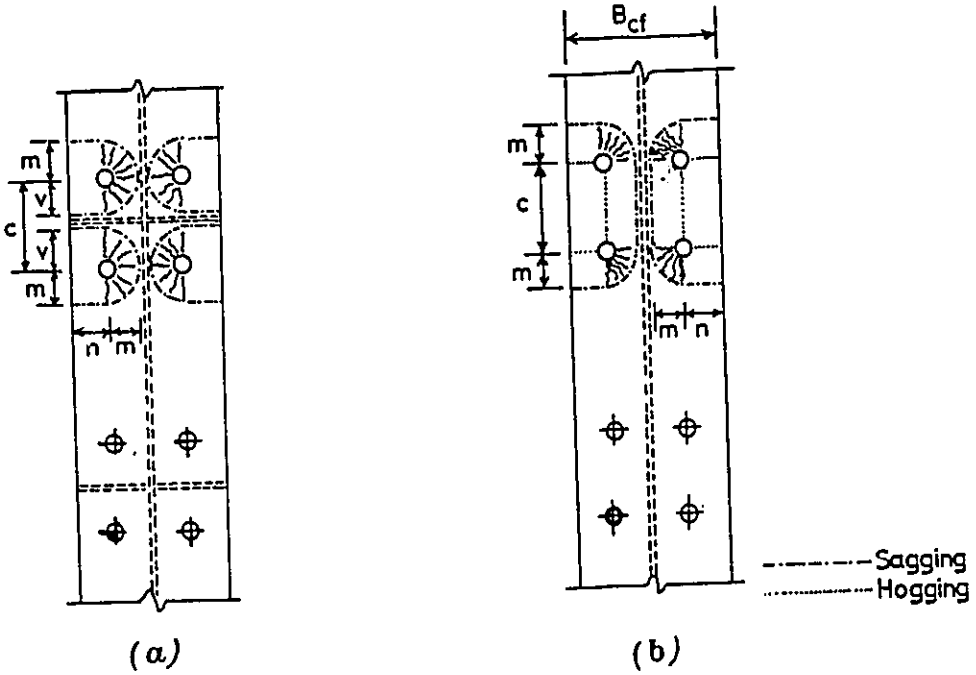

Fig. 2.50 Column flange mechanisms
a)stiffened; b)unstiffened.

CHAPTER 3

MOMENT-ROTATION RELATIONSHIP FOR EXTENDED END-PLATE CONNECTIONS

3.1 Introduction

The tests reported in Chapter 2 showed that the connection can experience large deformations especially in the post elastic range. As such, the actual response of frames utilizing this type of connection can be assessed only by incorporating the connection's flexibility in the analysis. This requires the development of a constitutive relationship capable of representing the connection response.

In the past, several researchers have tried to simulate connection behaviour under general loading conditions. Different models ranging from purely empirical curve fitting of test data (Frye and Morris, 1976; Ang and Morris, 1984), or by, analogy and semi-empirical techniques (Mzzalani, 1987), to comprehensive models have been presented. Some of these models are sophisticated and fairly accurate in predicting connection response; others were simple with only a limited ability to approximate the key parts of the connection response.

The degree of model sophistication required and its capability of predicting with sufficient accuracy the connection response depends mainly on the purpose for which the model is to be used. For example, if the overall response of MRFs is to be determined, simple models that are capable of handling only the key aspects of the connection response is adequate. Nethercot and Zandonini (1989) suggested that, in such cases, the adequacy of the predicted model should then be judged not merely on the basis of the level of accuracy achieved in approximating the actual connection moment-rotation curve, but rather on the effect of this approximation on the overall frame performance. On the other hand, if the influence of the end-restraint on strength or stability of the columns is to be investigated, Jones et al. (1982) have suggested that accurate prediction of the connection response is a necessity.

Therefore, in this chapter two models were developed to predict the moment-rotation relationship for extended end-plate connections. The first, is analytically sophisticated and is capable of predicting with high accuracy the connection response under both monotonic and cyclic loading conditions. The model uses parameters that are determined based on the geometrical and mechanical properties of the connection without the need for physical tests. The second, is a simple model that was developed to be used in studying the effect of connection flexibility on frame response. A connection element that can be easily incorporated in a computer program was introduced. The following sections describe in detail these models.

3.2 Sophisticated model

3.2.1 M-θ relationship under monotonic loading

In extended end-plate connections, the components that contribute to the connection deformation are:(1) end-plate flexure, Δ_{ep};(2) column flange flexure,Δ_{cf}; and(3) web compression,Δ_{cw} in the case of unstiffened connections. A schematic of the deformation for both stiffened and unstiffened connections is shown in Fig.3.1.

Yee and Melcher (1986) suggested that the connection deformation can be related to the connection moment through a four parameter exponential equation (Fig.3.2)given by

$$M=M_{pc}\{1-\exp[-(K_i-K_p+C\theta)\,\theta/M_{pc}]\}+K_p\theta \qquad (3.1)$$

Where

K_i = initial elastic stiffness,
K_p = post elastic stiffness,
M_{pc} = plastic moment capacity of the connection,
C = rate of decay parameter, and,
θ = connection rotation in radians.

This equation has the following characteristics; $dM/d\theta = K_i$ at $\theta = 0$ (the slope of the curve at the origin is equal to the initial elastic stiffness of the

connection); $dM/d\theta = K_p$ as θ tends to ∞ (as the rotation becomes large, the slope of the curve approaches the post elastic stiffness); and $M=0$ at $\theta=0$. However, the use of this equation requires the determination of the connection parameters K_i, K_p, C and M_{pc}. These parameters may be determined from experiment. However, this approach is impractical and uneconomical,since it requires extensive testing. Thus, in this study, efforts were directed towards calculating these parameters analytically. The methods used for such purpose will be explained in the following sections.

a) Evaluation of connection initial stiffness (K_i)

For evaluating the initial stiffness, the material was assumed to be linearly elastic and the deformations were assumed to be small. On the basis of these assumptions, the connection's initial stiffness is given by

$$K_i = M/\theta \qquad (3.2)$$

Referring to Fig.3.1, the connection rotation,θ ,can be related to the connection deformations by the formula

$$\theta = \Delta_T/(d_b - t_{bf}) \qquad (3.3)$$

where

Δ_T = total connection deformation,
d_b = beam depth, and
t_{bf} = beam flange thickness.

The connection moment, M, can be resolved into two equal and opposite forces acting through the beam flanges as

$$M = P(d_b - t_{bf}) \qquad (3.4)$$

Substituting Eqs. 3.3 and 3.4 into Eq. 3.2, the initial stiffness can be related to both the beam flange forces, P, and the total connection deformation, Δ_T by

$$K_i = P(d_b - t_{bf})^2 / \Delta_T \qquad (3.5)$$

Eq. 3.5 suggests that once Δ_T is calculated in terms of the beam flange force, P, the connection initial stiffness K_i can be determined. In calculating Δ_T, there should be a distinction between connections having stiffened column flanges and those without. In the former case, the total deformation, Δ_T, is due to both column flange deformation, Δ_{cf}, and end-plate deformation, Δ_{ep}. Using the assumption of material linearity and elasticity the total deformation can be calculated by superimposing the deformations of the individual components. Thus

$$\Delta_T = \Delta_{ep} + \Delta_{cf} \qquad (3.6)$$

However, in the latter case where the column flange bears into the column's unstiffened web, an additional deformation component, should be added, i.e.

$$\Delta_T = \Delta_{ep} + \Delta_{cf} + \Delta_{cw} \qquad (3.7)$$

These deformations can be determined in terms of the beam flange forces, P as described below.

i) End-plate deformation, Δ_{ep}

The end-plate in this model was idealized as a T-stub as shown by the shaded area in Fig. 3.3. The following assumptions were made to be consistent with the deformation model shown in the Fig. 3.4.

1) The bolts are fully pre-tensioned (i.e with infinite stiffness).

2) The end-plate allows deformation only between the bolts and the adjacent tensile beam flange.

3) Stiffening from the beam's web is neglected.

4) Prying action is concentrated at the tip of the end-plate.

Using the modified slope deflection equation derived by Azizinamini et al, (1987) to account for shear effects, the end-plate deflection is given by

$$\Delta_{ep}=P/12EI_{ep}\{\left(\frac{1}{b_1^3(1+r_2)}\left[\frac{3}{b_1(1+r_2)}\frac{1}{\left(\frac{12}{a(4+r_1)}+\frac{4+r_2}{b_1(1+r_2)}\right)}-1\right]\right)+$$

$$\left(\frac{1}{b_1^3(1+r_3)}\left[\frac{3}{b_2(4+r_1)}\frac{1}{\left(\frac{12}{a(4+r_1)}+\frac{4+r_2}{b_2(1+r_3)}\right)}-1\right]\right\} \qquad (3.8)$$

where

r_i = $12EI_{ep}/L_i^2GA_s$,(r_1 in Eq. 3.8 is associated with the length a, r_2 and r_3 are associated with b_1 and b_2)
E = Young's modulus of elasticity,
L_i = The length of the segments such as b_1, b_2, and a,
I_{ep} = Moment of inertia the end-plate,
G = Shear modulus,
A_s = Effective shear area of the end-plate,
B_{ep} = The end-plate width, and
t_{ep} = The end-plate thickness.

In the case of $b_1=b_2$ (Fig.3.3), Eq.3.8 can be reduced to

$$\Delta_{ep}=P/12EI_{ep}\left\{\left[\frac{1}{b_1^3(1+r_2)}\left(\frac{6}{b_1(1+r_2)}\frac{1}{\left(\frac{12}{a(4+r_1)}+\frac{(4+r_2)}{(1+r_2)b_1}\right.}\right.\right.\right.-2)\Big]$$

ii) Column flange deformation,Δ_{cf}

Calculation of the column flange deformation depends on whether the column flange is stiffened or unstiffened. In the case of the unstiffened column flange, it can be idealized as an infinitely long elastic cantilever plate subjected to concentrated loads of magnitudes P/4 at bolt locations (Fig.3.5). The deformation at these locations is given by Jaramillo (1950) as

$$\Delta_{cf} = \frac{PB_{cf}^2}{16\pi D^*}(H+Z) \qquad (3.10)$$

where B_{cf} is the column flange width excluding the column web thickness, D^* is the flange plate's flexural rigidity and is equal to $Et^3_{cf}/12(1-\nu^3)$, ν being Possion's ratio, and H and Z are dimensionless coefficients that depend on the distance m (Fig.3.5), on the plate width, S, and on the distance between bolts. The values of H and Z for different cases are tabulated in Jaramillo's paper (1950).

In the case of a stiffened column flange, Eq.3.8 can be used to calculate, Δ_{cf}. The stiffening action from the column web can be compensated for by excluding the column web thickness in the calculation of column flange inertia and reduced area.

iii) Web compression zone deformation, Δ_{cw}

In the case of a connection with stiffened column flanges, the web compression deformation is negligible. However, for unstiffened column flanges this deformation is significant and should be taken into account. This can be done by idealizing the effective compression zone of the web as being a rectangular plate of dimensions d_c' X d_s', subject to uniform compression from the beam compression force, P, and with the plate fully restrained in the y-direction as shown in Fig.3.6.The obtained web compression deformation, Δ_{cw}, is given by

$$\Delta_{cw} = \frac{d_c' P(1-\upsilon^2)}{d_s' E t_{cw}} \qquad (3.11)$$

where

d_s' = (t_{bf} + 6K + $2t_{ep}$ + $2t_{wf}$),
t_{ep} = the end-plate thickness,
t_{wf} = the size of the weld between the end-plate and the beam flange,
t_{cw} = the column web thickness,
K = the column "K" distance, and
t_{bf} = the beam flange thickness.

b) Evaluation of connection plastic moment capacity (M_{pc})

The plastic moment capacity of the connection, M_{pc}, is defined as the

maximum moment that can be transmitted by the connection prior to yielding of one of its components. It represents the smallest moment that will cause yielding to either the column flange, the end plate or the column web at the compression zone when applicable.

i) Yielding of Column Flange

Packer and Morris (1977) proposed the following relations to calculate the beam flange load, P_p, required to yield the column flange based on conical yield line analysis. In the case of the stiffened column flange (Fig.3.7(a)), P_p is given by

$$P_p = t_{cf}^2 \sigma_{yc} \left[\left(\frac{1}{V} + \frac{1}{W} \right) (2m+2n-D) + \frac{2V+2W-D}{m} \right] \qquad (3.12)$$

where

m and n are dimensions shown in Fig.3.7,
W = $[m(m+n-0.5D)]^{1/2}$,
D = bolt hole diameter,
V = $0.5(c-t_s-2x\ t_{wf})$ and > W,
σ_{yc} = yield stress of column flange,
t_{cf} = thickness of column flange, and,
t_s = thickness of the column flange stiffeners.

For the unstiffened column flange (Fig.3.7(b))

$$P_p = \sigma_{yc} t_{cf}^2 \left[\pi + \frac{2n-c-D}{m} \right] \qquad (3.13)$$

where c is the vertical distance between the bolts' centres as shown in Fig.3.7.

ii) Yielding of the End-plate

Two different details for the end-plate were considered in this study. In the first, the customary end-plate was used. In the second, the end-plate was stiffened by welding small triangular plates to further attach it to the beam flanges. For ordinary end-plates, Fig.3.8(a) shows straight line yield mechanisms for two possible cases. Packer and Morris (1979) showed that for the case of model 1 in Fig.3.8(a) P_p is

given by

$$P_p = \sigma_{ye} t_{ep}^2 B_{ep} / X \qquad (3.14)$$

where the symbols not previously defined in this chapter are shown in Fig. 3.8.

Later, Walpole (1985) recommended that the above equation be used when the beam is fillet welded to the end-plate. When the beam is connected to the end-plate by butt welds, he recommends another equation formulated based on the model 2 mechanism shown in Fig.3.8(a). In such a case, P_p is given by

$$P_p = \sigma_{ye} t_{ep}^2 \left[\frac{2B_{ep}}{C - t_{bf} - 2t_{wf}} + \frac{2p}{A - t_{bw} - 2t_{ww}} \right] \qquad (3.15)$$

Here, A is the horizontal distance between the centre of the bolts in the tension region. Also, t_{wfb} and t_{wwb} are the splay of the weld fillet on both sides of the flange and web respectively while, $p = 0.6\,(d_b - t_{bf})$.

In the case of the stiffened end-plate, the mechanism shown in Fig.3.8(b) was used to calculate P_p. The value in this case is given by

$$P_p = \sigma_{ye} t_{ep}^2 \left[(B_{ep} - t_{se} - D)/X + (B_{ep} - t_{bw} - D)/X_1 \right.$$

$$\left. + (p - (t_{bf}/2) - D + a + x)/X_2 \right] \qquad (3.16)$$

where

t_{se} = the thickness of the end-plate stiffeners.

iii) Web Yielding at Compression Zone

Hendrick and Murray (1984) suggested that the beam flange load required to yield the column web in the compression region be estimated as

$$P_p = \sigma_{yc} t_{cw} (t_{bf} + 6k + 2t_{ep} + 2t_{wf}) \qquad (3.17)$$

According to Hendrick and Murray (1984), Eq. 3.17 is applicable for both stiffened and unstiffened end-plates.

Once the different values of P_p are calculated, the smallest value is selected. This value will correspond to the load required to yield the weakest element in the connection. This value is used to calculate the plastic moment capacity of the connection as

$$M_{pc} = F_p(d_b - t_{bf}) \qquad (3.18)$$

c) Evaluation of post elastic stiffness (K_p)

Yee and Melcher (1986) suggested that the post-elastic stiffness, K_p, can be assumed zero for all connections except those exhibiting web shear yielding or web buckling. However, tests conducted on full scale specimens show that such connections exhibit a significant post elastic stiffness especially when column flange stiffeners are present (Osman et al., 1990). This post elastic stiffness was observed to be between 10% and 20% of the initial stiffness. In the present study, K_p was taken equal to $0.15K_i$. Although , this value is higher than expected for the strain-hardening range, it appears that changes in the geometry of the column flange and the end-plate during loading account for part of the stiffening effect. In the case of unstiffened connections a value of K_p of $.05K_i$ seems reasonable.

d) Evaluation of parameter C

The value of the rate of decay parameter C cannot be analytically predicted, and must be determined from test results. Yee and Melcher (1986) recommend values of 3.5×10^6 and 1.5×10^6 kN.m for stiffened and unstiffened connections, respectively. However, in this study a slightly higher value of 4.5×10^6 kN.m for the stiffened connections was considered more appropriate.

e) Model verification

The accuracy of the previous model was verified by comparing its

predictions with these obtained from experimental tests. In this study, all the connections were tested under cyclic loads. The monotonic moment-rotation curves for the tested connections were constructed from the cyclic moment-rotation curves. This was carried out using the shifting rule. Comparison between the predicted and the experimental moment-rotation curves for some of the tested specimens are shown in Figs.3.9 through 3.12. As indicated from these figures, the model accurately predicts the monotonic moment-rotation relationship. Table 3.1 lists the predicted model parameters as compared to the experimental results. Close agreement between the experimental and predicted parameters is evident.

3.2.2 M-θ curve under cyclic loading

The developed analytical model can be extended to simulate the connection behaviour under cyclic loading. In such a case, two different rules for describing the response are required, one is a loading rule and the other an unloading rule. These are shown in Fig.3.13 for the nth cycle of load application.

a) Loading

During loading of the nth cycle, Eq.3.1 is used to evaluate the moment corresponding to each rotation value, θ_{act}. In these calculations a temporary origin o' is used and the value of θ introduced in Eq.3.1 is the actual rotation, θ_{act}, plus the residual rotation from the previous excursion, θ_n^-. As such,

$$\theta = \theta_{act} + \theta_n^- \qquad (3.19)$$

Tests conducted on extended end-plate connections under cyclic loading conditions showed that the connections exhibited stiffness degradation with the progression of loading. To express such stiffness degradation in the model, K_i was replaced by K_{in} in Eq.3.1, where K_{in} is defined as the initial stiffness at the nth cycle. Analysis has shown that the value of K_{in} is a function of the rotation experienced by the connection in the previous cycle, ((n-1)th cycle). Therefore, it was concluded that the maximum rotation experienced by the connection in a given cycle is a good measure for assessing this degradation. Thus,

$$K_{in} = K_i (\theta_{(n-1)max}/\theta_y)^{\beta} \qquad (3.20)$$

Where

K_{in} = The initial stiffness in the nth cycle,
β = Parameter determined experimentally,
$\theta_{(n-1)max}$ = Maximum rotation experienced by the connection in (n-1)th excursion measured from the zero moment intercept, and
θ_y = Rotation at first yield.

The values of β determined for some of the tested specimens are shown in Table.3.2. As can be observed, discrepancy exists among those values which suggest that one parameter, $\theta_{(n-1)max}$, only is not enough to describe this behaviour. At the same time, these values were determined for certain loading histories.

(b) Unloading

When the rotation reaches a maximum value, θ^+_{nm}, and the load is reversed, the connection begins to unload. During this process the connection behaves as if it possesses a very high stiffness, approaching the initial stiffness, K_i. As unloading is continued, the connection shows softening until it reaches the cycle initial stiffness, K_{in} at zero load. A reasonable representation of this response is curve-line unloading. The tangent is taken equal to K_i at θ^+_{nm} after which there is a gradual decrease in the slopes of the lines connecting the unloading curve with the point (θ^+_{nm}, M^+). This continues until the slope reaches K_{in} at the point $(\theta^+_n, 0)$.

The change in the slope of these lines can be written as

$$K_n(\theta) = K_{in}\left[1+\frac{(K_i-K_{in})}{K_{in}}-\left(\frac{\theta^+_{nm}-\theta}{\theta^+_{nm}-\theta^+_n}\right)\left(\frac{K_i-K_{in}}{K_{in}}\right)\right] \qquad (3.21)$$

The value of θ^+_n can be obtained by

$$\theta^+_n-\theta^+_{nm}=\frac{M^+}{K_{in}} \qquad (3.22)$$

Here, M^+ is the maximum moment attained during the excursion.

Substituting Eq.3.22 into Eq.3.21 gives

$$K_n(\theta) = K_{in}\left[1+\frac{(K_i-K_{in})}{K_{in}}-\left(\frac{\theta^+_{nm}-\theta}{M^+}\right)(K_i-K_{in})\right] \qquad (3.23)$$

Once the slope of the line connecting the curve with the point (θ^+_{nm}, M^+) is determined for any θ value from Eq.3.23, the corresponding moment can be determined as follows

$$M=M^+ + (\theta-\theta^+_{nm})\,K_n(\theta) \qquad (3.24)$$

c) Model verification

The effectiveness of this model in predicting the cyclic response of the connections was verified by comparing its results with those obtained experimentally. Figs.3.14 and 3.15 show the results from two of the tested specimens. In these figures, the experimental results are shown by solid lines and the predicted results by dotted lines. The predicted results correlate well with the test results. It should be mentioned that, in predicting these curves, the degradation in connection stiffnesses was taken into account. As such, the values of β used were those corresponding to each tested specimen (Osman et al.,1990a).

3.3 Simple model

Although the model just described can predict accurately the connection

response, it is considered too complex and sophisticated to be incorporated into computer programs. Thus, a more simplified model is suggested for such purposes. Although, it is not as accurate as the earlier one, it approximates the key aspects of the connection response in an overall sense.

This second model is a bi-linear pieceline approximation for the connection moment-rotation relationship. The model needs only three parameters to describe the M-θ curve. The parameters are: (1) the connection initial stiffness, K_i, which can be determined as described in section 3.2.1; (2) the plastic moment capacity of the connection, M_{pc}, which can be calculated according to section 3.2.2; and (3) the connection post elastic stiffness, K_p, as determined in section 3.2.3. The model can easily be used to simulate the connection behaviour either under monotonic or under cyclic loading conditions as shown in Fig.3.16.

It should be noted that this model ignores the effect of connection stiffness degradation. However, in the view of the proposed design method (see Chapter 2), it is expected that connections designed in accordance with the proposed method will experience only minimal stiffness degradation.

3.3.1 Nonlinear connection element

If only flexural deformation of the connection is considered, a one degree of freedom connection element can be introduced at the beam-column intersection to model the M-θ relationship as shown in Fig.3.17. The connection element is placed between two nodes and is only influenced by the relative rotation between the nodes. The deformation of the element represents the angle changes between the connected beams and columns due to connection rotation. In this element, translational displacements of the nodes at both ends of the element are constrained to be identical. Also, they assigned similar coordinates to satisfy equilibrium.

Basically, the element consists of an elastic and elasto-plastic component in parallel as shown in Fig.3.18. A plastic hinge is introduced into the elasto-plastic component once the connection yield moment is reached. Kinematic hardening of the connection is modeled by specifying the appropriate strain hardening ratio of the M-

θ relationship.

In this element, the relative rotation between the connected nodes is related to the node rotations as follows

$$d\Gamma = \langle 1 \ldots -1 \rangle \begin{Bmatrix} d\theta_i \\ d\theta_j \end{Bmatrix} \qquad (3.25)$$

in which $d\Gamma$ = increment of relative rotation (element deformation), while $d\theta_i$ and $d\theta_j$ = increments of rotation of the connected nodes. The inelastic deformation is the amount of relative rotation beyond yield of the elasto-plastic component of the element.

With regard to the stiffness, the element tangent stiffness relationship is given by

$$dM = K_T d\Gamma \qquad (3.26)$$

3.4 Summary

Two analytical models that are capable of predicting the moment-rotation relationship for extended end-plate connections are proposed. One belongs to the category of a sophisticated model; the other is a simple one. The models were calibrated by comparing their predictions with that of experiments. On the basis of the presented analysis the following can be concluded:

1) The models predict the connection behaviour solely on the basis of its geometrical and mechanical properties without requiring physical tests on actual connections.

2) The sophisticated model is able to predict the M-θ relationship for the connection under both monotonic and cyclic loading conditions with high accuracy. This model can be used when the analysis significantly affected by the model sensitivity such as in the case of dealing with restrained members.

3) Comparison between experimental and analytical results for the sophisticated model shows that:

i) The experimental and predicted initial stiffness correlates well.

ii) Under low levels of load cycles just beyond yield, the model hysteretic energy dissipation exceeds that of experiment.

iii) The model hysteretic energy dissipation correlates better with the experimental results under large load cycles.

iv) The model predicts accurately the connection rotation at all load levels.

4) The proposed computer model is simple and was easily adopted for formulating a connection element that is capable of simulating the connection response. This element can be incorporated into a plane-frame computer program to assess the influence of connection flexibility on frame response.

Table 3.1 Comparison between predicted and observed connection parameters

Specimen No.	Predicted K_i	Predicted K_p	Predicted M_{pc}	Observed K_i	Observed K_p	Observed M_{pc}
A-1	46897	2345	170.4	51510	1449	166.7
A-2	65451	9817	209.4	63751	8178	200.7
A-3	83342	12501	224.1	79370	12150	222.2
A-4	55301	2765	149.8	52000	4710	150.0
A-5	67129	10069	155.6	65000	5790	153.4
B-1	72844	10926	216.0	74685	8233	202.0
B-2	66774	10016	221.6	65924	13333	203.0

Table 3.2 β values

Specimen No.	β Values
A-2	-.55419
A-3	-.93118
B-1	-.51020
B-2	-.55457

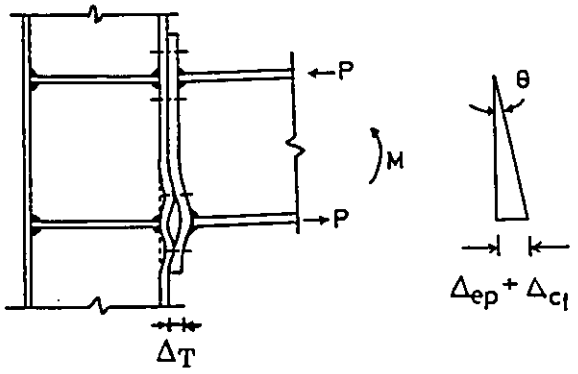

$\Delta_T = \Delta_{ep} + \Delta_{cf}$

a) stiffened

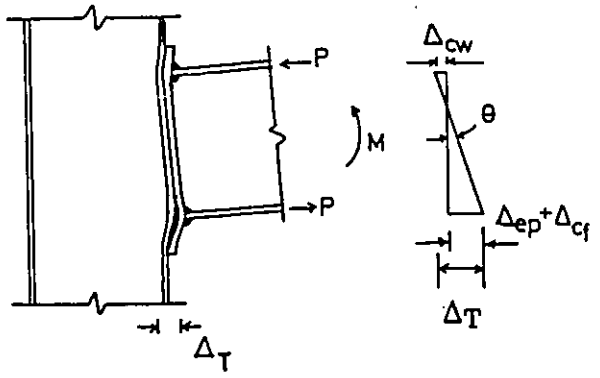

$\Delta_T = \Delta_{ep} + \Delta_{cf} + \Delta_{cw}$

b) unstiffened.

Fig. 3.1 Deformation of end-plate connection.

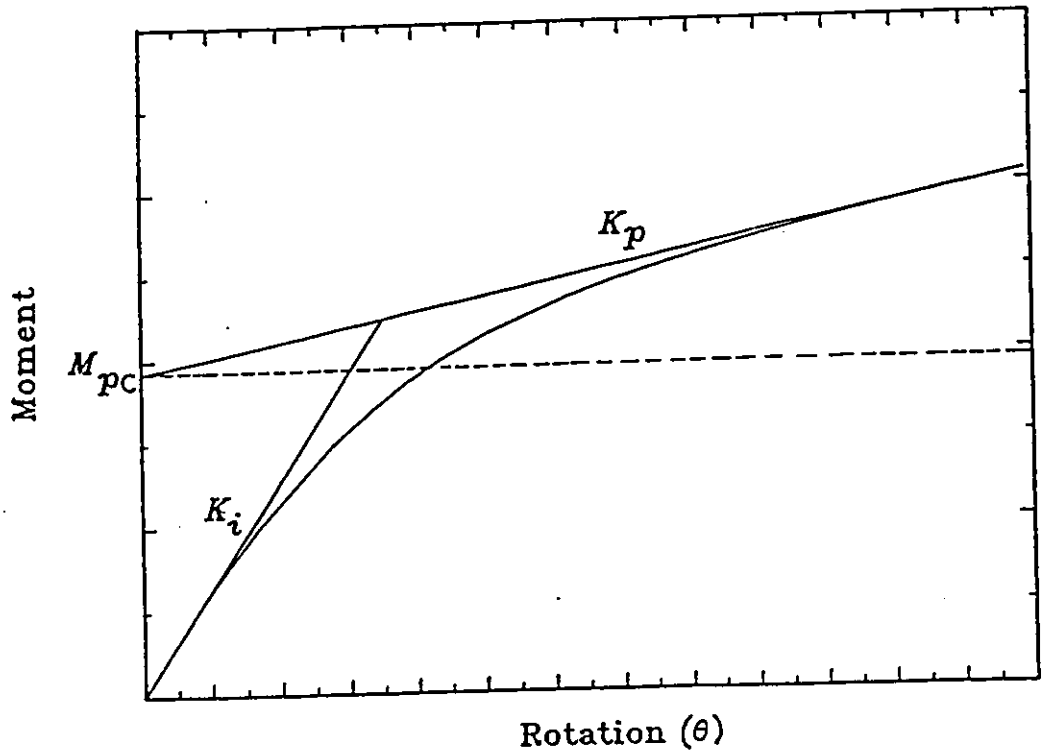

Fig. 3.2 Typical moment–rotation curve shows the model parameters.

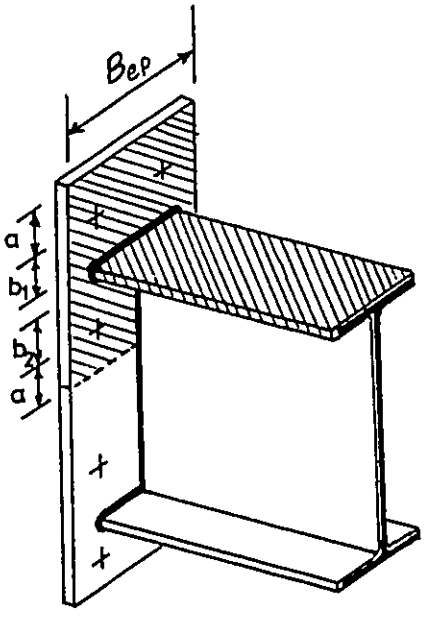

Fig. 3.3 End–plate T–stub model.

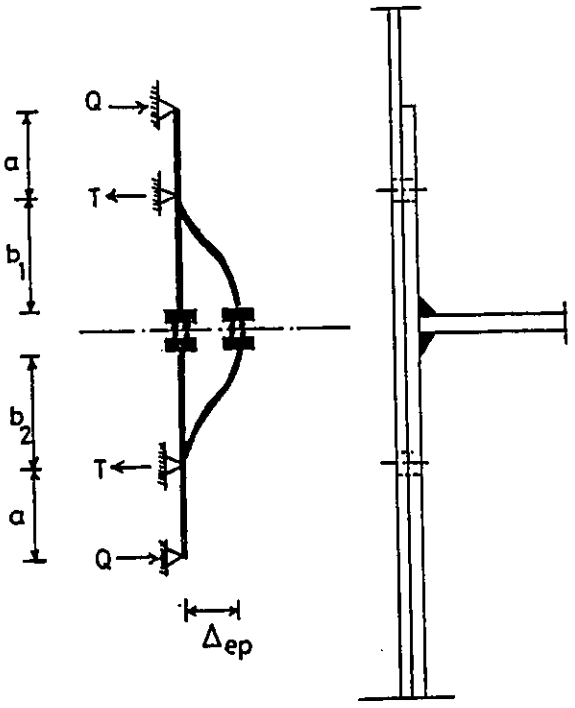

Fig. 3.4 Idealization of end–plate.

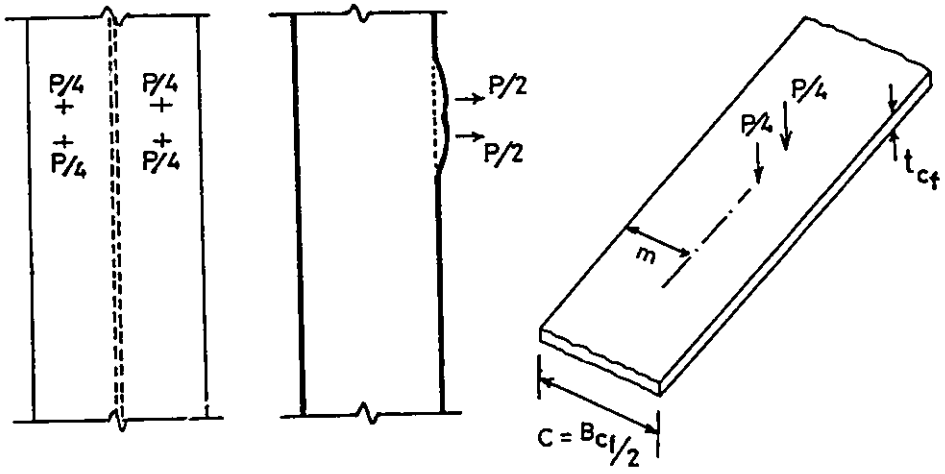

Fig. 3.5 Idealization of unstiffened column flange.

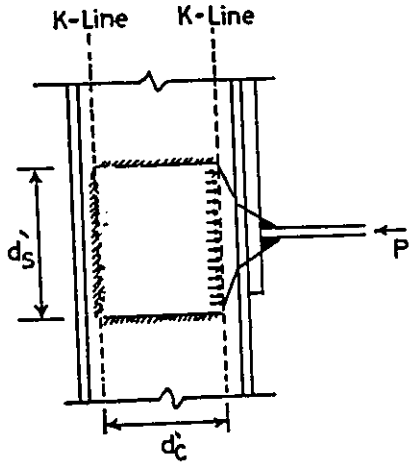

Fig. 3.6 Compression region of column flange.

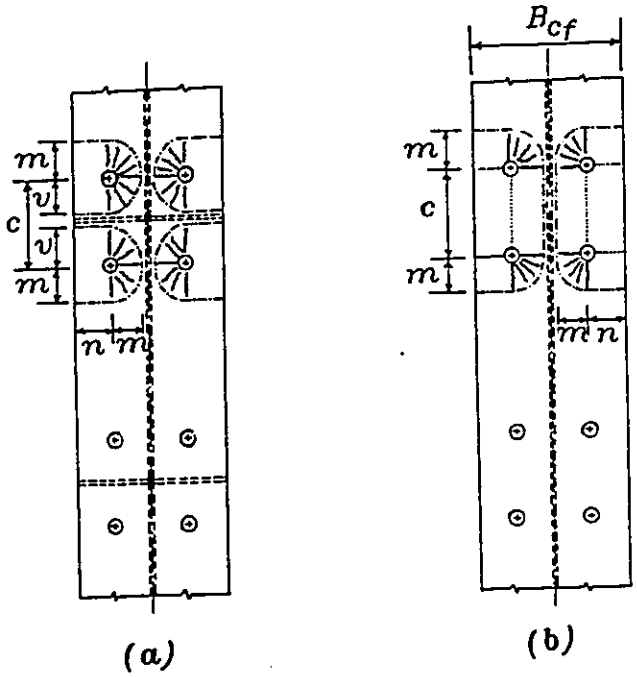

Fig. 3.7 Column flange mechanisms
a) Stiffened , b) Unstiffened.

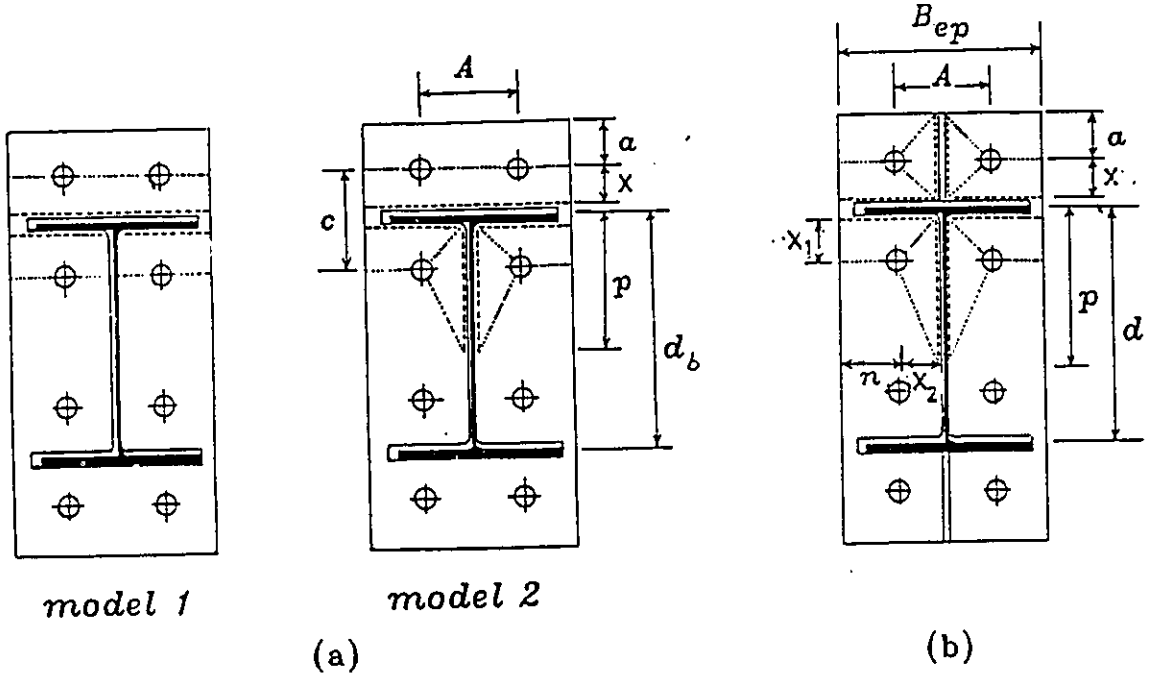

Fig. 3.8 End-plate mechanisms.

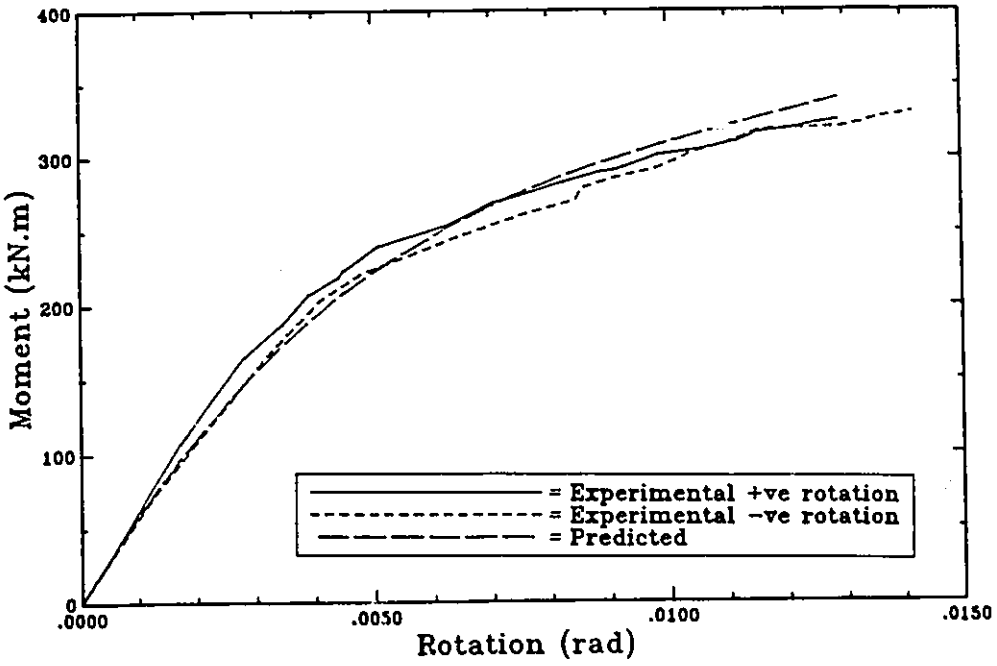

Fig. 3.9 Experimental vs. predicted moment rotation relationship for specimen A-2.

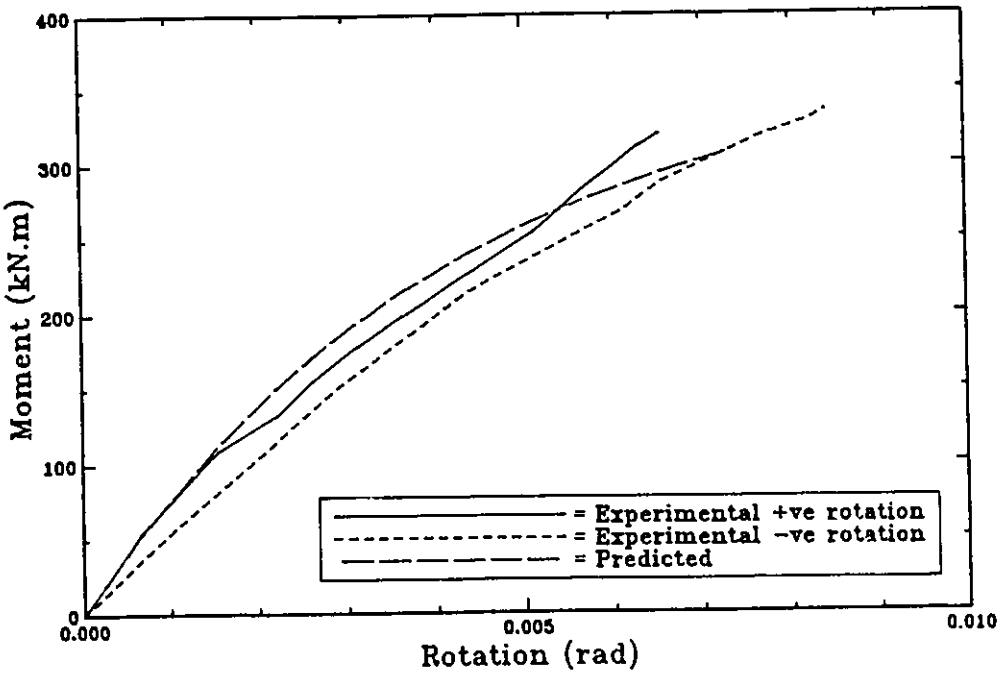

Fig. 3.10 Experimental vs. predicted moment rotation relationship for specimen A-3.

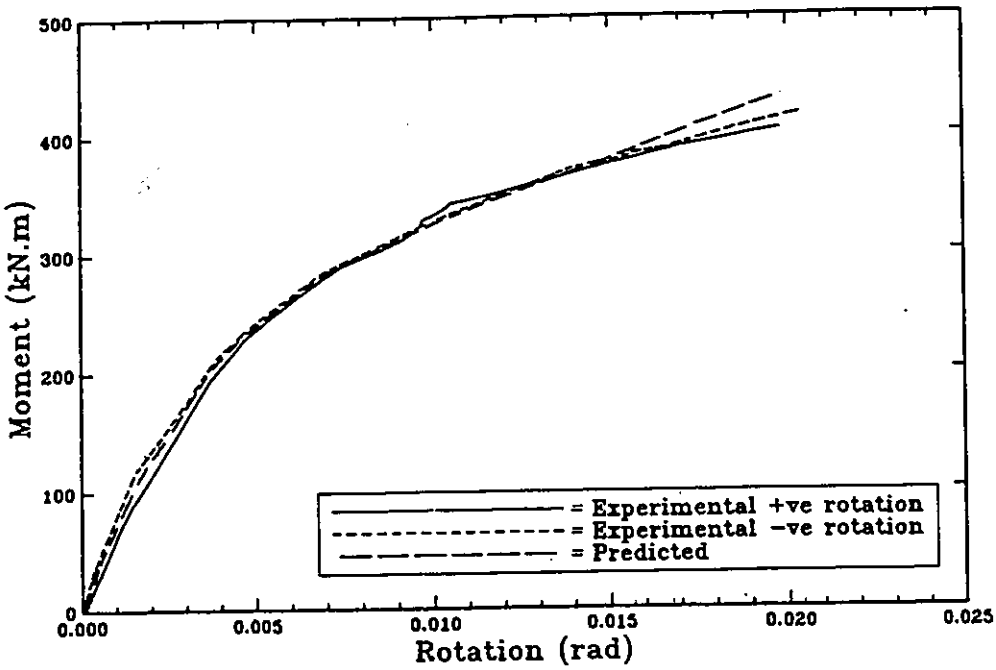

Fig. 3.11 Experimental vs. predicted moment rotation relationship for specimen B-1.

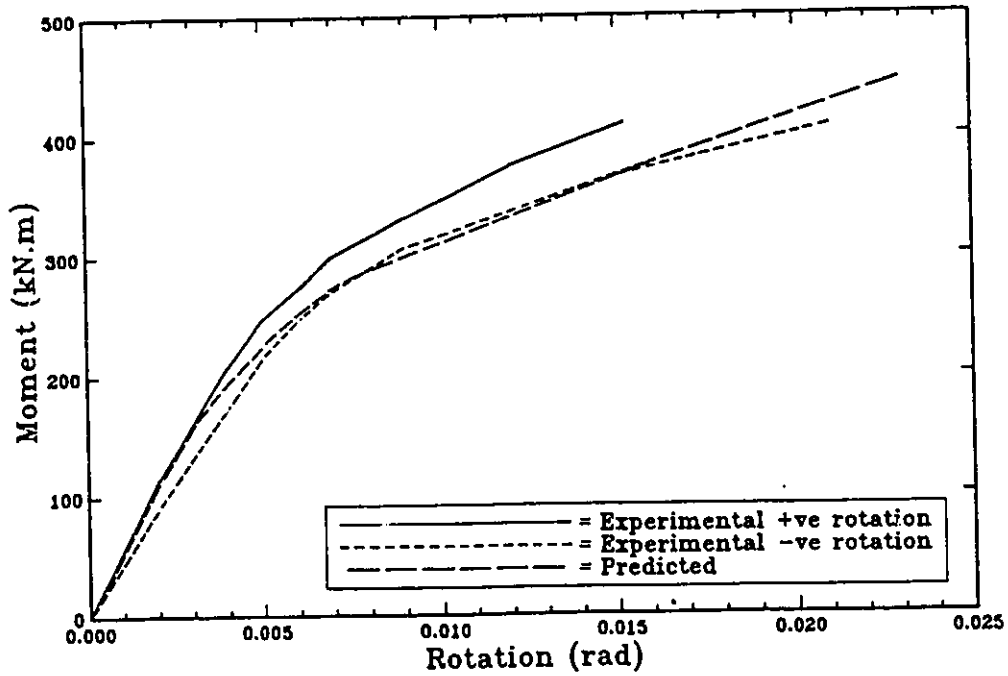

Fig. 3.12 Experimental vs. predicted moment rotation relationship for specimen B-2.

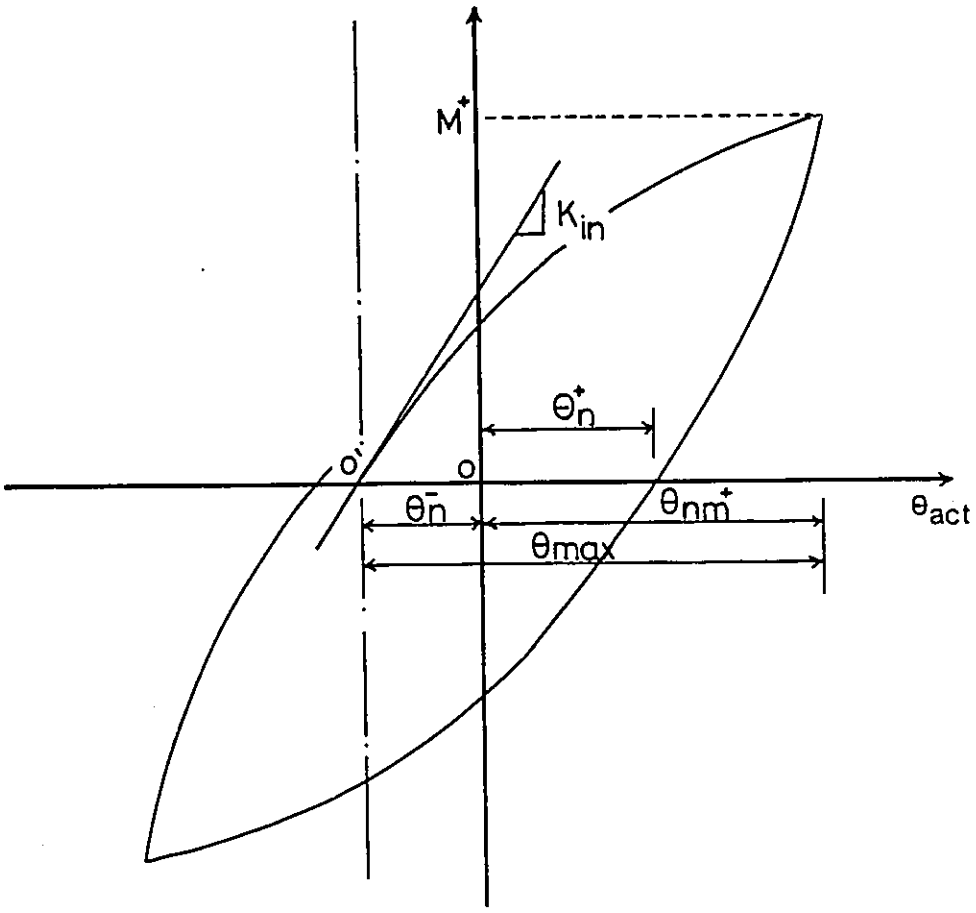

Fig. 3.13 Hysteretic model.

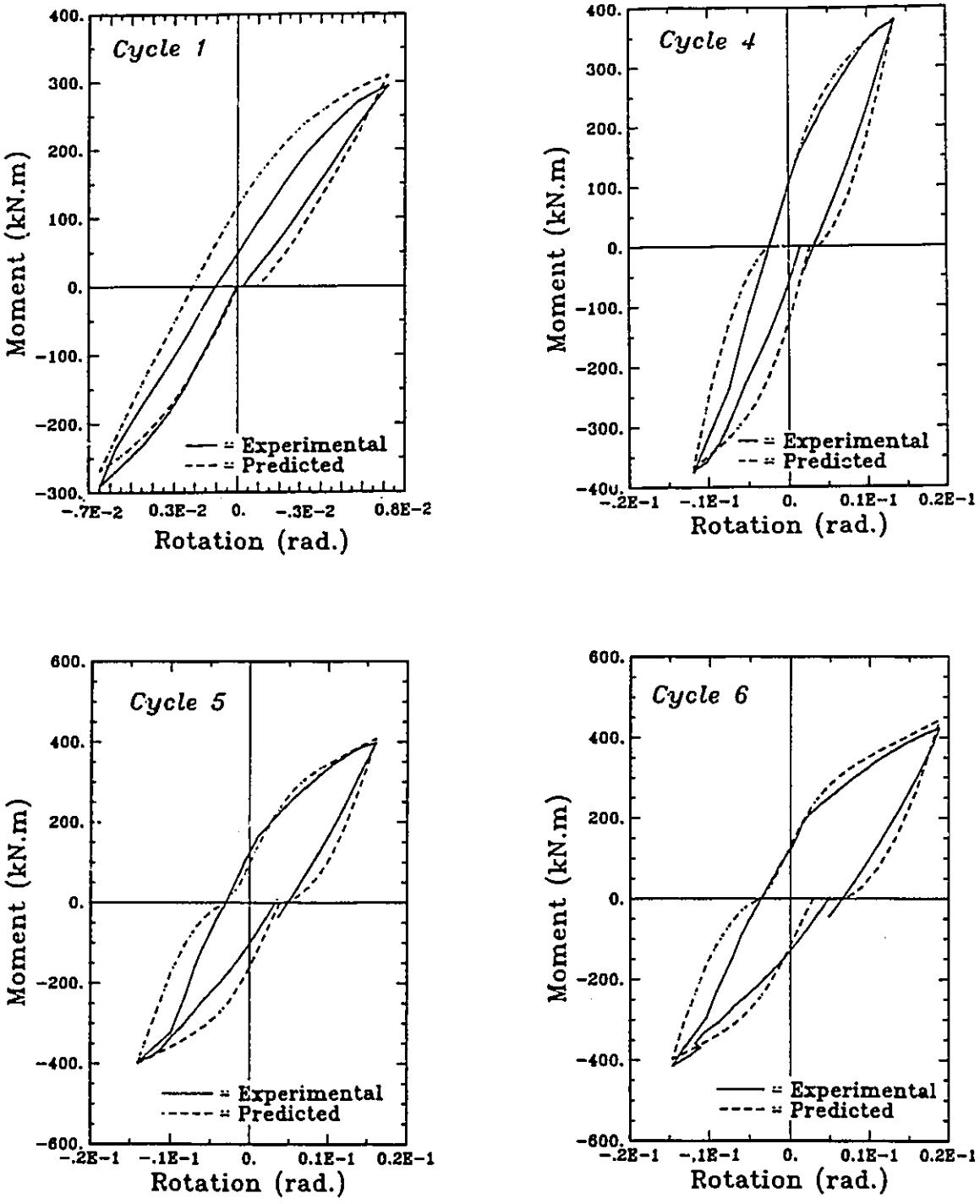

Fig. 3.14 Experimental vs. predicted hysteretic moment-rotation curves for specimen A-2.

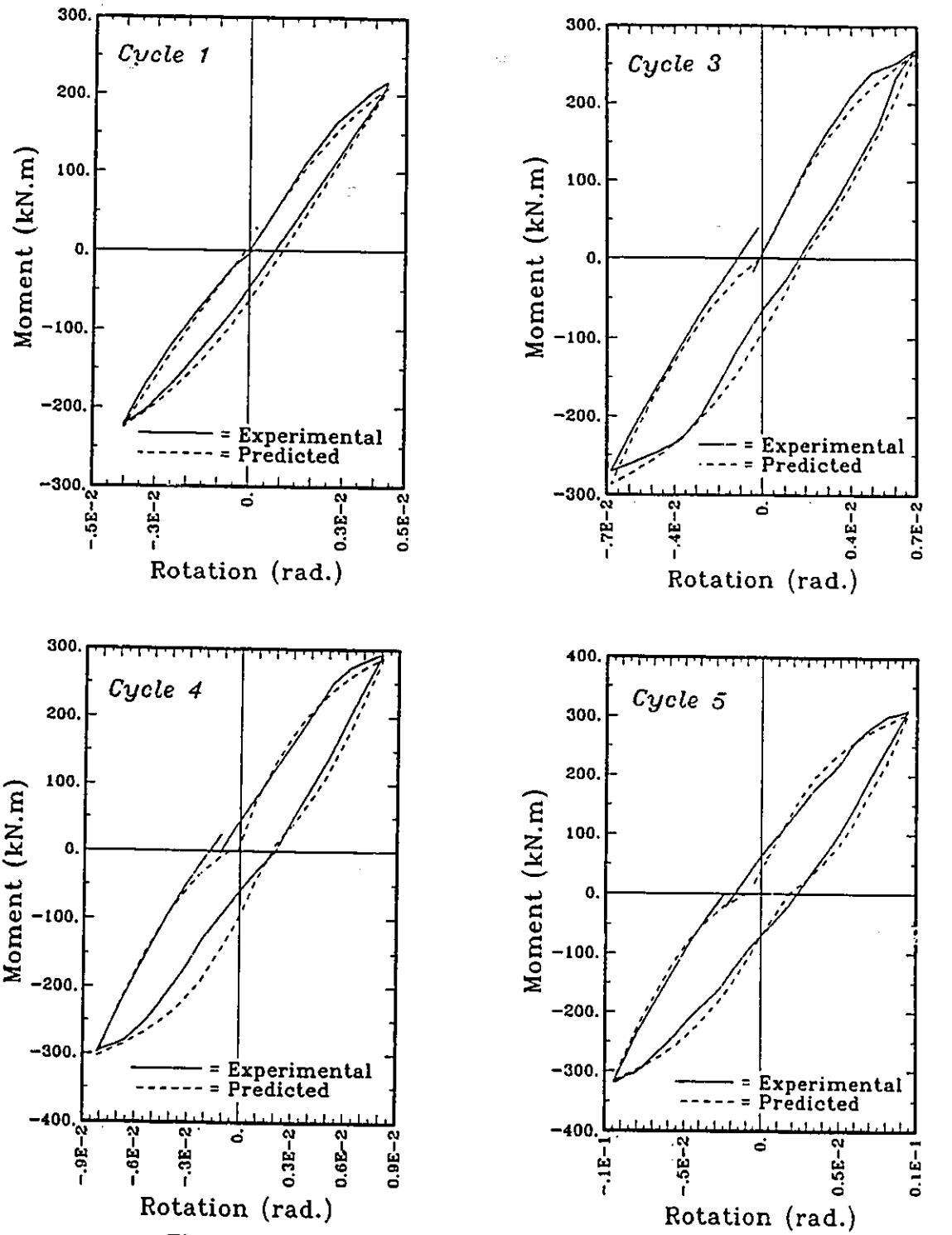

Fig. 3.15 Experimental vs. predicted hysteretic moment–rotation curves for specimen B-2.

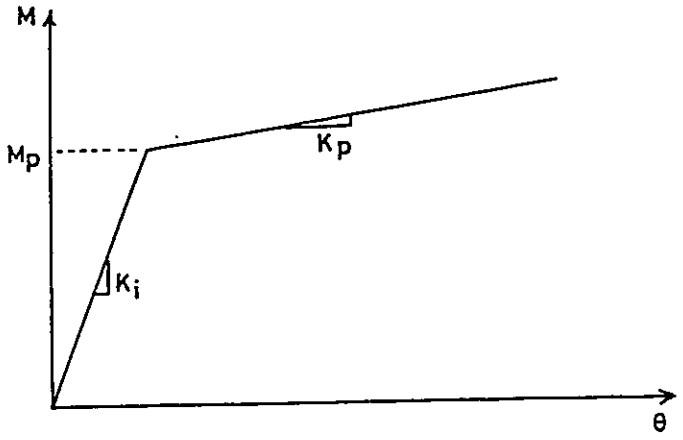

(a)

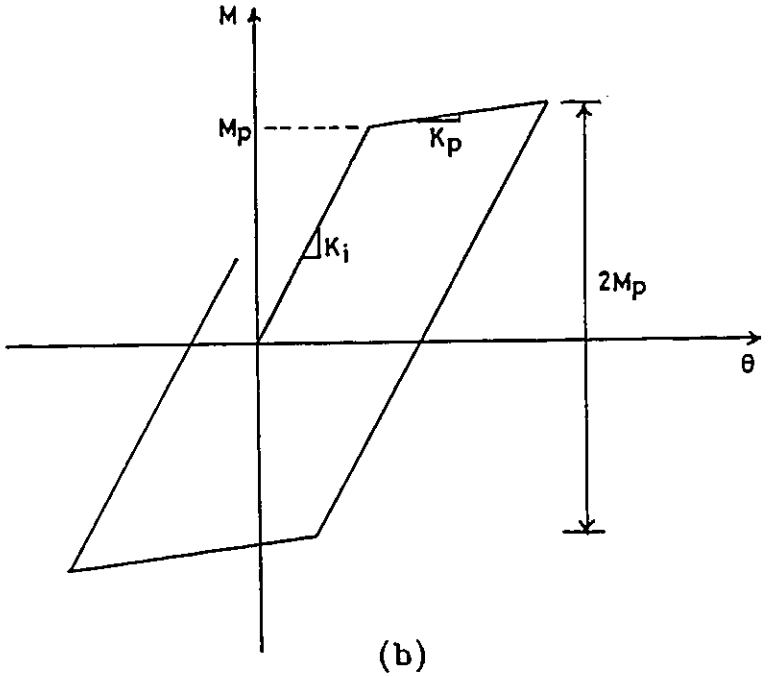

(b)

Fig. 3.16 Moment–rotation simple model
a) Monotonic ; b) Cyclic

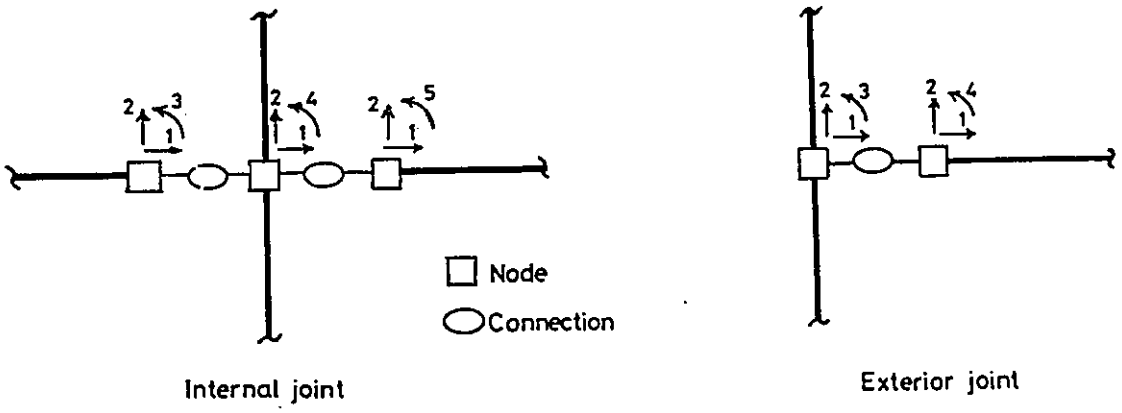

Fig. 3.17 Idealization of the semi-rigid connection element.

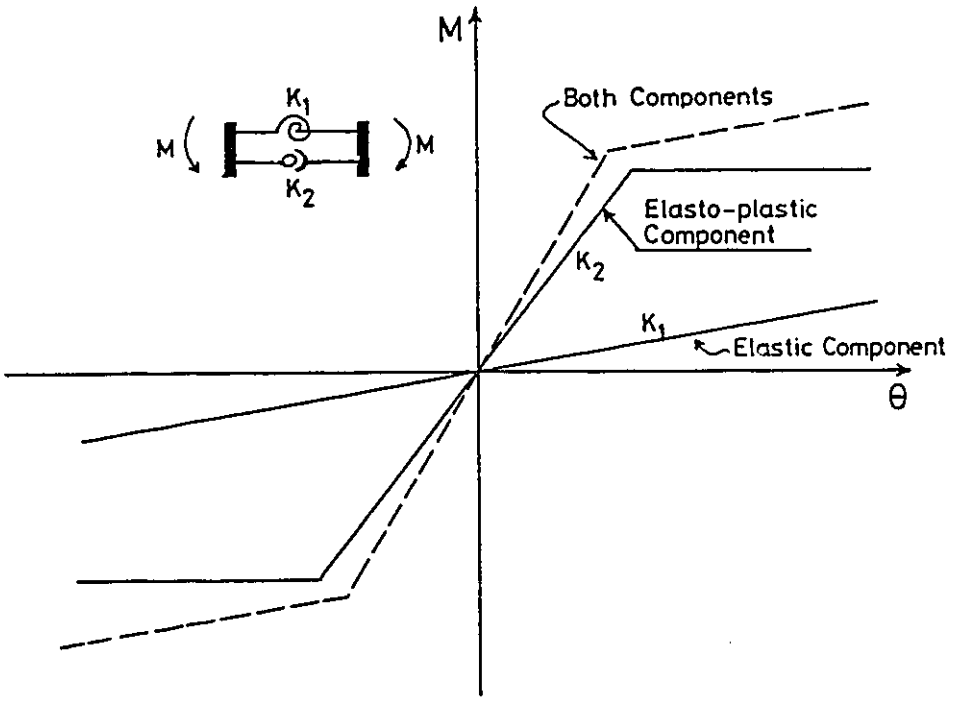

Fig. 3.18 The connection element components.

CHAPTER 4

BEHAVIOUR OF EXTENDED END-PLATE PANEL JOINTS

4.1 Introduction

Current design specifications for steel structures in seismically active areas (UBC ,1988 ; CAN3-S16.1-M89, 1989) recommend that, the joints' panel zones in ductile MRFs be designed to participate efficiently with the beams in dissipating the earthquake input energy. As a result, a design criterion for detailing the panels was introduced. It is recommended that the panel zones be designed to yield and undergo sufficient inelastic deformation (more than $4\gamma_y$, where γ_y is the panel average shear strain at yield) prior to the yielding of the beams. In establishing such a criterion, the experimental results reported by Bertero et al.(1972) and Krawinkler and Popov (1982) were taken as the basis. The tests were conducted on beam-to-column subassemblages utilizing fully welded connections or connections with beam flange welded and beam web bolted. No attempt was made to investigate the implication of adopting such a design approach when other connecting media such as extended end-plate connections are employed. In this case, the proposed design criterion may not be able to represent the actual joint behaviour as can be noted from examining Fig.4.1. The figure shows the deformed shapes of the panel zones when both fully welded and extended end-plate connections are employed. According to the deformed shape plots, the end-plate has to deform in order to allow for panel deformation, i.e the end-plate flexural stiffness contributes to the panel zone shear resistance. Thus, direct application of the current design approach for such a joint type is expected to result in underestimating the panel zone shear resistance. The result will be reduction in the panel zone ability to dissipate energy and the requirement that most of the energy dissipation occurs in the beams. The significance of this design on the panel zone response is not known and further investigation is

needed.

Another important aspect that needs to be studied is the effect of the panel zone flexibility on the overall response of the subassemblage.

In the second phase of the experimental study, four full scale beam-to-column subassemblages representing parts of a typical MRF, were tested under a cyclically controlled displacement program. The behaviour of the subassemblages and their individual components were investigated with special emphasis on studying the response of the panel zones in the tested subassemblages.

4.2 Description of subassemblages

Four exterior joint subassemblages were selected for testing. The joints were designated as CB-1, CC-1, CC-2 and CC-3. Each specimen consisted of a single column 2800 mm long with a cantilever beam on one side of the column at its mid-height. The length of the cantilever beam was taken to be 2300 mm, measured from the point of load application to the centre line of the column. The material used for all the specimens was in accordance with CSA-G40.21-M300W steel. Tensile test coupons were cut from the sections used in the experiments to determine their mechanical properties as summarized in Table 4.1.

Specimen CB-1

This specimen was fabricated by fillet welding a W360X57 beam section to a 28 mm thick end-plate. Then, the end-plate was bolted to a W360X64 column section. Eight 25 mm diameter, grade ASTM A490M bolts were used to fasten the end-plate to the column flange. Continuity plates, 9 mm thick, were provided to stiffen the column flanges. In this specimen, the panel zone was designed to be the weakest element in the subassemblage. As a result, the specimen behaviour was expected to be dominated by that of the panel zone. Details of the test specimen are shown in Fig.4.2.

Specimen CC-1

Specimen CC-1 was fabricated by welding a W410X60 beam section to a

28 mm thick end-plate. A W310X129 section was used for the column. As in the case of specimen CB-1, four 9 mm thick continuity plates were used to stiffen the column flange. The flanges and web of the beam were welded to the end-plate using 12mm and 6mm fillet welds, respectively. The panel zone was expected to yield at approximately the same load as the beam. Thus, the participation of both the beam and the panel zone during inelastic action could be expected. The overall fabrication details of the specimen are shown in Fig.4.3.

Specimen CC-2

Specimen CC-2 was designed to be similar to specimen CC-1, except that a 9 mm thick plate was all around welded to the column web at the panel zone area to increase the panel shear capacity. The result was a relatively strong panel. The behaviour of this specimen was expected to be dominated by the behaviour of the beam. This specimen was intended to provide necessary information on the effectiveness of shear reinforcement in resisting panel zone deformation. Fabrication details of the specimen are shown in Fig.4.3.

Specimen CC-3

In specimen CC-3, the beam section was welded to a 22 mm thick end-plate stiffened by two 9 mm thick small triangular plates. This connection detailing is effective in reducing the design thickness of the end-plate. The beam and column sections used were identical to those used in specimen CC-1. Both the panel zone and the beam were expected to yield at the same load. The details of this specimen are shown in Fig.4.3.

In all specimens, the bolts used were 25 mm diameter, grade ASTM A490 M. Direct Tension Indicating washers (DTI) were used to check the achievement of the minimum bolt Pre-tension forces required by the code (CAN3-S16.1-M89).

4.3 Test setup

The experimental setup previously discussed in chapter 2, was modified to accommodate the subassemblages so that an axial load could be applied to the

column while the beam was being loaded in bending. A schematic illustration of the test setup with one of the test specimens installed, is shown in Fig. 4.4. The test specimen is shaded for clarification. A photograph for the test arrangement is shown in Fig.4.5.In this setup, the reaction frame was used to brace the test fixture in order to minimize the lateral movement of the upper hinge support. The bottom hinge support was fastened directly to the test floor. Similar to the case in chapter 2, a hydraulic actuator was used to apply cyclic controlled displacement to the beam-tip. A 2000 kN jack was used to apply an axial force to the column top. A couple of angles were used to laterally brace the beam at its end to prevent lateral out-of-plane movement.

4.4 Instrumentation

The instrumentation of the specimens was designed to determine the applied loads, the deformation of various components, and the internal stresses in the specimens. Typical instrumentation mounted on one of the specimens is shown in Fig.4.6.The applied beam tip displacements were controlled by a cable LVDT, and the corresponding loads were measured by a special load cell mounted on the actuator rod. The applied axial load on the column was monitored by a load cell at its top. LVDTs were installed diagonally over the panel zone to measure the average panel zone deformation. Another group of LVDTs was used to measure the rotation of the connection. Strain gauges were mounted on the column flanges to determine the forces in the column. Rosettes glued to the panel zone were used to determine the shear stress distribution and to monitor the progress of plastification in the panel zone. An Autodata 9 data acquisition system was used to scan the data from the instrumentation and record it onto a computer disk for later processing and plotting.

Before each test, the specimens were whitewashed or stress coated to visually observe yield patterns that might develop during loading.

4.5 Loading sequence

In each experiment, a controlled cyclic displacement program was adopted

for testing. The displacement program consisted of 12 to 14 cycles. The first two cycles were elastic to check the instrumentation and to determine the elastic properties of the subassemblages. Following these two cycles, another two cycles of amplitude Δ_y were applied, where Δ_y is defined as the displacement required to initiate yielding of the beam. This value was determined theoretically prior to the tests using the section properties, a nominal yield of 300 MPa, and assuming infinitely rigid panel zones and connections. For the following 8 cycles, the displacement was increased by $\Delta_y/2$ for each cycle. Then, for the last two cycles increments of Δ_y were applied. The loading program is show in Fig.4.7.

4.6 Experimental results

For each test, the maximum attained load, the initiation of yielding and the ultimate inelastic deformation of the beams and panel zones, were recorded. The hysteretic behaviour of each specimen and that of its individual components were also documented. More results can be found in Osman et al (1991c). The failure modes were recorded as will be presented for each test case.

Specimen CB-1

Twelve displacement cycles were applied to the beam tip as shown in Fig.4.8 while a constant axial force of 600 kN was applied to the column. This axial force corresponds to 25% of the column yield axial load calculated on the basis of a nominal yield stress of 300 MPa. The overall behaviour of the connection, represented by the beam tip load versus the beam tip deflection, is shown in Fig.4.9. Examining this figure shows that the specimen yielded during the third cycle (downward loading) and yielding was initiated in the panel zone. During yielding of the panel zone, the theoretically calculated average shear stress was equal to .87 γ_y , where γ_y is the yield stress in shear of the web material given by the Von Mises yield criterion. It is believed that this early web yielding is attributed to the presence of the axial force.

The applied moment versus the measured average panel zone shear strain, is shown in Fig.4.10. As can be observed, the panel zone was completely plastified

during the fifth cycle (downward loading). Following the panel's complete plastification, the panel web buckled. However, strength deterioration did not result due to the formation of a diagonal tension field in the panel zone. Further loading resulted in progressive increase in the strength of the panel due to strain hardening. The progress of plastification throughout the panel zone was studied from the readings recorded by the rosettes glued to the panel. The measured shear strain contours for different loading conditions during the third cycle are show in Fig.4.11.

During the test, the beam yielded in the eighth cycle as noted from the strain gages mounted on its flanges. However, due to the weakness of the panel, the beam's participation in the inelastic action was minimal. Observed behaviour as noted by Fig.4.9 and Fig.4.10, shows that the overall behaviour of this specimen was dominated by the behaviour of its panel as would be expected in the case of a weak panel zone. As for the connection behaviour, yielding was observed during the third cycle while a yielding mechanism was clearly evident in the column flange during subsequent cycles. When a high ductility level was reached, the test was terminated. A photograph of the joint area at the end of the test is shown in Fig.4.12. Severe buckling of the panel web is apparent. In this test, the maximum recorded beam tip load was 175 kN at a beam tip displacement of 145 mm.

Specimen CC-1

A total of 14 displacement cycles was applied to the beam tip as shown in Fig.4.13. Again, an axial force of 600 kN was applied to the column, which in this case corresponds to 12% of the yield axial load of the column. The results for the beam tip deflection versus the beam tip load are shown in Fig.4.14.

In this test, the panel zone yielded first as was observed from the flaking of the stress coat. Very soon thereafter, the beam yielded. The applied moment versus the average panel zone shear strain hysteretic behaviour for this specimen is shown in Fig.4.15. The yielding of both components,i.e the panel zone and the beam, occurred at approximately the same time because the theoretically calculated load required to yield the two components, was the same. This close yielding gave both components a chance to participate in the inelastic action. No signs of web panel

buckling were evident throughout the loading history. At later stages of testing, the beam flange slightly buckled but this slight buckling did not cause any deterioration in the specimen's strength. The maximum load attained during the test was 250 kN at a beam tip displacement of 130 mm. The tested specimen is shown in Fig.4.16. Throughout the test, the shear strain at various locations in the panel zone was measured. These measurements are shown in Fig.4.17 as recorded by the rosettes. The rosette at the centre recorded the highest shear strain. Also, the shear strain decreases as we move away from the centre towards the corners.

Specimen CC-2

In this specimen, the panel web was strengthened by fillet welding a doubler plate around its perimeter on one side. With a 600 kN axial force acting on the column, twelve displacement cycles were applied to the specimen (Fig.4.18). The measured overall behaviour of the specimen represented by the beam tip load versus the beam tip deflection, is shown in Fig.4.19. As can be observed, deterioration of strength occurred near the final stages of the test. The loss in strength can be explained by examining Fig.4.20 which shows the inelastic rotation of the beam versus the beam moment. It is evident that the beam experienced severe yielding at the final stage of the test with the occurrence of buckling of the beam's web and flanges. Buckling of the beam appeared to be the major cause of deterioration in specimen strength. Analysis indicates that strengthening the panel zone forced most of the inelastic action to occur in the beam, imposing high ductility demands on the beam and causing its instability. Meanwhile, the overall behaviour of the panel zone remained essentially elastic although local yielding did occur at the centre, as observed by strain rosette readings late in the experiment. The overall behaviour of the panel is shown in Fig.4.21.

To determine the effectiveness of the doubler plate, several rosettes were glued to both the panel web and its stiffening plate at similar locations. The responses of the two rosettes mounted at the centres of the panel web and the doubler plate and another two glued at the corner of the panel are shown in Figs.4.22 and 4.23, respectively. These figures show that the doubler plate

experienced roughly the same amount of inelastic action as the panel web. On this basis, it can be concluded that the assumption of full participation of the doubler plates in resisting the shear deformation of the panel zone is quite reasonable. The condition of the specimen after the test is shown in Fig.4.24. Flaking of the whitewash on the beam's web and flanges shows that severe yielding of the beam occurred. Also to be noted is that the panel retained its whitewash thus indicating little or no panel participation in the inelastic action that took place. The maximum load reached in this test was 250 kN at a beam tip deflection of 115 mm.

Specimen CC-3

This specimen was similar to specimen CC-1 except for the different detailing of the connection. In this test specimen, a triangular plate was used to stiffen the end-plate. This modification proved to be effective in reducing the thickness of the end-plate (Chapter 2). The specimen was subjected to 12 displacement cycles as shown in Fig.4.25 and a 600 kN axial force. Figures 4.26 through 4.29 show the beam tip load versus the beam tip deflection , the applied moment versus the average panel shear strain, the beam moment versus the connection rotation and the beam moment versus the beam inelastic rotation, respectively. Similar to specimen CC-1, the beam and the panel zone participated effectively through inelastic action and the connection behaved well. It is evident from the figures that the specimen components provided excellent energy dissipation properties. The hysteresis loops continued to expand throughout the course of the loading history. Gauges mounted on the end-plate stiffeners showed that they yielded in tension and in compression as shown in Fig.4.30. The condition of the specimen after the test is shown in Fig.4.31. Flaking of the whitewash on both the beam and the panel zone indicates that the beam and the panel web underwent significant inelastic action. It can also be observed that the beam's bottom flange buckled severely. However, this buckling did not cause any strength deterioration since it was not accompanied by beam web buckling. The maximum load reached in this test was 260 kN at a beam displacement of 140 mm.

4.7 Discussion of test results

All of the specimens carried loads well above the nominal yield strength of the cantilever beams. This can be seen from the experimental skeleton curves for the load-deformation relationship shown in Fig.4.9, 4.14,4.19 and 4.26. Also, from these figures, the connection and panel zone yielding limits based on a nominal yield strength of 300 MPa are noted.

In specimen CB-1, the yielding was mainly confined to the panel zone with little indication of beam yielding. The strength of this specimen was primarily governed by the strength of the panel zone. In this specimen the panel zone went through several severe inelastic strain reversals. A high ductility ratio of the panel was observed (more than 30). Even though the panel web buckled, no deterioration in the panel strength was observed due to the formation of a diagonal tension field.

In specimens CC-1 and CC-3, better behaviour was observed. In these specimens both the panel zone and the beam participated in the inelastic action because both components yielded at approximately a load of about 170 kN as illustrated from Figs.4.14 and 4.26. An improved distribution of energy dissipation resulted between the beam and the panel zone.

In the case of specimen CC-2, deterioration in the specimen strength was observed because of severe buckling of the beam. This local buckling occurred due to the high demand imposed on the beam as a result of stiffening the panel zone. Although, the panel zone participated in dissipating the input energy during the later loading stages, the panel's high shear strength confined most of the inelastic action to the beam.

On the basis of the above observations and results, it seems that designing both the beam and the panel zone to participate efficiently in dissipating the earthquake input energy while the connection undergoes local plastification, is the appropriate approach for designing the bolted joints to sustain severe earthquake loading.

4.7.1 Components of deflection

The contribution of the specimens' components to the overall deflection of the subassemblages was determined from measured data. The influence of the panel zone deformation on the overall behaviour of specimen CB-1 was found to be dominant. Approximately 65% of the total deformation resulted from the panel zone deformation. In the case of specimens CC-1 and CC-3, equal contributions from both the beam and the panel zone to the total deformation were observed. In the case of specimen CC-2, the influence of the beam on the total behaviour was found to be dominant. As an example of the results, the contributions of the column, panel zone, beam and connection to the overall deformation of specimen CC-3 is illustrated in Fig.4.32. In this figure, the contributions of the various components of the specimen to the beam-tip deflection are plotted with the applied load. The connection elements which include the end-plate, bolts and the column flange contributed very little to the total deformation of the joint. The contributions of the beam and panel zone were about equal. These contributions were consistent throughout the elastic and inelastic ranges of behaviour as a result of yielding of the beam and panel zone commencing at approximately the same time.

4.7.2 Energy dissipation capacity

The amount of energy dissipated by each component in the specimen versus the number of inelastic excursions is shown in Figs 4.33 (a,b,c,d). For specimen CB-1, about 80% of the total energy was dissipated by the panel zone. This shows the high demand that is imposed on the panel zone when it is designed to be the weakest element in the specimen. In specimens CC-1 and CC-3, the energy dissipated was shared by the panel zone and the beam as shown in Figs.4.33(b) and 4.33(d). In both specimens about 33% of the total energy was dissipated by the panel with the remainder dissipated by the beam and the connection. In the case of specimen CC-2, the beam was the main energy dissipator because of the high strength of the panel. Severe damage to the beam occurred which resulted in reducing its ability to dissipate more energy. The amount of energy dissipated by each element in this

specimen is shown in Fig. 4.33(c).

The energy dissipation capability of the various components of a connection is dependent on their design. The designer may choose to have a weak panel zone, a strong panel zone or a panel zone and beam that yield about simultaneously. Requiring one component only to provide all the demanded ductility will result in severe damage to that component. The best performances, measured as high load carrying capacity and ductility levels, were found to be that for specimens for which the panel zone and the beam were allowed to yield together. The two components could share in providing higher load carrying capacity through strain hardening and higher ductility values by permitting large inelastic deformations. Meanwhile, the connection itself(end-plate, bolts and column flange), were required to remain elastic.

4.7.3 Response of panel zone

A careful study of the hysteretic curves for the applied moment versus shear strain relationships for the panels of the tested specimens revealed the following distinctive characteristics: 1) Every panel exhibited a high reserve strength beyond first yielding; and 2) The panels are very ductile elements with stable hysteretic behaviour. The hysteretic diagrams also show that the response of the panel is characterized by an elastic behaviour followed by a post-elastic response in which the rate of strain increases until it finally reaches a stage of constant strain hardening rate. This behaviour is similar to the behaviour observed in the case of panels of fully welded joints reported by Bertero et al. (1972). However, to investigate the effect of changing the type of connection on the response of the panels, the change of the panel shear was examined. The panel zone shear resistance of the tested specimens, V_p, were calculated using the equation recommended by the CAN3-S16.1-M89 (1989) and UBC(1988) codes and ignoring any shear resistance provided by the end-plates. The results are summarized in Table 4.2. These results were compared with those measured from the test, V_a . It should be noted that, the code equation gives the panel zone shear resistance at a distortion of approximately $4\gamma_y$ (where γ_y is defined as the panel average shear strain at yield). Thus, in determining V_a , the

strain of $4\gamma_y$ was used. As can be observed from the table, neglecting the shear resistance provided by the end-plate resulted in underestimating the panel shear strength by 17 to 40%. As such, if the panel for an extended end-plate joint is detailed based on the code equation, it will be stronger than anticipated and as a result will impose higher demands on the beams. This can have a damaging effect on the beams, especially in the case of thick end-plates. When the end-plate thickness was accounted for, together with the column flange thickness, V_{pc}, a 12% difference, was obtained when the predicted results were compared with the measured ones.

4.8 Summary

Based on this experimental study, the following observations are of importance:

1) The hysteresis curves of response for the four tested specimens were stable during their entire loading regimes with the exception of specimen CC-2 (with strengthed panel zone) which suffered deterioration in its strength at the end of the test due to severe beam buckling.

2) The panel zone is a very ductile element with high post-elastic strength that can undergo a large number of strain reversals without signs of distress.

3) Doubler plates that are directly fillet welded all around to the column web proved to be effective in increasing the shear capacity of the panels.

4) In the seismic design of MRFs, it appeared to beneficial to allow yielding to take place in the panel zone to reduce the demand on the beam and consequently prevent any local instability.

5) The end-plate participated effectively in controlling the inelastic deformation of the panel zone. This contribution resulted in up to a 40% increase in the panel's shear strength.

6) The panel and the connection can significantly affect the strength and the stiffness characteristics of the frames. In the analysis and the design of MRFs, their responses should be taken into account.

7) Direct application of the current design criteria for detailing the panel zones, may

be questionable when applied to connections other than the fully welded connections. This issue will be further addressed in Chapter 5.

Table 4.1 Mechanical properties of tensile coupons

Specimen No.	Coupon location	Yield stress (MPa)	Tensile strength (MPa)
CB-1	Beam web	346	530
	Beam flange	331	496
	Column web	360	538
	Column flange	327	528
CC-1	Beam web	359	535
	Beam flange	326	518
	Column web	333	507
	Column flange	300	494
CC-2	Beam web	391	595
	Beam flange	330	527
	Column web	354	526
	Column flange	319	518
CC-3	Beam web	357	536
	Beam flange	323	512
	Column web	326	502
	Column flange	333	495

Table 4.2 Panel shear strength

Specimen No.	Calculated panel shear V_p (kN)	Measured panel shear V_a (kN)	Predicted panel shear with end-plate V_{pc} (kN)	V_a/V_p	V_a/V_{pc}
CB-1	607	768	803	1.26	0.96
CC-1	940	1105	1266	1.17	0.87
CC-2	1557	1835	1903	1.18	0.96
CC-3	920	1298	1158	1.41	1.12

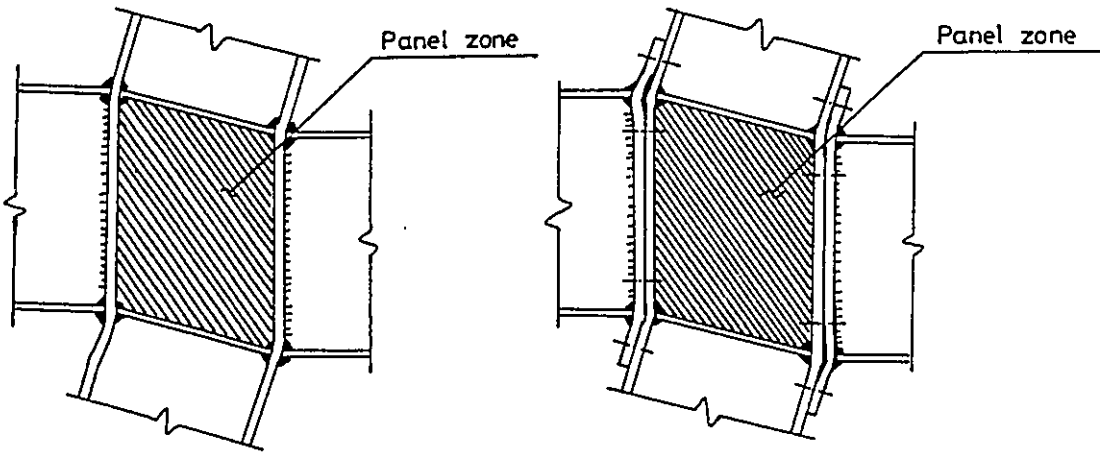

Fig. 4.1 Deformed panel zones.

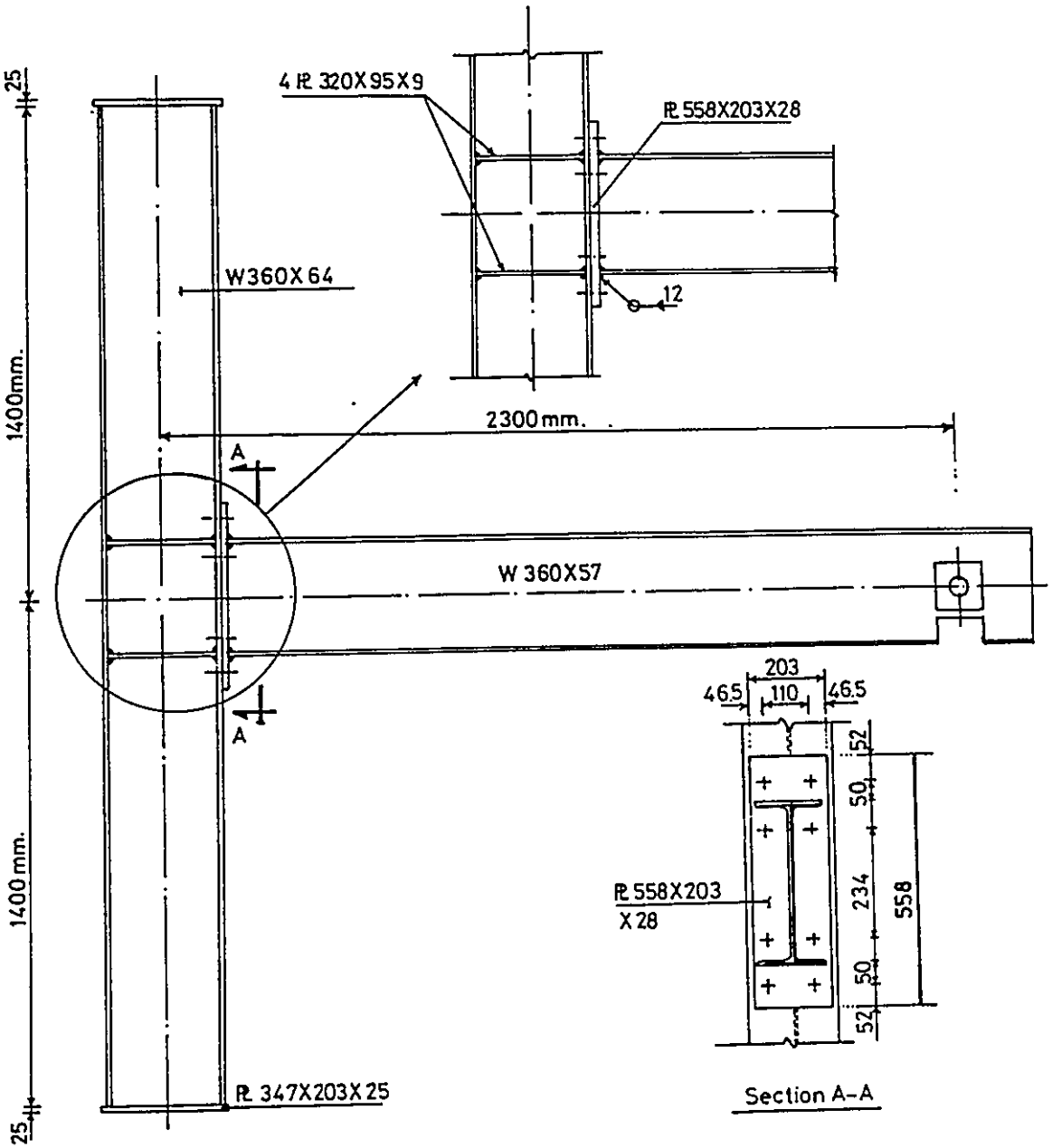

Fig. 4.2 Details of specimen CB−1.

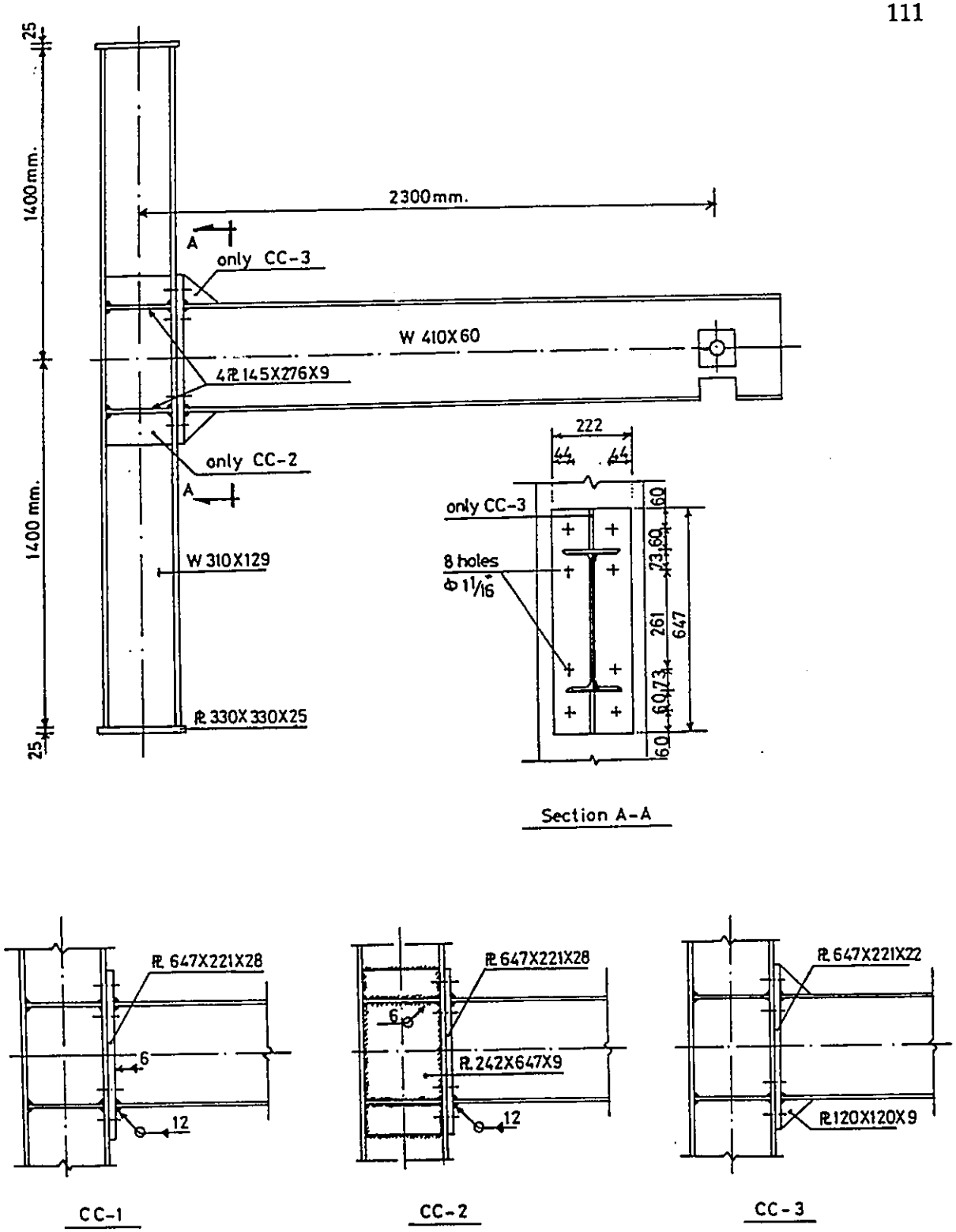

Fig. 4.3 Details of specimen CC-1, CC-2 and CC-3.

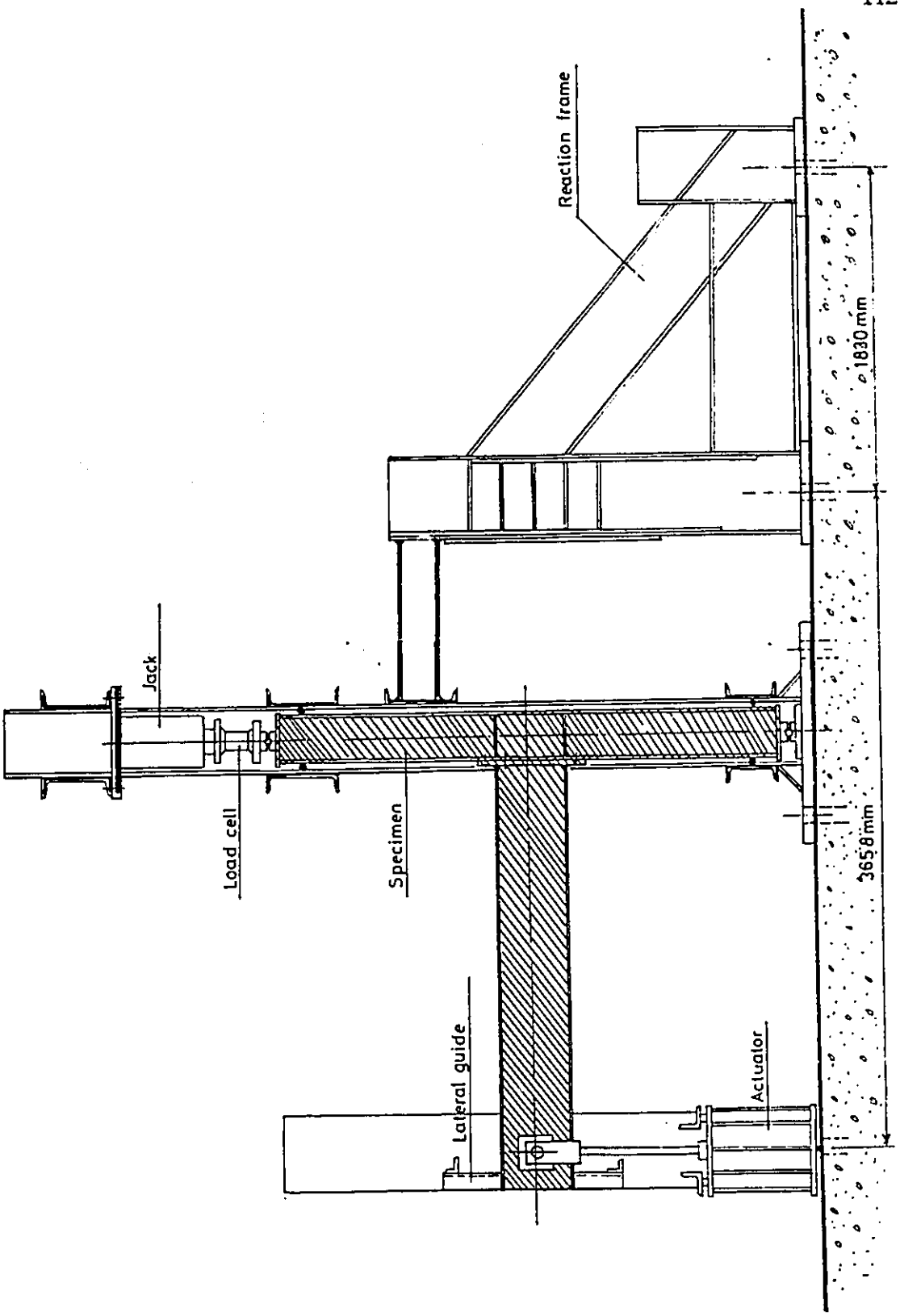

Fig. 4.4 Test setup

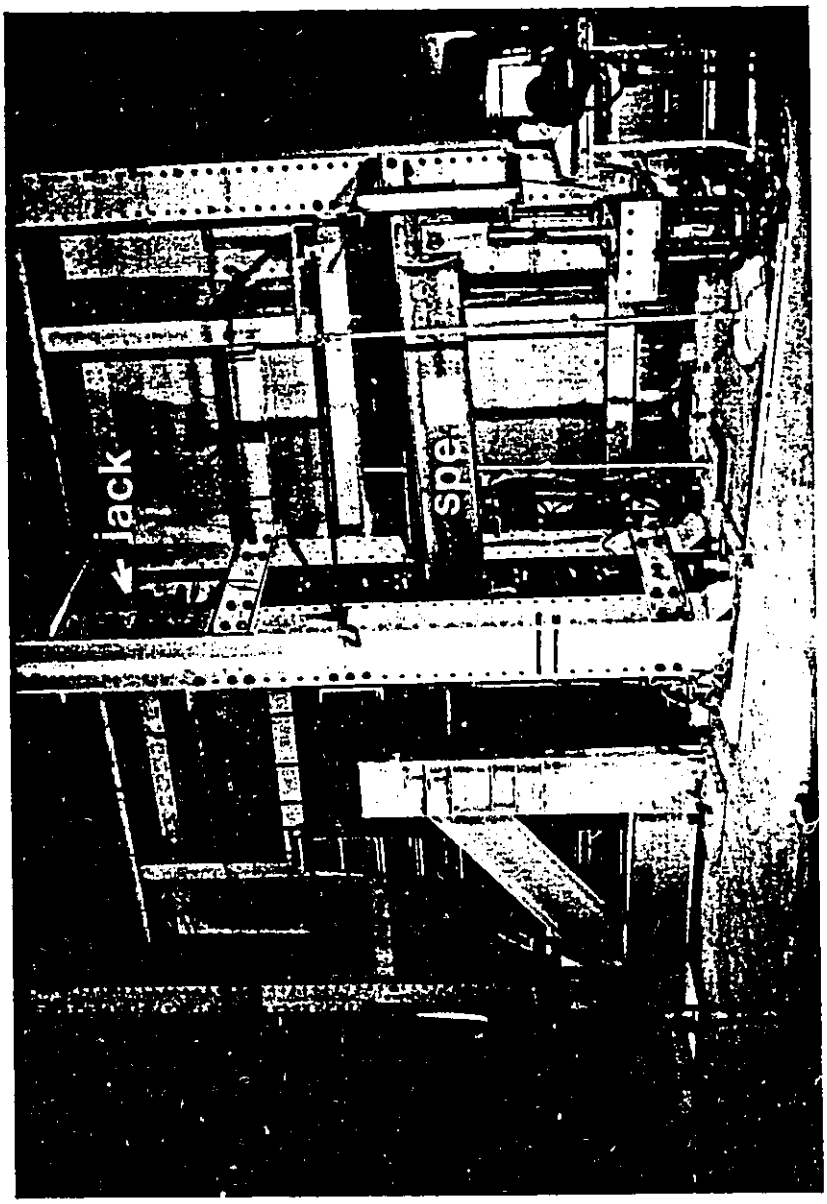

Fig. 4.5 Test arrangement.

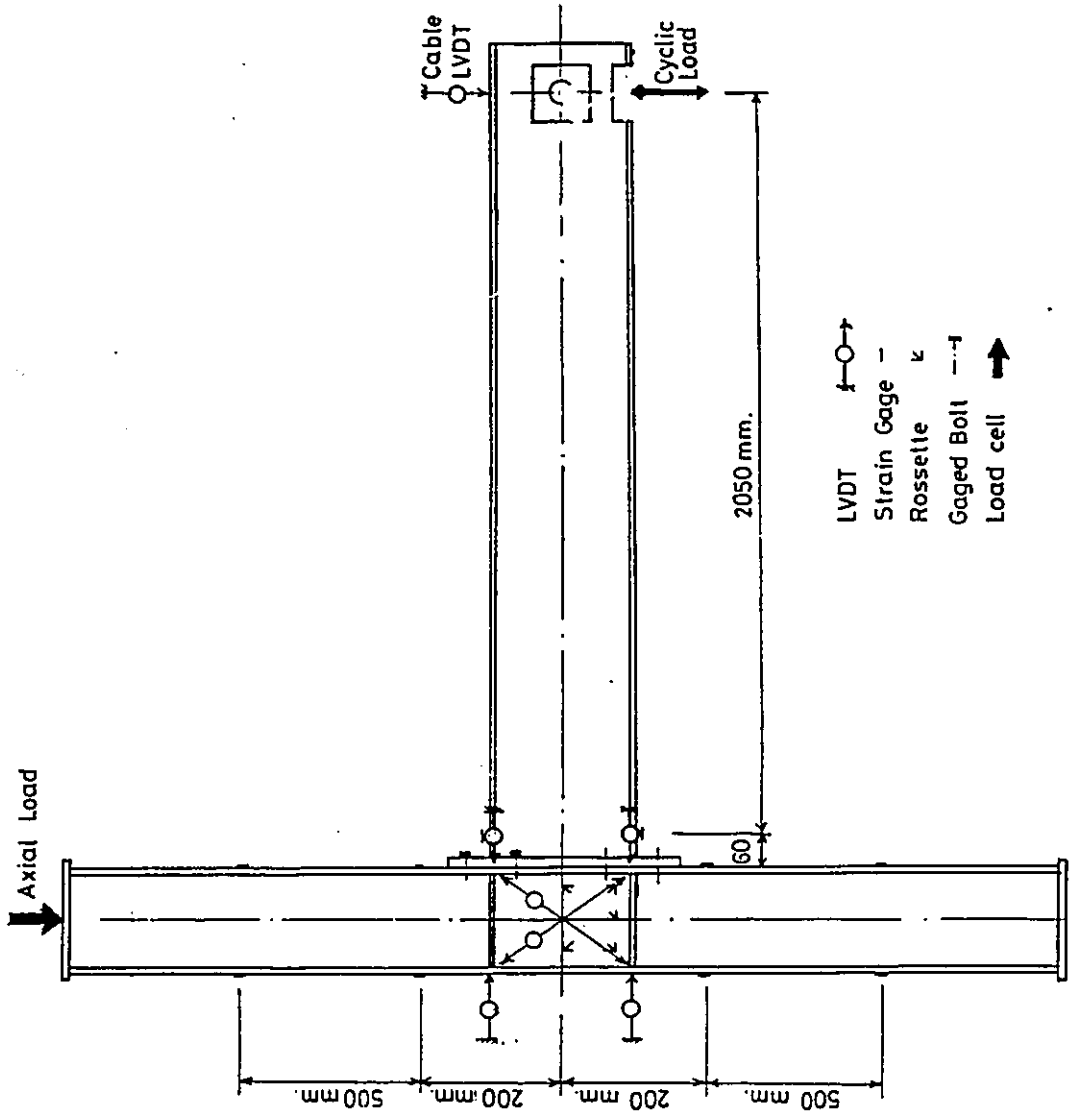

Fig. 4.6 Specimen instrumentation

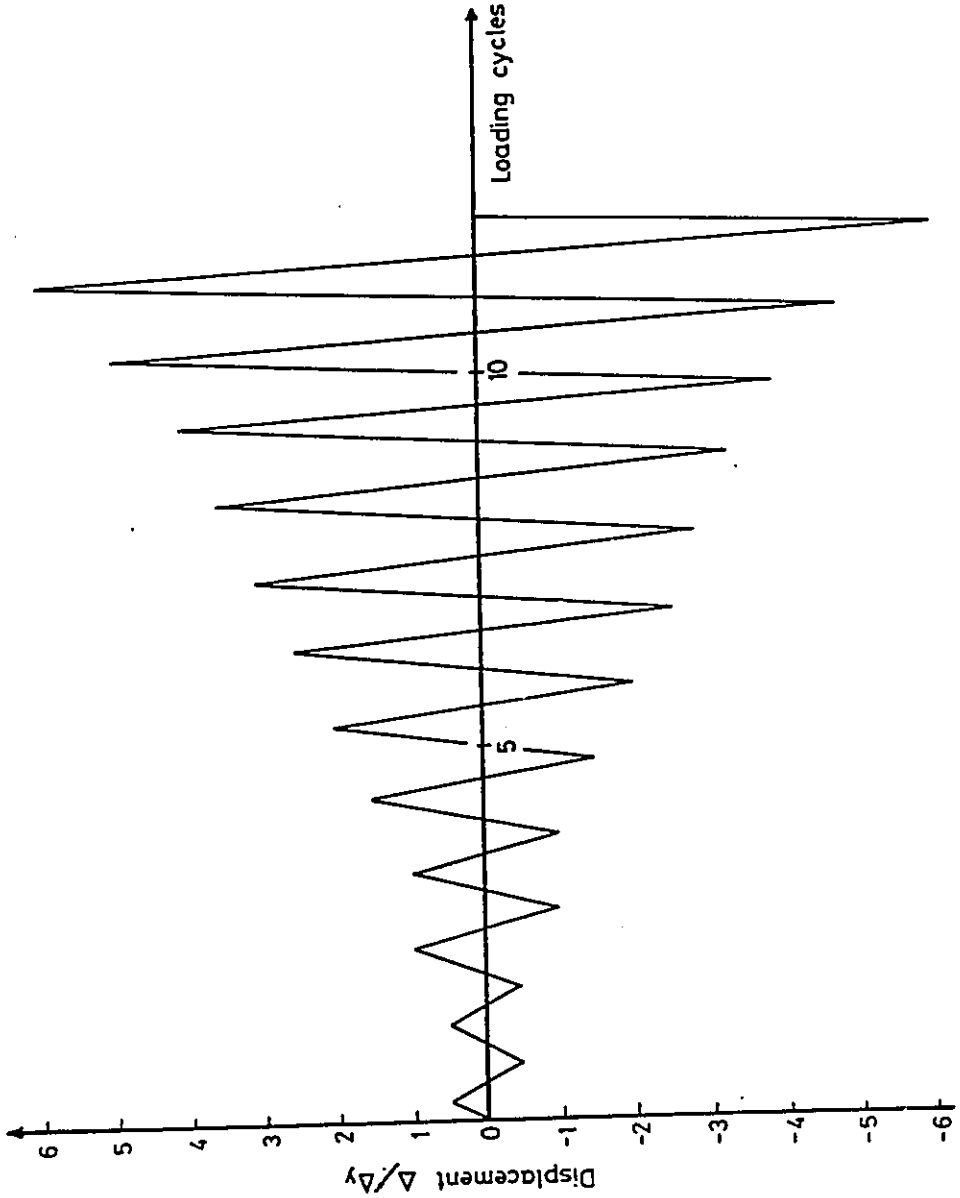

Fig. 4.7 Loading sequence

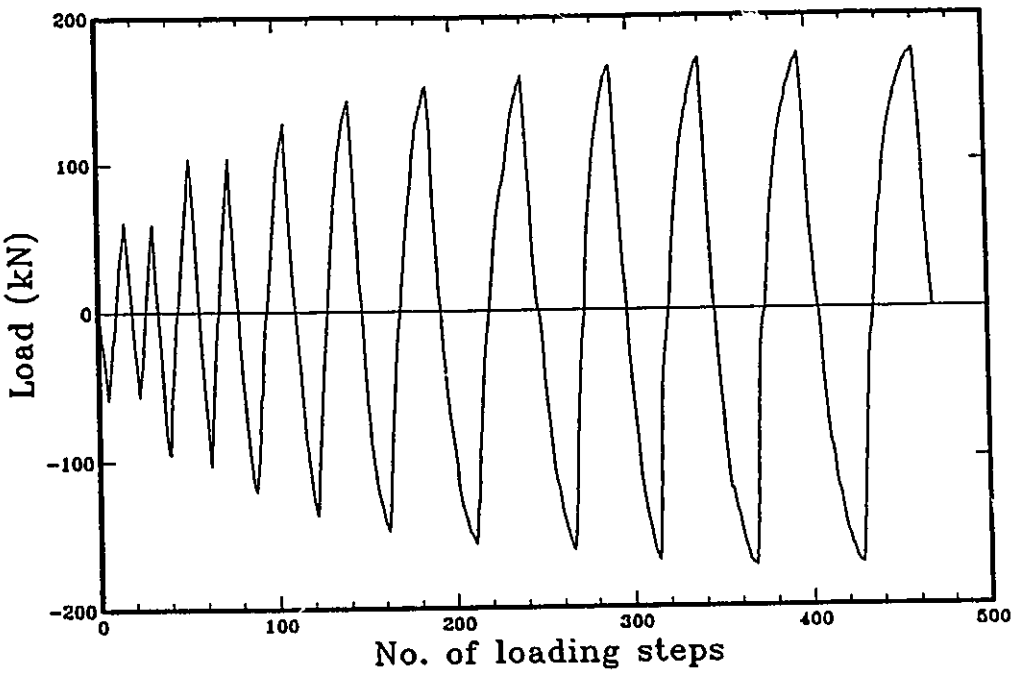

Fig. 4.8 Loading history for specimen CB−1.

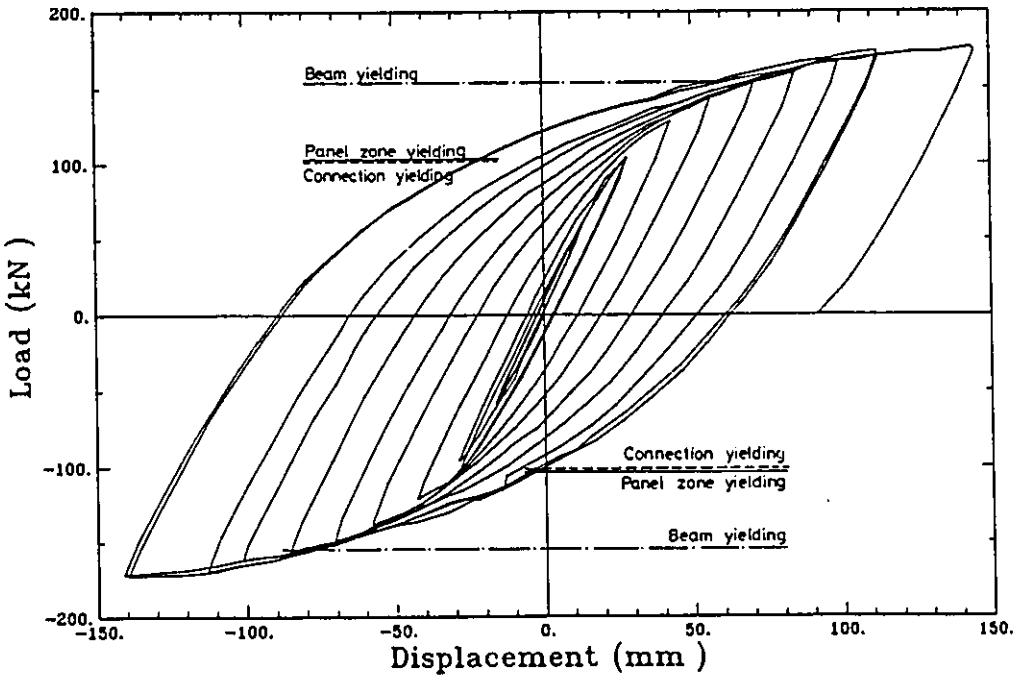

Fig. 4.9 Beam tip load−deflection relationship for specimen CB−1.

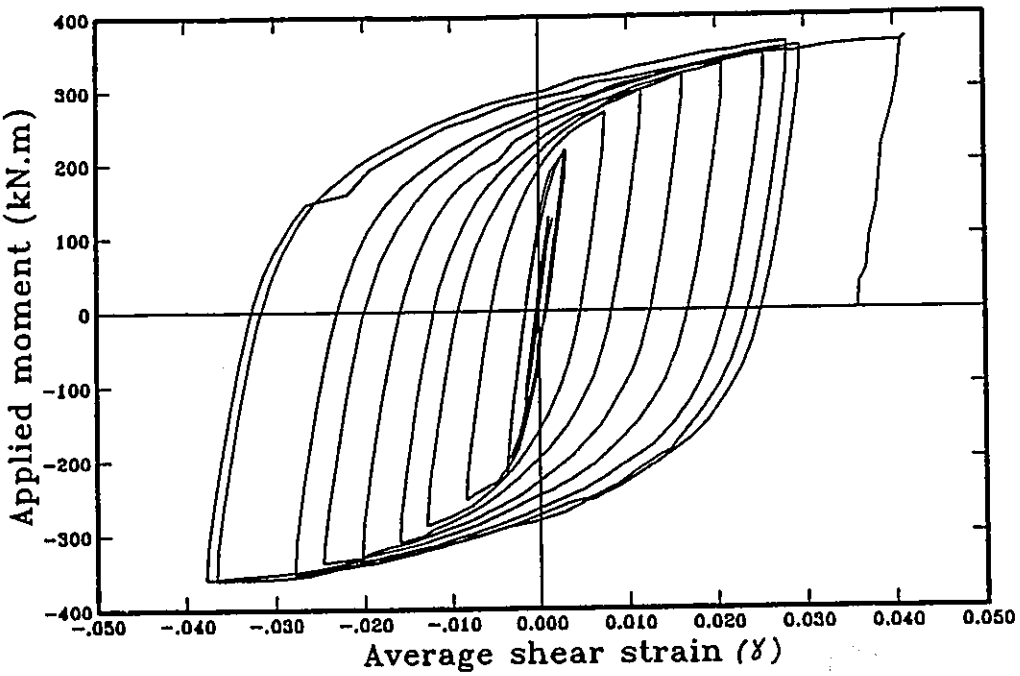

Fig. 4.10 Applied moment versus panel shear strain for specimen CB-1.

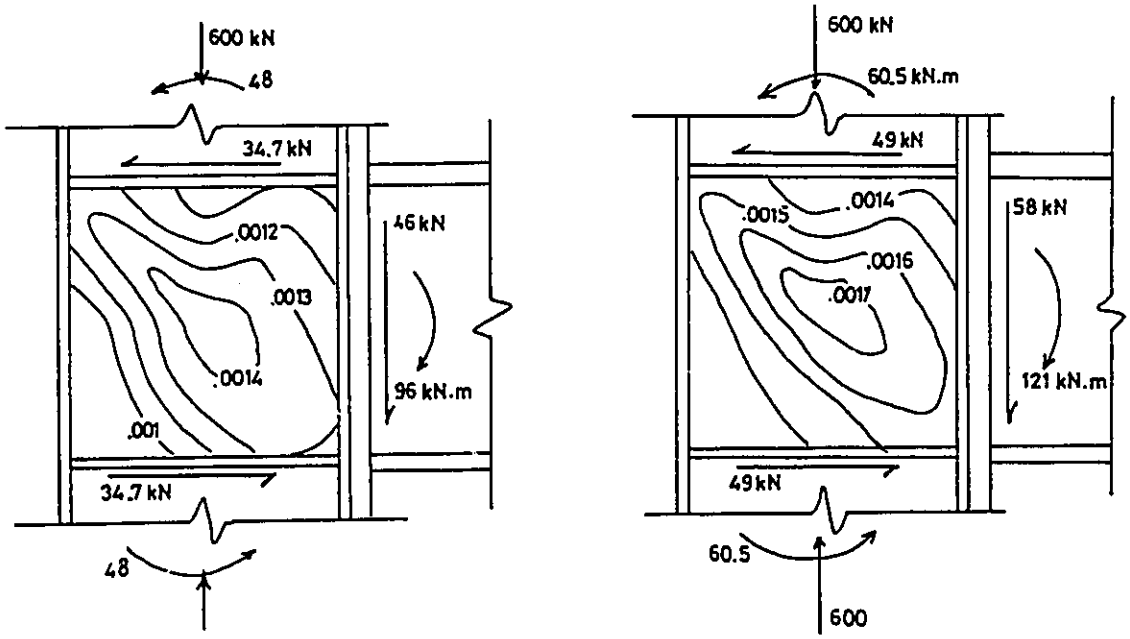

Fig. 4.11 Shear strain contours throughout the panel for different loading conditions.

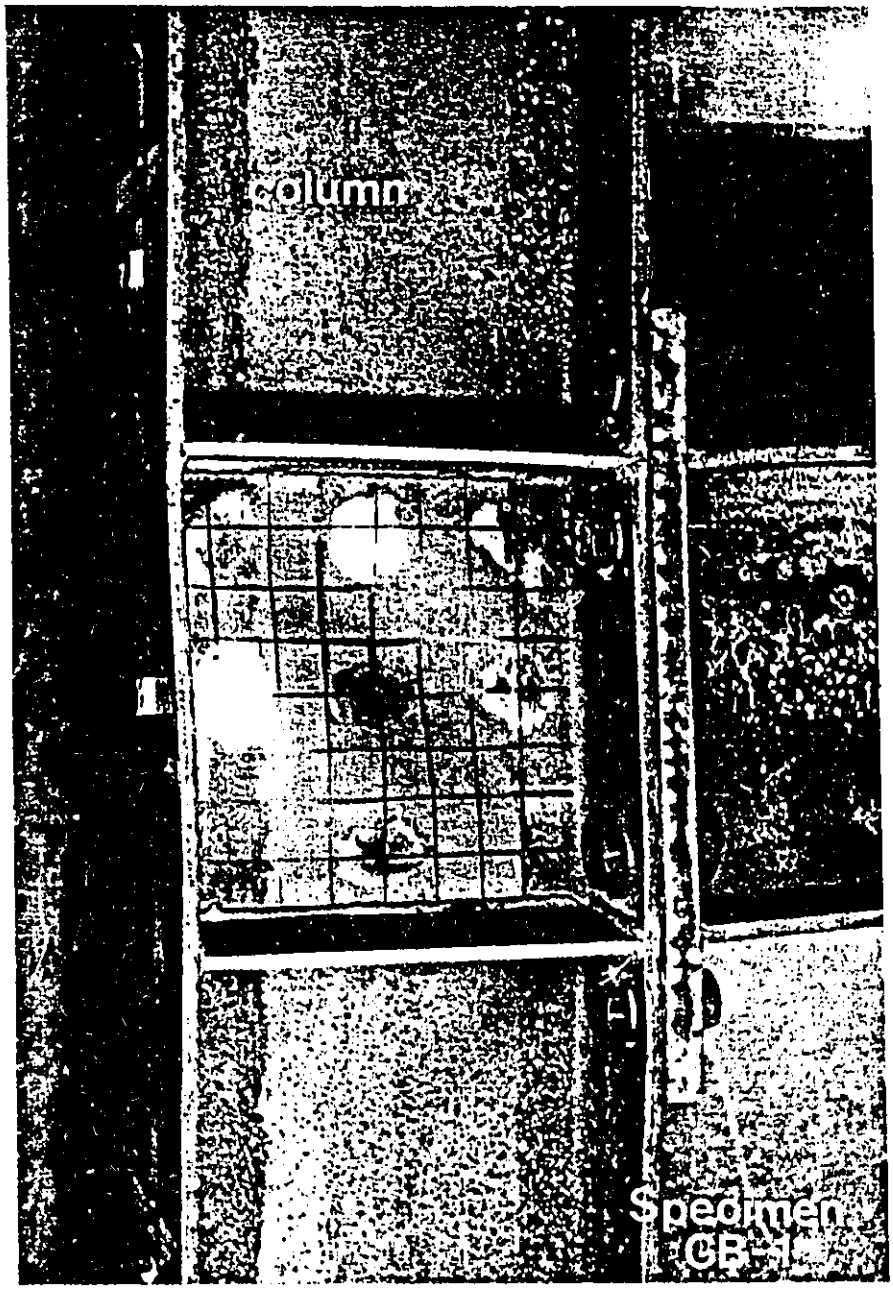

Fig. 4.12 Specimen CB–1 at failure.

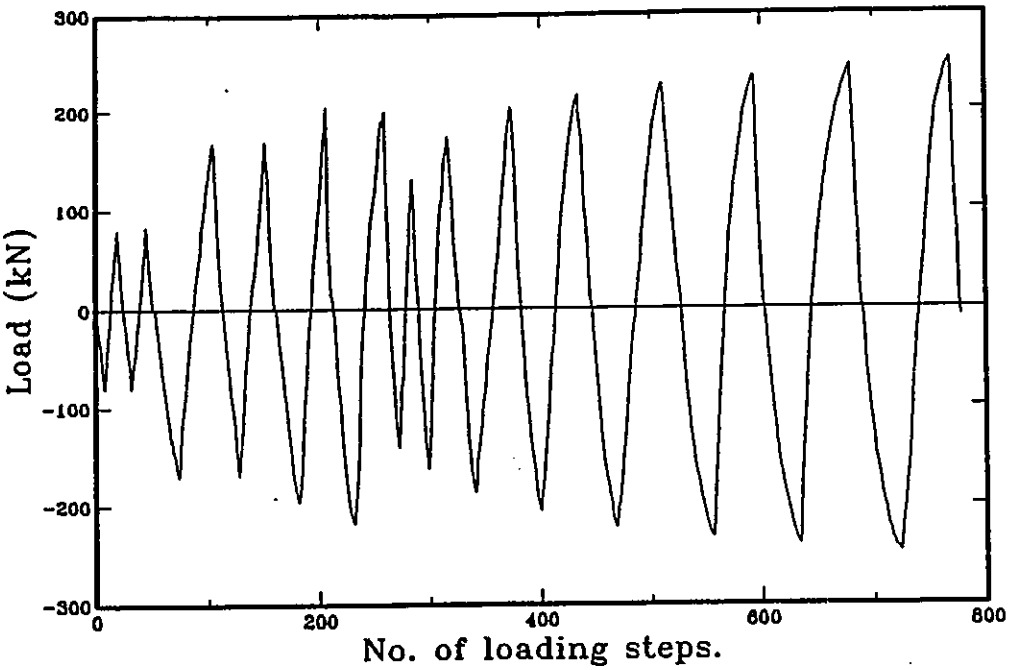

Fig. 4.13 Loading history for specimen CC-1

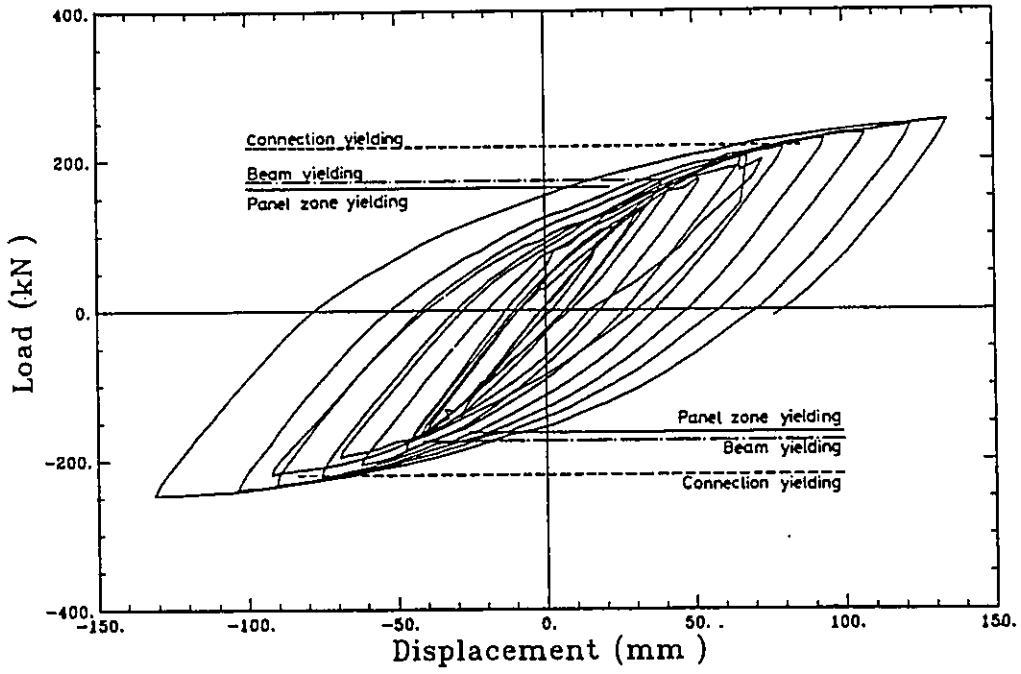

Fig. 4.14 Beam tip load-deflection relationship for specimen CC-1.

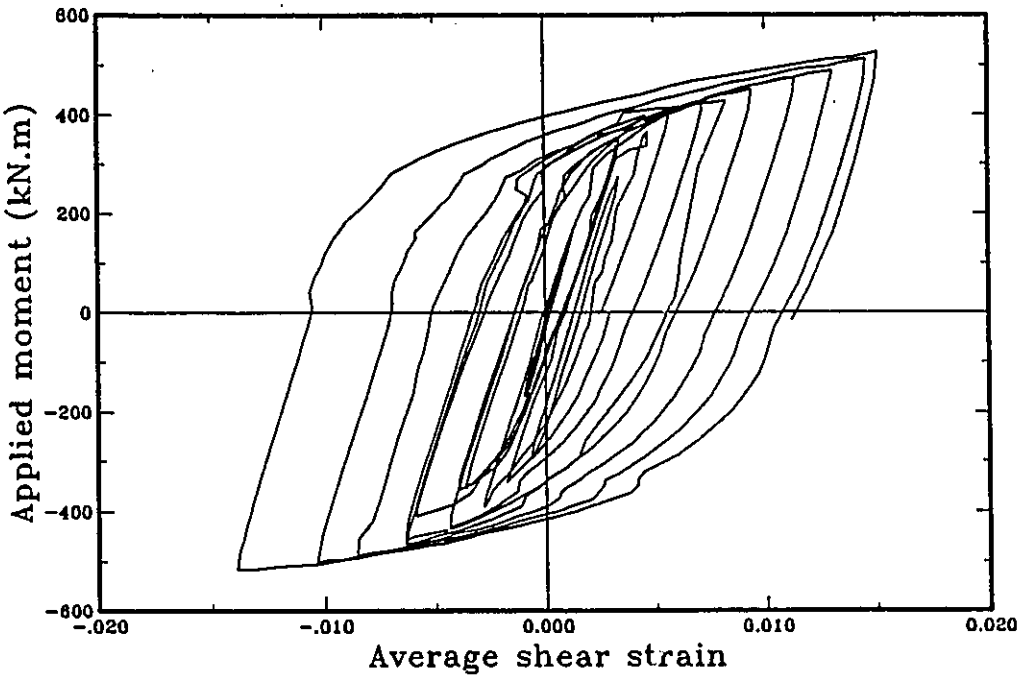

Fig. 4.15 Applied moment versus panel shear strain for specimen CC-1.

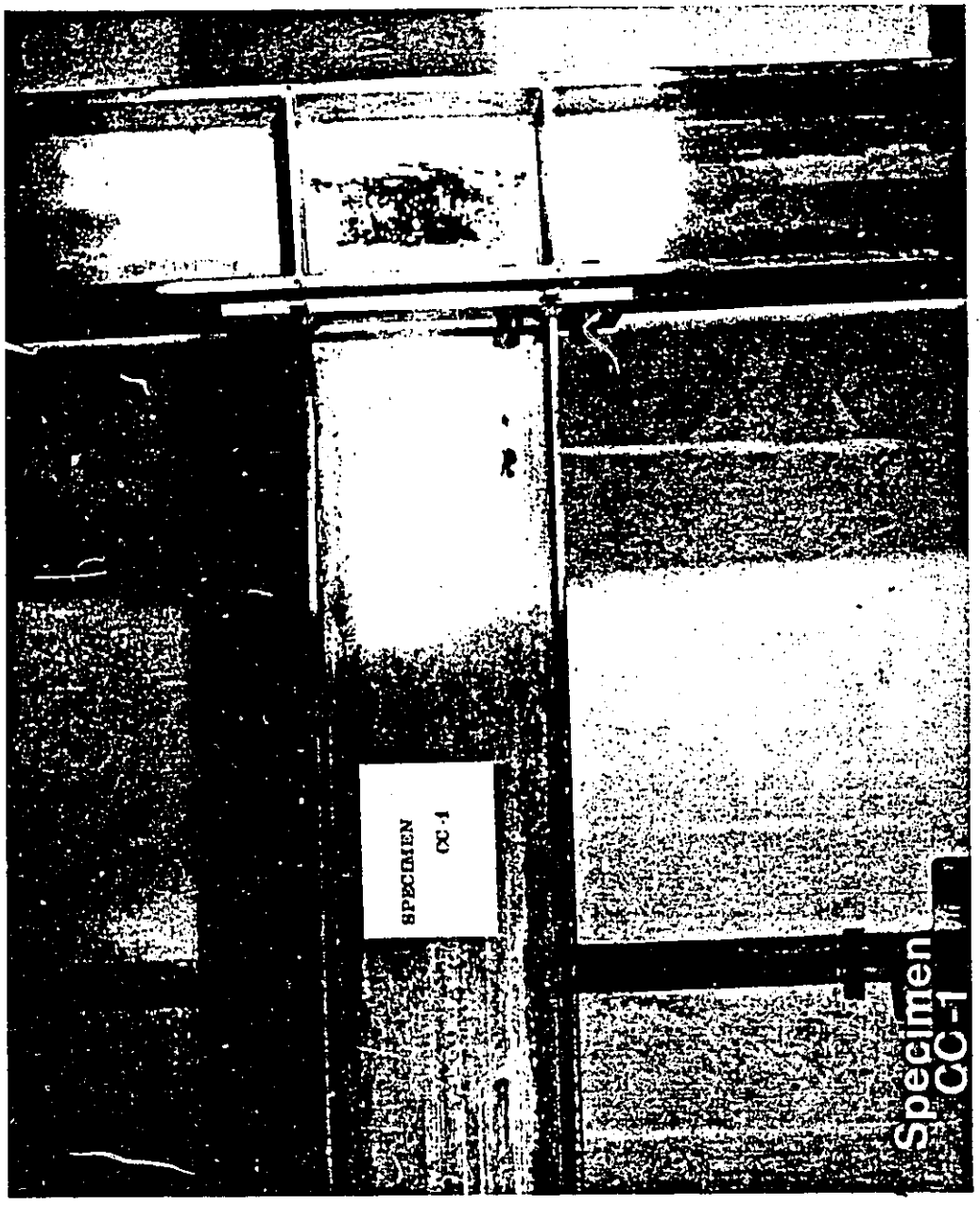

Fig. 4.16 Specimen CC–1 at failure.

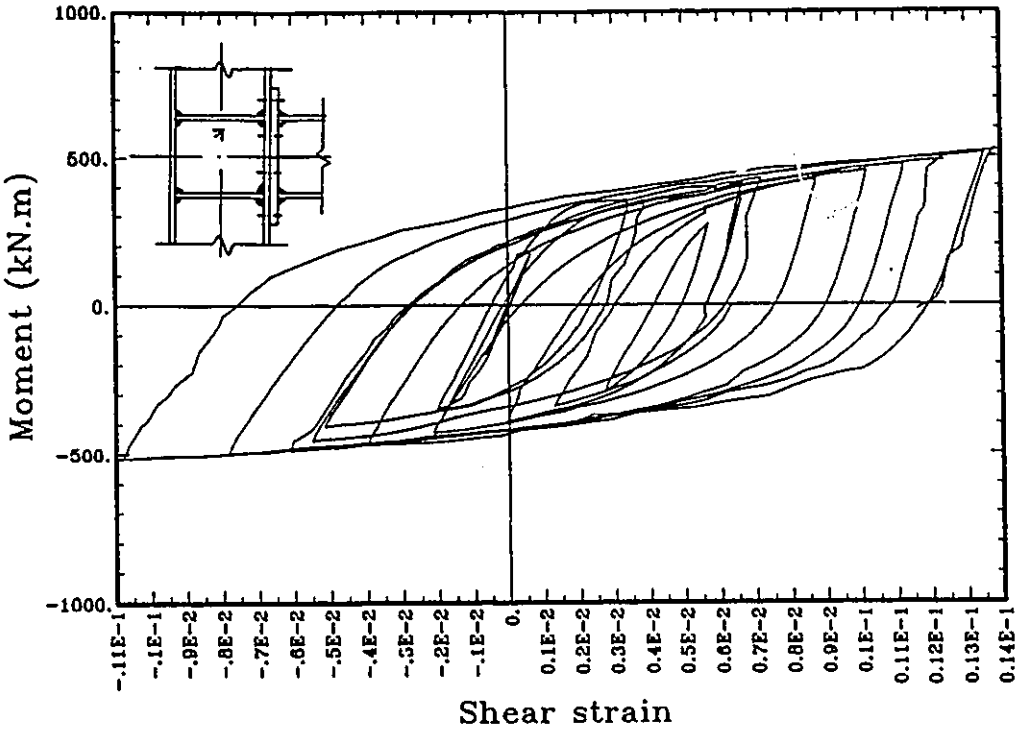

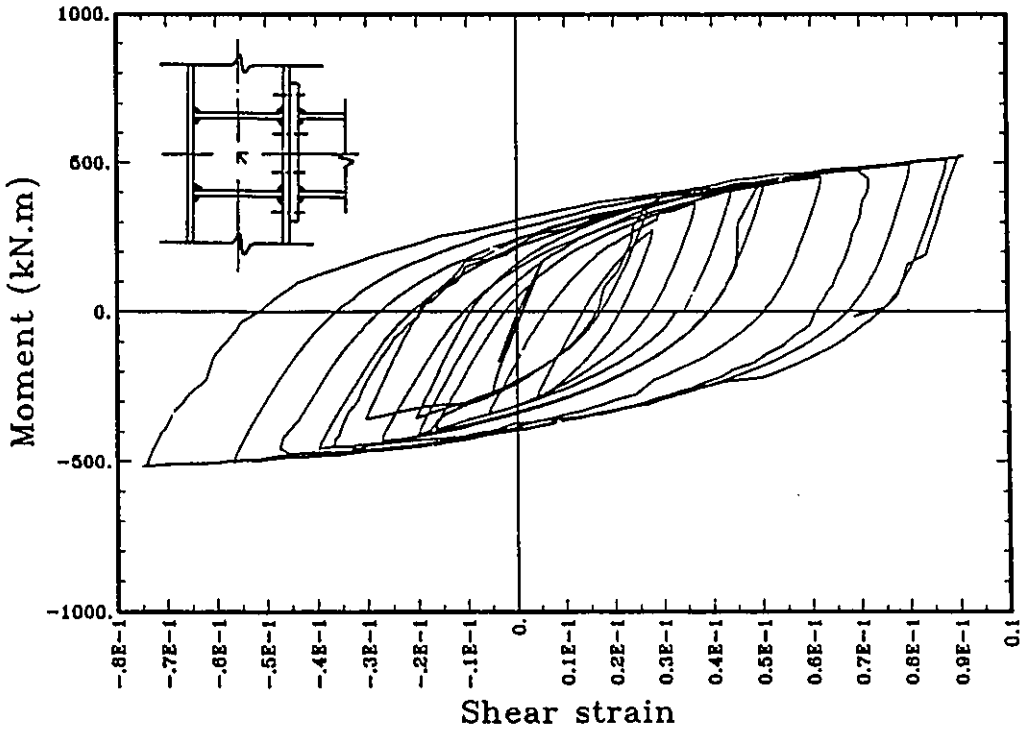

Fig. 4.17 Contd.

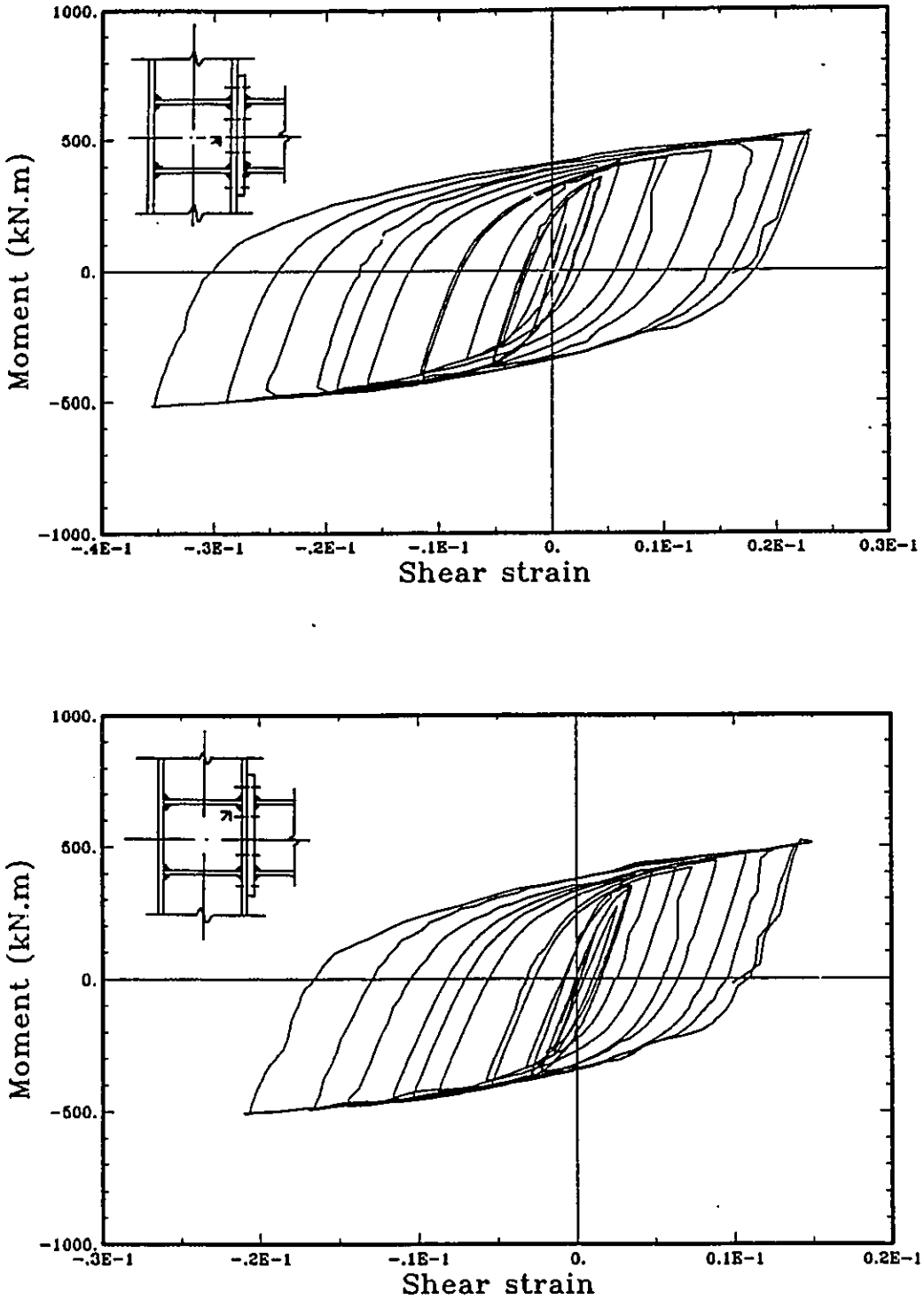

Fig. 4.17 Applied moment versus shear strain at various locations in the panel.

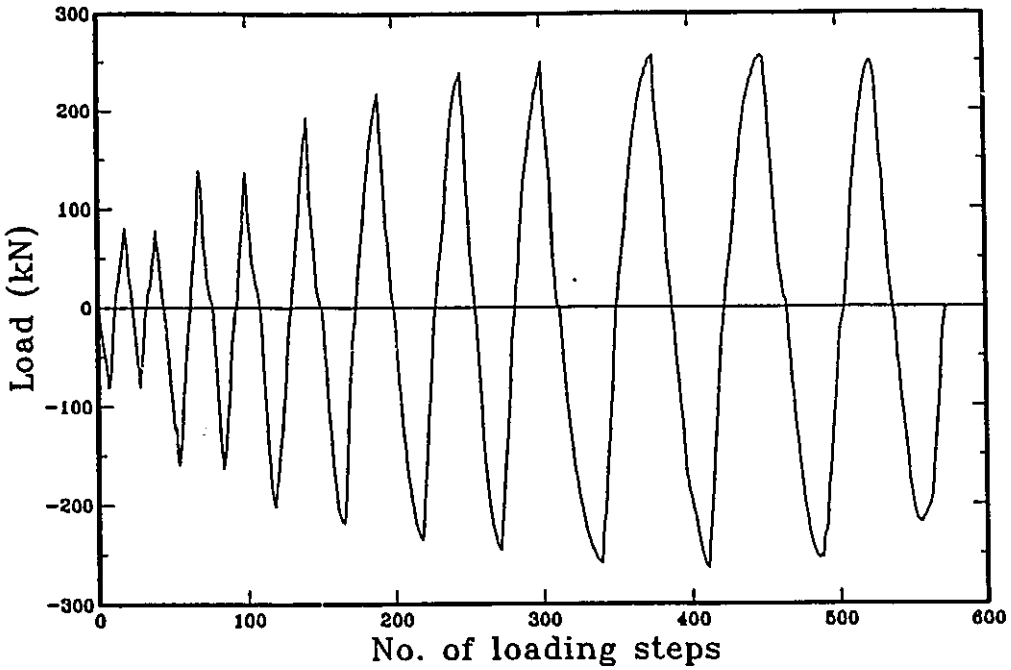

Fig. 4.18 Loading history for specimen CC-2.

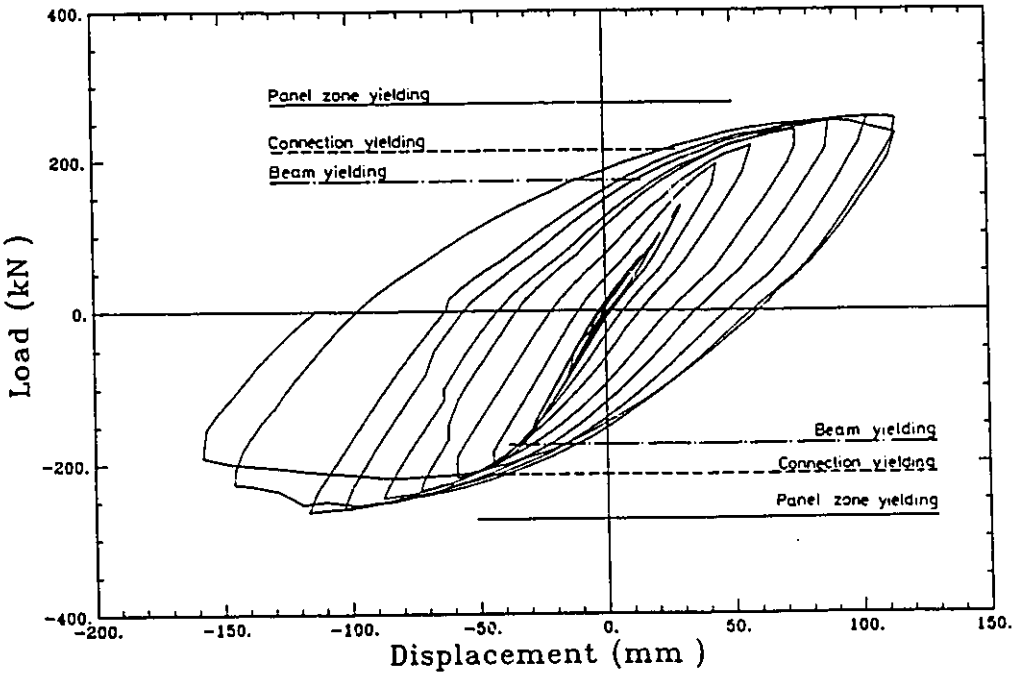

Fig. 4.19 Beam tip load-deflection relationship for specimen CC-2.

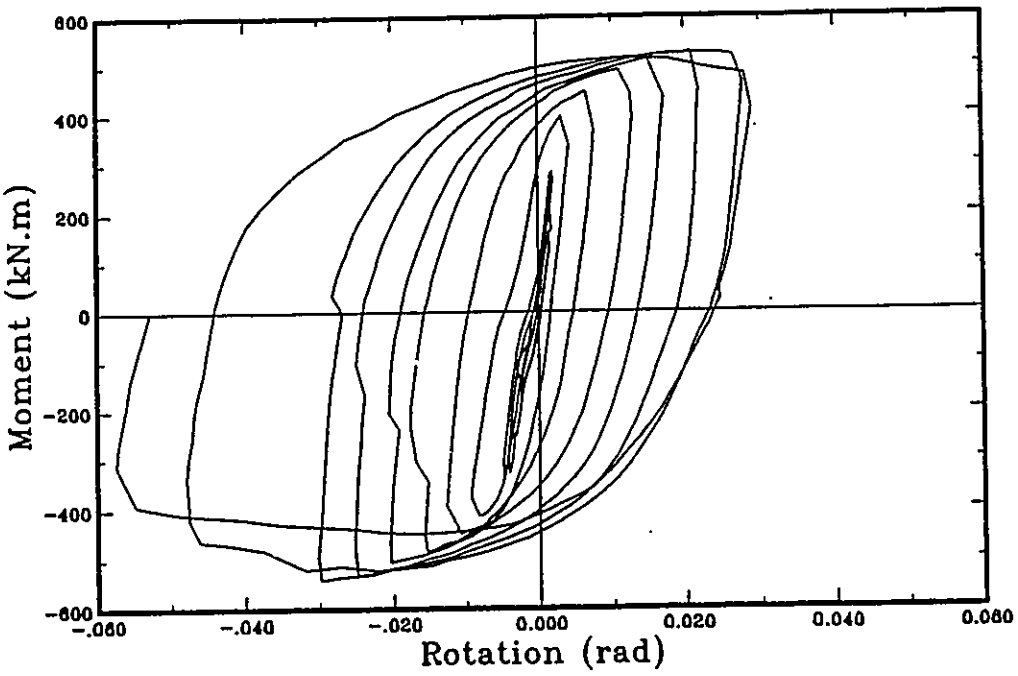

Fig. 4.20 Beam moment versus beam inelastic rotation for specimen CC-2.

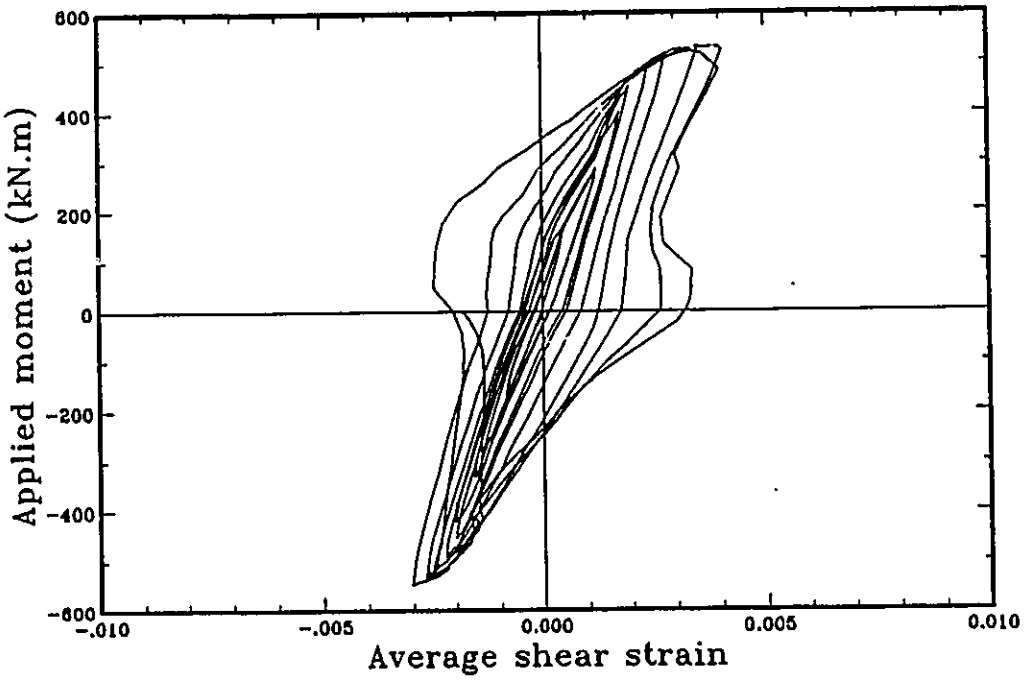

Fig. 4.21 Applied moment versus panel shear strain for specimen CC-2.

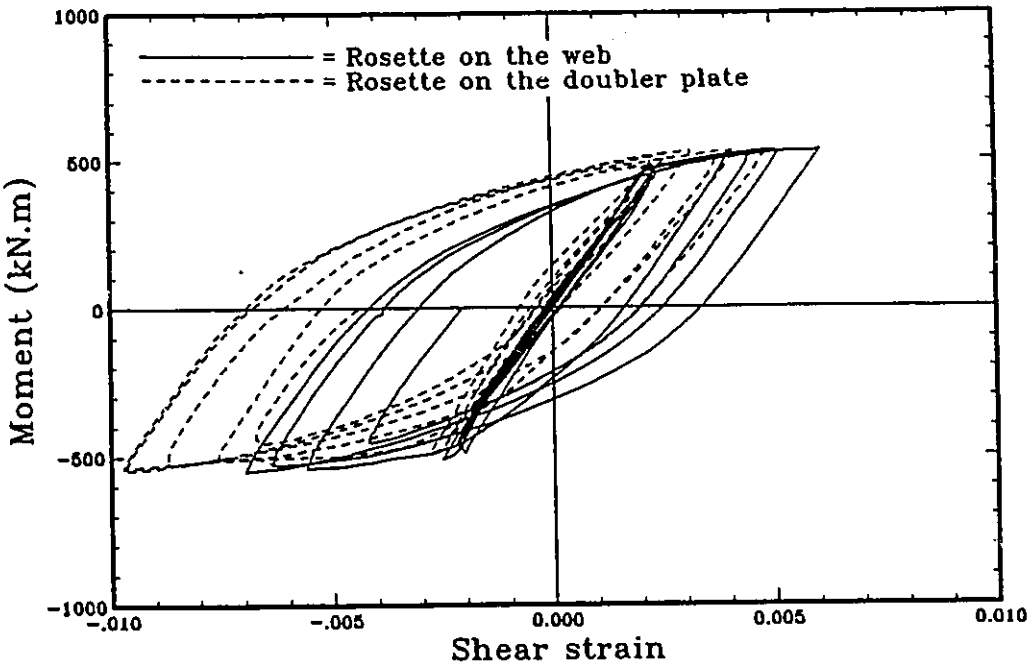

Fig. 4.22 Shear strains measured at the centers of the panel web and the doubler plate.

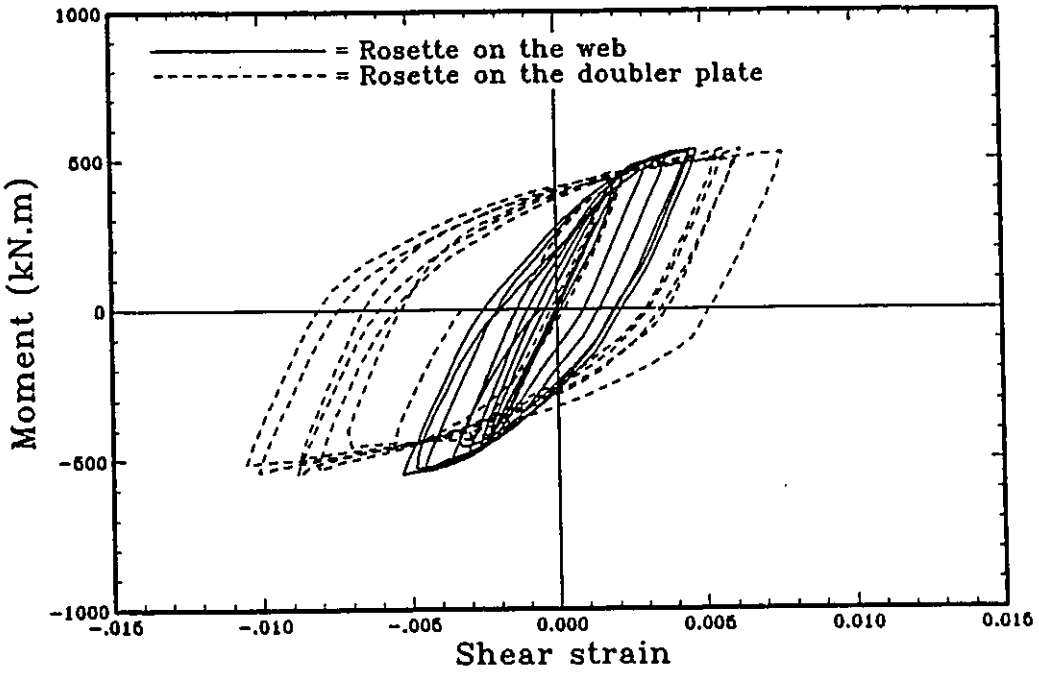

Fig. 4.23 Shear strains measured at the corners of the panel web and the doubler plate.

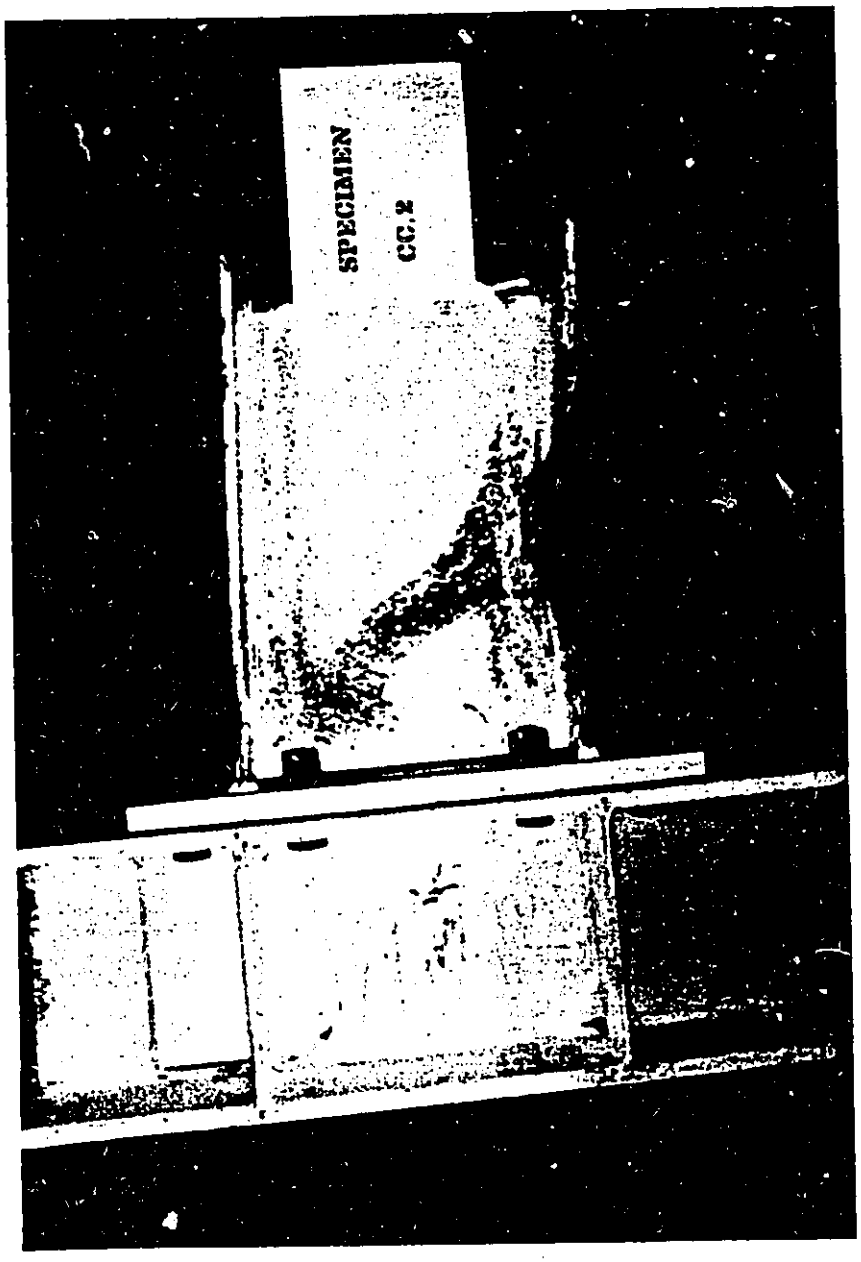

Fig. 4.24 Specimen CC-2 at failure

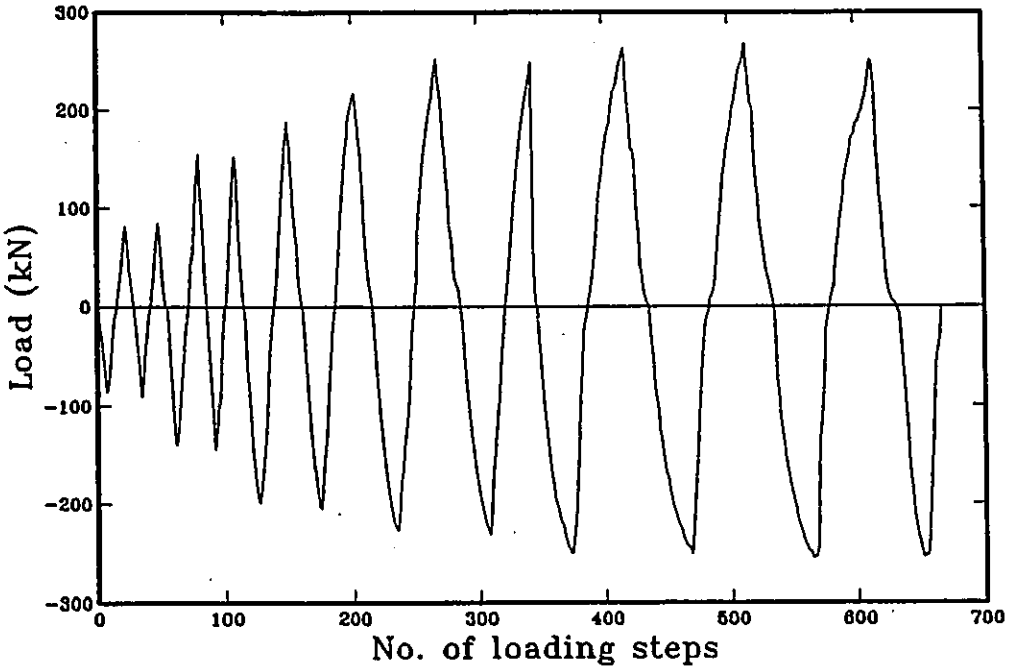

Fig. 4.25 Loading history for specimen CC-3.

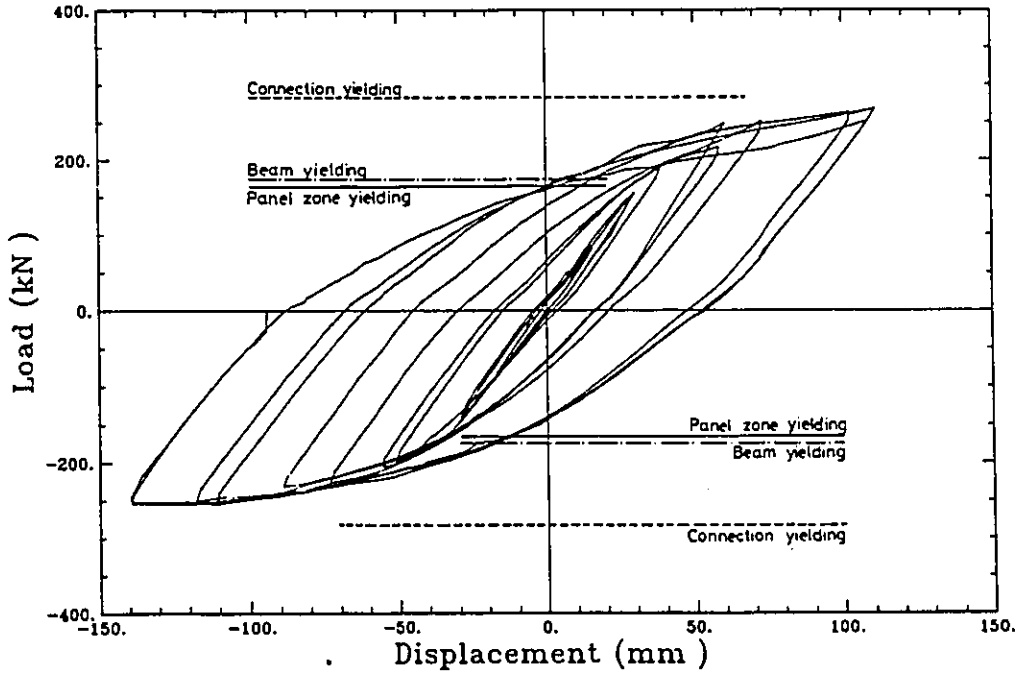

Fig. 4.26 Beam tip load-deflection relationship for specimen CC-3.

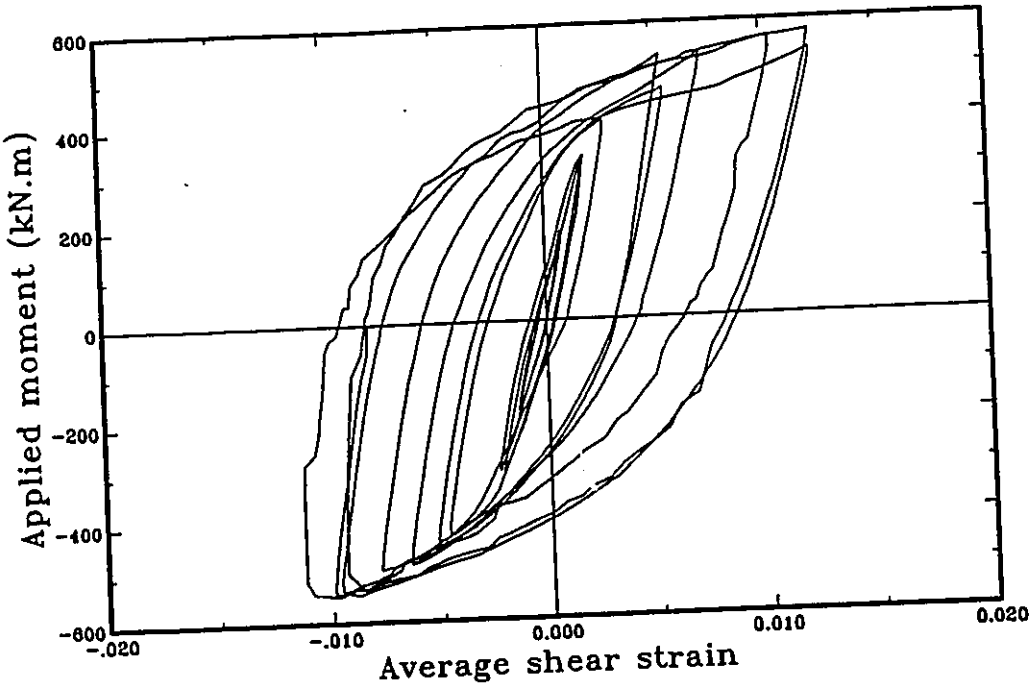

Fig. 4.27 Applied moment versus panel shear strain for specimen CC-3.

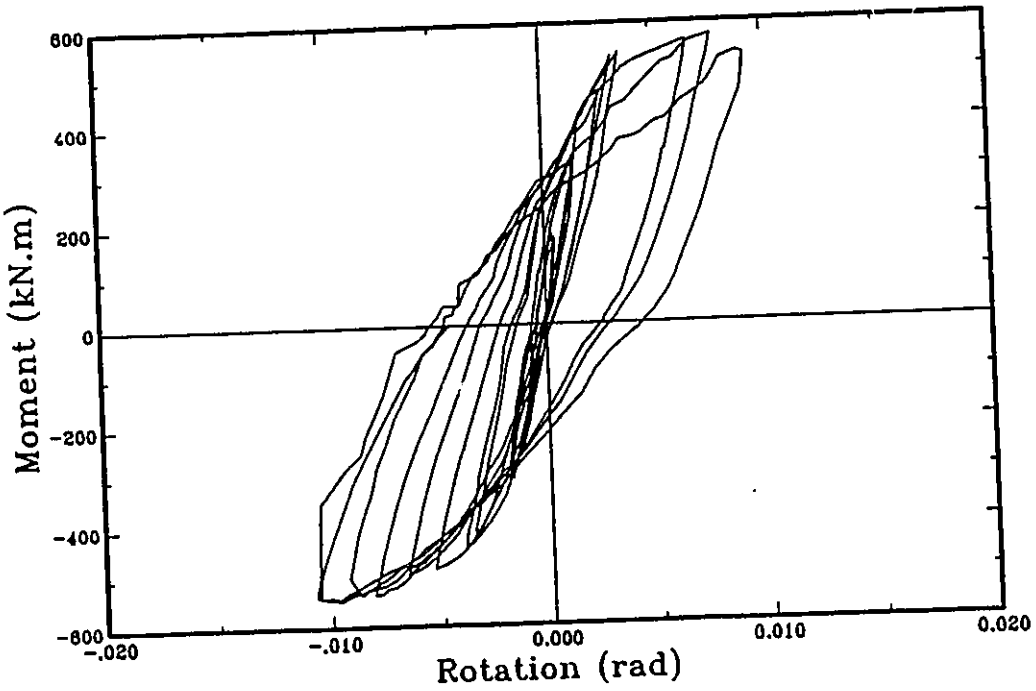

Fig. 4.28 Beam moment versus connection rotation for specimen CC-3

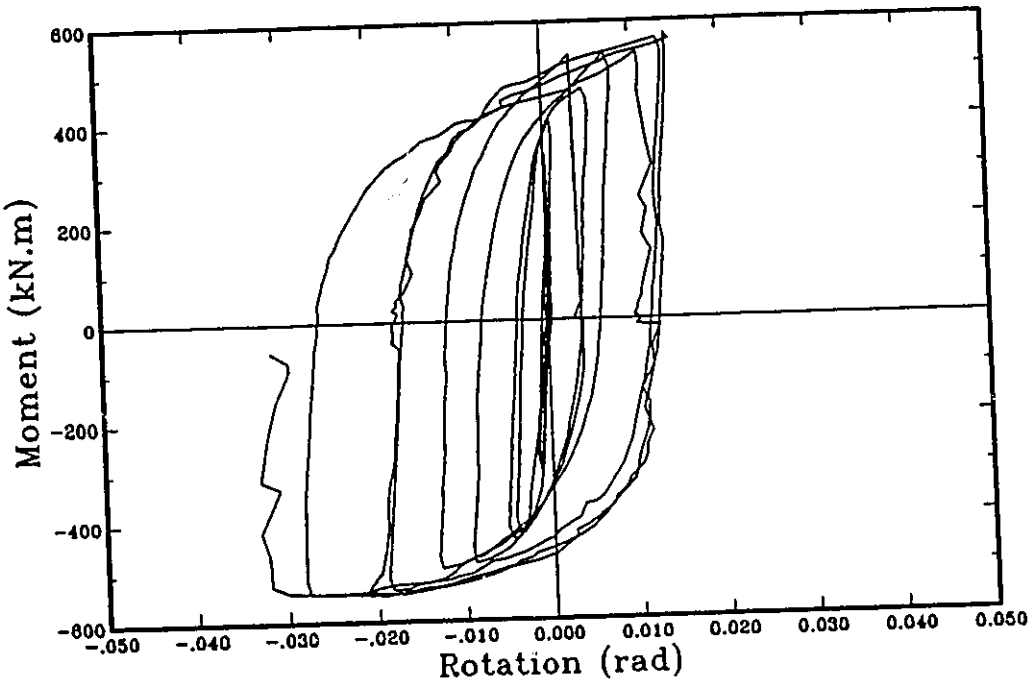

Fig. 4.29 Beam moment versus beam inelastic rotation for specimen CC-3.

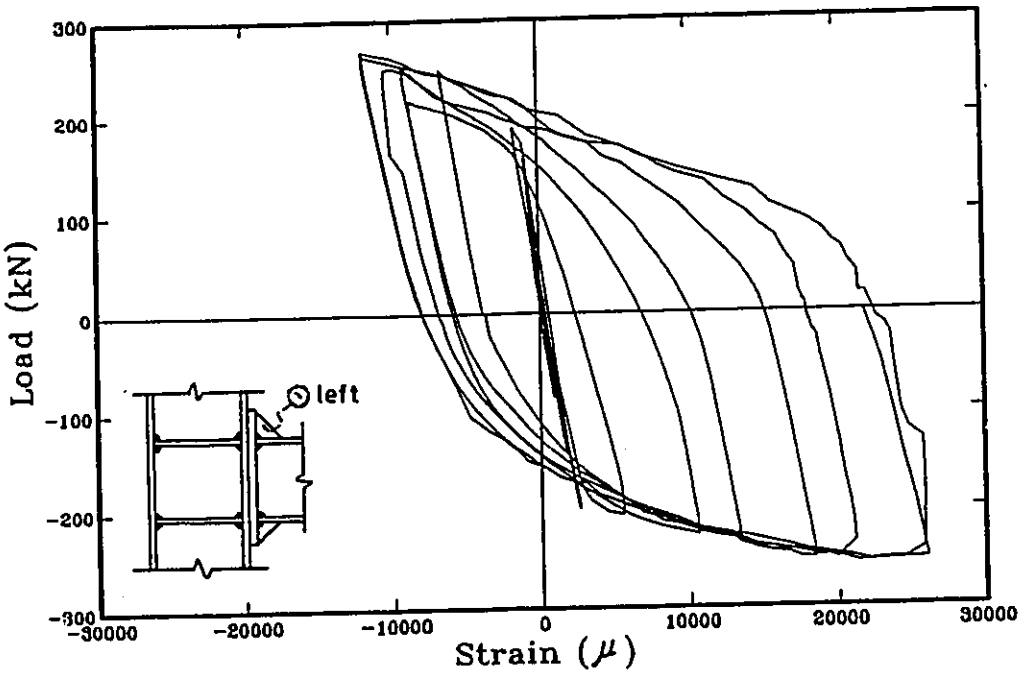

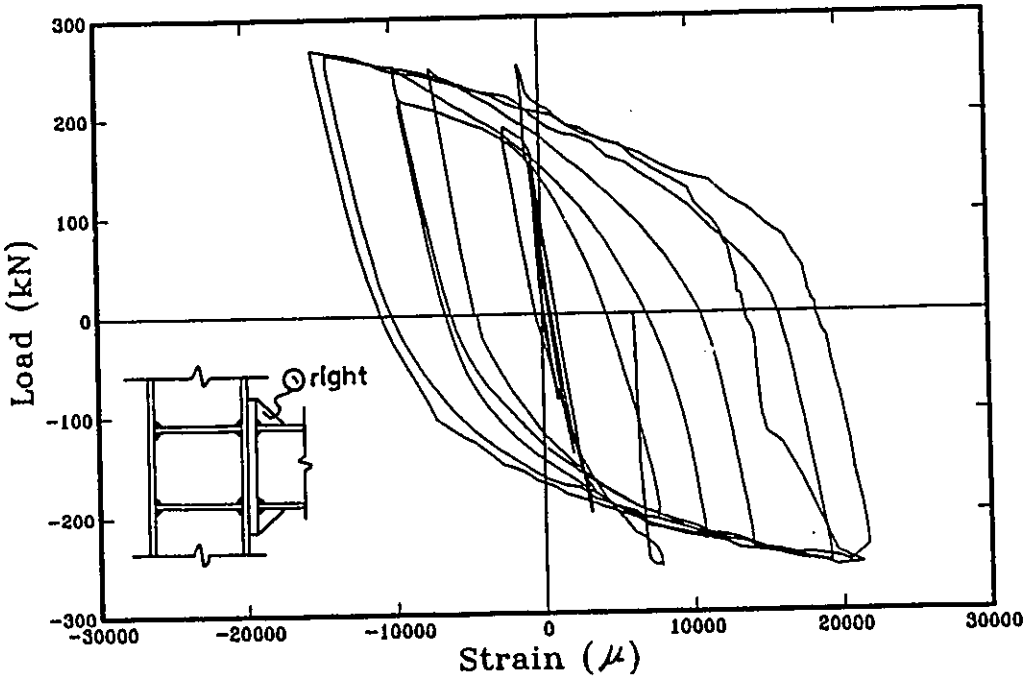

Fig. 4.30 Contd.

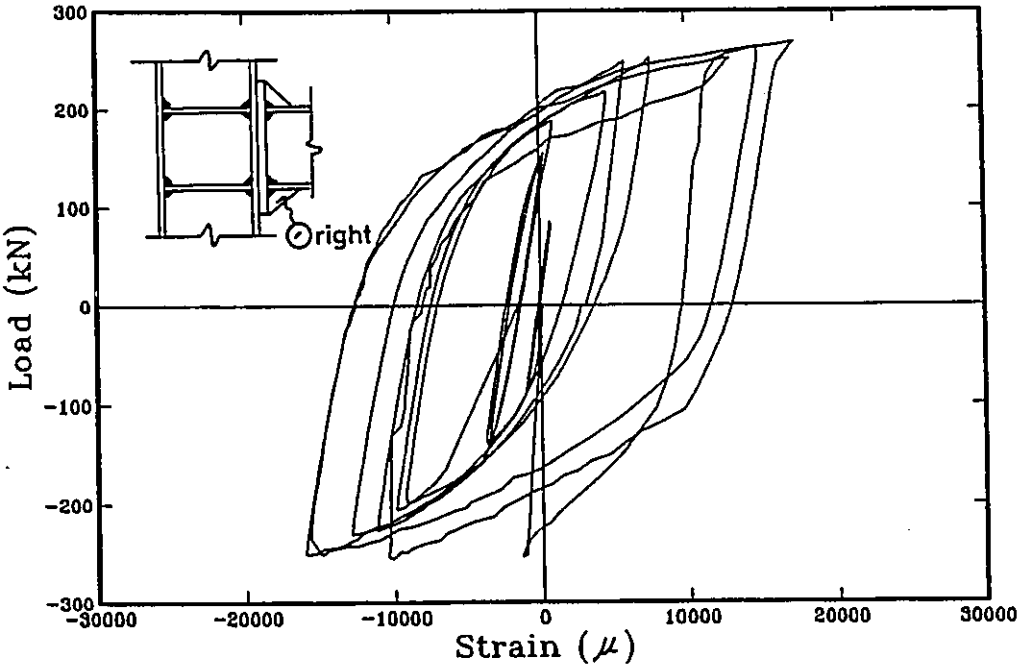

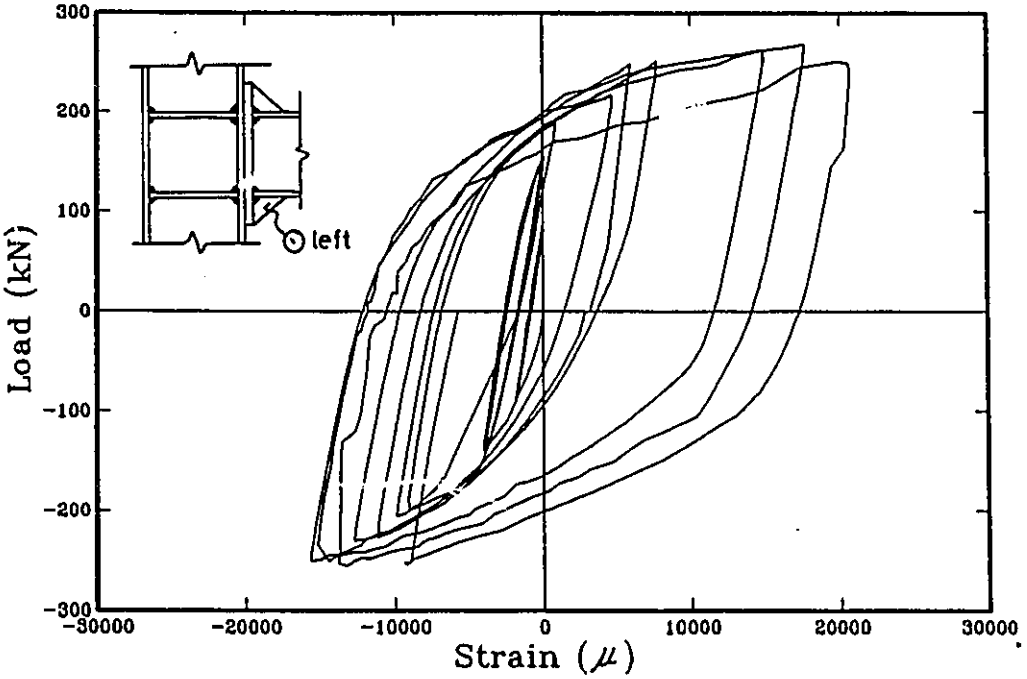

Fig. 4.30 Strains measured on the end-plate stiffeners.

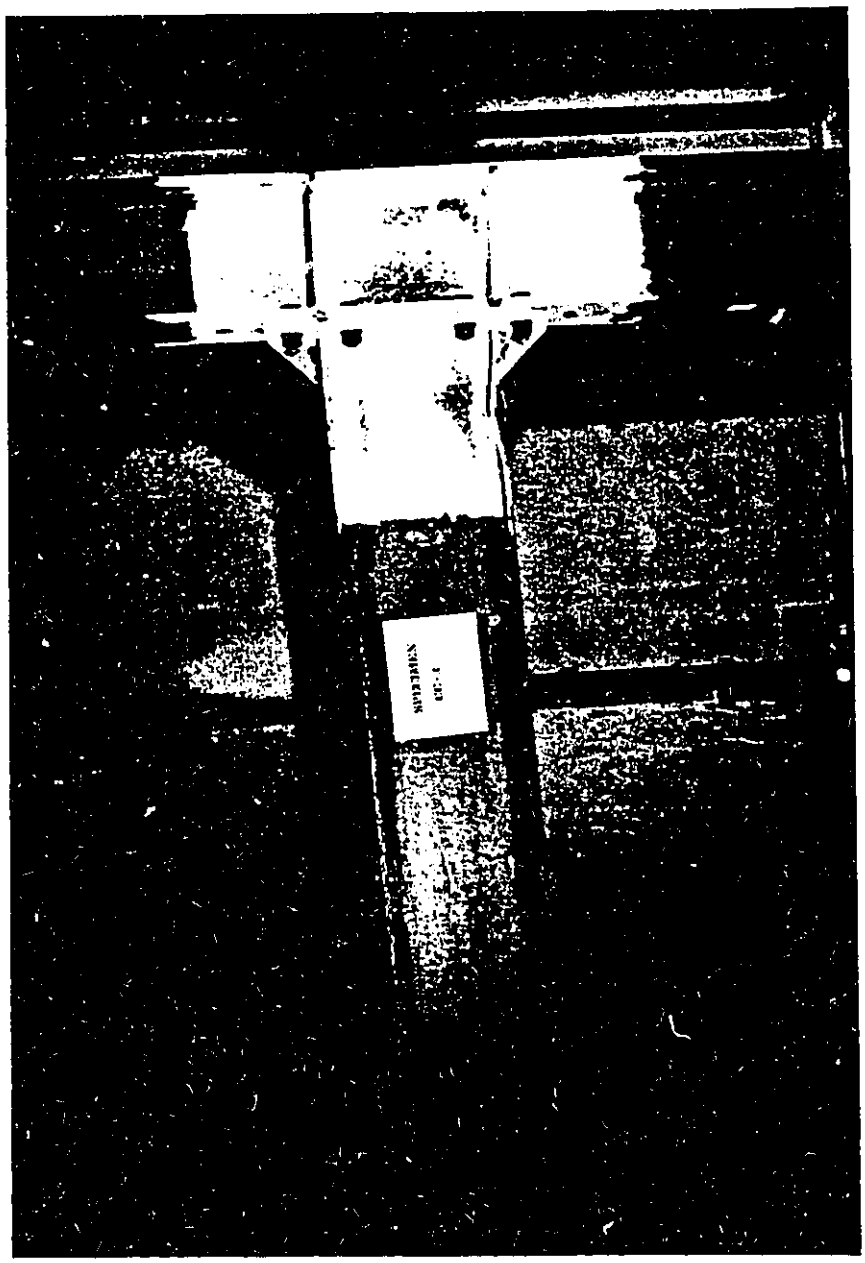

Fig. 4.31 Specimen CC-3 at failure.

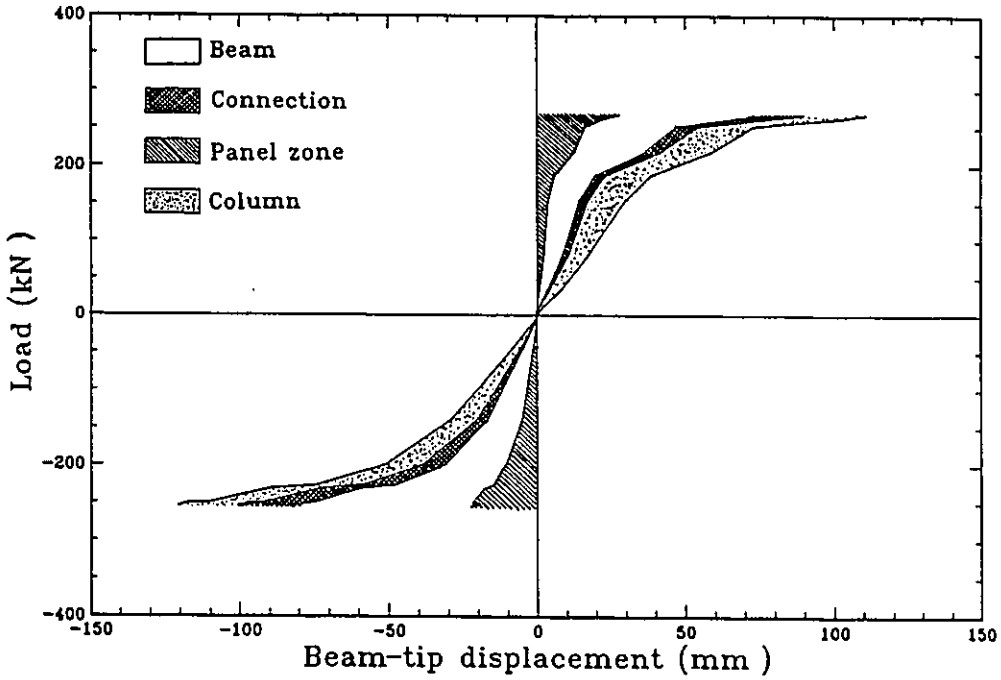

Fig. 4.32 Contribution of specimen CC-3 components to beam-tip deflection.

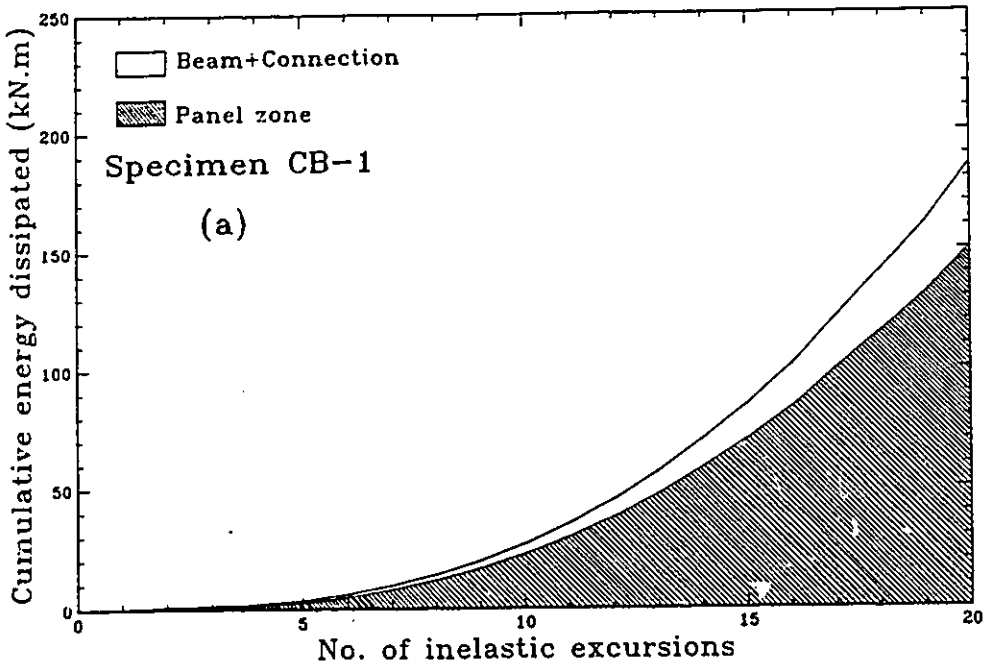

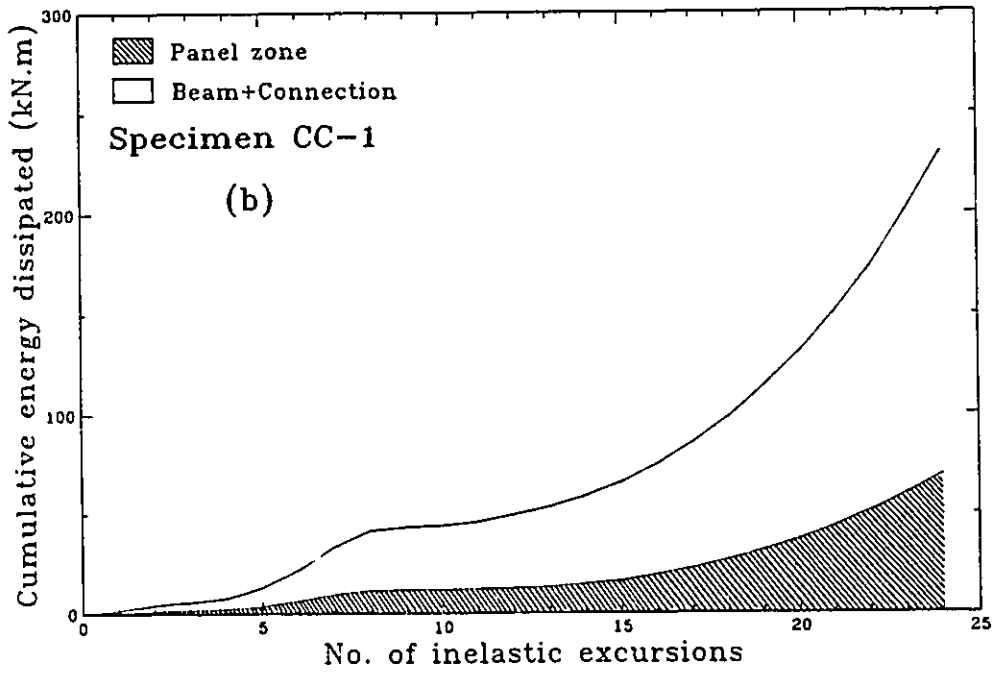

Fig. 4.33 Contd.

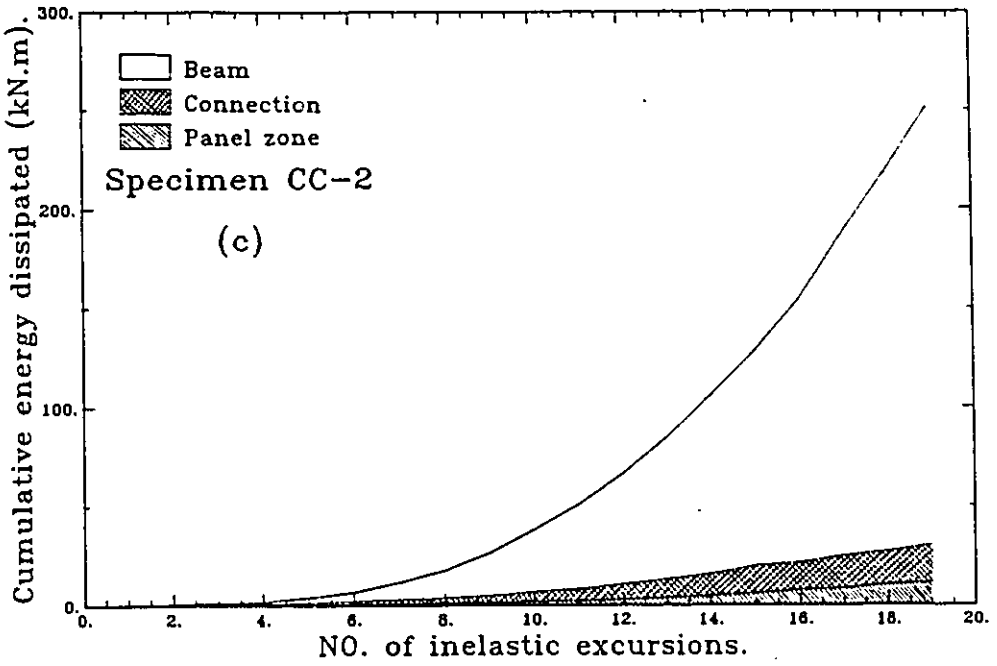

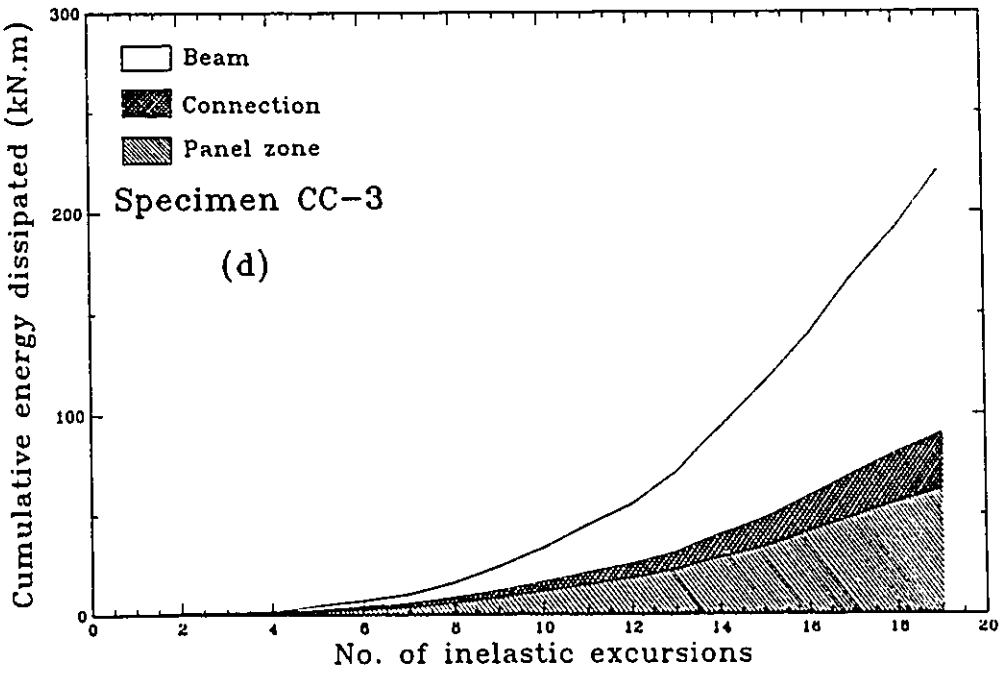

Fig. 4.33 Cumulative energy dissipated by each component in the tested specimens.

CHAPTER 5

APPLIED MOMENT-SHEAR STRAIN RELATIONSHIP FOR THE PANEL ZONE

5.1 Introduction

Tests conducted on beam-to-column subassemblages utilizing extended end-plate joints, showed that the panel zone contributes significantly to the total deformation of the specimen. In addition, tests showed that the performance of the specimens can be improved by allowing the panel zone to participate in dissipating the earthquake input energy jointly with the beams.

The panel zone's contribution to the frame's overall deflection and its shear capacity can be evaluated using an analytical model. The model should be capable of simulating the panel zone applied moment-shear strain relationship, M-γ. In this model, two requirements should be satisfied, simplicity and practicality. Simplicity is required to ensure that the model can be easily incorporated into a computer program for analyzing the frame's response taking into account the effect of panel zone deformation. Practicality implies that the model should depend on geometrical and mechanical properties of the panel zone without the need for other parameters to be determined experimentally.

In this chapter, an analytical model that is capable of predicting the M-γ relationship for the panel zones in extended end-plate joints, is proposed. The model's accuracy was verified by comparing its predictions with the experimental results previously obtained from testing beam-to-column joints.

5.2 Behaviour of joint-panels

When a steel frame is subjected to horizontal earthquake forces, high shears are developed in the beam-to-column joint-panels. The forces acting around an interior structural joint of a MRF are shown in Fig.5.1.The shear force in the panel, Q, can be estimated by the following formula

$$Q = \frac{M_{b1}+M_{b2}}{d_b} - H_c \qquad (5.1)$$

where,

$$H_c = \frac{M_{b1}+M_{b2}}{L_c} \qquad (5.2)$$

in which M_{b1}, M_{b2} are the beam bending moments acting on either side of the joint, d_b is the beam depth and L_c is the column height as shown in Fig.5.1. It should be noted that in Eq.5.1, it is assumed that most of the bending moment in the wide flange members is carried by the flanges. Examining Fig.5.1 shows that the panel moment, M_{pn}, is equal to

$$M_{pn} = (M_{b1}+M_{b2}) - (M_{c1}+M_{c2}) \qquad (5.3)$$

By substituting Eq.5.3 into Eq.5.1, the panel shear, Q, is given by

$$Q = \frac{M_{pn}}{d_b}(1-\alpha) \qquad (5.4)$$

where $\alpha = d_b/L_c$.

An examination of the experimental response of a panel zone indicates that its behaviour can be characterized as follows:

1. When the joint is subjected to lateral loads, shear stresses develop with their highest value at the panel centre. These shear stresses propagate from the centre of the panel towards its corners until the whole panel has completely yielded. During this stage which will be called the elastic range, the panel possesses very high stiffness.
2. Once the panel is fully yielded, the surrounding elements such as the column flanges and the end-plates are the main components that are resisting the panel zone deformation. This resistance continues up to the formation of a mechanism in these elements. At this stage, the panel stiffness decreases gradually until it reaches a stiffness with constant slope equal to strain

hardening stiffness. This stage will be called the transition range.

3. Once a mechanism is formed in the elements surrounding the panel, the only resistance provided by the panel is due to its material strain hardening. This stage will be called the strain hardening range.

These three distinctive stages were typical for all tested panels.

5.3 M-γ relationship under monotonic loading

Based on the observed behaviour of the panel zones, it was found that panel response can best be approximated by a tri-linear curve such as shown in Fig.5.2. The curve consists of three segments corresponding to the three stages of response described in section 5.2.

5.3.1 Elastic range

In deriving the stiffness and defining the yield surface of the panel zone in the elastic range, the following assumptions were made:

1. Yielding of the panel web will occur as the state of the average stress reaches the yield surface described by the Von Mises criterion.
2. The panel zone deformation or distortion remains small throughout.
3. The shear stresses are assumed to be uniformly distributed throughout the panel.
4. Local buckling of the panel is precluded.

regarding the third assumption, experimental measurements indicate that an elastic strain distribution is closer to being nearly uniform than parabolic, as predicted by the elastic solution (Kato et al.1988). The adoption of this assumption will simplify the proposed model substantially with little loss of accuracy.

In the elastic range, the panel experiences two different modes of deformations, shear and bending. Since, the panel is assumed to be elastic and its deformations small, the total panel deflection can be computed by directly superimposing the deflections due to pure shear and bending, as shown in Fig.5.3, therefore

$$W_T = W_s + W_b \tag{5.5}$$

where W_T is total panel deformation and W_s and W_b are the panel deformations due to shear and bending, respectively.

Using principles of strength of materials, W_s and W_b can be determined as

$$W_s = \frac{Qd_b}{G(d_c - t_{cf})\, t_{cw}} \tag{5.6}$$

and

$$W_b = \frac{Qd_b^3}{12EI_c} \tag{5.7}$$

where

d_c = the column depth,
d_b = the beam depth,
t_{cf} = the thickness of column flange,
t_{cw} = the thickness of column web,
I_c = the column section inertia,
E = Young's modulus, and
G = shear modulus

By substituting Eqs.5.6 and 5.7 into Eq.5.5, Eq.5.8 is obtained as follow

$$W_T = Qd_b\left(\frac{1}{G(d_c - t_{cf})\, t_{cw}} + \frac{d_b^2}{12EI_c}\right) \tag{5.8}$$

The panel shear strain γ, is given by

$$\gamma = \frac{W_T}{d_b} \tag{5.9}$$

while the panel elastic stiffness, K_e, is written as

$$K_e = \frac{M_{pn}}{\gamma} \tag{5.10}$$

The panel elastic stiffness can be determined by substituting Eqs.5.4, 5.8 and 5.9 into Eq.5.10 as follow:

$$K_e = \frac{d_b}{\left(\frac{1}{G(d_c - t_{cf})\, t_{cw}} + \frac{d_b^2}{12EI_c}\right)} \frac{1}{(1-\alpha)} \qquad (5.11)$$

Applying this equation to most of the available standard wide flange column sections, reveals that the stiffness due to panel bending accounts for only about 10% of the total elastic stiffness.

In deriving Eq.5.11, it should be noted that no contribution from the end-plates to the panel shear resistance was considered, since the panel zone deformations are small and complete contact between the end-plate and the column flange cannot be assumed.

The plastic shear capacity of a panel, Q_p, subjected to pure shear deformation can be calculated as

$$Q_p = \tau_y t_{cw} (d_c - t_{cf}) \qquad (5.12)$$

where τ_y is the panel shear yield stress and is equal to $\sigma_y/\sqrt{3}$

Substituting Eq.5.12 into Eq.5.4 gives

$$M_{pnl} = \tau_y t_{cw} d_b (d_c - t_{cf}) \frac{1}{(1-\alpha)} \qquad (5.13)$$

When the column is subjected to an axial force, early yielding of the panels is observed. Using Von Mises yield criterion, the plastic panel moment, M_{pnl}, can be calculated by using reduced plastic shear stress, τ'_y, which is given by (Popov, 1968)

$$\tau'_y = \tau_y [1 - (P/P_y)^2]^{1/2} \qquad (5.14)$$

where, P, is the column axial force and P_y is the axial force required to yield the column. In practical terms, the effect of axial force seems to be small. For example, if P = 0.5 P_y, Eq.5.14, gives $\tau'_y = 0.87\ \tau_y$. In effect, a 13% reduction in shear yield stress results. Considering the fact that 0.5 P_y is nearly the maximum compressive column load used in practical design, its influence on the reduction in shear yield stress, is relatively small.

5.3.2 Transition range

Following the full plastification of the panel web, the panel stiffness starts to decrease gradually. During this stage, the column flanges and the end-plates are the main source for providing the panel shear resistance. To evaluate the model during this range, the following assumptions were made:

1. Both the column flanges and web outside the panel area remain elastic.
2. Fracture and instability are not considered.

Throughout this range, the panel zone can be idealized as a closed frame consisting of two columns connected by two infinitely rigid beams, as shown in Fig.5.4. The beams represent the column section below and above the panel zone area which is assumed to remain elastic according to the first assumption. The flexible columns represent the column flanges and the adjoining end-plates. In this idealization, the panel zone itself is represented as a material with low shear modulus equal to the plastic shear modulus of the steel, G_{st}. This plastic shear modulus is equal to $\rho E/3$ in accordance with Prandl-Reuss theory (Malvern, 1969), where ρ is defined as the uniaxial strain hardening ratio.

The closed frame is subjected to two equal and opposite forces, Q, acting at the levels of the top and bottom beam flanges and represents the panel shear. These Q forces are increased until they reach a level that causes the formation of a sway mechanism in the closed frame as shown in Fig.5.4. This mechanism was visually observed during the tests by the flaking of whitewash on the column flanges, as shown in Fig.5.5. At this point, any further increase in panel resistance is expected to be due to panel strain hardening.

The shear capacity of the panel at the end of this stage can be found by calculating the load required to develop a mechanism formed by plastic bending of the flanges and end-plates. Using the theories of plastic analysis, the associated additional moment resistance ,ΔM, can be determined as

$$\Delta M = (2M_{pf1} + 2M_{pf2}) + Q^* d_b \qquad (5.15)$$

where M_{pf1} and M_{pf2} are the plastic moment of the flanges on either side of the panel including the adjoining end-plate and Q^* is the additional resistance provided by the strain hardened panel web.

From observations during the tests, it was evident that the end-plate participated efficiently in resisting the panel zone deformation in this stage. However, it was not clear whether the assumption of a complete or partial contact between the end-plate and the column flange is the valid one. Calibration of the model results, indicated that the assumption of complete contact improves the accuracy of the results as will be explained later (Osman et al, 1991b).

The moment, M_{pfi} can be calculated by using simple plastic theory as follows (Neal, 1963)

$$M_{pfi} = \sigma_y Z_{fe} [1 - (N/A_f \sigma_y)^2] \qquad (5.16)$$

where

Z_{fe} = the plastic modulus of the column flange and the adjoining end-plate as one unit,

A_f = the cross sectional area of both the column flange and the end-plate, and

N = the axial force in the column flange and is equal to half the column's axial force.

The evaluation of Eq.5.15 requires that Q^* is determined. The calibration of the model indicated that the effect of Q^* is significant and cannot be neglected. Thus, a unique technique for calculating Q^* was developed. In this technique the deflection at the point of mechanism formation in the closed frame is determined. Once this deflection is determined, the shear strain at this instant, γ_T, can be found

by dividing the deflection by the beam depth. Knowing γ_y (the shear strain at panel yield), Q^* can be determined by the formula:

$$Q^* = (\gamma_T - \gamma_y) G_{st} t_{cw} (d_c - t_{cf}) \qquad (5.17)$$

The value of γ_T can be determined using the slope deflection theory in plastic analysis (Neal,1963). In this approach, the last hinge to form in the closed frame is determined. Then, using the slope deflection equations, the deflection can be found. Analysis showed that the last hinge always formed at the thinnest column flange and end-plate, i.e the ones with the smallest M_{pfmin} and I_{fmin}. Thus, γ_T is given by

$$\gamma_T = \frac{M_{pfmin} d_b}{6 E I_{fmin}} \qquad (5.18)$$

As a result, M_{pn2} is given by

$$M_{pn2} = M_{pn1} + \Delta M \qquad (5.19)$$

Once ΔM and γ_T are determined, K_T can be calculated as follow

$$K_T = \frac{\Delta M}{(\gamma_T - \gamma_y)} \qquad (5.20)$$

5.3.3 Strain hardening range

Following the formation of the sway mechanism, the strength of the panel increases slightly due to material strain hardening. In this range, the stiffness, K_s is given by

$$K_s = \frac{E_{st}}{E} K_e \qquad (5.21)$$

5.3.4 Model verification

To verify the model accuracy, results of the four tested panels were compared with the experiment. Since the panels were mainly tested under cyclic loading conditions, the monotonic M-γ relationships for the tested panels were constructed from the cyclic curves using the approach suggested by Kato et al.(1981). In this approach, the monotonic curve can be found from the cyclic curves by the shifting rule shown in Fig.5.6. The resulting curves are shown by solid lines in Figs. 5.7 to 5.10. The model predictions are shown by dotted lines on the same plots. Examining these figures reveals the following:

1. The model was able to predict the initial elastic stiffness for all tested panels with adequate accuracy.
2. Assuming complete contact between the column flanges and end-plates gives better results as compared with the partial contact assumption. These data are plotted in Fig.5.7.
3. In the case of specimen CC-2 (Fig.5.9), the doubler plates are assumed to fully participate in resisting the panel zone deformation. Based on this assumption, accurate prediction was obtained.
4. With the exception of specimen CC-3 (Fig.5.10), which has a stiffened end-plate, the model correlates well with the experimental results in both the transitional and strain hardening zones. Underestimation of the panel shear strength in specimen CC-3, resulted from neglecting the effect of the end-plate stiffeners.

5.4 M-γ relationship under cyclic loading

The analytical model was extended to simulate the panel zone behaviour under cyclic loading conditions. The hysteretic M-γ model is shown in Fig.5.11. This model was proposed on the basis of the experimental results reported in chapter 4. The following features describe the panel's behaviour:

1. As long as the panel moment, M_{pn}, remains below the yield value, M_{pn1}, the panel behaves elastically with stiffness equal to the initial elastic stiffness, K_e

(Fig.5.11).

2. Once the panel moment exceeds the yield value, M_{pn1}, the panel is considered to yield and its stiffness becomes equal to K_T.
3. The panel unloads with stiffness equal to K_e up to a moment equal to $2M_{pn1}$ subtracted from the maximum previous attained moment, then unloads with stiffness equal to K_T.
4. If the panel moment exceeds the panel strength, M_{pn2}, the panel stiffness becomes equal to the strain hardening stiffness, K_s.
5. Straight-line strain hardening envelopes in both directions define a constant strength range.

On the basis of the previous discussion, it can be concluded that the entire panel response can be described by five parameters, three stiffnesses, K_e, K_T, and K_s , and two limiting moments, M_{pn1} and M_{pn2}. All these parameters are easily obtainable. It should be noted that this model can only simulate the kinematic hardening which was evident from the tests. No attempt was made to model the isotropic hardening which is considered to be insignificant.

5.4.1 Model verification

The predicted and the experimentally applied moment-panel zone deformation relationships for specimens CB-1 and CC-1, are plotted in Figs.5.12and 5.13. It is observed that the model performed satisfactorily especially in representing the elastic stiffness of the panel zone.

5.5 Computer modelling

To represent the behaviour of the panel zone in computer analysis, a one degree-of-freedom panel zone element was introduced. This element consists of two elasto-plastic components acting in parallel with an elastic component as shown in Fig.5.14. The effect of axial forces in formulating the element was neglected due to its insignificance. In the analysis, the panel zone element is introduced at the beam-column intersection as shown in Fig.5.15. The deformation of the element represents

the panel zone deformation. In this element, translational displacements of the nodes at both ends of the element are constrained to be identical. Also, the nodal coordinates were taken to be identical to satisfy equilibrium.

Another approach to simulate the panel tri-linear behaviour is to use two bi-linear elements in parallel such as those described in Chapter 3. In this case, an elastic-perfectly plastic behaviour with initial stiffness of $(k_e\text{-}K_T)$, yield moment equal to $\gamma_y(K_e\text{-}K_T)$ and zero strain hardening is assigned for the first element. An elastic-strain hardening response with initial elastic stiffness equal to K_T, post elastic stiffness equal to K_s and yield moment equal to $\gamma_T K_T$ is assigned to the second element, as shown in Fig.5.16. It should be noted that in this approach two degrees of freedom are added at each beam-to-column intersection instead of only one.

5.6 Summary

A tri-linear model capable of predicting the panel M-γ relationship, was proposed. The model is based solely on the geometrical and mechanical properties of the panel zone. The model sensitivity was assessed by comparing its results with the experimental measured results from the tests. A panel zone element that can be used in computer analysis is thus introduced. The element is simple and is proven to be easy to incorporate into computer programs.

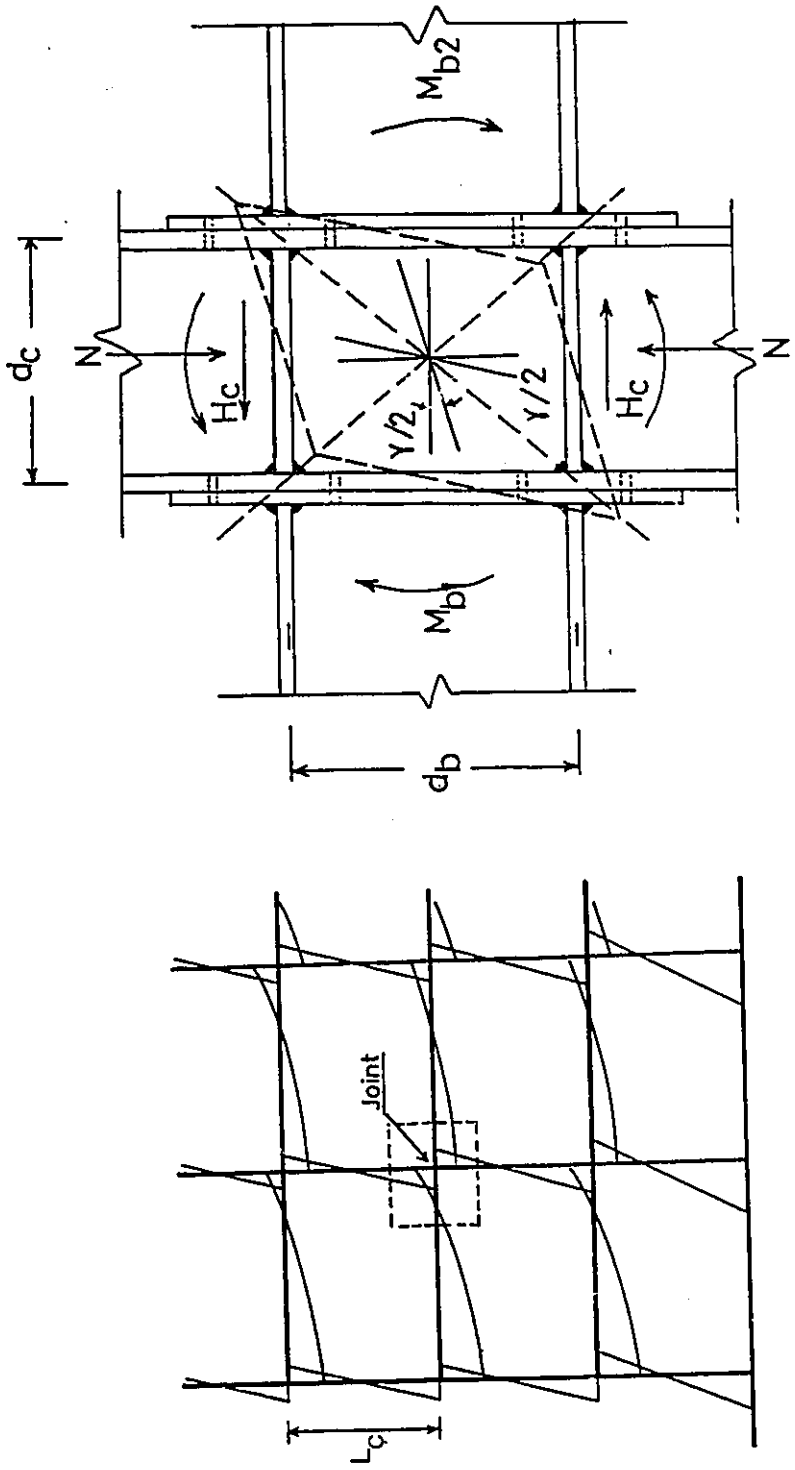

Fig. 5.1 Forces acting on the joint-panel

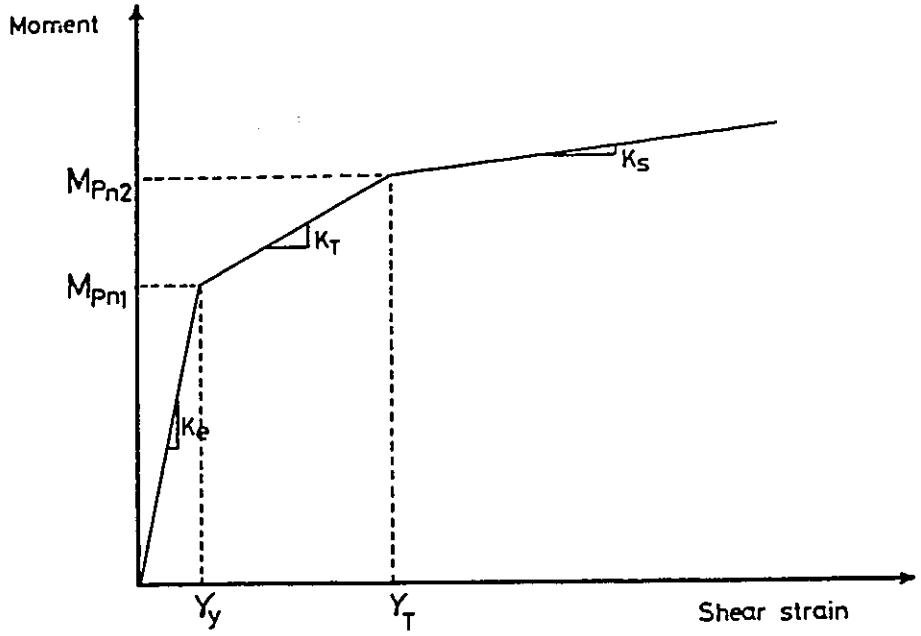

Fig. 5.2 Proposed Model

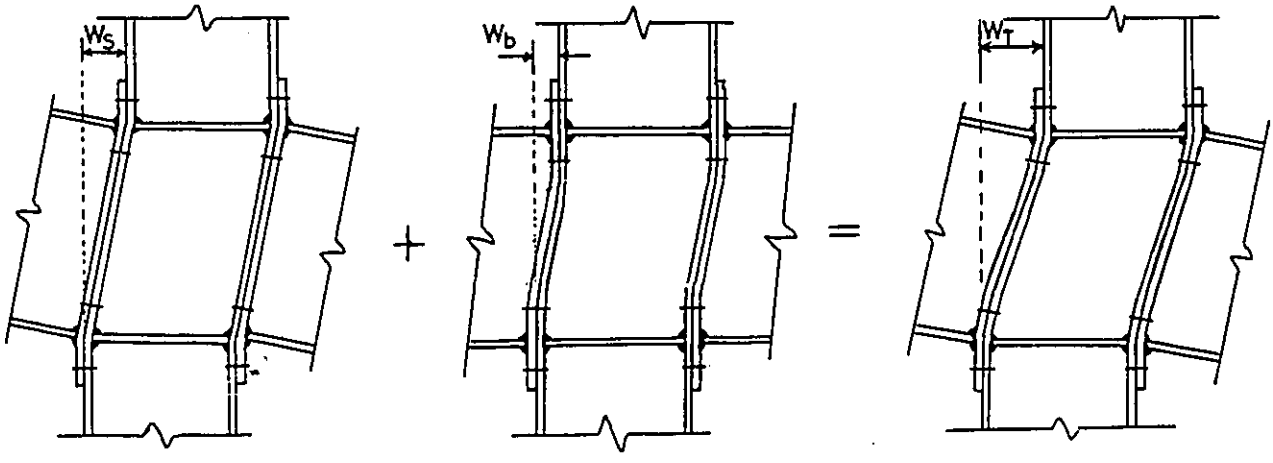

pure shear deformation pure bending deformation total deformation

Fig. 5.3 Panel zone deformation in the elastic range.

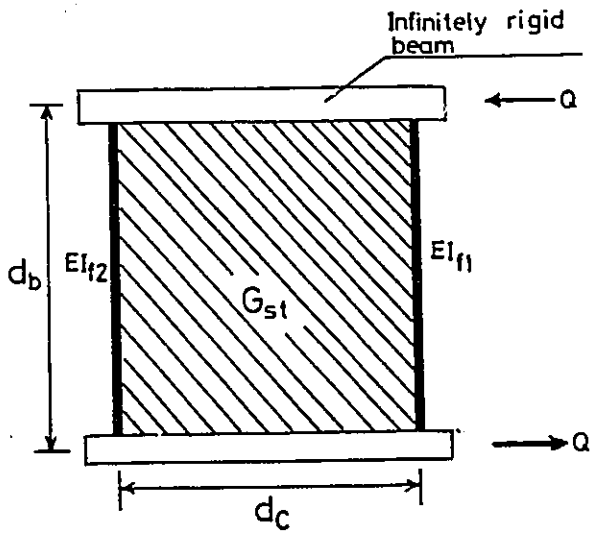

Panel zone idealization

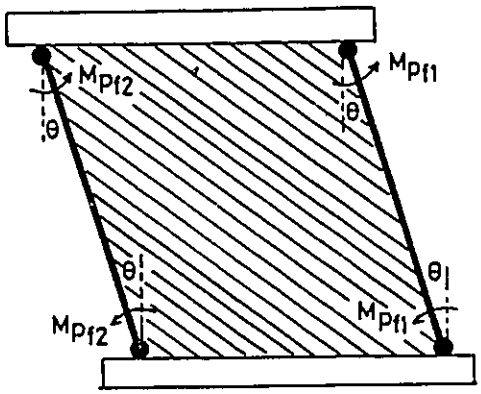

Sway mechanism

Fig. 5.4 Panel zone in the transition zone.

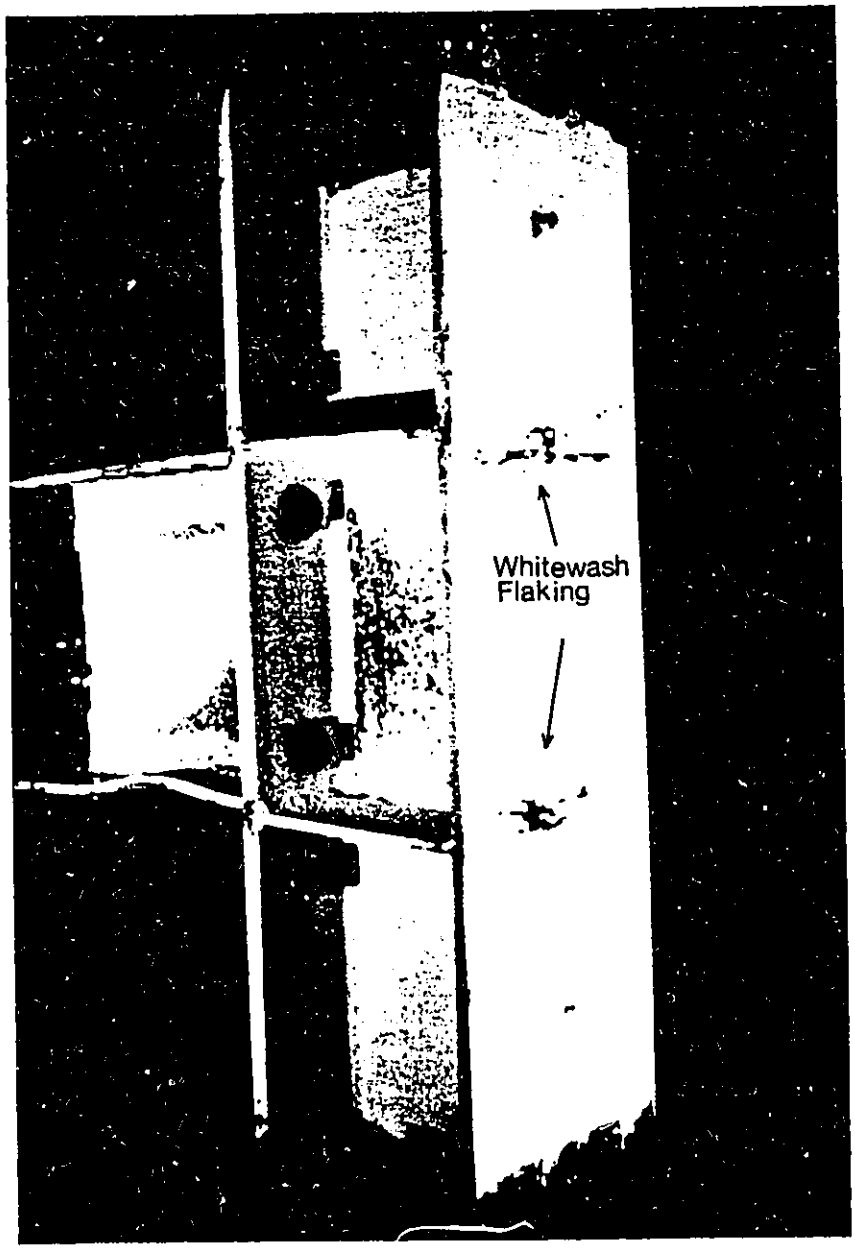

Fig. 5.5 Sway mechanism

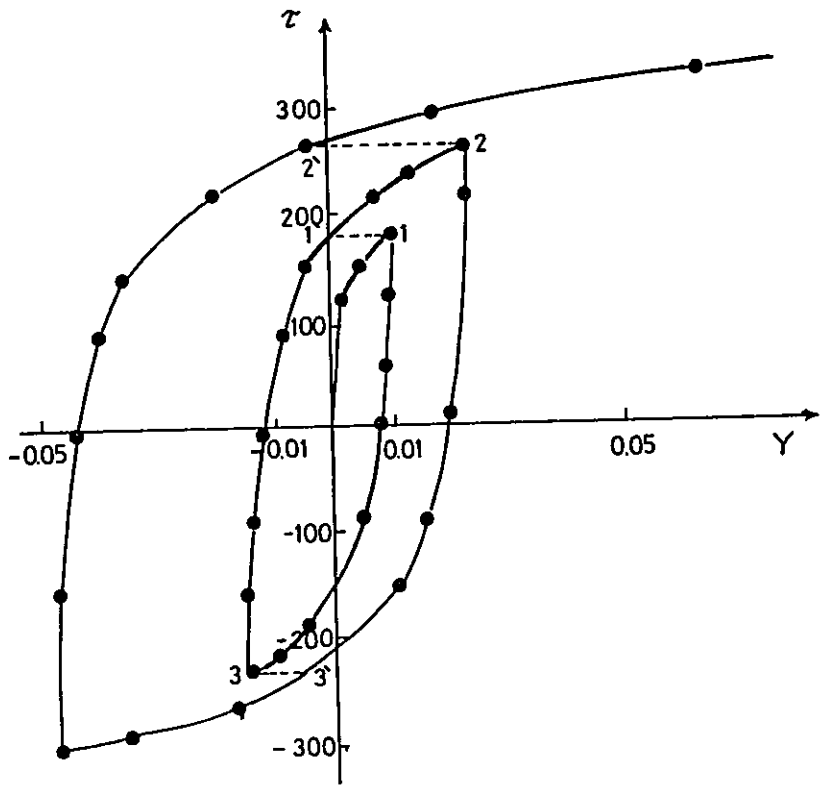

a) hysteretic curves

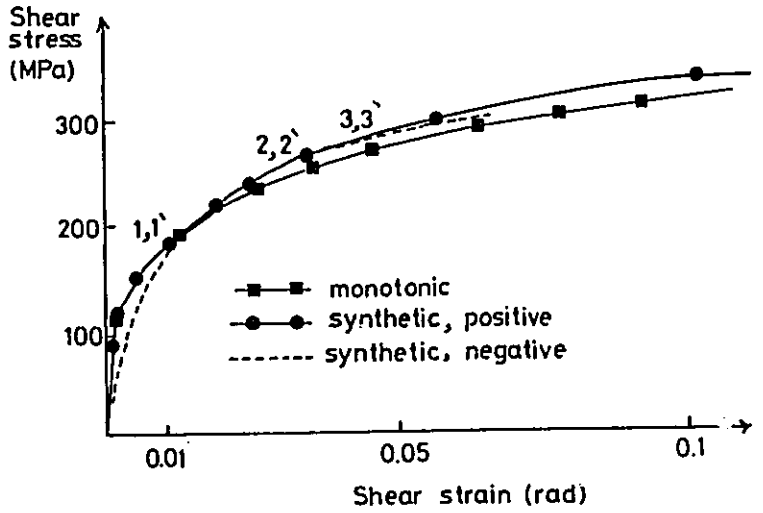

b) monotonic and synthetic curves.

Fig. 5.6 Relation between monotonic and hysteretic curves (Kato et al. 1981).

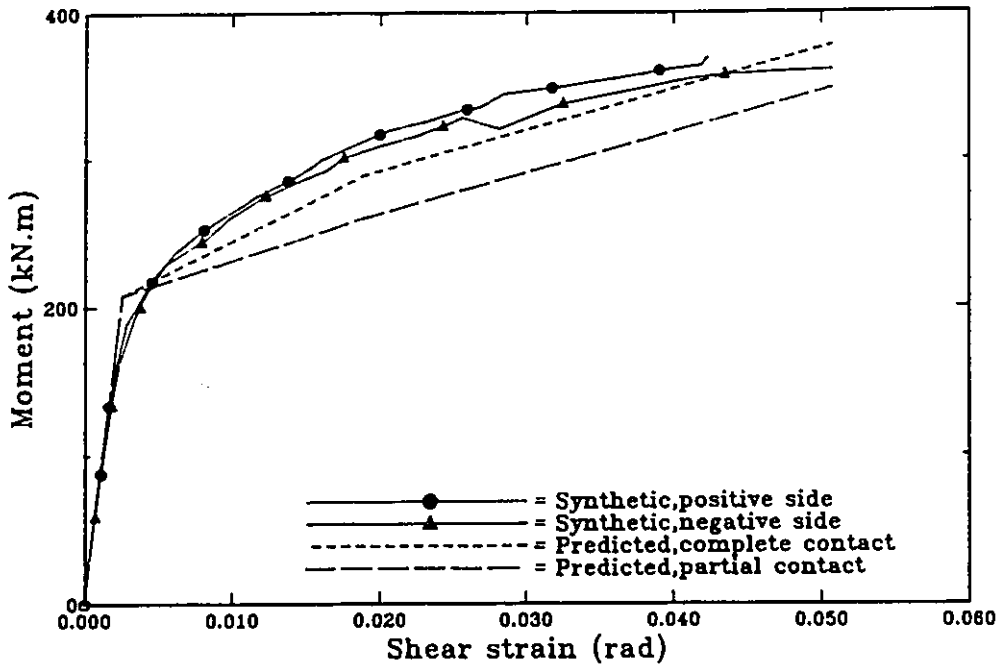

Fig. 5.7 Predicted vs. experimental M–γ relationship for specimen CB–1 panel.

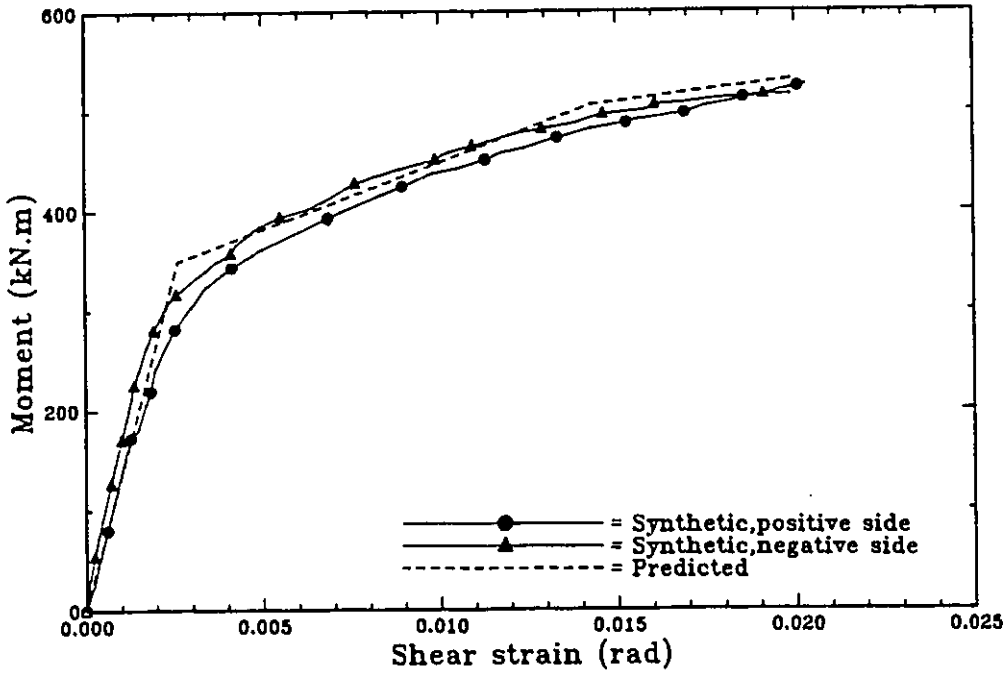

Fig. 5.8 Predicted vs. experimental M–γ relationship for specimen CC–1 panel.

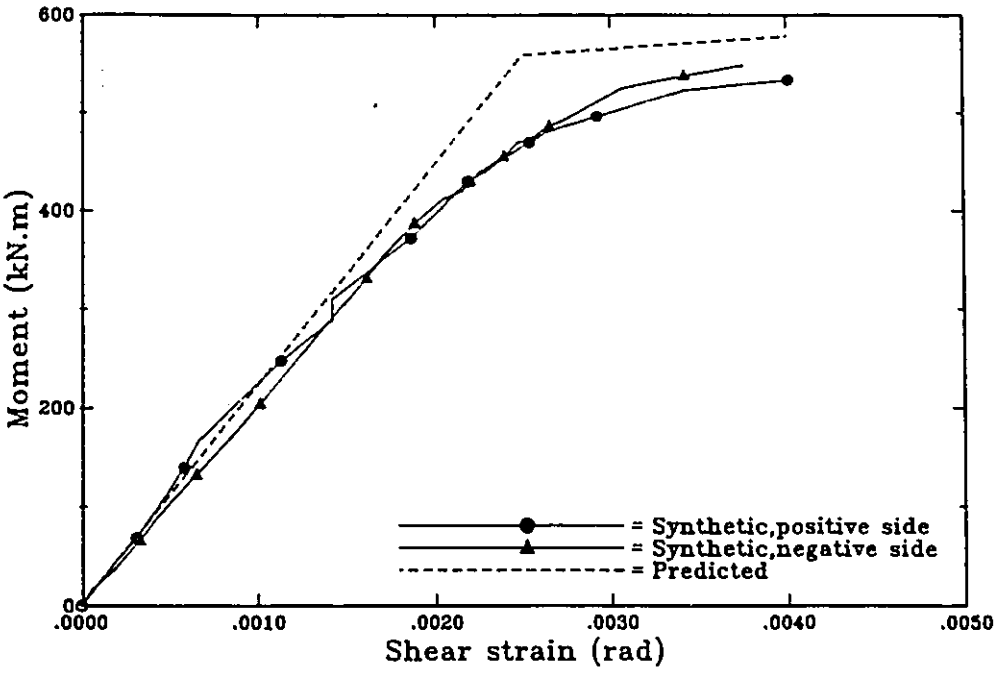

Fig. 5.9 Predicted vs. experimental M–Y relationship for specimen CC-2 panel.

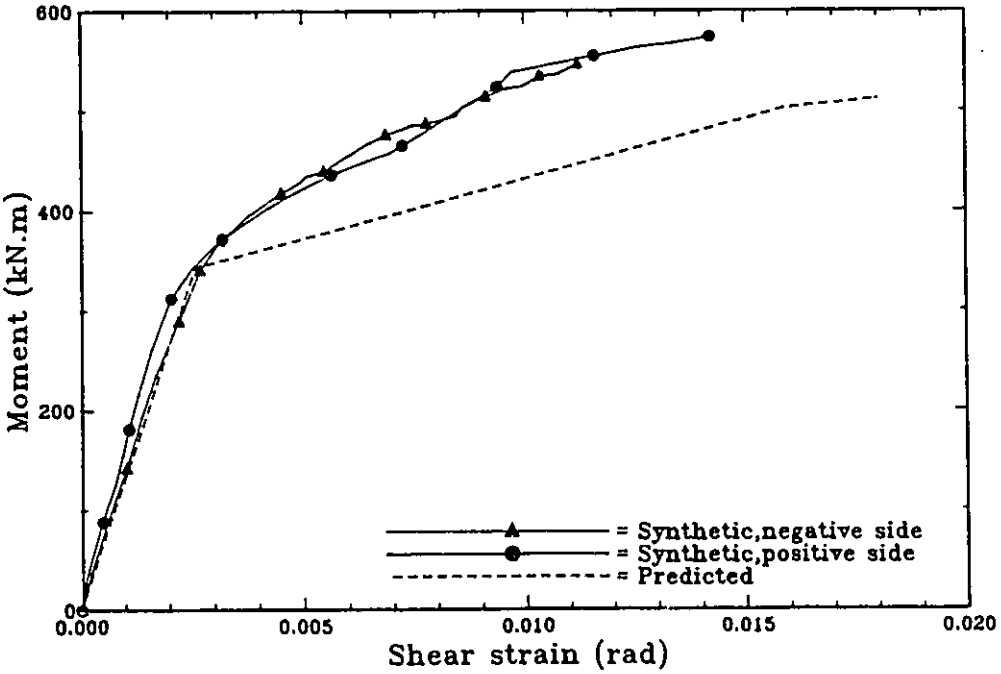

Fig. 5.10 Predicted vs. experimental M–Y relationship for specimen CC-3 panel.

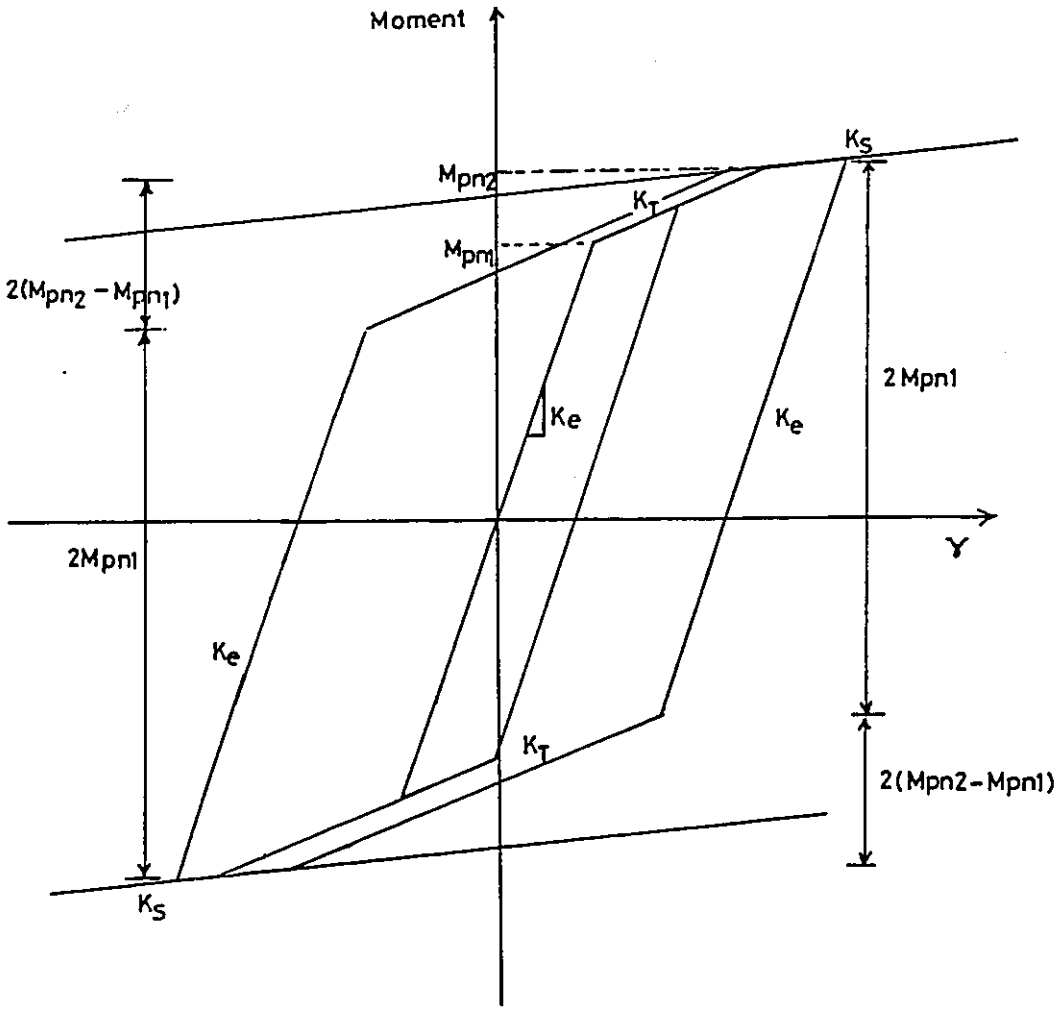

Fig. 5.11 Hysteretic model

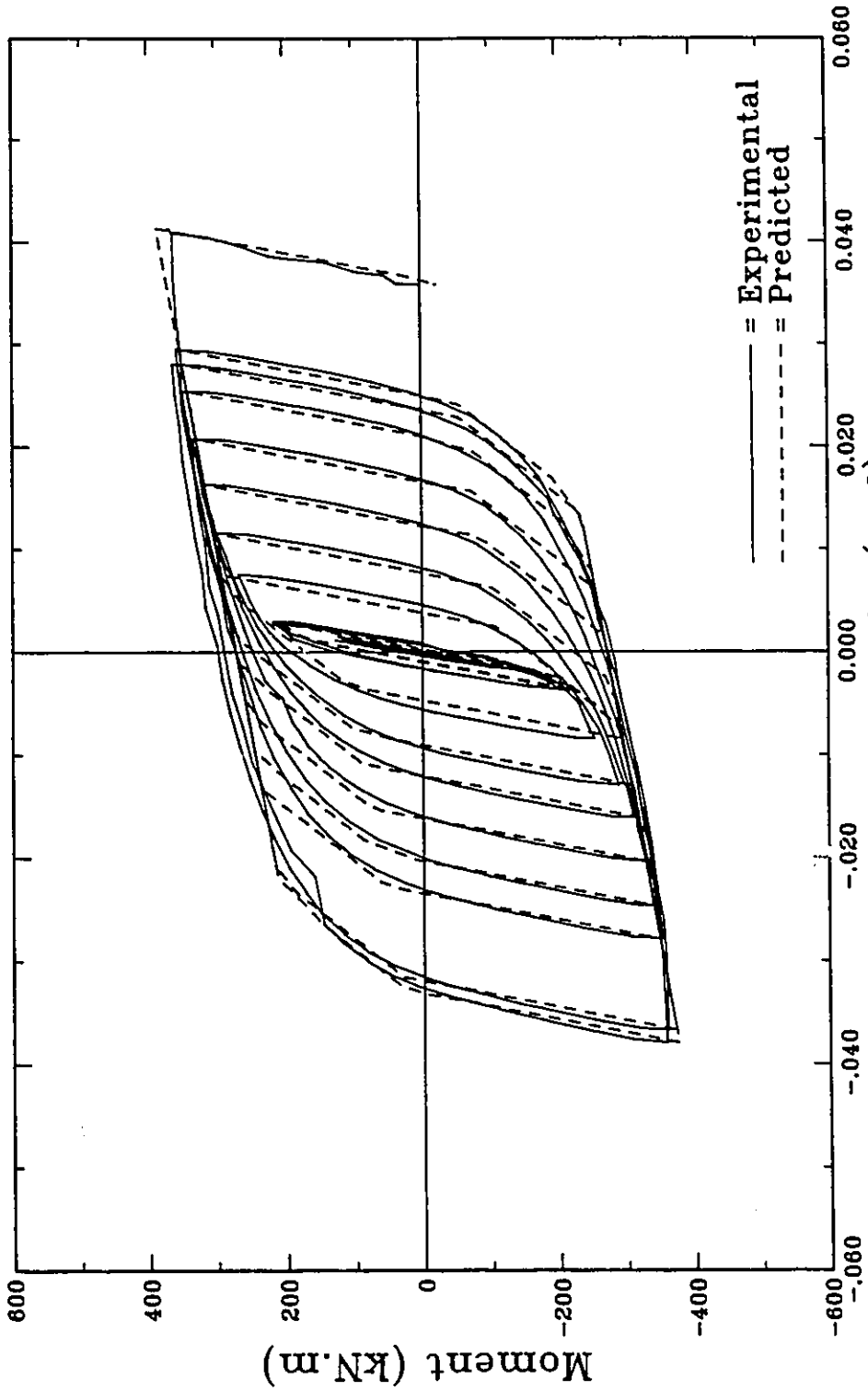

Fig. 5.12 Comparison between experimental and predicted panel response for specimen CB-1

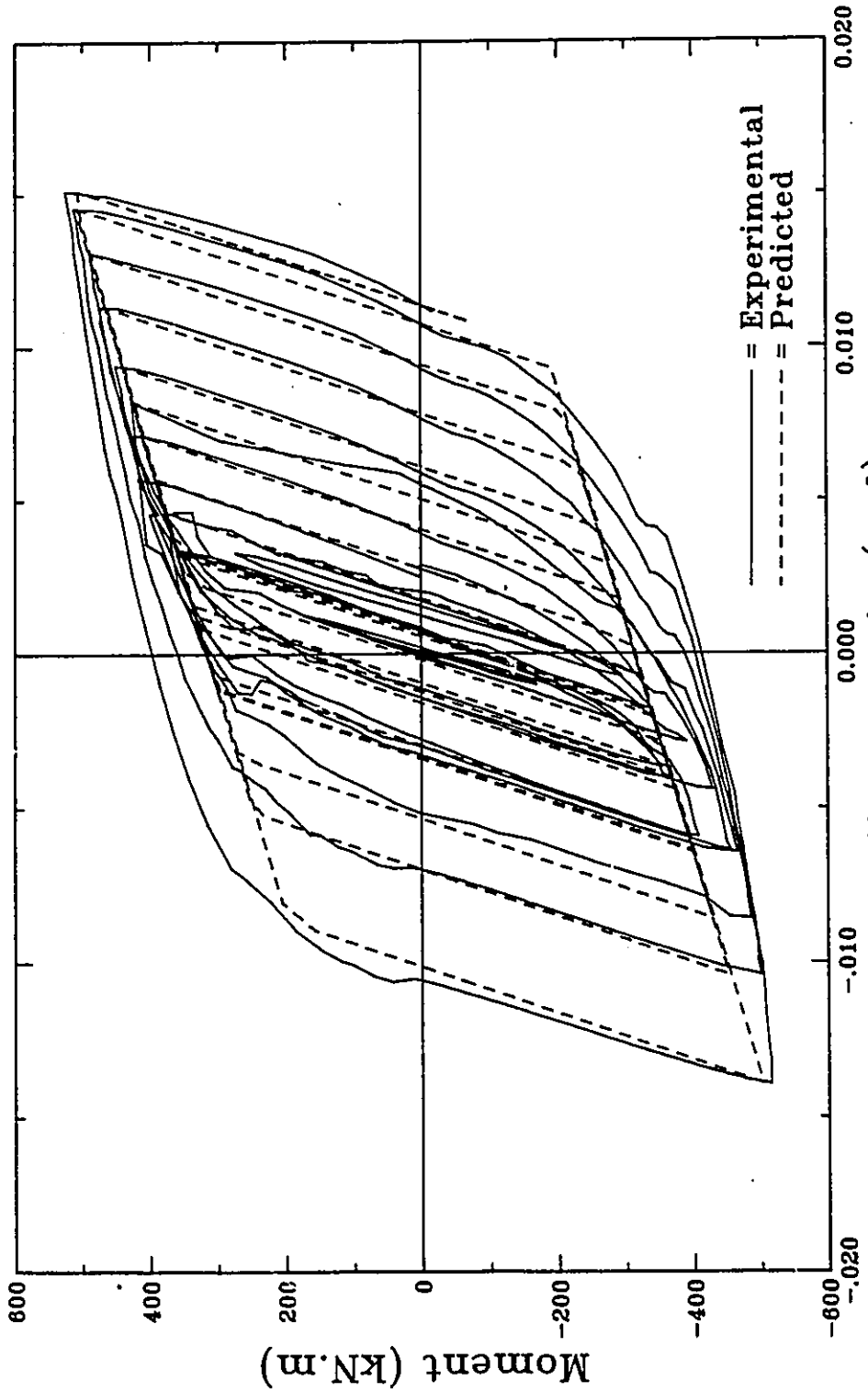

Fig. 5.13 Comparison between experimental and predicted panel response for specimen CC-1

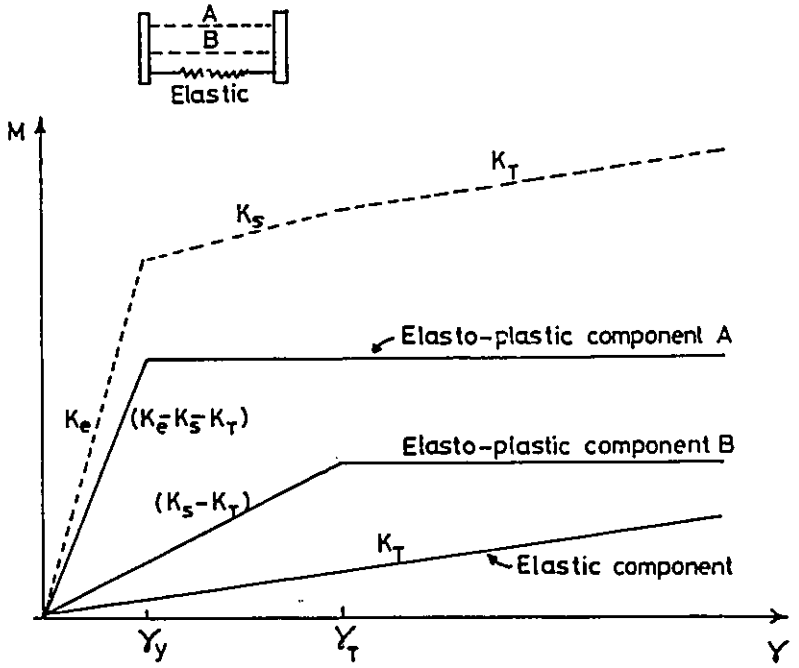

Fig. 5.14 The panel zone element components.

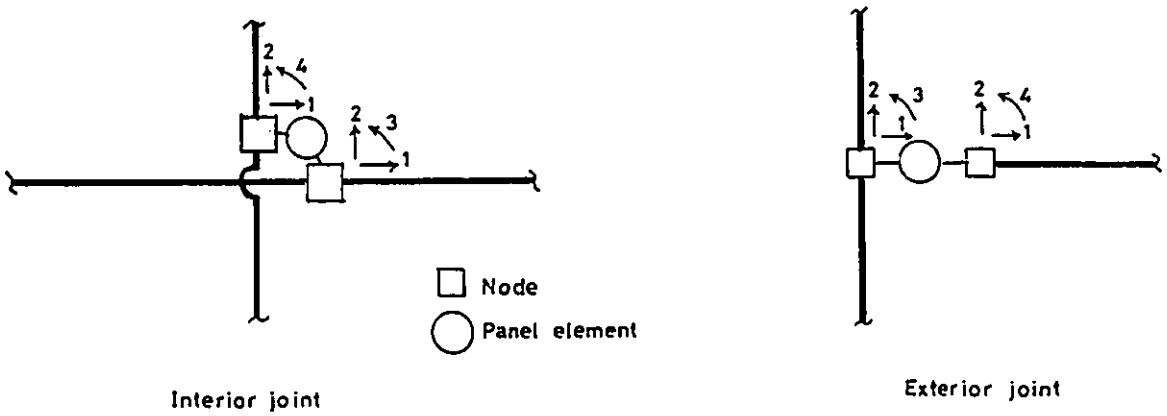

Fig. 5.15 Idealization of the panel zone element in frame analysis.

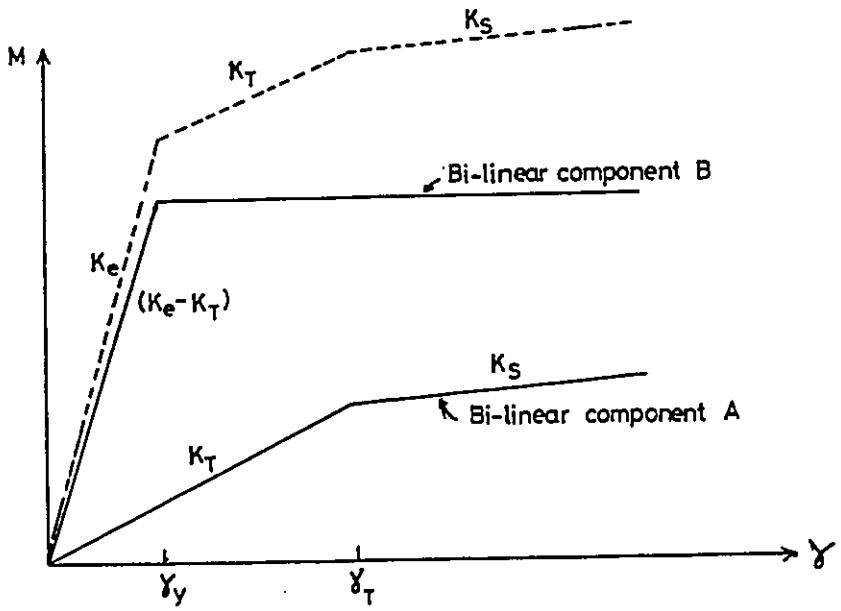

Fig. 5.16 Simulation of the tri-linear model by using two bi-linear models.

CHAPTER 6

ANALYSIS OF 8-STOREY BUILDING

6.1 Introduction

As previously mentioned, the design and detailing of the beam-to-column joints can significantly affect the static and dynamic characteristics of the MRFs. In chapters 2 and 3, it was observed that employing extended end-plate connections to join beams to columns can contribute significantly to the frame interstorey drift. Also, it was observed that yielding of such a connection type may lead to its failure. Based on these observations, a design criterion which limits a connection's inelastic action and minimizes its contribution to the overall drift of the structure was proposed. In chapter 4, the contribution of the panel zone to the response as determined experimentally was reported. From examining these results, it was concluded that the panel zone is a very ductile element and is capable of dissipating the input energy jointly with the beam.

However, several questions remained outstanding. For example: how will such a connection that meets the proposed design criterion affect the frame response?; or how should the panel zone be detailed in order to ensure its participation in dissipating the input energy with the beam? and then, how will such detailing affect the overall response of the frame?

To answer such questions and draw final conclusions about these larger issues, the connection model and the panel zone model (described in chapters 3 and 5, respectively), were incorporated into computer program Drain-2D (Kannan and Powell, 1973). The program was used to investigate the effect of the connection flexibility and the panel zone deformation on the response of multi-storey steel frames. Non-linear inelastic frame analyses were performed on frames employing extended end-plate joint between beams and columns. In detailing these joints the previously proposed criterion for designing the connection was employed. Also,

different design criteria for the panel zones were suggested and their effects on a frame's response were examined. As a result, design criteria for the panel zone are recommended.

6.2 Design procedure

For the purpose of this analytical study, the selected structure was an eight-storey, three-bay by four-bay rectangular steel office building located at Vancouver, British Columbia. As shown in Figs. 6.1 and 6.2, the total height of the building is 33.5 meters and the plan area is 972 m^2. The lateral load resisting system consists of a perimeter moment resisting frame in the E-W direction and braced frame in the N-S direction. The gravity load is supported by interior core columns in conjunction with the perimeter framing system. As a result, each frame in the E-W direction is expected to resist 50% of the lateral load but carry only 12.5% of the gravity loads. This framing system is similar to systems widely used in North America (Tahara and Kamei, 1988).

The storey height for the building was selected to be 4 meters for typical floors and 5.5 meters for the ground floor. The nominal yield stress of the structural steel used in the various structural elements is 300 MPa. The building was designed in accordance with CAN3-S16.1-M89 (1989) and the National Building Code of Canada NBCC (1990).

6.2.1 Loads

a) Gravity loads and floor system:

The structure was designed to sustain two types of gravity load; dead and live. The dead loads were assumed to originate mainly from the weight of the flooring system. The typical floor construction was presumed to consist of a beam and girder composite floor system. Except for a mechanical floor, all other floors and the roof consisted of 75 mm metal deck with 65 mm concrete cover. For the mechanical floor, a 90 mm concrete cover slab was provided. The concrete was taken as normal density of 20 MPa compressive strength. In addition to the floor dead

weight, loads due to fire protection, mechanical services and ceiling fixtures and materials were considered also. The exterior window wall system was assumed to weigh 1.65 kPa over the exterior surface of the building for the office floors. For the mechanical floor and the interior core walls, 2.0 kPa load over the walls surface area was superimposed. A 2.0 kPa load was applied over the mechanical floor to account for the presence of permanent equipment.

With regard to the live loads, a distributed load of 2.4 kPa was applied to all office floors. For the mechanical floor a 3.6 kPa distributed load was applied. These loads were subjected to tributary area reduction according to the NBCC (1990). A 1.0 kPa partition load was applied to the office and mechanical floors.

The roof was subjected to vertical loads due to self weight, wind and snow. A uniformly distributed snow load was calculated to be 1.76 kPa, which corresponds to 80% of the ground snow load, with the probability of being exceeded in 30 years on average.

b) Lateral loads

The building was designed to sustain two types of lateral loads, wind and earthquake. In the design, the equivalent lateral forces recommended by the NBCC (1990) were used. With regard to wind, the reference velocity pressure "q" for designing the members was taken to be equal to 0.44 kPa Which is "$q_{1/30}$" for the Vancouver area. Variation of the wind load with building height was also considered. The unfactored base shear due to wind load was calculated to be 878 kN (E-W direction).

With regard to earthquake, the base shear was given by $V=(V_e/R)U$, where U is equal to 0.6, R is the force modification factor and is equal to 4 in the case of a ductile moment resisting frame, and $V_e = vSIFW$. Here, v is defined as the zonal velocity ratio and is equal to 0.2 for Vancouver, while S represents the seismic response factor and is equal to $1.5/\sqrt{T}$. T is the period of the structure, which for unbraced steel frames may be taken as 0.1 N and N is the total number of storeys. The foundation factor F was taken as 1.3 which corresponds to coarse-grained soil,

while I is the importance factor and assumed to be equal to 1. W is the building dead load, which includes the weight of permanent equipment and 25% of the snow load.

Based on these inputs, the base shear acting on each frame was found to be 1267 kN, distributed to each floor using the following equation given in the NBCC (1990).

$$F_i = (V - F_t)\ (W_i h_i / \Sigma W_i h_i) \qquad (6.1)$$

Where

F_t = Concentrated force at the top of the structure and equal to 0.07 TV and considered zero if T>0.75.
V = Base shear
W_i = The portion of W that is located at the floor level i.
h_i = The height of the ith floor.

For this building, the storey shear forces due to earthquake loads were higher than that due to wind loads. Thus, the earthquake governed the strength design of the building.

6.2.2 Design of frame

After determining the applied loads, the second step is to design the frames. In contrast to frames designed to sustain gravity and wind loads only, frames designed to sustain earthquake loads are expected to experience inelastic action in the case of a major event. Therefore, these frames are not designed only to provide the strength and satisfy the code drift limitations under the applied loads, but also to satisfy the requirements for ductility. In the following, the steps for designing the 8-storey frame will be explained in detail.

a) Design for strength

The " portal frame method" was used to obtain the preliminary moments and axial forces in the beams and columns due to both gravity and lateral loads. Then, the moments and the axial forces were factored and combined for trial selection of the beams and columns. It was found that the combination (1.25 D+Q),

where Q represent the earthquake load, governs the design for all the columns and the beams.

Preliminary column and beam sizes were then selected, after which an elastic first order analysis of the structure was performed using the ETABS (Wilson et al, 1978) computer program. In this analysis, the members were checked for the following load combinations

1) 1.25 D + Q
2) 1.25 D + 0.7(1.5 L+Q)
3) 1.25 D + 1.5 L

The analysis was refined until final member sizes were selected. In selecting these members, the ductile requirements concerning the local stability of the members were satisfied in accordance with the Canadian Code (CAN3-S16.1-M89, 1989), i.e the sections were selected from class 1 sections and were properly laterally braced. It should be noted that in these analyses, the structural stiffness were formulated based on centre line dimensions and infinitely rigid panel zones and connections.

B) Drift limitation

Interstorey drift is one of the major aspects in assessing the performance of a structure under wind and earthquake loads. Usually, drift is controlled to assure satisfactory occupancy requirements under wind loads and to minimize nonstructural damage during earthquakes. When the building is subjected to specified earthquake loads, the NBCC (1990) recommends that interstorey drifts should not exceed .02 h_i/R ,where h_i is the height of the ith floor and R is the force modification factor. Also, the NBCC recommends that the interstorey drift should not exceed $h_i/500$ when the building is subjected to specified wind loads. The reference velocity pressure "q" used for the deflection calculation due to the wind loads is based on "$q_{1/10}$" value with a 10% probability of being exceeded in any one year. The building was checked for the previous drift limitations and the design was refined until it met the code requirements. The results of the analysis are shown in Fig. 6.3. First and second order analyses were performed under each loading case. For the second order

analysis, the fictitious column method developed by Rutenberge (1981) was used to account for the P-Δ effect. Analysis showed that the structural design was controlled by drift limitations from wind loading rather than strength requirements.

c) Strong column-weak girder concept

In the seismic design of steel frames, it is an accepted philosophy to design the girders to be weaker than the columns. As such, inelastic action is expected to take place in the beams which are capable of developing large inelastic rotations without strength deterioration. In the absence of an approach to satisfy such a requirement in CAN3-S16.1-M89 (1989), the building was checked using the equation recommended by the Uniform Building Code , UBC(1988).

$$\Sigma Z_c(\sigma_y-\sigma_a)/\Sigma Z_b\sigma_y>1.0 \qquad (6.2)$$

and

$\sigma_a > 0.0$

Where

Z_c= Column plastic section modulus.
Z_b= Beam plastic section modulus.
σ_y= Yield stress.
σ_a= Axial stress in columns.

It was decided to waive the strong column weak beam requirement in the upper floors, where P/P_y is less than 0.2.Taking these aspects into account led to the final member sizes for the 8-storey building shown in Fig.6.4.

6.2.3 Design of end-plate connections

Following the selection of the frame's members, the connections were designed according to the method proposed in chapter 2, after which the parameters that describe the moment rotation relationship of each connection were calculated. Tables 6.1 through 6.4 show the connections dimensions and the connections' model parameters.

6.2.4 Design of panel zones

Following detailing of the connections, the panel zones were designed. Four different design criteria were employed to assess the thickness requirements for the web. In all these methods, yielding of the panel zone was ensured in order to allow the panel to participate in dissipating the input energy jointly with the beam. However, the degree of inelastic action expected to be experienced by the panel zone was varied to examine the effect of changing the panel zone strength on the overall response of the frames. Since earthquake intensity can not be accurately predicted, it appeared prudent to design the panel zones for the capacity of the members framing into them (capacity design).

Design 1

In this method, the panel zones were designed to develop the beam strength. This was achieved by ensuring that the expected design shear, V_{des}, is equal or less than the shear capacity of the panel, V_{cap}. i.e

$$V_{des} \leqslant V_{cap} \qquad (6.3)$$

Where the shear capacity of the panel was taken equal to the panel shear at yield, and is given by

$$V_{cap} = 0.55 \sigma_y d_c t_{cw} \qquad (6.4)$$

and the design shear, V_{des}, is given by Eq. 6.5 as was previously explained in Chapter 5

$$V_{des} = \frac{M_{p1}}{0.95 d_{b1}} + \frac{M_{p2}}{0.95 d_{b2}} - H_c \qquad (6.5)$$

where

σ_y = The yield stress of steel,
d_c = The column depth,
t_{cw} = The thickness of the column web panel including the thicknesses of the doubler plates if any,
H_c = The column shear equal to $\Sigma M_{pi}/L_c$,
L_c = The storey height, and
M_{pi} = The flexural strength of the ith beam framing into the joint.

Applying such a design criterion results in relatively thick doubler plates and causes the panel zone to yield either with or after the yielding of the beam. As such, relatively small inelastic action is expected to take place in these panels. The thicknesses of the doubler plates and the resulting parameters that describe the panels models for the 8-storey frame are listed in Table 6.5.

Design 2

In this design method the design shear for the panel, V_{des}, was increased by a factor of 1.25 to account for possible overstrength of the beams. Therefore,

$$V_{des}=1.25\left(\frac{M_{p1}}{0.95d_{b1}}+\frac{M_{p2}}{0.95d_{b2}}-H_c\right) \qquad (6.6)$$

At the same time the panel shear capacity , V_{cap} ,was taken equal to the panel ultimate shear strength derived in Chapter 5 and given by

$$V_{cap}=0.55\sigma_y d_c t_{cw}+\left[\frac{2M_{f1}}{d_{b1}}+\frac{2M_{f2}}{d_{b2}}+\frac{M_{fmin}d_b}{6EI_{fmin}}G_{st}t_{cw}(0.95d_c)\right] \qquad (6.7)$$

where

M_{f1} and M_{f2} = The flexural strength of the column flanges including the end-plate thicknesses,
M_{fmin} = The minimum of M_{fi},
I_{fmin} = The minimum moment of inertia of the column flanges including the end-plates,
E = The modulus of elasticity,
G_{st} = Strain hardening shear modulus.

The first term of Eq. 6.7 represents the shear strength of the panel at the yield. The second term represents the additional resistance provided by the column

flange and the end-plates to the shear deformation, i.e the expected overstrength of the panel. Designing the panel zones according to this method ensures yielding of the panels prior to or approximately with the beams. This occurs without the panels' shear deformation encountering strain hardening.

In this method the panels are allowed to participate efficiently in dissipating the input energy but with controlled panel shears. Compared to Design 1, this method resulted in relatively thinner doubler plates as can be observed from Table 6.6.

Design 3

Design 3 is a mix of both designs 1 and 2. In this approach, the design shear force is determined using Eq. 6.5 and the panels' capacity as determined from Eq. 6.7. This design method resulted in weak panel zones and reduced drastically the thicknesses of the doubler plates. The panels designed according to such method would be expected to yield before the beam and to experience large deformations. The thicknesses of the doubler plates resulting from applying such a method to the 8-storey building and the associated models parameters are listed in Table 6.7.

Design 4

In this method, the strong column-weak panel principle which was suggested by Kawano (1984) was adopted. In this approach, the panel is designed to be the weakest element in the frame. This was achieved by linking the panel shear strength to the column's flexural shear strength through a factor ι, defined as $\Sigma M_{pn} / \Sigma M_{pco}$. The former is the summation of the beam moment required to yield the panel and is equal to $(t_{cw}\, \sigma_{yc}\, d_b\, d_c)$ while the latter represents the summation of the plastic moments of the columns framing into the joint. Kawano suggested a value of 0.42 for ι. Applying this approach results in very weak panels and confines all the inelastic action to the panels. Although, this approach is questionable except in special cases (Popov, 1987) it was adopted in this study to investigate frame response at the extreme case when the panels constitute the weakest elements in the structure. The thicknesses of doubler plates and panel model parameters that resulted from following this design approach are reported in Table 6.8.

6.3 Computer modelling

Once the 8-storey frames were designed and the connections and the panel zones detailed, the frames were modeled for the purpose of the analysis.

6.3.1 Inelastic elements for the analysis of MRFs

In modelling the frames, the two dimensional beam-column elements described in Appendix I was used to represent the beams and the columns. The beams were treated as beam-column elements with plastic hinges assumed to take place only in concentrated points at the element ends. The beams' shear deformations were neglected and the yield interaction limits were assumed to be affected by bending moment only. The effect of the axial forces were neglected. As such, beam strength is limited to ($Z\sigma_y$), where Z is the plastic modulus of the beam section and σ_y is the yield stress. In the case of the columns where the axial forces are high and cannot be neglected, beam-column elements possessing flexural and axial stiffness were used. Member stability considerations were excluded while yielding was assumed to take place only in concentrated hinges at the element ends. Yield interaction relationships given below were assumed to govern the strength (CAN3-S16.1-M89, 1989)

$$\frac{C_f}{C_y} + 0.85\frac{M_{fx}}{M_p} \leqslant 1.0 \qquad (6.8)$$

and

$$\frac{M_{fx}}{M_p} \leqslant 1.0$$

In inequalities 6.8, C_f and M_{fx} are the axial load and the bending moment about major axis due to gravity and lateral loads while C_y and M_p are the axial compressive resistance $A\sigma_y$, and moment resistance, respectively. Such a strength limit is applicable for steel welded wide flange and wide flange sections bent about their major axes. For modelling the connections between the beams and the columns, bilinear springs as described earlier were used. The spring parameters such as the

initial stiffness, K_i, the post elastic stiffness, K_p, and the connection plastic moment, M_{pc}, were calculated as previously described in chapter 3.

In modelling the panel zone behaviour, the tri-linear model described in chapter 5 was used. For the beam and the beam-column elements a strain hardening modulus of .03E was used. The modulus of elasticity and the shear modulus for steel were assumed to be 200,000 MPa and 77,000 MPa, respectively.

In the analysis, the effect of the column axial force on the panel zone behaviour was neglected. Neglecting the effect of the column axial force, will result in an error not more than 5% as stated by Tsai and Popov (1988).

6.3.2 Damping

A damping proportional to both the mass and the tangent stiffness was used. A damping ratio of 3% was assigned to the first two modes. The damping cofficients η and ζ were determined as explained in Appendix II. It is believed that the error in the damping approximated in this manner is within an acceptable range of accuracy implicit in the analysis undertaken.

6.3.3 Loads and masses

The frames were subjected to gravity loads that included specified dead (unfactored) and live loads. The live loads were subjected to tributary area reduction as permitted by the NBCC (1990). Gravity loads applied to the beams were modelled by specifying fixed end forces at the beam ends. Masses of the tributary floor areas, wall units and glazing were all assumed to be lumped to the column-beam joints and were associated with the horizontal displacement of the floors only. In addition, 25% of the snow load on the roof and 100% of permanent equipments in the mechanical floor were included.

6.4 Cases studied

In order to study the effect of the connection flexibility and the panel zone deformation on the response of an 8-storey frame, both static and dynamic analyses

were performed. In each case, six different frames were studied. Each frame represents a case study with a special configuration for the connections and the panel zones. For the sake of comparison, the beams and columns sections in all six frames were kept constant and only the stiffness of the connections and the panel zones were changed. Table 6.9 summarizes the studied cases.

As can be observed, in case 1 the connections and the panel zones were assumed to be infinitely rigid. In practice this represents the case when fully welded connections are used to join the beams to the columns and diagonal stiffeners are used to stiffen the panel zone. In such a case, all the inelastic action is expected to be confined to the beams and the columns. This design was taken as the base-line for comparison.

In the case 2, the panel zones were assumed to be infinitely rigid. However, the connections were modeled using bilinear springs. In reality, this frame represents the case when extended end-plate connections are used to join the beams to the columns while diagonal stiffeners are employed to stiffen the column panel zones. Comparing the response in this case with that in case 1 reveals the effects of employing extended end-plate connections in moment resisting frames on the frame response.

In case 3, the connections were modeled using bilinear springs to simulate the connections' moment-rotation relationships ,and, tri-linear springs were used to simulate the applied moment-shear strain relationships for the panel zones. In assigning the values for the connections' model parameters, similar values to the ones used in frame case 2 were adopted. However, in assigning the values for the parameters used to describe the panel zones' behaviour, the values calculated based on panel zone 1st design criterion were used. As a result, this frame represents the case when extended end-plate connections are used to join the beams to the columns with the panel zones detailed according to design 1 criterion. Since this case, and frame case 2 have identical connections, the difference in response is expected to be due to the effect of employing design 1 criterion in detailing the panel zones.

Frame cases 4 ,5 and 6 were similar to frame case 3 with the exception that

the panel zones in these cases were detailed according to the 2nd , the 3rd and the 4th design criteria previously described, respectively. Comparing the responses in these cases to the response of frame case 2 reveals the effect of employing design 2, 3 and 4 criteria on the response of MRFs.

6.5 Static Characteristics of the 8-storey MRFs

6.5.1 Effects of connection flexibility

To examine the effect of the connection flexibility on the static behaviour of the 8-storey frame, the frames case 1 and case 2 were subjected to the code specified lateral earthquake loads. The resulting frames' lateral displacements are shown in Fig. 6.5. As can be observed, the frame case 2 with extended end-plate connections exhibited larger drifts than the rigidly connected frame in case 1. The contribution of the connections' flexibility to the increase of the roof lateral deflection was about 9%. Thus, it can be concluded that employing extended end-plate connections, designed and detailed in accordance with the previously proposed design criteria (Chapter 2) tends to increase the frame lateral deflection. With regard to the forces generated in the members, no significant differences were observed except that the exterior columns in frame case 2 shed some of their moments to the interior columns.

6.5.2 Effects of panel zone flexibility

Similarly, frame cases 3, 4, 5,and 6 with panel zones designed according to design criteria 1, 2, 3,and 4,respectively , were subjected to the code specified earthquake loads. The resulting lateral deflections for the four cases with the lateral deflection for frame case 2, are shown in Fig. 6.6. Since all the frames have identical connections and were subjected to same loads, the differences in the response are attributed only to the flexibilities of the panel zones. Comparing the lateral deflection of the roof of frames in cases 3, 4, 5,and 6 with that of frame case 2 shows that 19.3% ,23.3% ,28.4% ,and 35.5% increase in the roof deflection were observed,respectively due to the reduction in the panel zones stiffness. It should be

noted that in all analyses the frame stiffness were formulated based on member clear spans.

6.6 Dynamic characteristics of the MRFs

Inclusion of the connections and the panel zones in the analysis is expected to affect the dynamic characteristics of the frames,i.e the vibration periods and the mode shapes. Incorporating the connections and the panel zones reduced the stiffness of the frames while the masses remain constant. It is expected that the connections and the panel zone flexibilities lengthen the vibration periods of the frames. The computer program ETABS was used to determine the periods of free vibrations of the frames. Since the ETABS program does not contain any connection or panel zone elements, a unique technique was used to account for their effect. This was done by adjusting the structure's stiffness matrix coefficients. These coefficients were calculated on the basis of the initial stiffness of the connections and the panel zones using the methods suggested by Gerstle (1988) and Kato et al. (1988).

The resulting first seven vibration periods for each frame are shown in Table 6.10. It can be observed, that the fundamental period of frame case 2 with flexible connections and infinitely rigid panels is 1.05 times that of frame case 1 with infinitely rigid connections and panels. At the same time, frame cases 3, 4, 5,and 6 have a first mode with periods 1.060, 1.067, 1.092,and 1.1 that of frame case 2. Therefore, it can be concluded that the inclusion of the connections and the panel zones flexibilities in the analysis indeed lengthens the natural periods of the frames. However, in any case this effect is not more than 10%. The mode shapes differ from each other only slightly. Also, analysis shows that in all frames, about 80% of the effective model mass is associated with the first mode.

6.7 Nonlinear dynamic analysis of MRFs

6.7.1 Selection of ground excitations

Three different earthquake records were used to assess the dynamic performance of the 8-storey MRFs. The ground motions were selected from actual

earthquake records that have a predominant natural period close to the natural periods of the frames.

Accordingly, the three selected ground motion records were:

1) The NS (Bucharest) component of the original 1977 Bucharest earthquake with a peak ground acceleration of .205g and a peak ground velocity of 0.75 m/sec. The most notable feature of the Bucharest earthquake was the single strong pulse with a period of about 1.4 seconds recorded in the N-S and E-W components that resulted in damage to flexible, low frequency structures.

2) The N90W (SCt) component of the 1985 Mexico earthquake with peak ground acceleration of 0.17g and a peak ground velocity of 0.605 m/sec.

3) The EW component of the Near Coast of Honshu 1968 earthquake of peak ground acceleration of 0.2g and a peak ground velocity of 0.32 m/sec. This time history was recorded on soft soils and at a long epicentral distance of 243 km.

The MRFs were designed for a location in the Vancouver area. According to the NBCC (1990), Vancouver is located in zone 4 which is expected to experience earthquakes with peak ground acceleration and peak ground velocity of 0.23g and 0.23 m/sec with a 10% probability of exceedence in 50 years. All the selected earthquakes have peak ground accelerations less than 0.23g, but the peak ground velocities were higher than 0.23 m/sec. The time histories were used as recorded and no attempt was made to scale the records.

The ground acceleration history, the associated Fourier spectrum and the linear elastic pseudo-acceleration spectra for 3% damping were computed and plotted in Figs. 6.7 through 6.10.

Examining Fig. 6.10 which shows the periods of the MRFs and the corresponding spectral pseudo-acceleration reveals that, during Bucharest and Honshu events, in addition to the first mode the second and the third modes may be contributed to the frames response. However, during the Mexican event the first mode is expected to dominate the frames response.

6.7.2 Response to the earthquakes

The three selected earthquake records were used as the input ground motions for each frame. In the analysis, the equation of dynamic equilibrium was formulated at any instant of time. Then, it was solved. Various explicit and implicit, single and multiple step integration schemes have been used to solve the incremental equations of motion for linear and nonlinear systems (Newmark, 1959; Wilson et al. 1973 and Hibler et al. 1977). However, two basic requirements should be satisfied in the method used, namely its accuracy and stability.

In Drain-2D program, a method based on constant acceleration within the time step has been adopted. This method has the advantage of being stable for all periods and time steps, and of not introducing damping into the system. The basic equations for this method with the solving technique used by the program are explained in Appendix III.

The results of the storey displacements, storey drifts and storey shears obtained from these analyses were studied. The effects of the connections and the panel zone deformations on the response of the frames were evaluated. Also, the maximum plastic hinge rotation experienced by the beams, the columns and the panel zones during each event, were examined. The results of the analyses are summarized for each event as follows. Additional information can be found in Osman et al (1991a)

a) Response to Bucharest earthquake

The floor displacement envelopes and the floor displacements at the instant of the peak roof displacement for the MRFs are shown in Figs. 6.11 and 6.12. Examining Fig. 6.11 shows that, frame case 2 with flexible connections exhibited larger lateral deflections than frame case 1 with rigid connections. The increase in the roof deflection in this case was only about 2.8%, a value that is considerably less than the 9% increase observed under static loads. Fig. 6.11(b) Shows that the responses of frames cases 1 and 2 are dominated by their first mode with only small contribution from the third mode. From Fig. 6.12(a), it can be observed that, Frames

cases 5 and 6 with relatively weak panels exhibited less positive displacement as compared to frame case 2 with infinitely rigid panels. On the contrary, frame cases 3 and 4 which have relatively strong panels exhibited 8.6% and 11% increases in the roof displacement, respectively as compared to frame case 2. Again, these increases were much less than the 19.3% and 23.3% observed in the case of static loads. Also, Fig. 6.12(b) shows that the response of the frames with flexible panel zones was dominated by the first mode, but with noticeable participation from the third mode. The study of the roof displacement histories of the MRFs provides further insight into the frame response. As can be seen from Fig. 6.13, frame cases 1 and 2 vibrate approximately in the same manner, with frame case 2 exhibiting slightly larger deformation. However, from Fig. 6.14 it can be observed that all the frames vibrated in the same manner up to 5 seconds after the event started, after which differences occurred. Again, the figures show that the deflection is not as pronounced as in the case of static loads. This can be explained by examining Figs. 6.15 and 6.16 which show the frames' storey shears and storey drifts. Obviously, frame case 1 with rigid panels and connections experienced the highest storey shears, followed by frame cases 2 to 6 in that order. As would be expected, as a frame's stiffness decreases its storey shear decreases.

The maximum base shear experienced by frame cases 1, 2, 3, 4, 5, and 6 respectively were 2.77, 2.76, 2.67, 2.57, 2.30 and 2.25 times the design base shear. Also, The maximum storey drift that occurred in the frames respectively were 2.67%, 2.66%, 2.94%, 3.18%, 2.87%, and 3.6% . It should be noted that these drift values exceeded the 2% drift limitation prescribed by the code (NBCC, 1990) for the case of inelastic response. As such, it would be expected that the P-delta effects could be significant and would need to be accounted for.

Incorporation of panel zones and connection flexibilities in the analysis can significantly change the distribution of the internal forces throughout the structure. Figs. 6.17 through 6.20 show the columns' axial forces and the column moment envelopes for two columns, column 1 which is an exterior column aligned with axis 1 and column 2 which is an interior column aligned with axis 2. By examining Figs

6.17 and 6.19, it can be noted that as the frames stiffness decreases, the moments experienced by the columns decrease. This can be attributed to the fact that less stiff structures attract less forces. By examining Figs. 6.18 and 6.20, a similar conclusion can be drawn for the columns' axial forces. However, this behaviour is noticeable in the case of exterior columns where a large portion of the axial force result from the storey moments. In the case of interior columns, where the main source of axial forces is the gravity loads, this behaviour can not be easily detected.

The maximum panel zone joint, beam, and column plastic hinge rotations that occurred during the event are shown in Figs. 6.21 through 6.26. As can be observed, frame case 1 with rigid connections and panel zones had the highest rotational demands of the beams and columns compared to the other frames. Also, Comparing frame case 2 with frame case 1 reveals that the inclusion of the connection did not affect the distribution of the plastic hinges throughout the frame, but only reduced slightly the demand on the beams and on the columns.

Examining frame cases 3, 4, 5 and 6 which have flexible panel zones showed that once the panel zone stiffness and strength decreased, the rotational demands on the beams and columns decreased, as well. In the case of frame case 3 only the interior panels yielded, but for frames cases 4, 5 and 6 both the interior and exterior panels yielded. Some panels in frames cases 5 and 6 approached strain hardening conditions. This can be seen from Figs. 6.27 and 6.28 which show the behaviour of two panels, one an interior and the other is exterior, for the different frame designs. In general, all the frames formed hinges at the bottom end of columns at ground level. However, the magnitude of such rotations decreased with the decrease in a frame's stiffness as a result of incorporating the connection and panel zone flexibilities. It should be mentioned, that in view of the high rotational demand and high axial forces experienced by the columns at the ground level, frame case 1 would have the least chance to survive such a major event,due to the high possibility of occurrence of local instability.

b) Response to Mexico earthquake

In addition to Bucharest earthquake, the frames were analyzed for Mexico

event. The maximum floor displacements, storey shears, storey drifts, as well as the plastic hinge deformation for the beams, columns and panel zone joints are presented in Figs 6.29 through 6.38. Examining Figs. 6.29 and 6.30 supports the previous conclusion regarding the effects of the connections and the panel zones in increasing the frame's lateral deflections. also, they suggest that the response of the MRFs during the Mexican event were dominated by the first mode. During this event and after 57.5 seconds from its start, the large negative peaks produced severe inelastic action in the MRFs causing them to deform significantly. Subsequent vibrations were about a deformed position. This was the reason that in Fig. 6.30 frame cases 3, 4, 5,and 6 experienced significantly higher negative and less positive displacement compared to frame case 2 with rigid panels. Again, the less stiff frames experienced less storey shear as shown in Figs. 6.31 and 6.32. The maximum storey drift that occurred in frame cases 1, 2, 3, 4, 5 and 6 were 3.5%, 4.2%, 3.9%, 3.7%, 3.2% and 3.8% , respectively. With the exception of frame case 6 where the maximum drift occurred at the seventh floor, all other frames' maximum interstorey drifts occurred at the ground floor level. These drifts were significantly higher than the code limit for inelastic action,(2%). The severity of such an event can be noted from examining Figs. 6.33 through 6.38 which show the maximum plastic hinges formed in the beams, the columns and the joints. The magnitudes of the plastic hinge rotations at the base of the columns at ground floor were relatively high,indicating a high possibility of local instability. Also, in most of the frames, plastic hinges formed at the top and at the bottom of the same column. Although, this is not a mechanism nor did the plastification form at the same instant, the pattern of yielding shows the devastating effect of such an event. The Mexico earthquake is characterized by high input energy and high peak ground velocity and a predominant period that was close to the natural periods of the MRFs.

c) Response to Honshu earthquake

As a third example, the Honshu earthquake of 1968 was employed in a similar manner as for the other two described earlier. Plots of the maximum floor displacements, maximum storey shears, storey drifts and plastic hinge deformations

for beams, columns and panel zones are shown in Figs. 6.39 through 6.48. As can be observed from Fig. 6.39 frame case 2 experienced higher positive and fewer negative deflections compared with frame case 1. On the other hand, frames in cases 3, 4, 5,and 6 experienced still higher deflections in both directions compared to frame case 2 with rigid panels as shown in Fig. 6.40. The maximum base shear calculated for the six frames were 2.78, 2.856, 2.837, 2.78, 2.58 and 2.26 times the design base shear, respectively. Figs. 6.39 through 6.42 suggest that the participation of the higher modes in the response, especially in frame case 6 having weak panel zones, was noticeable. Examining Figs. 6.43 through 6.48 indicates how the inclusion of the connections and the panel zones changed the distribution of the plastic hinges throughout the structure. In general, as the panel zone becomes flexible ,the rotational demands on the beams are reduced.

6.7.3 The demand and the supply

As can be concluded from the previous analyses, the end plate joints when properly designed and detailed can perform reasonably well in severe earthquakes. However, the full significance of the previous observation can be realized only after the behaviour of individual elements in the frames are examined. As such, maximum plastic hinge rotations of the beams and maximum joint distortions at each floor were identified from the time history analyses. Then, these values were normalized with respect to the beams' plastic hinge rotations and joint distortions at yield to give an indication of the inelastic deformation demands for the beams and the joints. This was achieved by defining the normalized plastic hinge rotation of the beams, μ_θ,(rotation ductility) as follows:

$$\mu_\theta = 1 + \frac{|\theta|}{\theta_y} \qquad (6.9)$$

where

$|\theta|$ = The absolute maximum plastic hinge rotation of the beam.
θ_y = The rotation at yield and is equal to $M_pL/6EI$.
E = Modulus of elasticity.
L = Beam span.
M_p = Plastic moment of the beam.
I = Beams moment of inertia.

Also, the panel zone deformations were normalized with respect to panel shear strain at yield, γ_y, resulting in the following definition of joint ductility:

$$\mu_p = \frac{|\gamma|}{\gamma_y} \qquad (6.10)$$

where

$|\gamma|$ = The absolute maximum panel zone rotation.

The results of the beam and panel zone ductilities in the cases of the different events are shown in Figs. 6.49 through 6.51. These predicted ductilities are the values that must be achieved if the MRFs are to survive the earthquakes.

As can be seen from these figures, the beam ductility demands vary considerably from floor to floor, from frame to frame and from event to event. In general, frame cases 1 and 2 with rigid panel zones imposed the highest rotational demands on their beams. On the other hand, frames 5 and 6 with relatively weak panels imposed the lowest rotational demands on the beams. In this study, the predicted demands for the beams from the analytical analyses were compared with the beams' ductilities obtained experimentally (Chapter 2). To make the results comparable, the ductilities, R_u, in Table 2.3 which represent the ductilities that the beams can deliver, were used. The values of R_u is defined as the beam ductility achieved before failure or before beam plastic moment capacity is exhausted. The comparison reveals the following:

1- For the Bucharest, Mexico and Honshu events the required ductilities of the beams are not excessively large ($\mu_\theta < 6$), i.e the imposed rotational demands on the beams in the Bucharest, Mexico and Honshu events are within the rotation capacities

expected from class 1 sections when properly braced in accordance with plastic design requirements.

2- Local instability problems would be expected to occur in the case of Mexico earthquake, in frame cases 1,2 and 3, since θ in such cases were higher than θ_m values given in Table 2.3.

Form Figs 6.49 to 6.51, it can be observed that the joint distortions were within the accepted limits ($\gamma < 20\gamma_y$) for well designed joints (Kato et al, 1988). Thus, it can be concluded that, with the exception of frame cases 1, 2, 3 for the Mexican earthquake, the frames would be expected to behave satisfactorily under postulated earthquakes from the prospective of the ability of beams and joints to sustain the imposed demands.

Also, from the demand and the supply prospective, it is very important to examine the ability of columns, especially at the ground floor level(columns with highest axial forces), to deliver the required rotational demands. According to previous research conducted in this field (Bertero et al, 1973, Mitani et al, 1977; Suzuki and Ono, 1977 and Matsui and Yoshizumi, 1980) columns under high axial forces are more prone to buckling as compared to columns with less axial force under the same rotational demands. It is known that buckling leads to drastic deterioration in a column's resistance and a column's ductility. In these analyses, the axial force in ground floor columns approached 0.167 P_y, 0.30 P_y and 0.28 P_y for the cases of the Bucharest, Mexico and Honshu events, respectively. From the figures which show the maximum plastic hinges rotations in the MRFs, it can be concluded that, in the frames with flexible panel zones, the possibility of local buckling occurring in the ground floor columns is much less than for the case of frames with rigid panels.

6.8 Summary

Based on the previous analysis the following can be concluded:

1) Incorporating the connection in the analyses has demonstrated that, extended end-plate connections, detailed and designed according to the proposed design method,

do not change significantly the static and dynamic characteristics of frames.

2) Inclusion of the connections and panel zones lengthen the frames vibration periods. However, this effect appears to be insignificant.

3) Under static loads, frames with flexible connections and panel zones experienced higher lateral deflections. These deflections were highest in the case of frames with weak panel zones.

4) The increase in the lateral deflections of the MRFs with flexible connections and panel zones were not as pronounced in the case of dynamic loads as in the case of static loads.

5) Allowing yielding to take place in the panels resulted in a more uniform distribution of the dissipated energy and imposed less rotational demands on the beams in the MRFs.

6) Designing the panel zone according to design criterion 3 or 4 resulted in a drastic reduction in the frames stiffness and consequently unacceptable high deflections under static loads. Also, adopting the design 4 criterion for detailing the panels resulted in confining all the inelastic action to the panels, thus neglecting the beams which have good ductile potential. On the other hand, adopting design criterion 1 for detailing the panels required relatively thick doubler plates which may be impractical to design. Most of the inelastic action was confined to the beams.

7) In the view of this study, design 2 criterion in which the panel is detailed to yield approximately at the same time with the beam and deform without encountering strain hardening is the recommended design criterion for the panel zone.

8) This study highlightened the importance of including the effects of the connections and the panel zones in frame analysis.

Table 6.1 End-plate design for 8-storey frame (Interior connection)

Floor level	Dimensions (mm)	Thickness (mm)	Bolts diameter	Column flange stiffener
8th	480X230	25	7/8"	No
7th	822X260	40	1 1/8"	No
6th	822X260	40	1 1/8"	Yes
5th	822X380	45	1 1/2"	Yes
4th	822X380	45	1 1/2"	Yes
3rd	822X380	50	1 1/2"	Yes
2nd	822X380	50	1 1/2"	Yes
1st	970X400	45	1 1/2"	No

All bolts are A490.

Table 6.2 Connection model Parameters (Interior connections)

Floor level	K_i (kN.m/rad)	K_p (kN.m/rad)	M_{pc} (kN.m)
8th	$23.747X10^4$	$3.562X10_4$	312.65
7th	$429.59X10^4$	$64.44X10^4$	1641.8
6th	$429.59X10^4$	$64.44X10^4$	1641.8
5th	$206.30X10^4$	$30.94X10^4$	2300.0
4th	$206.30X10^4$	$30.94X10^4$	2300.0
3rd	$333.15X10^4$	$49.97X10^4$	2869.0
2nd	$333.15X10^4$	$49.97X10^4$	2869.0
1st	$310.60X10^4$	$46.59X10^4$	2714.3

Table 6.3 End-plate design for 8-storey frame (Exterior connections)

Floor level	Dimensions (mm)	Thickness (mm)	Bolts diameter	Column flange stiffener
8th	480X230	25	7/8"	Yes
7th	822X260	40	1 1/8"	Yes
6th	822X260	40	1 1/8"	Yes
5th	822X380	45	1 1/2"	Yes
4th	822X380	45	1 1/2"	Yes
3rd	822X380	50	1 1/2"	Yes
2nd	822X380	50	1 1/2"	Yes
1st	970X400	45	1 1/2"	Yes

All bolts are A490.

Table 6.4 Connection model Parameters (Exterior connections)

Floor level	K_i (kN.m/rad)	K_p (kN.m/rad)	M_{pc} (kN.m)
8th	$30.326X10^4$	$4.549X10^4$	312.65
7th	$137.85X10^4$	$20.67X10^4$	1211.8
6th	$429.59X10^4$	$20.67X10^4$	1211.8
5th	$206.30X10^4$	$30.94X10^4$	2003.0
4th	$206.30X10^4$	$30.94X10^4$	2003.0
3rd	$103.17X10^4$	$15.48X10^4$	2853.7
2nd	$103.17X10^4$	$15.48X10^4$	2853.7
1st	$117.26X10^4$	$17.59X10^4$	2542.6

Table 6.5 Panel zone joint for 8-storey building (Design 1)

Floor level	Doubler plate thicknesses	M_{pn1}	M_{pn2}	K_e	K_T	K_s
Interior columns						
8th	No	394.	864.	164233	151149	5583.9
7th	2PL#20	2149	2757	722279	180414	24557
6th	2PL#20	2149	2757	722279	180414	24557
5th	2PL#25	3214	4225	1044124	421106	35500
4th	2PL#25	3214	4225	1044124	421106	35500
3rd	2PL#30	4288	5540	1508753	518280	51297
2nd	2PL#30	4288	5540	1508753	518280	51297
1st	2PL#30	4011	5408	1468533	610776	49930
Exterior columns						
8th	No	224.1	350	93843	12983	3190.7
7th	2PL#10	1182	1667	372007	22832	12648
6th	2PL#10	1182	1667	372007	22832	12648
5th	2PL#16	1945	2643	527289	53800	17927
4th	2PL#16	1945	2643	527289	53800	17927
3rd	2PL#16	2323	3170	731629	96379	24875
2nd	2PL#16	2323	3170	731629	96379	24875
1st	2PL#14	2105	3029	802822	135848	27295

Moments are in kN.m.
Stiffnesses are in kN.m/rad.
Doubler plates thicknesses are in mm.

Table 6.6 Panel zone joint for 8-storey building (Design 2)

Floor level	Doubler plate thicknesses	M_{pn1}	M_{pn2}	K_e	K_T	K_s
Interior columns						
8th	No	394.	864.	164233	151149	5583.9
7th	2PL#10	1507	2059	428541	195038	14570
6th	2PL#10	1507	2059	428541	195038	14570
5th	2PL#22	2939	3965	1037046	388265	35259
4th	2PL#22	2939	3965	1037046	388265	35259
3rd	2PL#25	3752	4972	1355501	490037	46087
2nd	2PL#25	3752	4972	1355501	490037	46087
1st	2PL#25	3334	4702	1313944	551220	44674
Exterior columns						
8th	No	224.1	350	93843	12983	3190.7
7th	2PL#6	871.0	1273	300990	18706	10233
6th	2PL#6	871.0	1273	300990	18706	10233
5th	2PL#10	1541	2151	496720	44948	16888
4th	2PL#10	1541	2151	496720	44948	16888
3rd	2PL#12	1992	2791	687164	88157	23364
2nd	2PL#12	1992	2791	687164	88157	23364
1st	2PL#8	1642	2508	624346	127466	21228

Moments are in kN.m.
Stiffnesses are in kN.m/rad.
Doubler plates thicknesses are in mm.

Table 6.7 Panel zone joint for 8-storey building (Design 3)

Floor level	Doubler plate thicknesses	M_{pn1}	M_{pn2}	K_e	K_T	K_s
Interior columns						
8th	No	394.	864.	164233	151149	5583.9
7th	2PL#10	1507	2059	428541	195038	14570
6th	2PL#10	1507	2059	428541	195038	14570
5th	2PL#16	2388	2958	746348	250401	25375
4th	2PL#16	2388	2958	746348	250401	25375
3rd	2PL#20	3216	4404	1193817	463410	40589
2nd	2PL#20	3216	4404	1193817	463410	40589
1st	2PL#18	2765	4092	1085425	536875	36904
Exterior columns						
8th	No	224.1	350	93843	12983	3190.7
7th	1PL#6	653.3	916	171800	12760	5841.2
6th	1PL#6	653.3	916	171800	12760	5841.2
5th	2PL#6	1217	1602	365582	28938	12429
4th	2PL#6	1217	1602	365582	28938	12429
3rd	2PL#6	1992	2791	687164	88157	18584
2nd	2PL#6	1992	2791	687164	88157	18584
1st	1PL#8	1305	2132	497856	121624	16927

Moments are in kN.m.
Stiffnesses are in kN.m/rad.
Doubler plates thicknesses are in mm.

Table 6.8 Panel zone joint for 8-storey building (Design 4)

Floor level	Doubler plate thicknesses	M_{pn1}	M_{pn2}	K_e	K_T	K_s
Interior columns						
8th	No	394.	864.	164233	151149	5583.9
7th	No	716.	1212	278660	131398	9474.5
6th	No	716.	1212	278660	131398	9474.5
5th	2PL#8	1653	2599	641224	326256	21801.
4th	2PL#8	1653	2599	641224	326256	21801.
3rd	2PL#10	2144	3268	842212	414550	28635.
2nd	2PL#10	2144	3268	842212	414550	28635.
1st	2PL#15	2507	3815	982862	530306	33417
Exterior columns						
8th	No	224.	350.	93843	12983	3190.7
7th	No	435.	714.	156870	12897	5333.6
6th	No	435.	714.	156870	12897	5333.6
5th	No	730.	1192	270006	33095	9180.2
4th	No	730.	1192	270006	33095	9180.2
3rd	1PL#6	1256	1948	469901	74405	15976.
2nd	1PL#6	1256	1948	469901	74405	15976.
1st	2PL#12	1930	2834	744759	132401	25321.

Moments are in kN.m.
Stiffnesses are in kN.m/rad.
Doubler plates thicknesses are in mm.

Table 6.9 Cases studied

Cases	Connection Configuration	Panel Zone Configuration
Case 1	Infinitely rigid	Infinitely rigid
Case 2	Deformation permitted	Infinitely rigid
Case 3	Deformation permitted	Design 1 criterion
Case 4	Deformation permitted	Design 2 criterion
Case 5	Deformation permitted	Design 3 criterion
Case 6	Deformation permitted	Design 4 criterion

Table 6.10 Vibration periods of MRFs

Modes	Vibration Periods (s)					
	Case 1	Case 2	Case 3	Case 4	Case 5	Case 6
1st	2.170	2.279	2.412	2.431	2.490	2.507
2nd	0.823	0.850	0.893	0.906	0.927	0.935
3rd	0.489	0.512	0.532	0.536	0.544	0.548
4th	0.359	0.375	0.385	0.388	0.391	0.393
5th	0.267	0.283	0.289	0.289	0.291	0.293
6th	0.196	0.210	0.214	0.214	0.215	0.217
7th	0.155	0.168	0.169	0.170	0.170	0.170

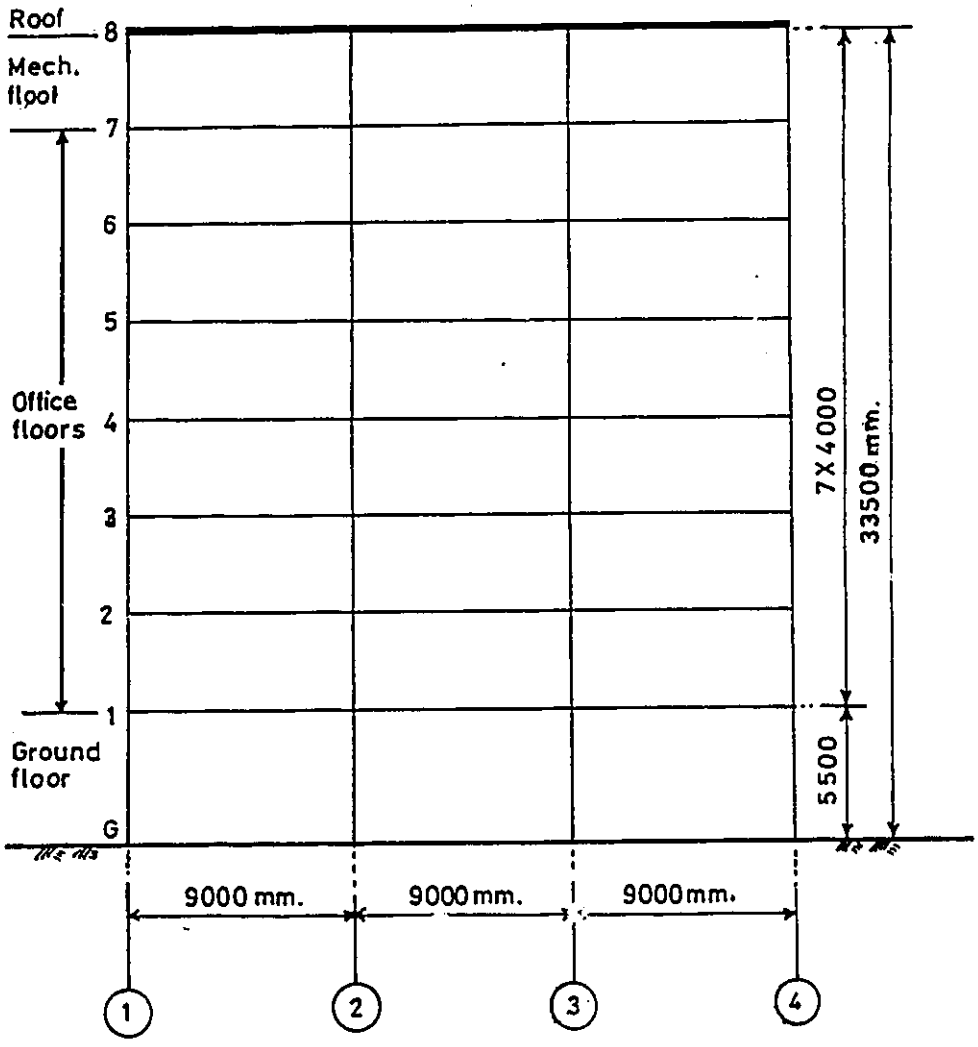

Fig. 6.1 Elevation of the 8-storey building.

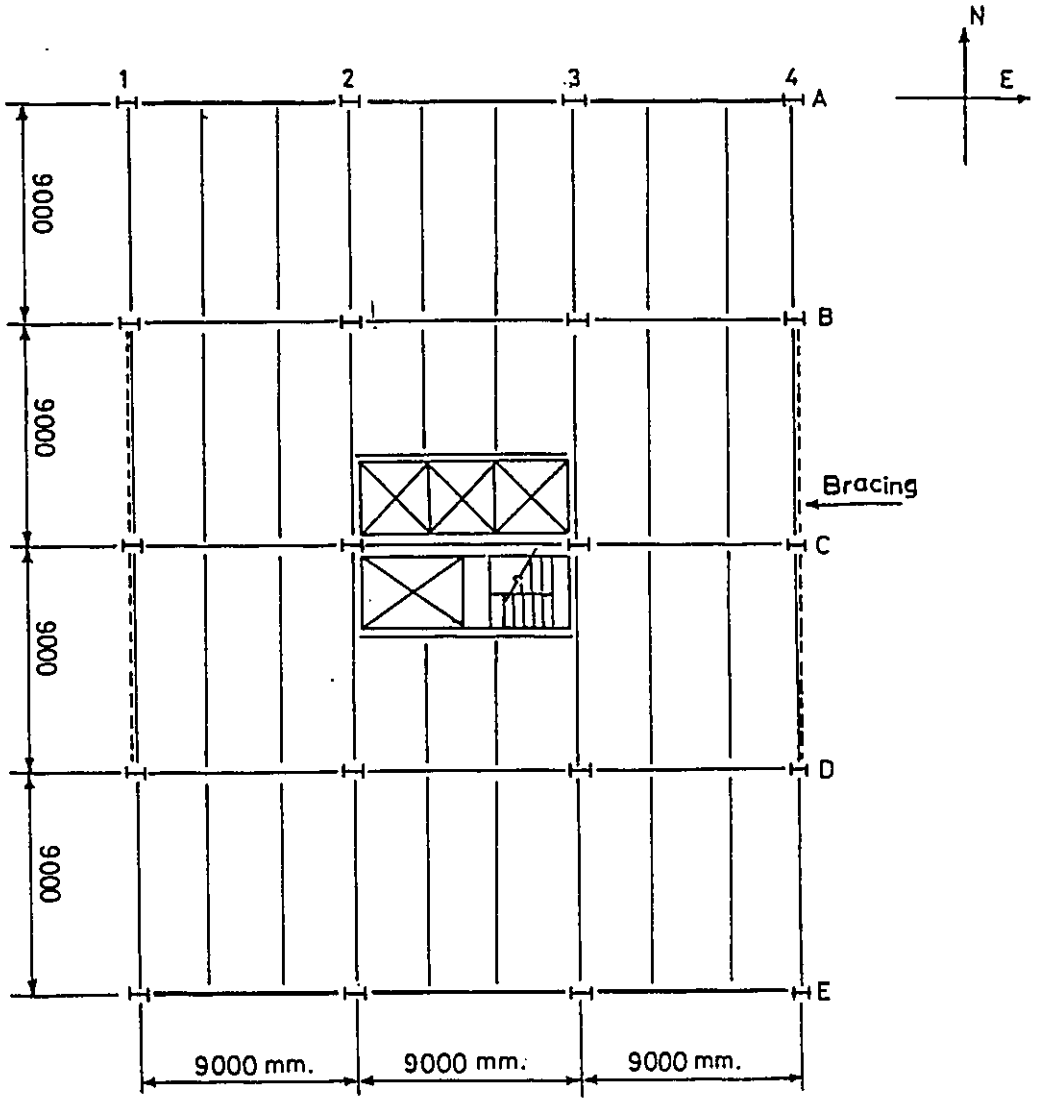

Fig. 6.2 Plan of the 8-storey frame.

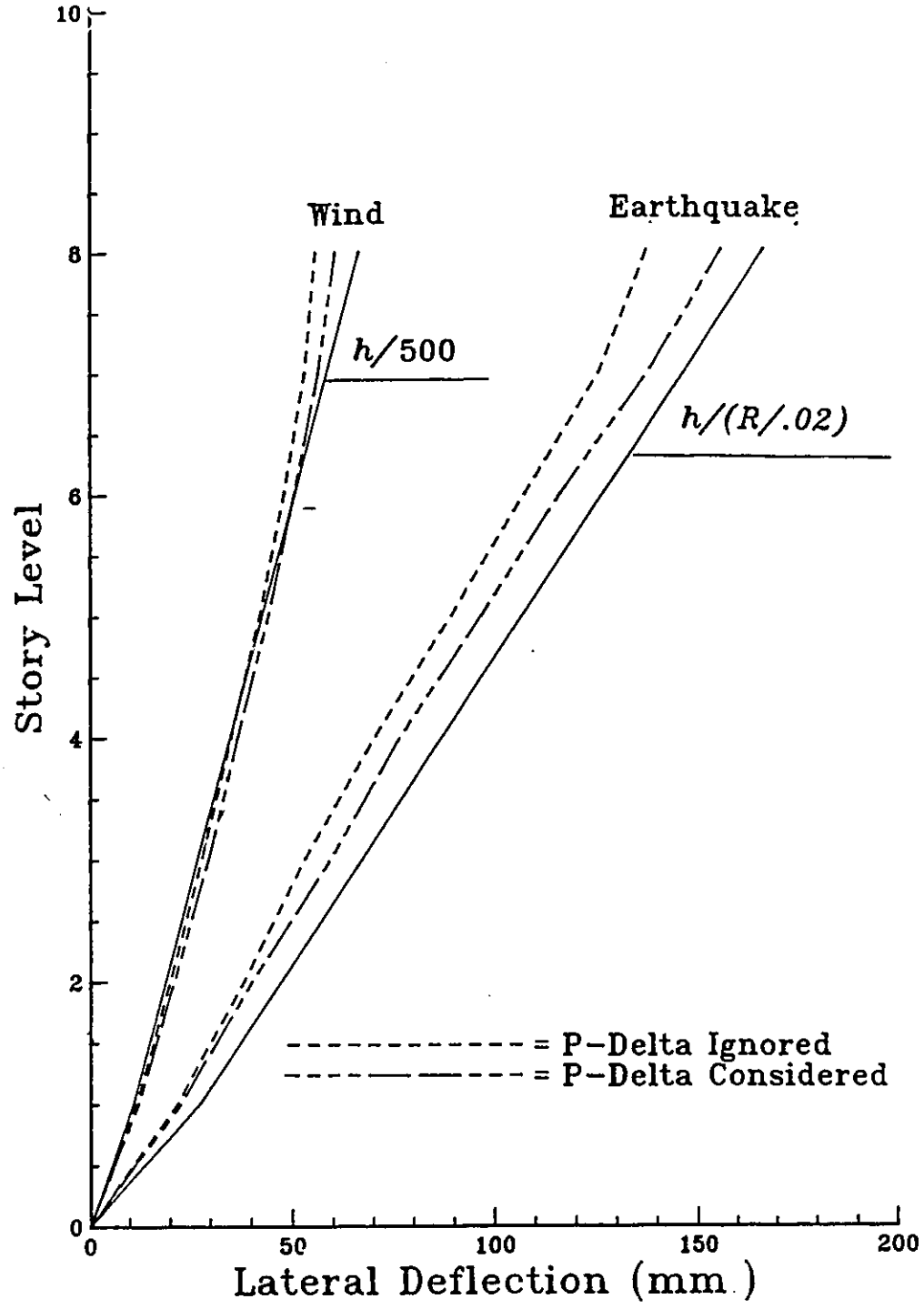

Fig. 6.3 Frame lateral deflection.

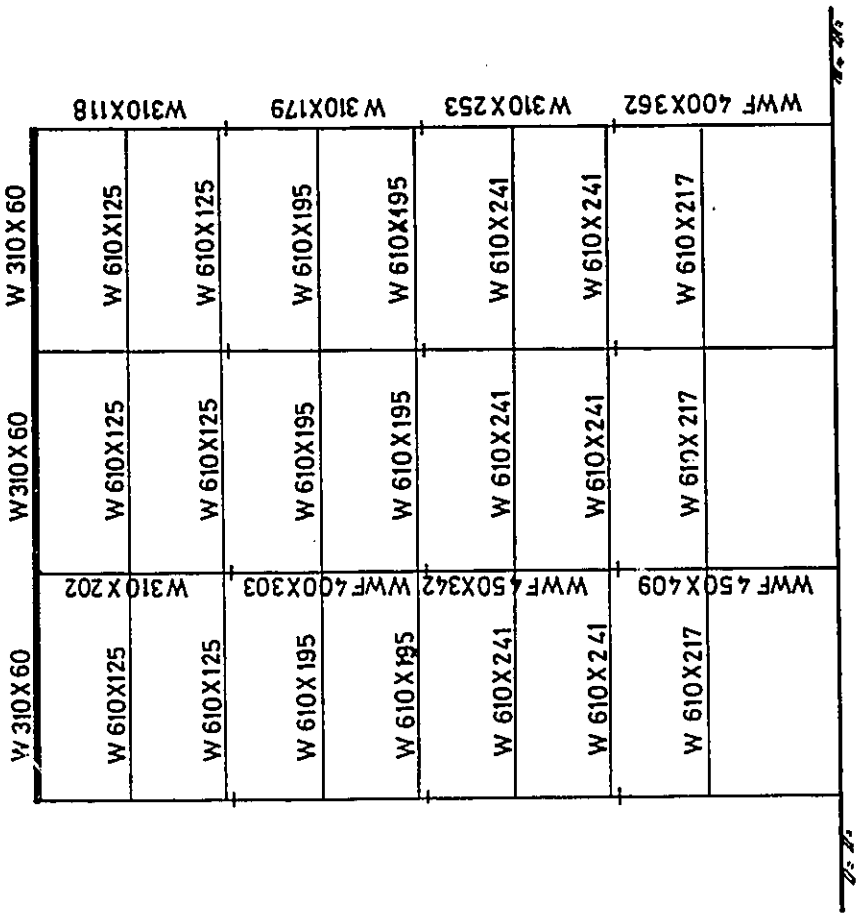

Fig. 6.4 Beams and columns sections.

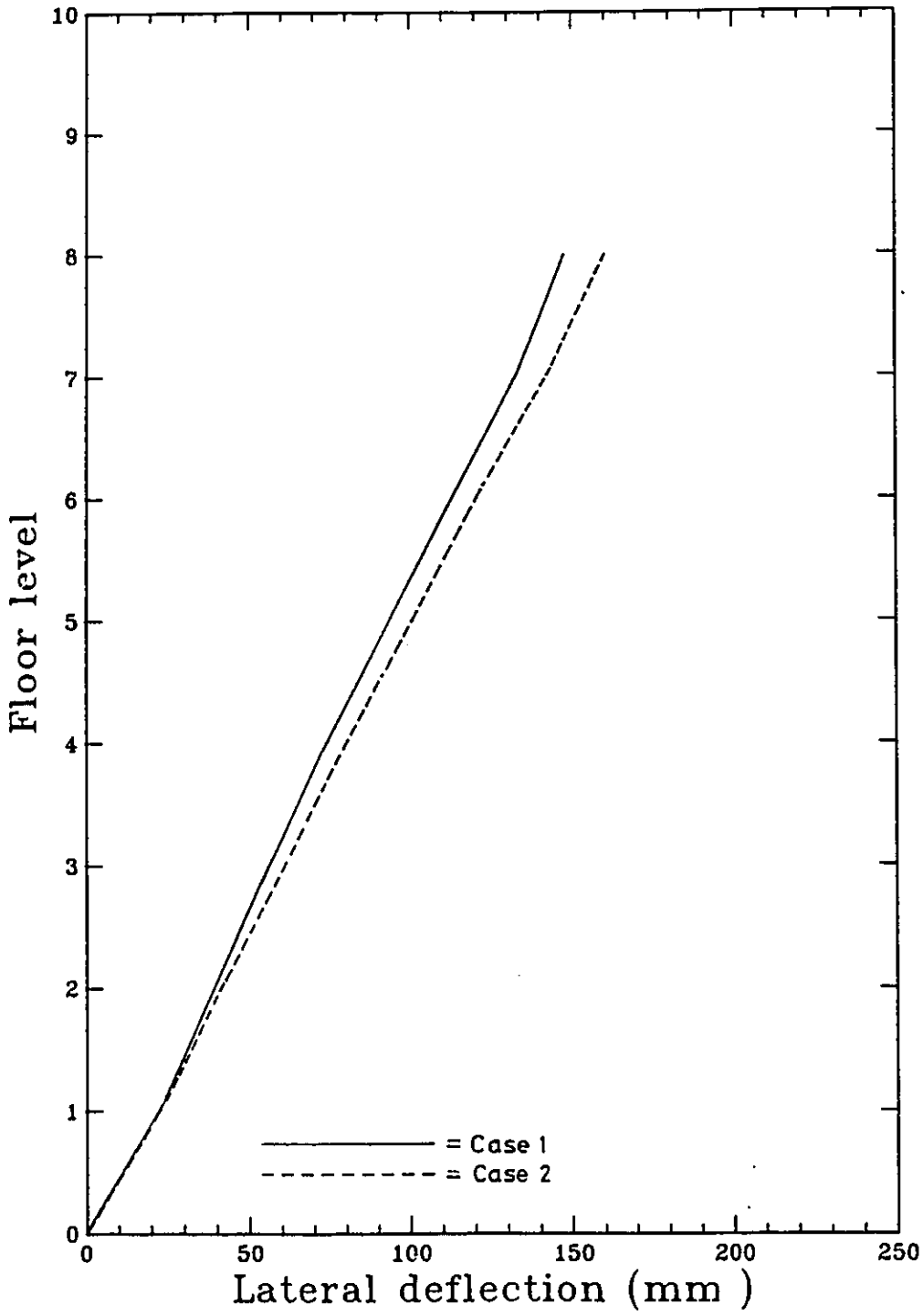

Fig. 6.5 Effect of connection flexibility on the static deflection of the 8-storey frame.

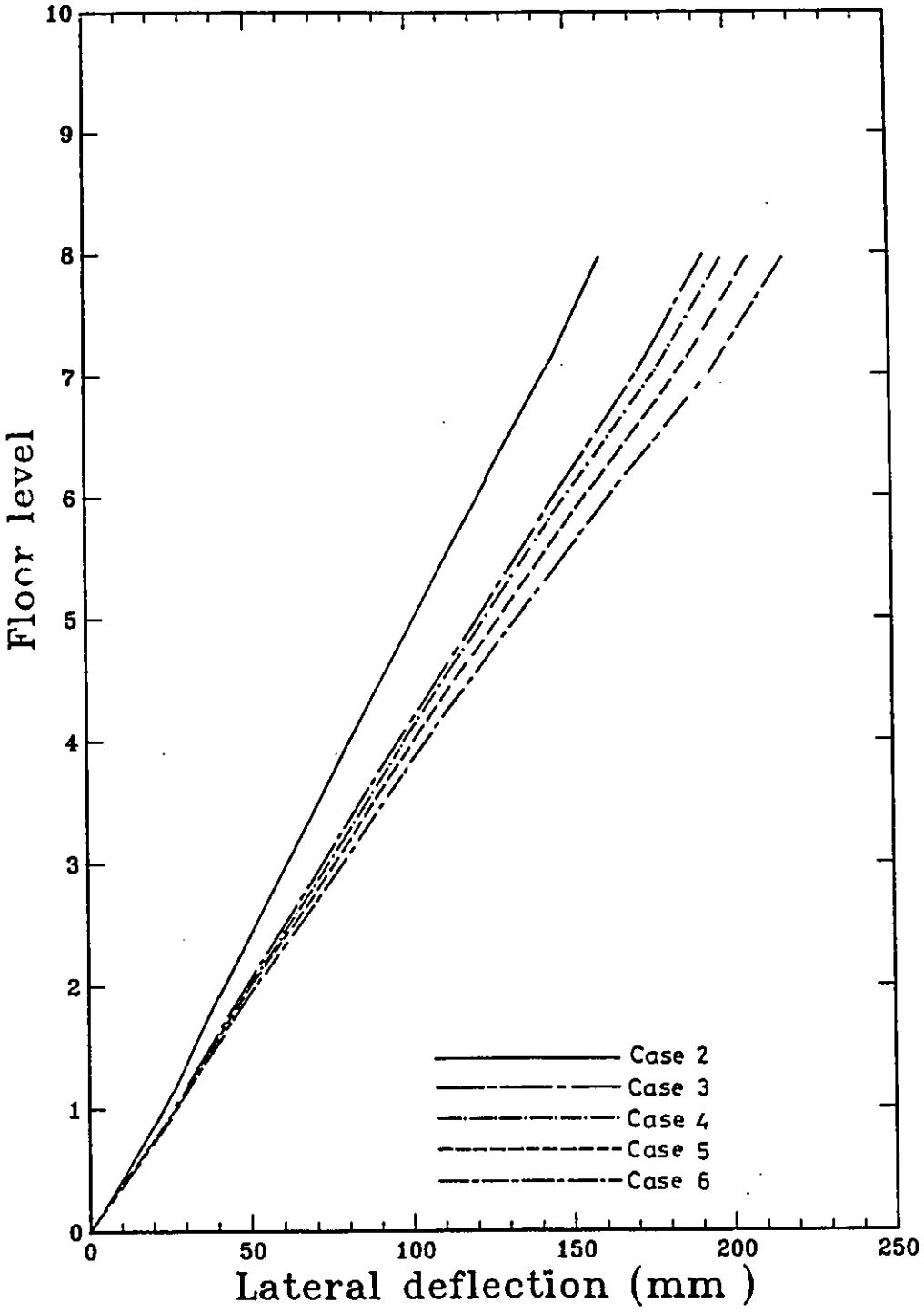

Fig. 6.6 Effect of panel zone deformation on the static deflection of the 8-storey frame.

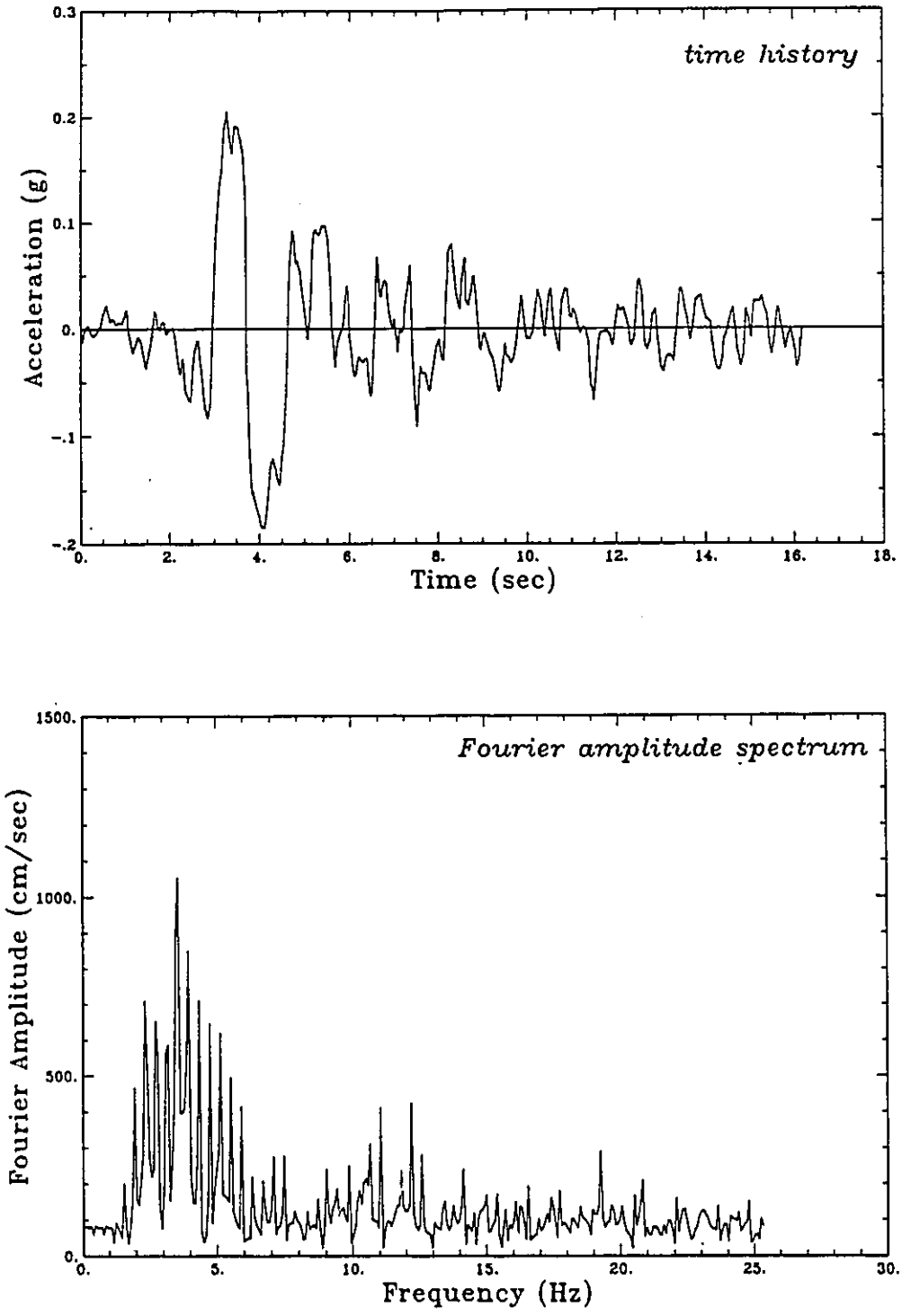

Fig. 6.7 Time history and Fourier spectrum for Bucharest earthquake.

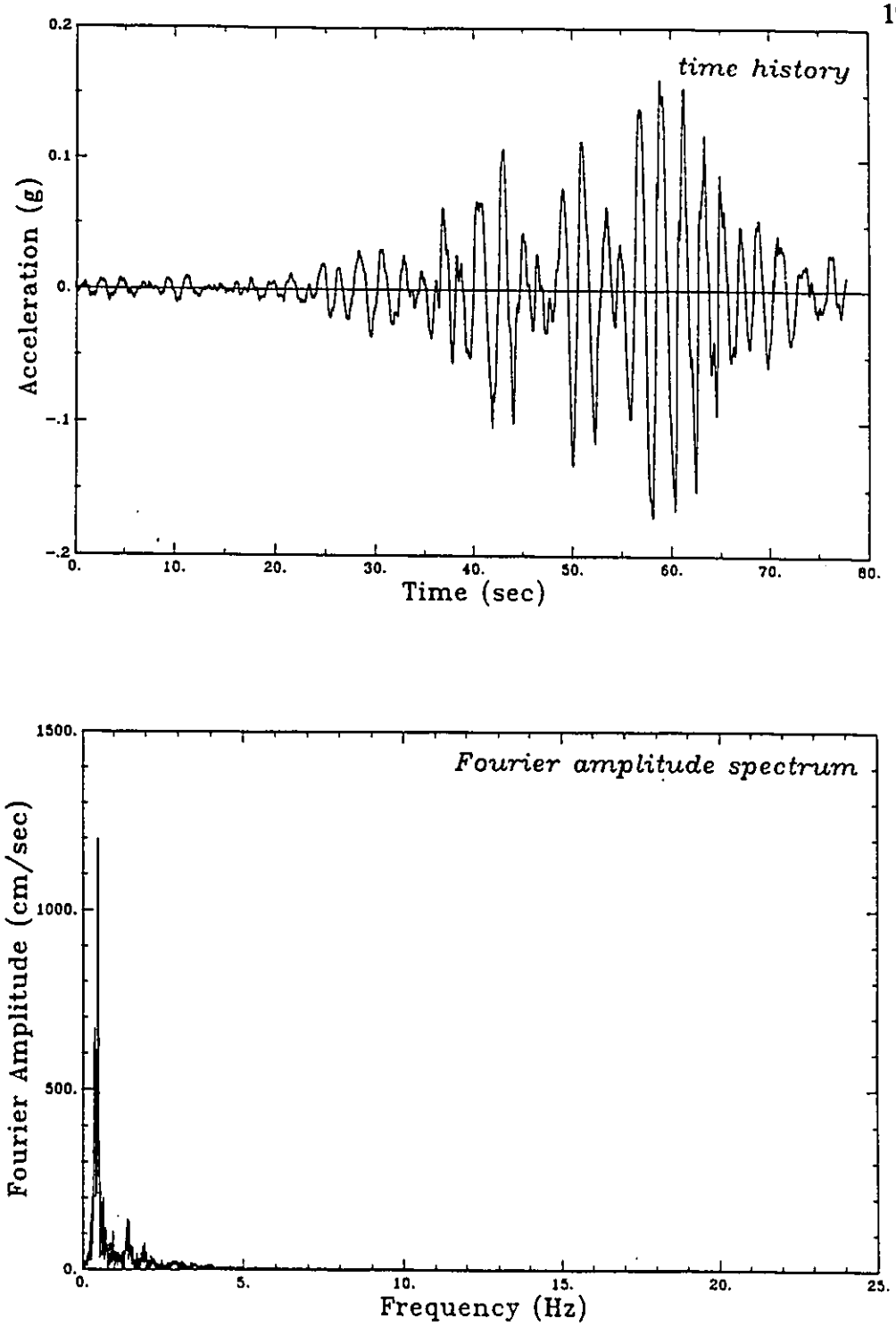

Fig. 6.8 Time history and Fourier spectrum for Mexico earthquake.

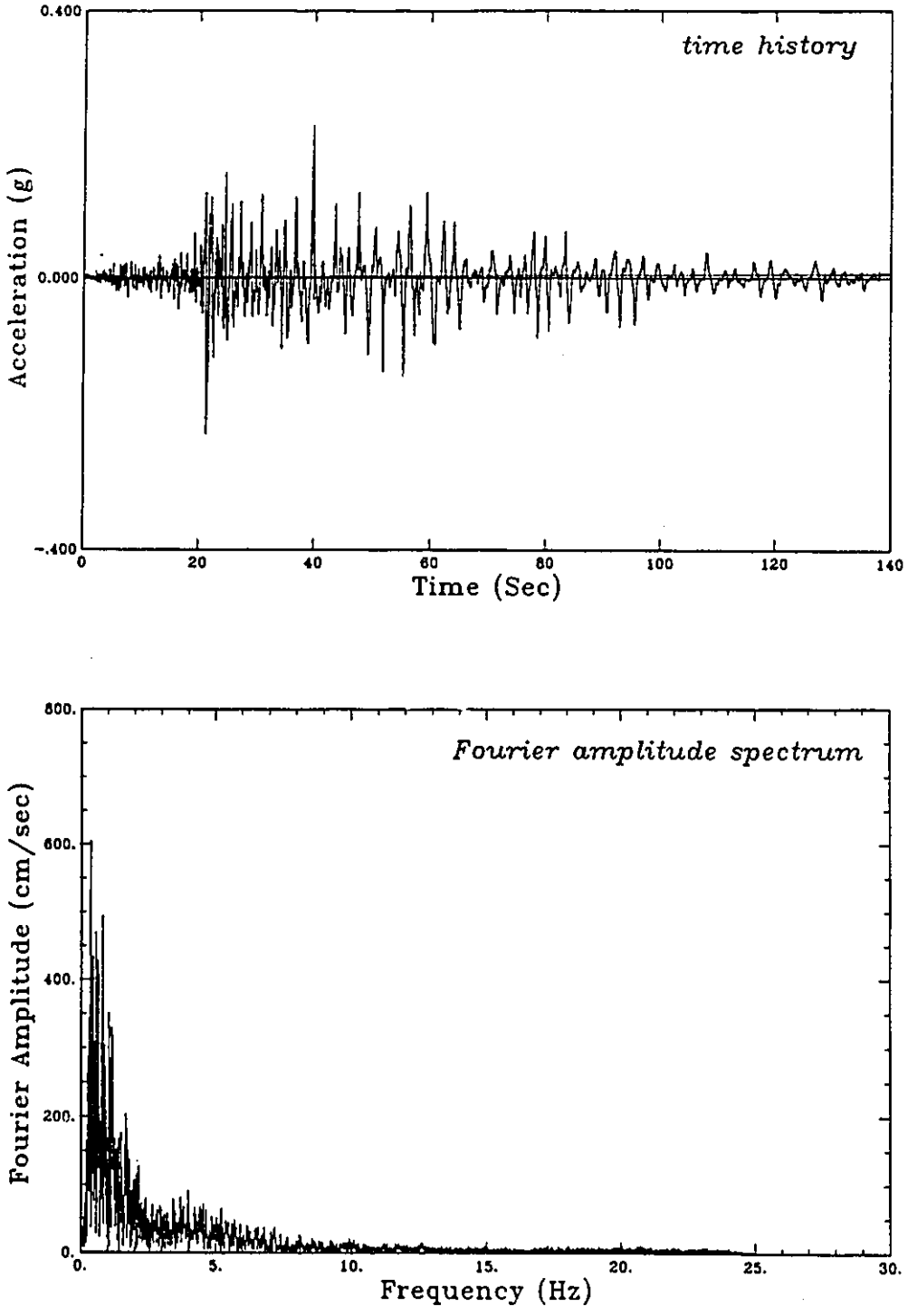

Fig. 6.9 Time history and Fourier spectrum for Honshu earthquake.

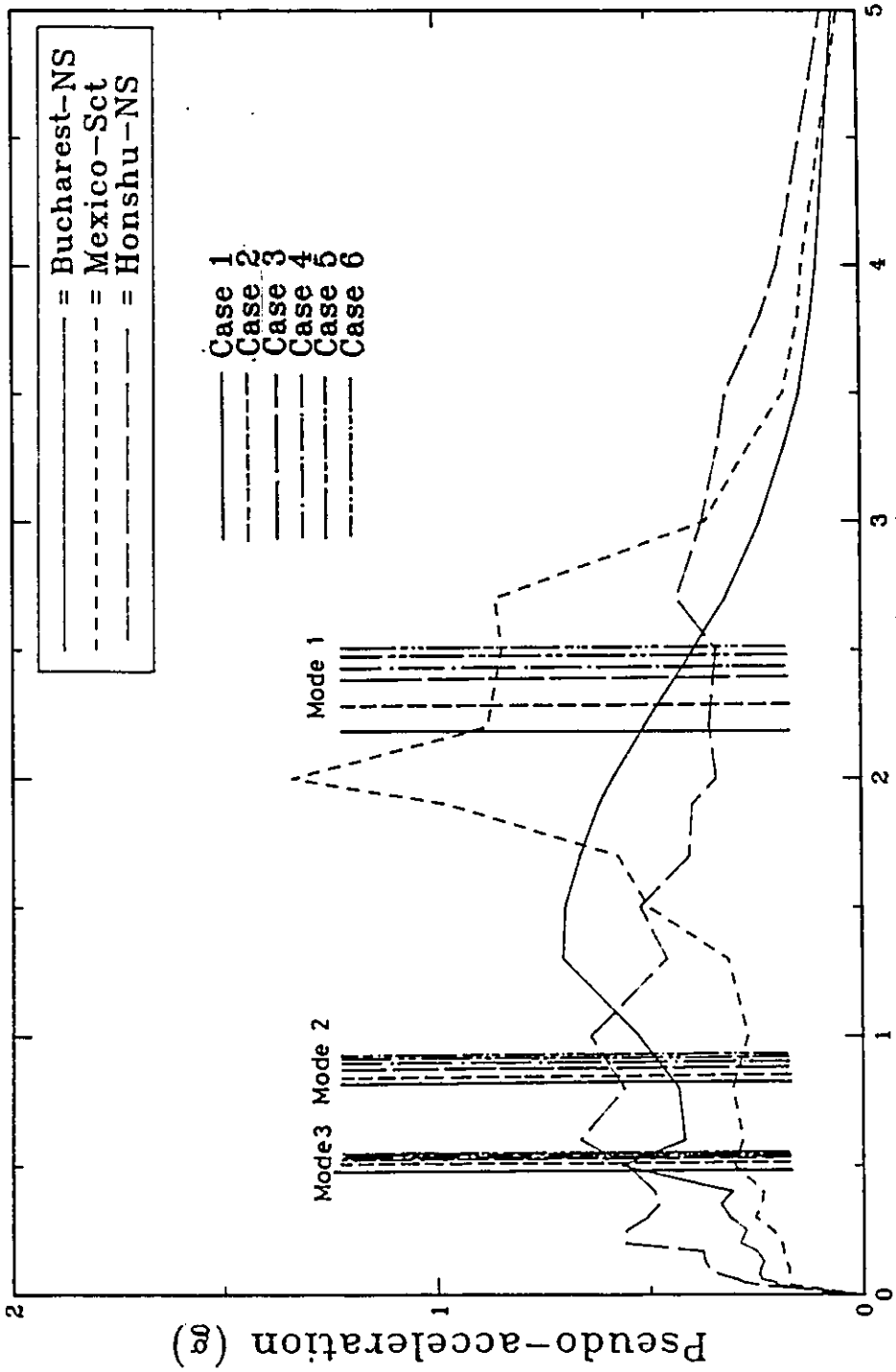

Fig. 6.10 Linear elastic pseudo-acceleration spectra for the selected ground accelerations (3% Damping).

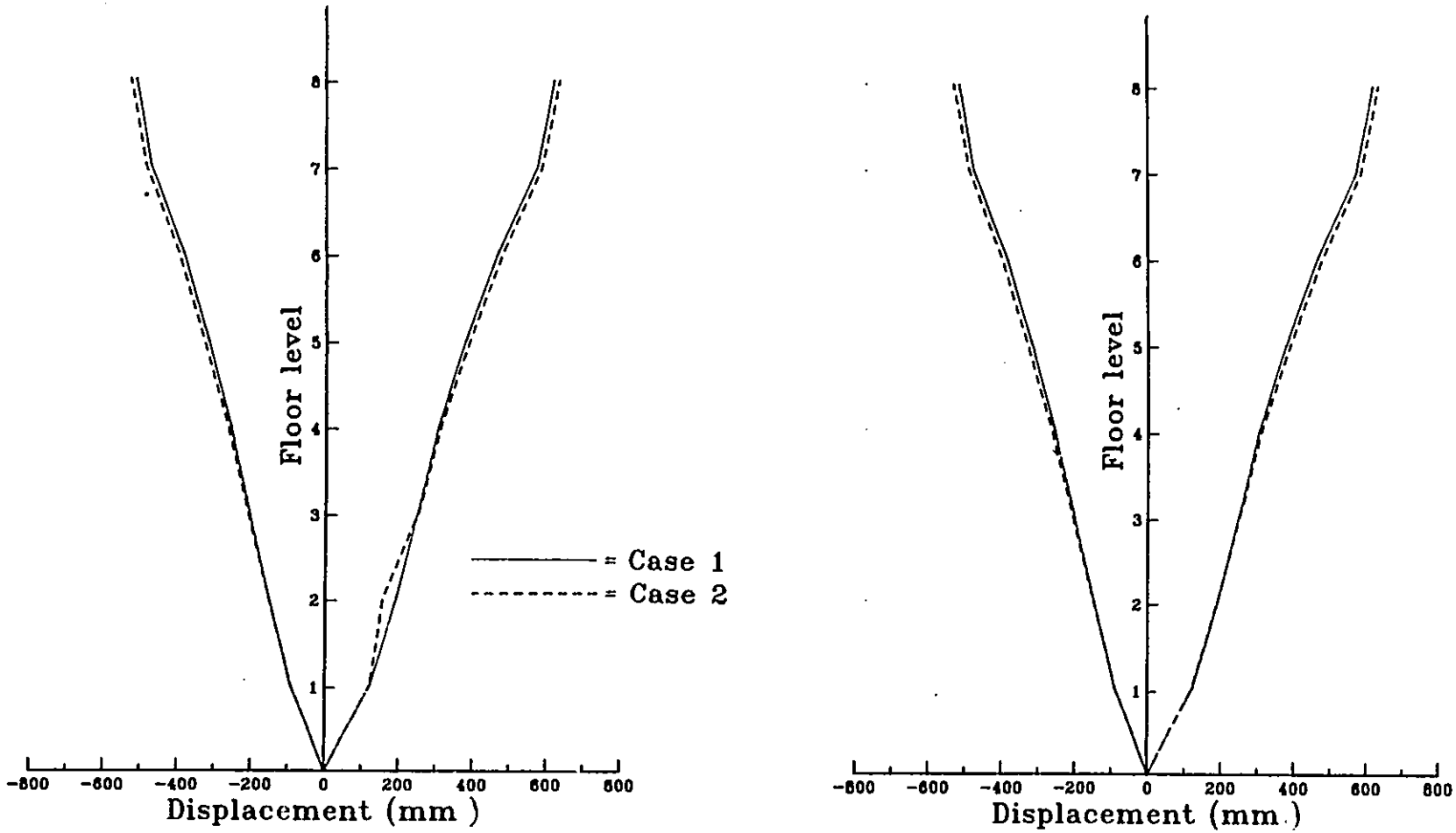

a) Maximum floor displacement

b) Floor displacement at peak roof displacement

Fig. 6.11 Effect of connection flexibility on the dynamic lateral displacement of the 8-storey frame

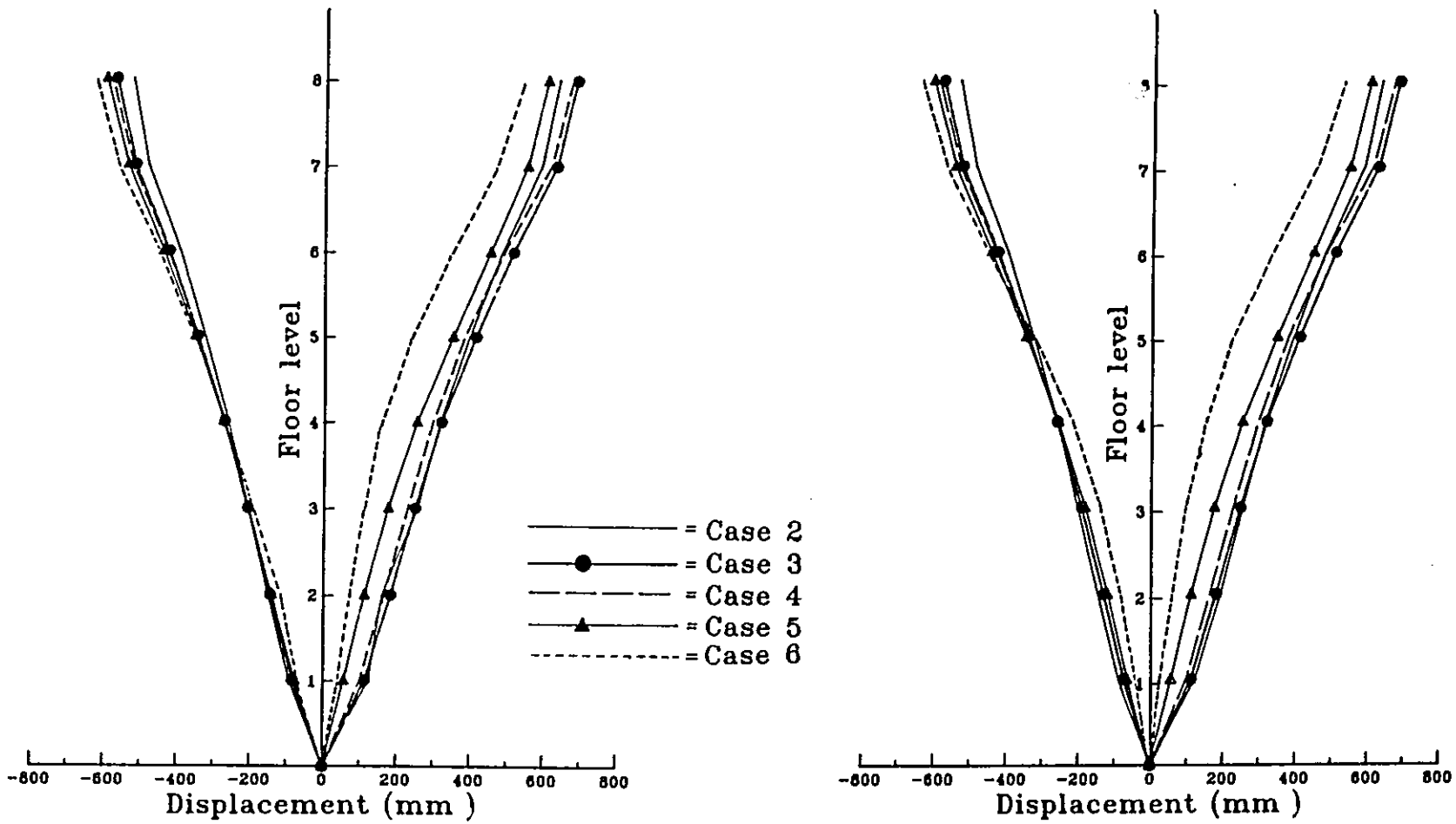

a) Maximum floor displacement

b) Floor displacement at peak roof displacement

Fig. 6.12 Effect of panel zone deformation on the dynamic lateral displacement of the 8-storey frame

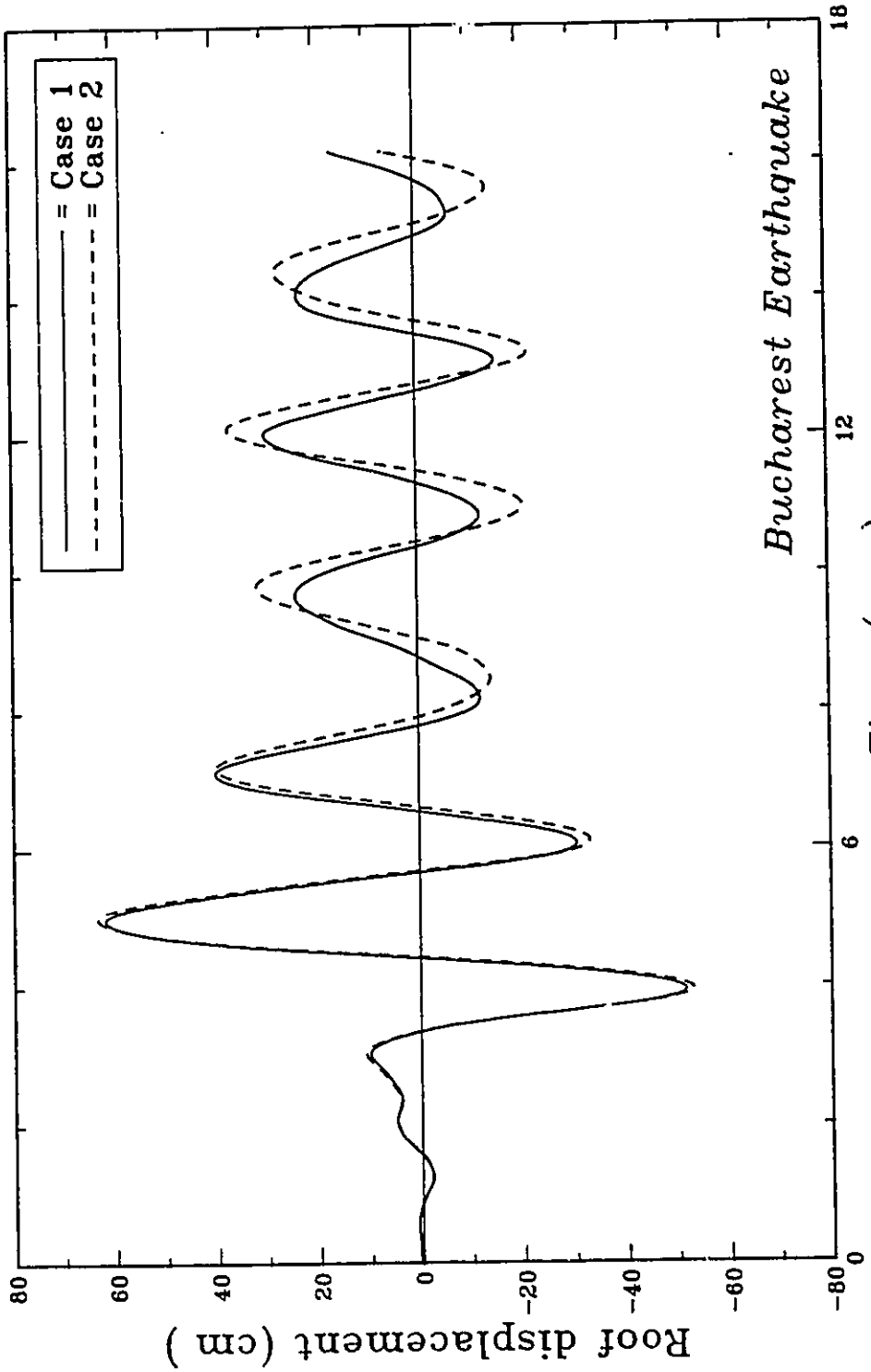

Fig. 6.13 Effect of connection flexibility on the roof displacement history.

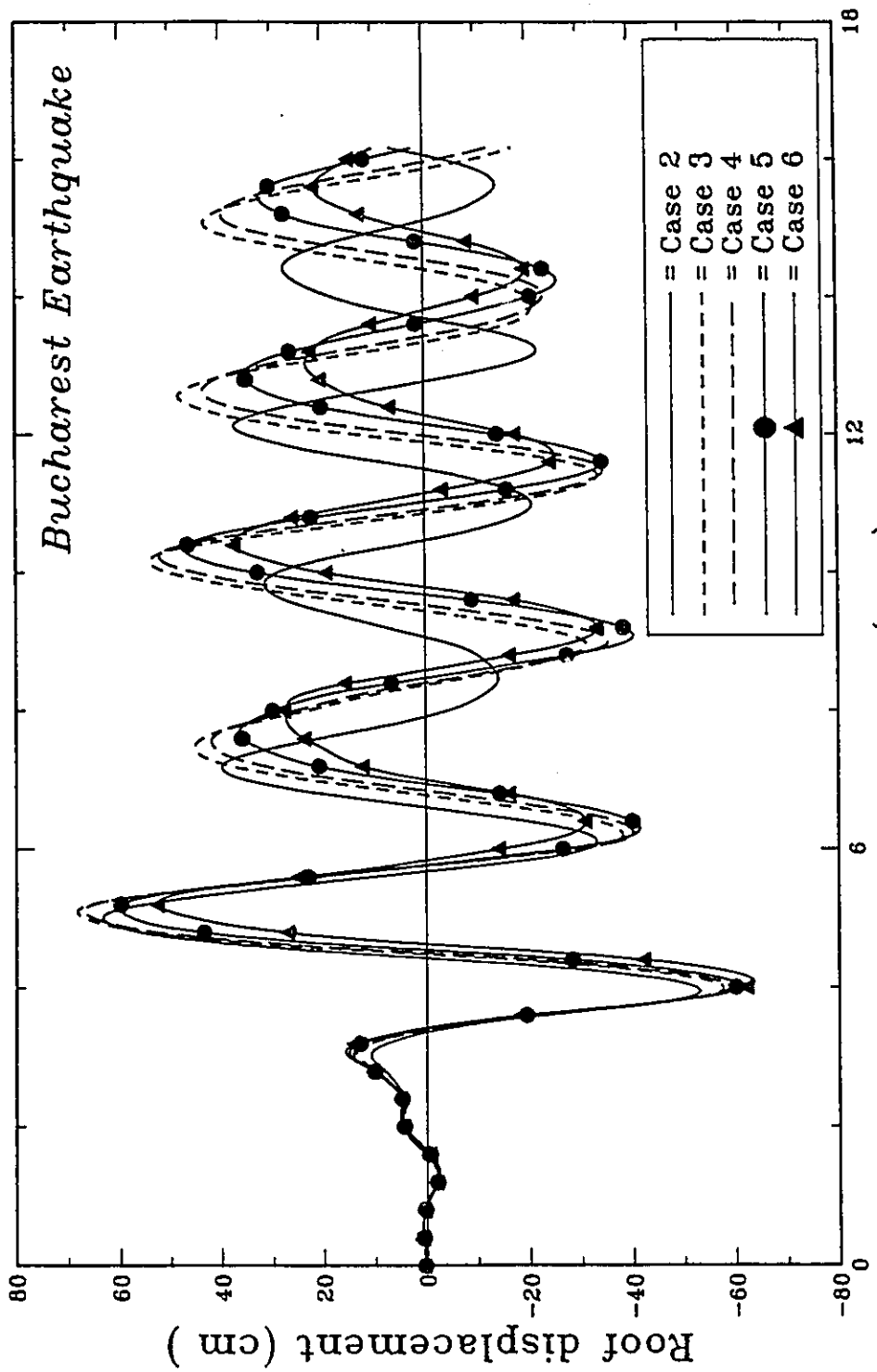

Fig. 6.14 Effect of panel zone deformation on the roof displacement history.

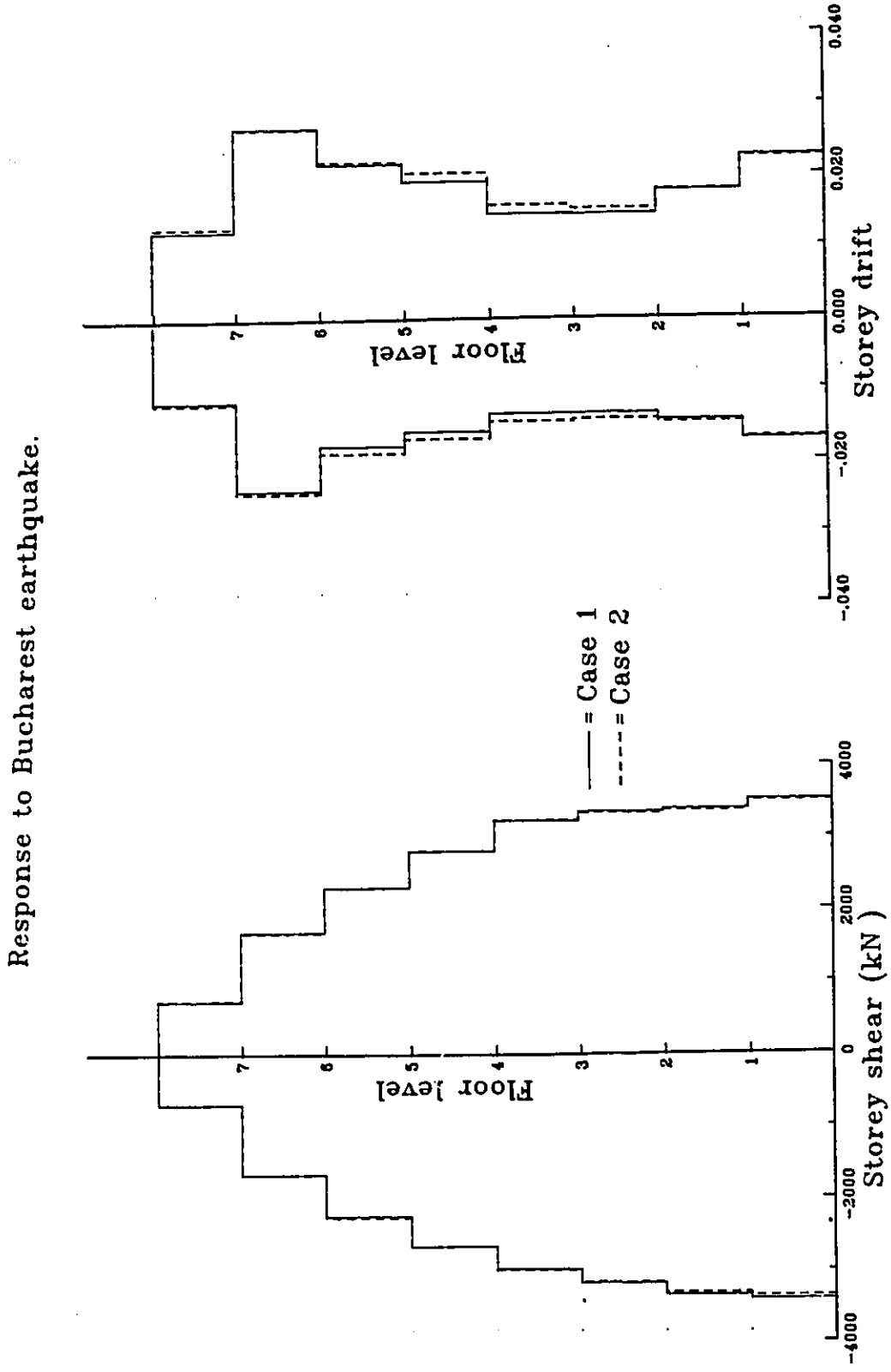

Fig. 6.15 Effect of connection flexibility on the storey shear and storey drift.

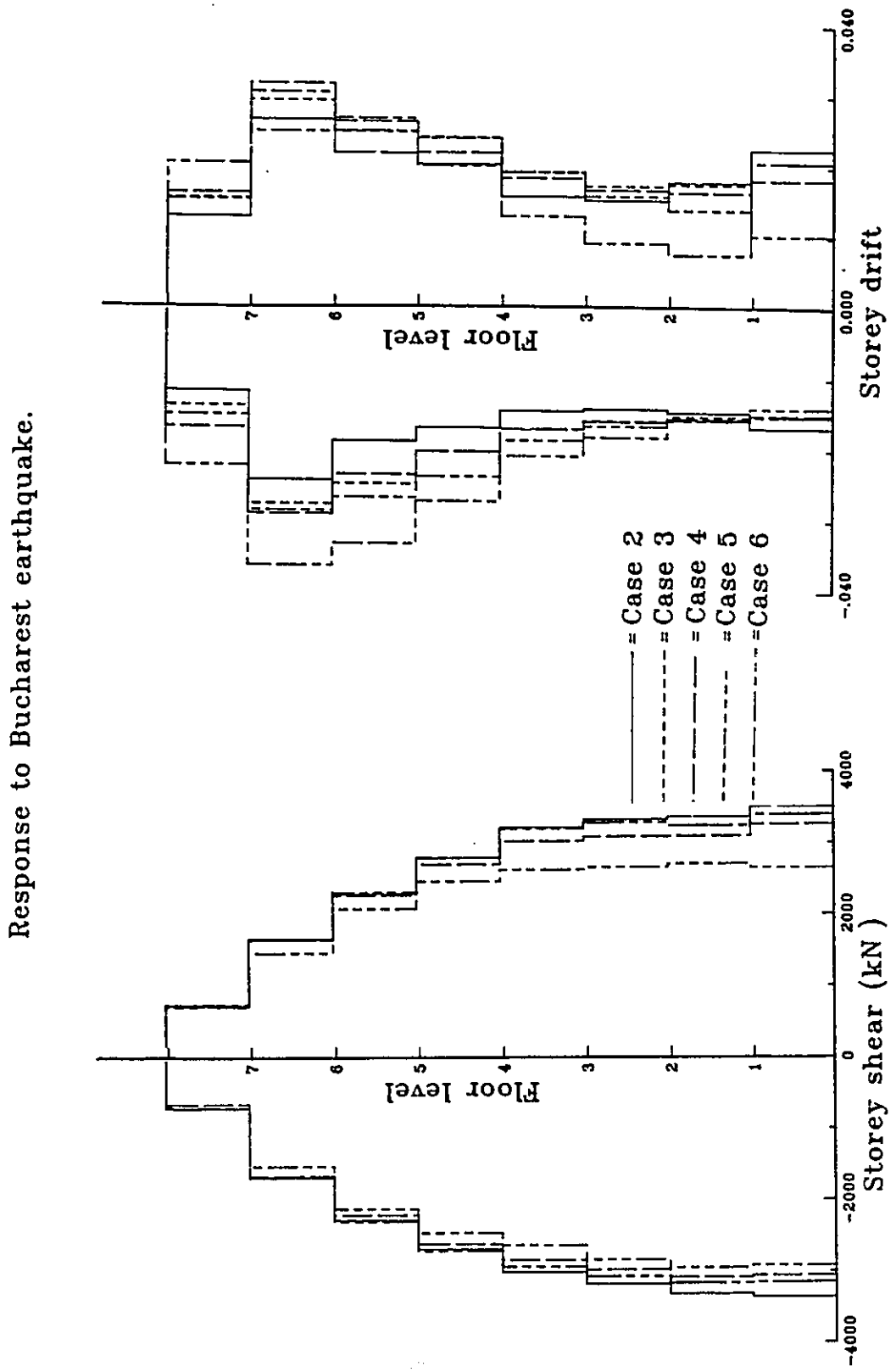

Fig. 6.16 Effect of panel zone deformation on the storey shear and storey drift.

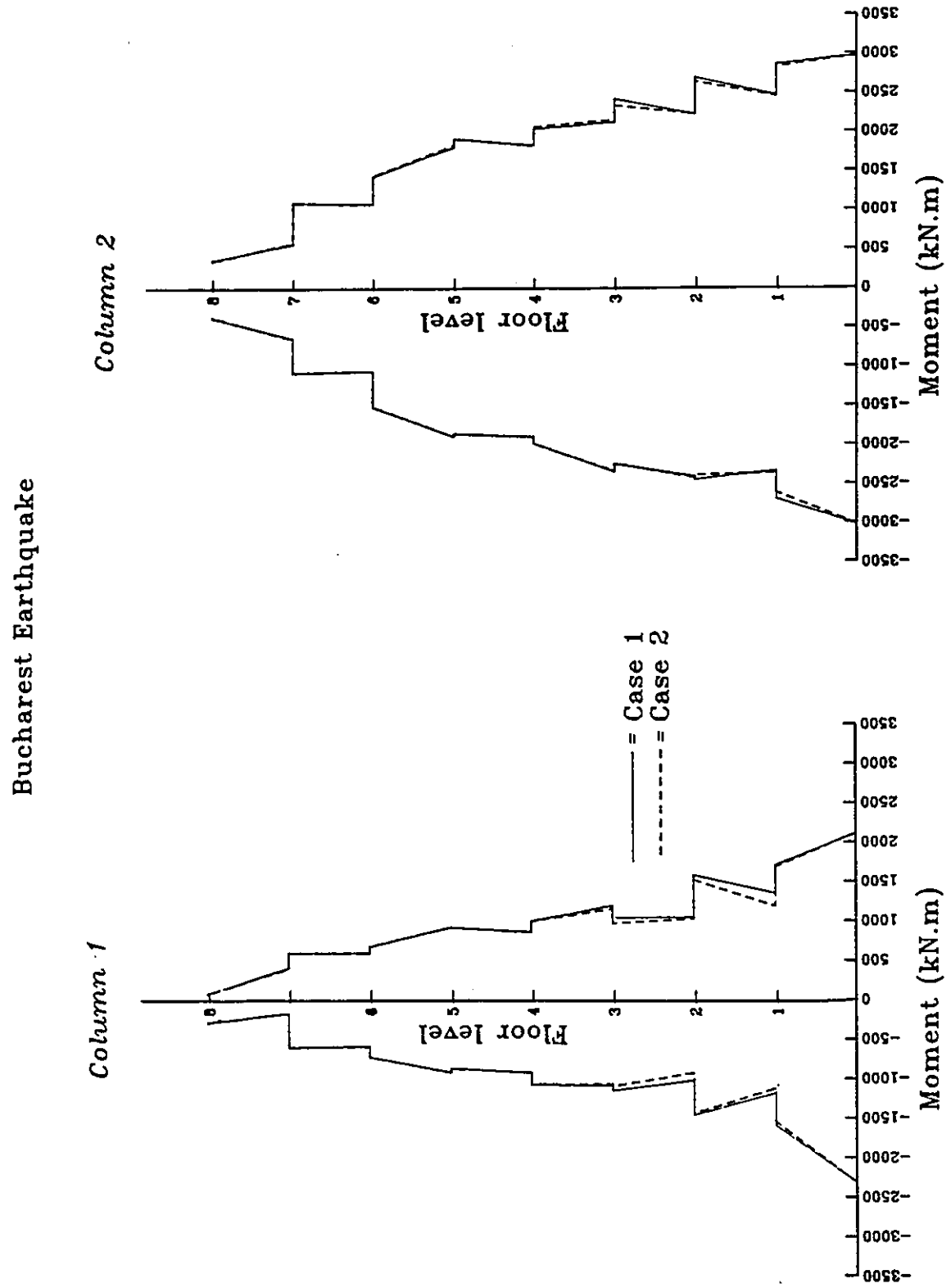

Fig. 6.17 Effect of connection flexibility on the columns' moment envelopes

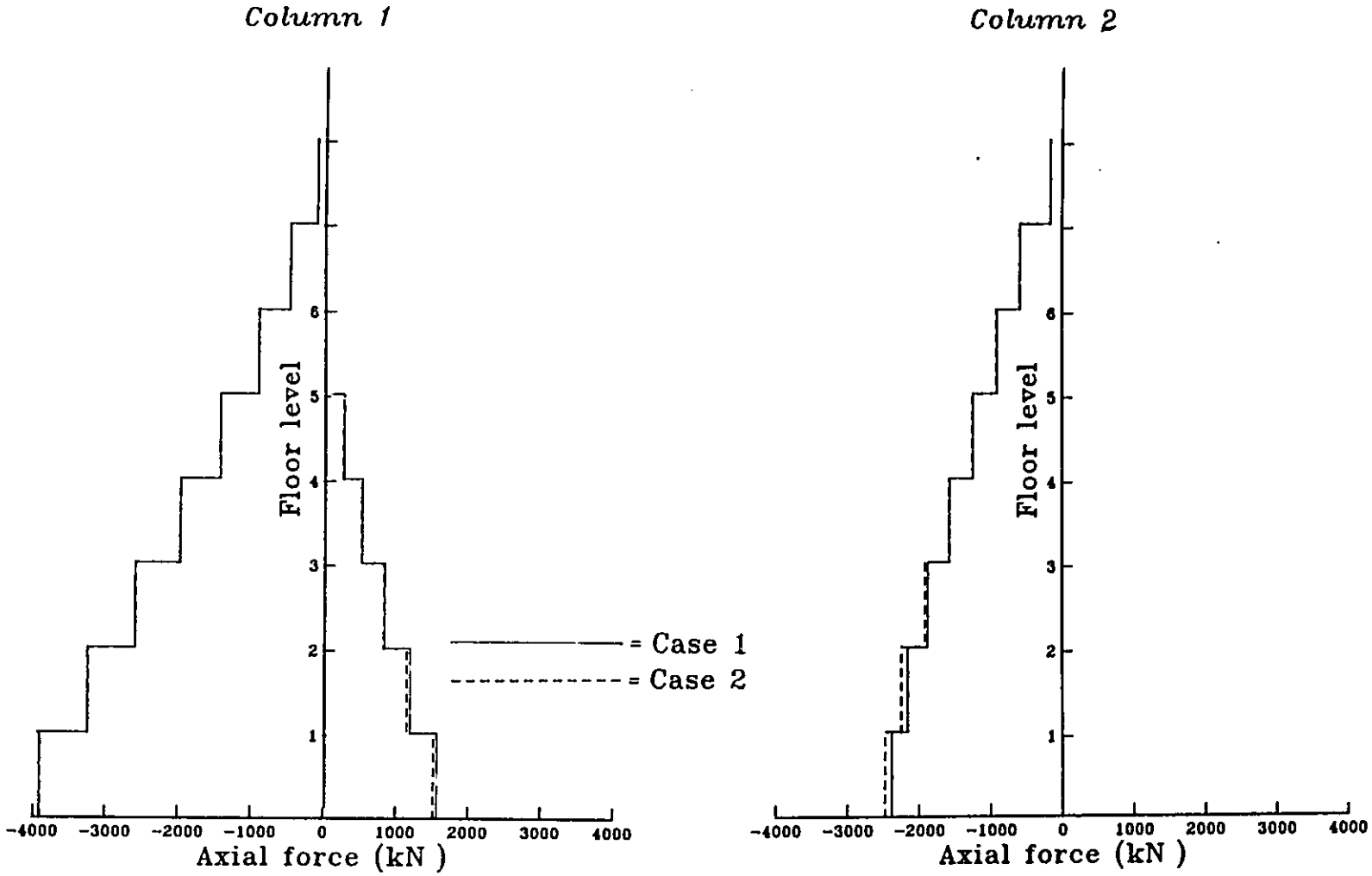

Fig. 6.18 Effect of connection flexibility on the columns' axial force envelopes.

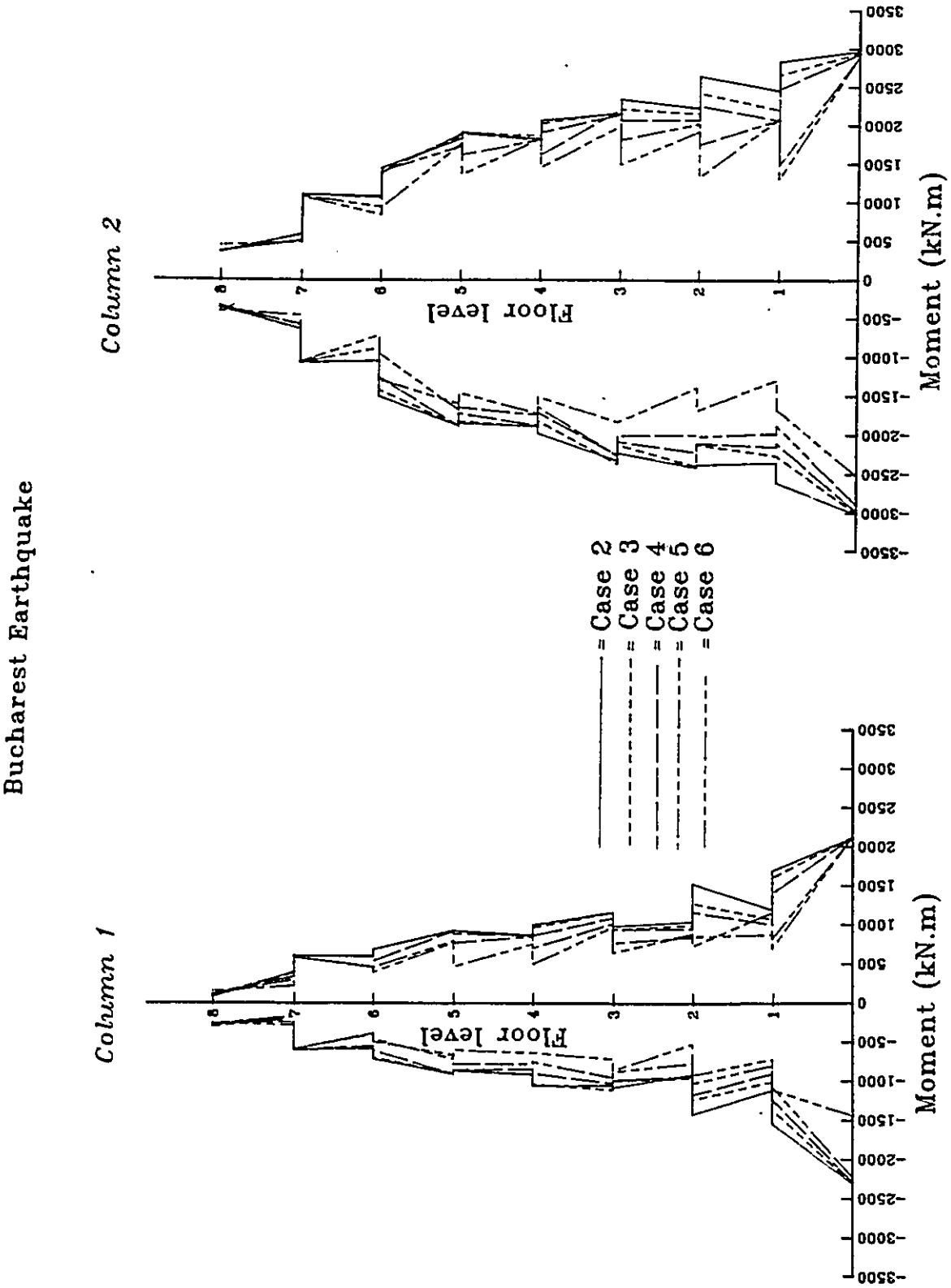

Fig. 6.19 Effect of panel zone deformation on the columns' moment envelopes.

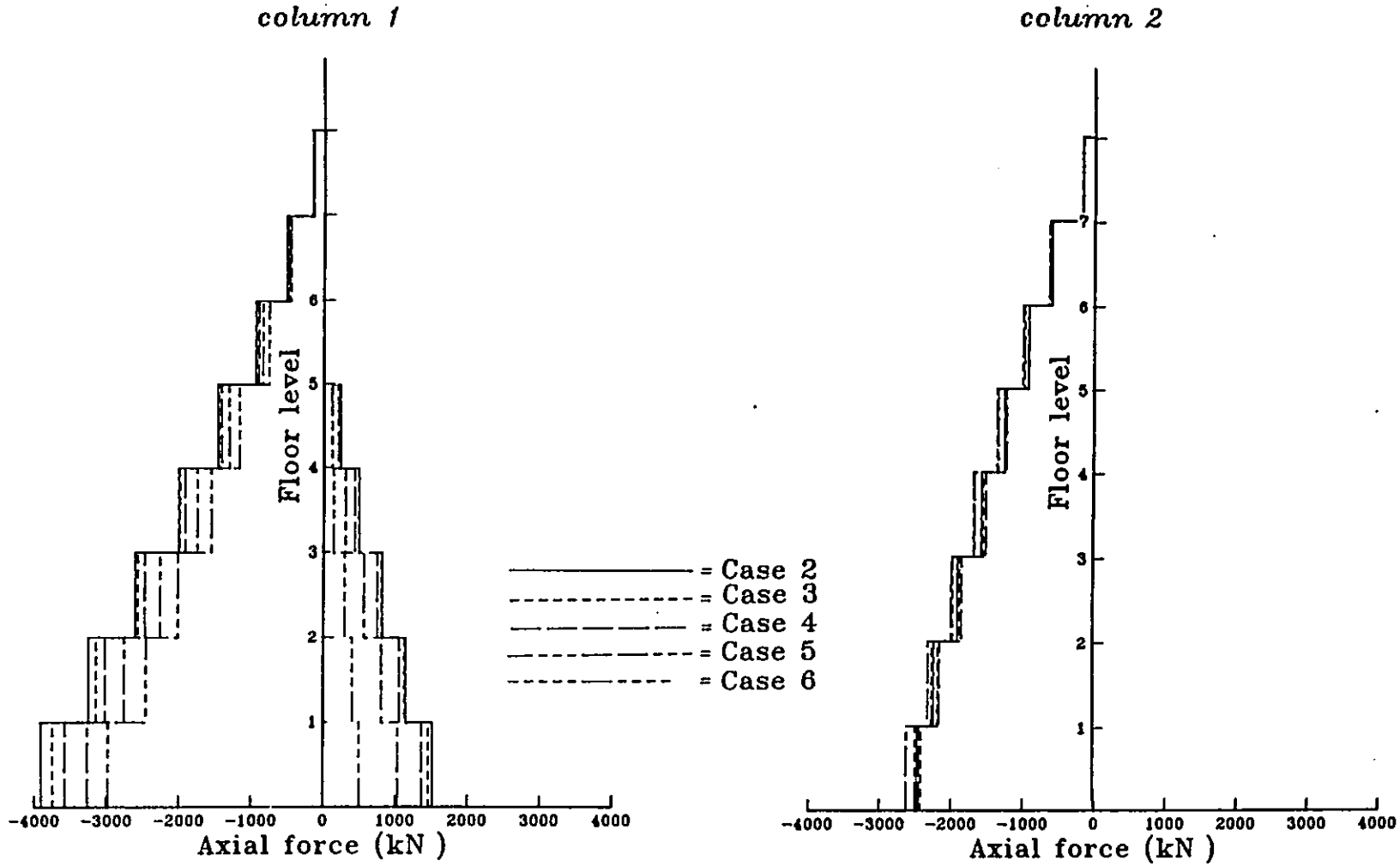

Fig. 6.20 Effect of panel zone deformation on the columns' axial force envelopes.

Bucharest Earthquake

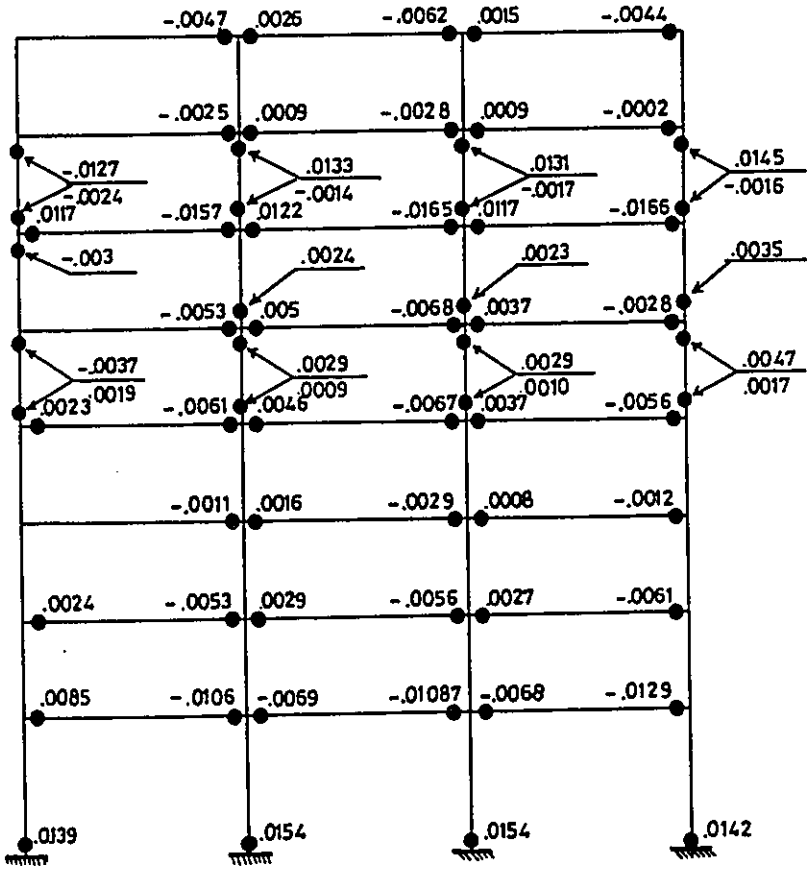

Fig. 6.21 Maximum beam and column plastic rotations for MRF case 1 (in radians).

Bucharest Earthquake

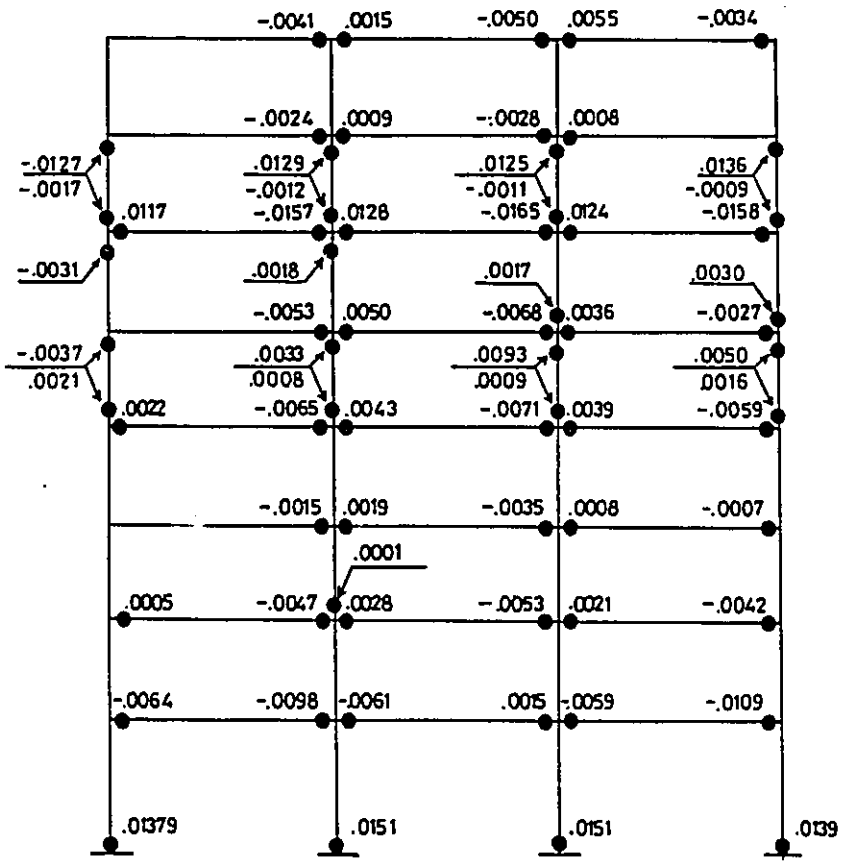

Fig. 6.22 Maximum beam and column plastic rotations for MRF case 2.(in radians).

Bucharest Earthquake

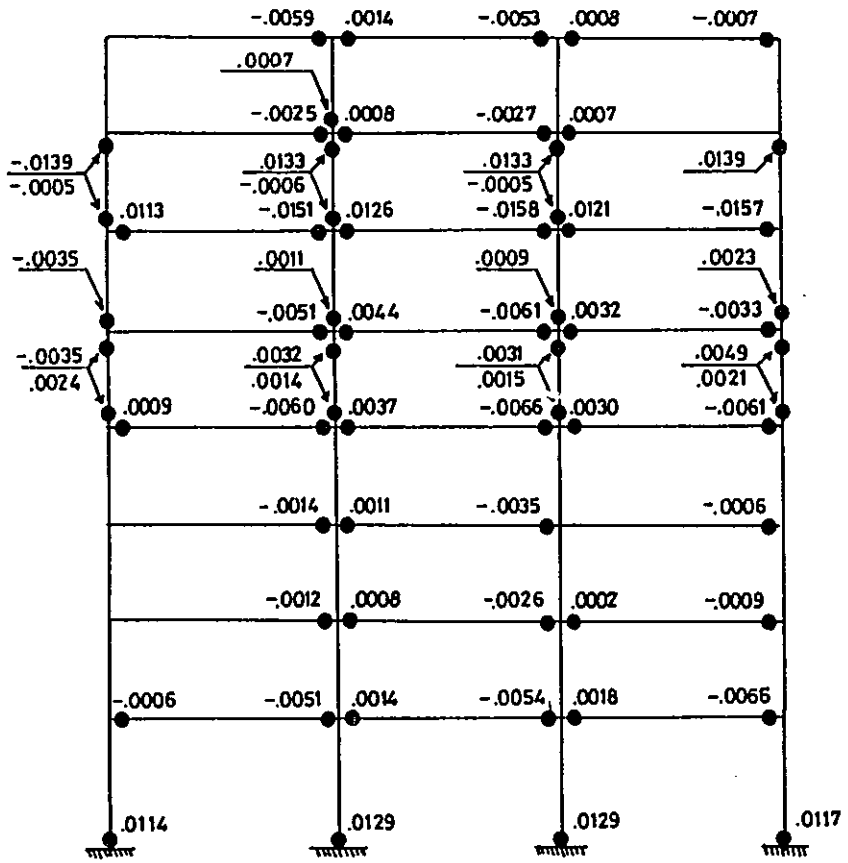

Beams and columns

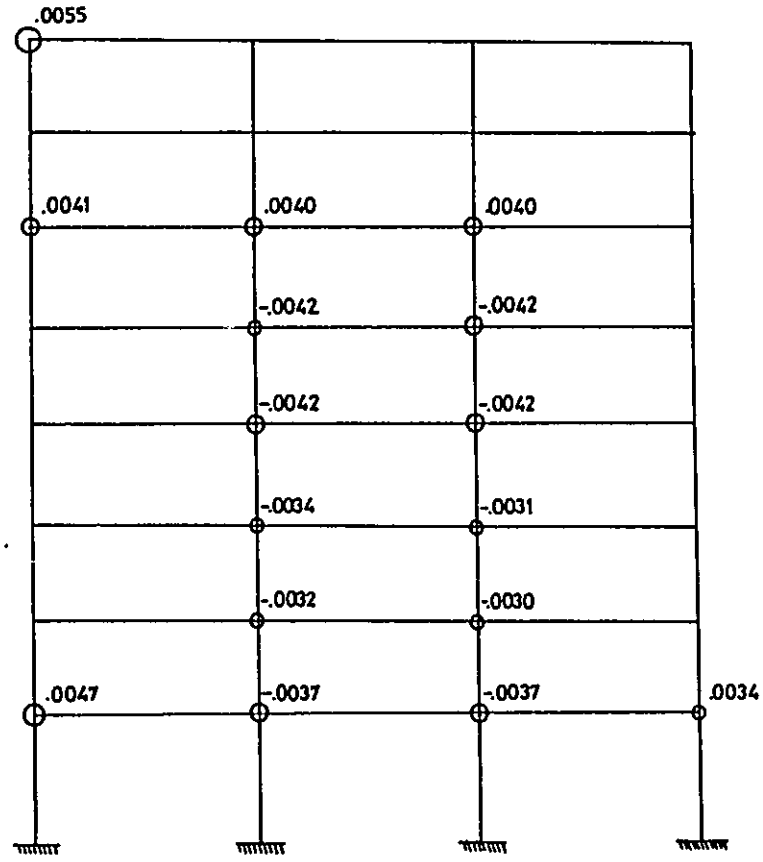

Panel zones

Fig. 6.23 Maximum beam, column and panel zone joint plastic rotations for MRF case 3. (in radians)

Bucharest Earthquake

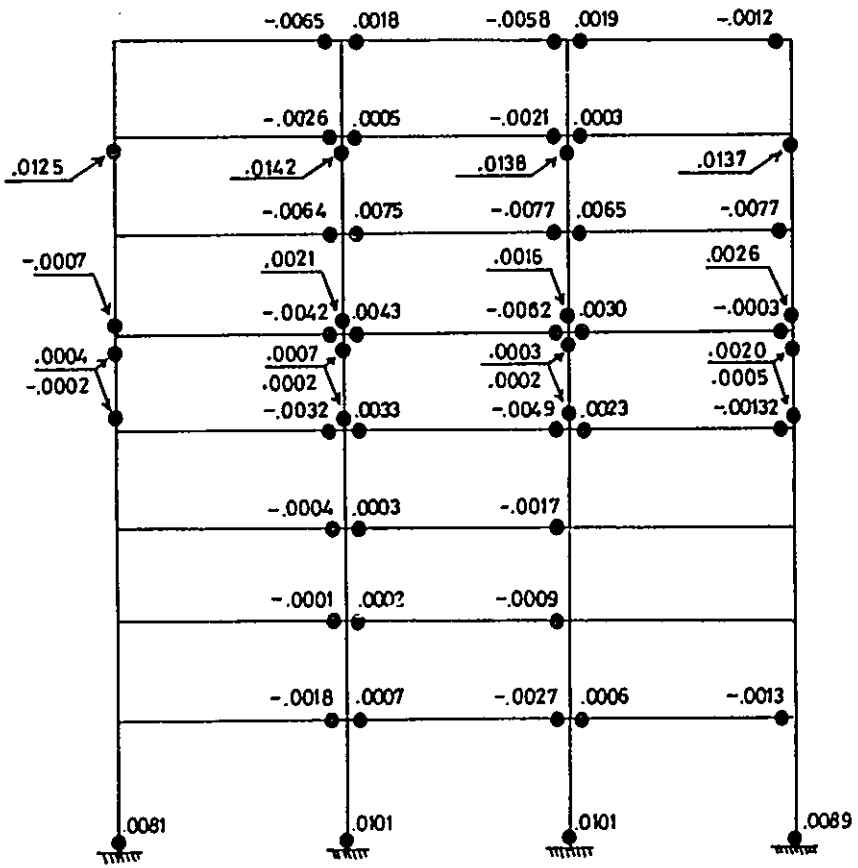

Beams and columns

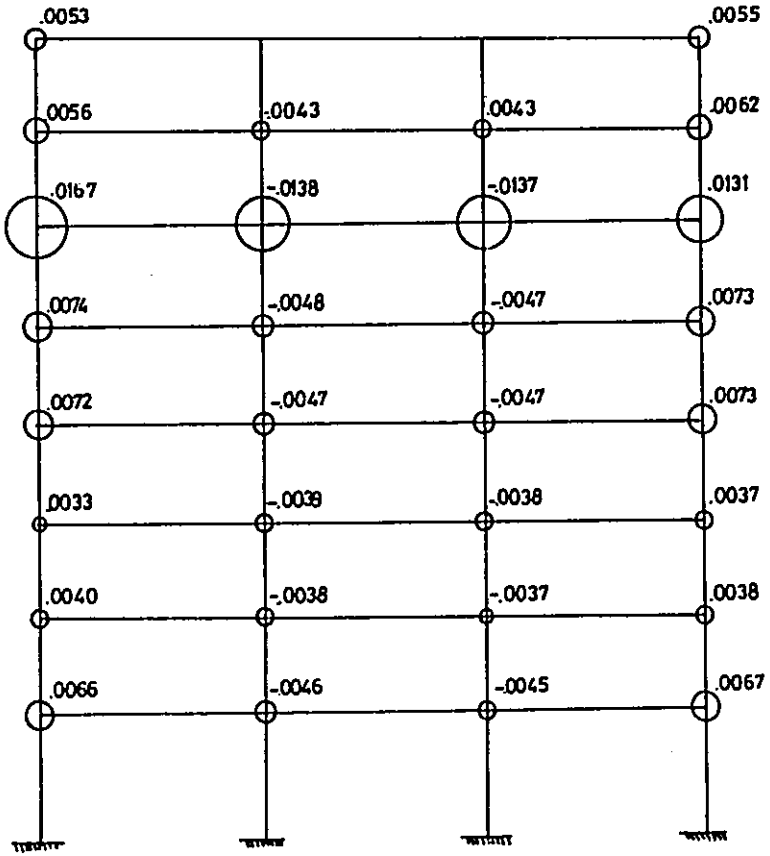

Panel zones

Fig. 6.24 Maximum beam, column and panel zone joint plastic rotations for MRF case 4. (in radians)

Bucharest Earthquake

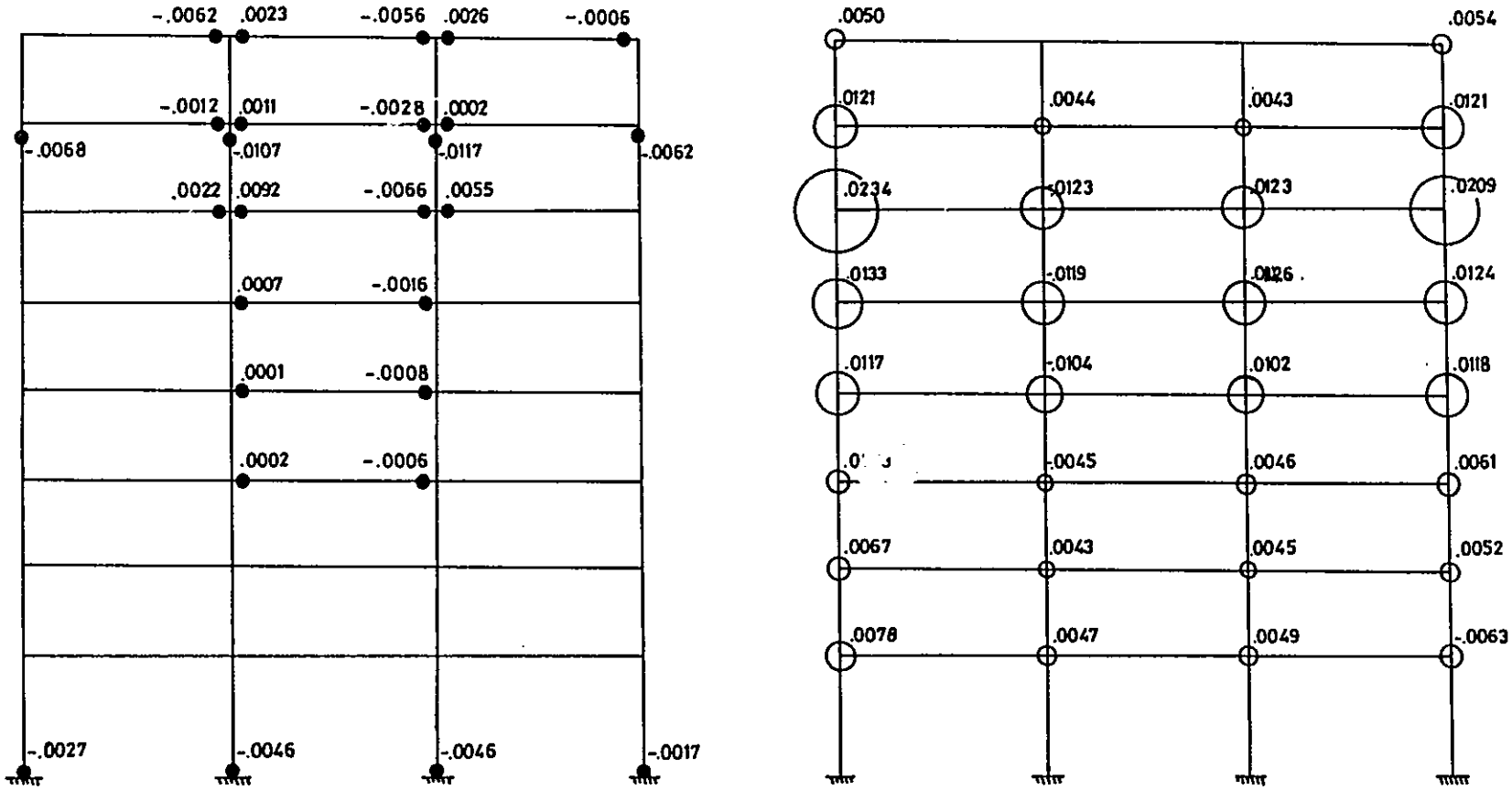

Beams and columns

Panel zones

Fig. 6.25 Maximum beam, column and panel zone joint plastic rotations for MRF case 5. (in radians)

Bucharest Earthquake

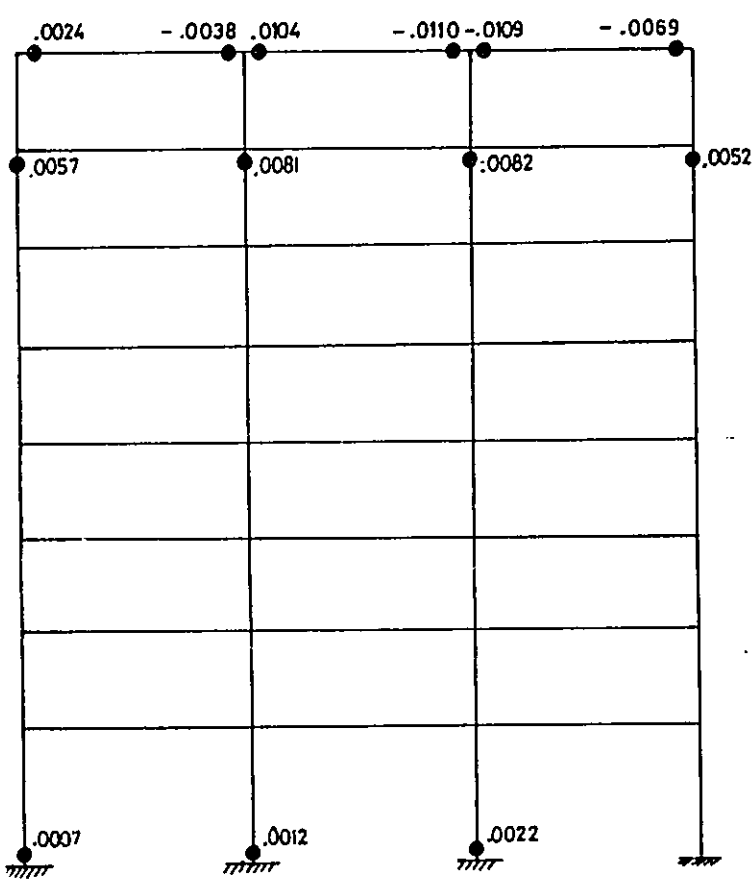

Beams and columns

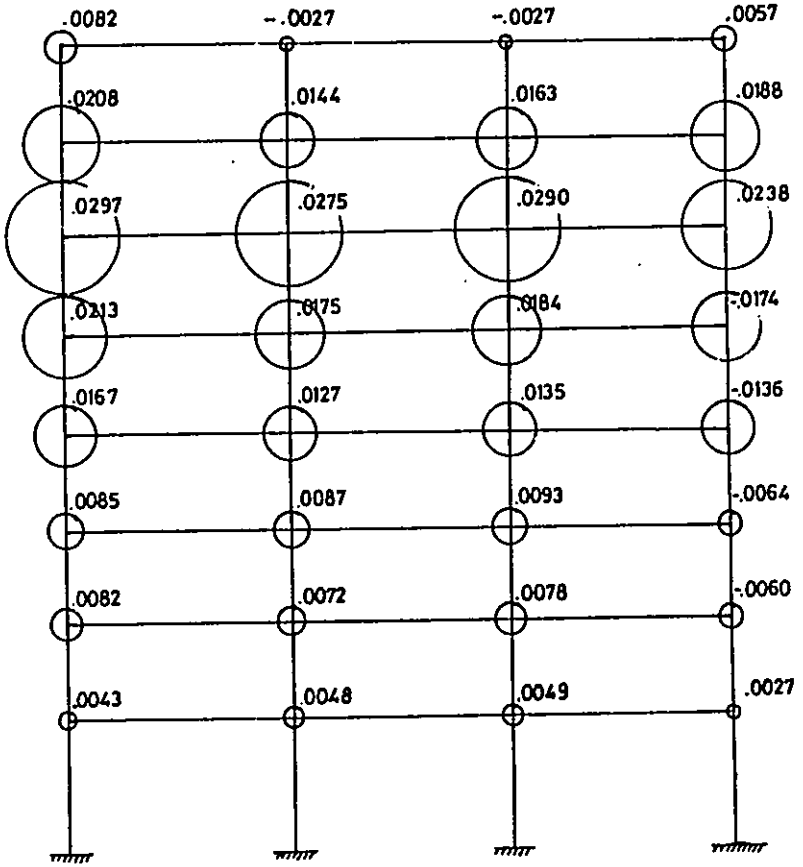

Panel zones

Fig. 6.26 Maximum beam, column and panel zone joint plastic rotations for MRF case 6. (in radians)

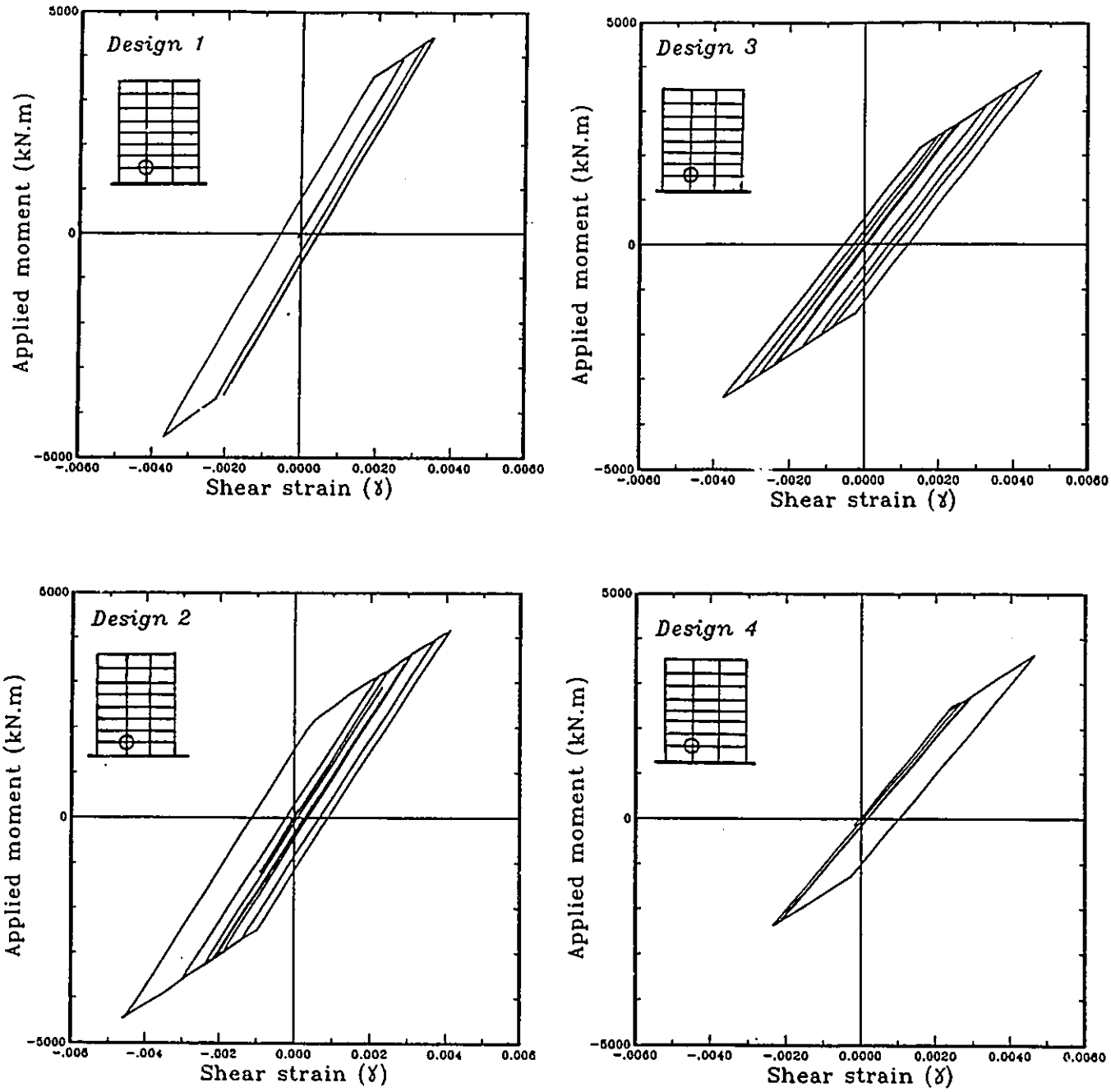

Fig. 6.27 Interior panel zone deformation versus applied moment hysteretic loops.

Bucharest Earthquake

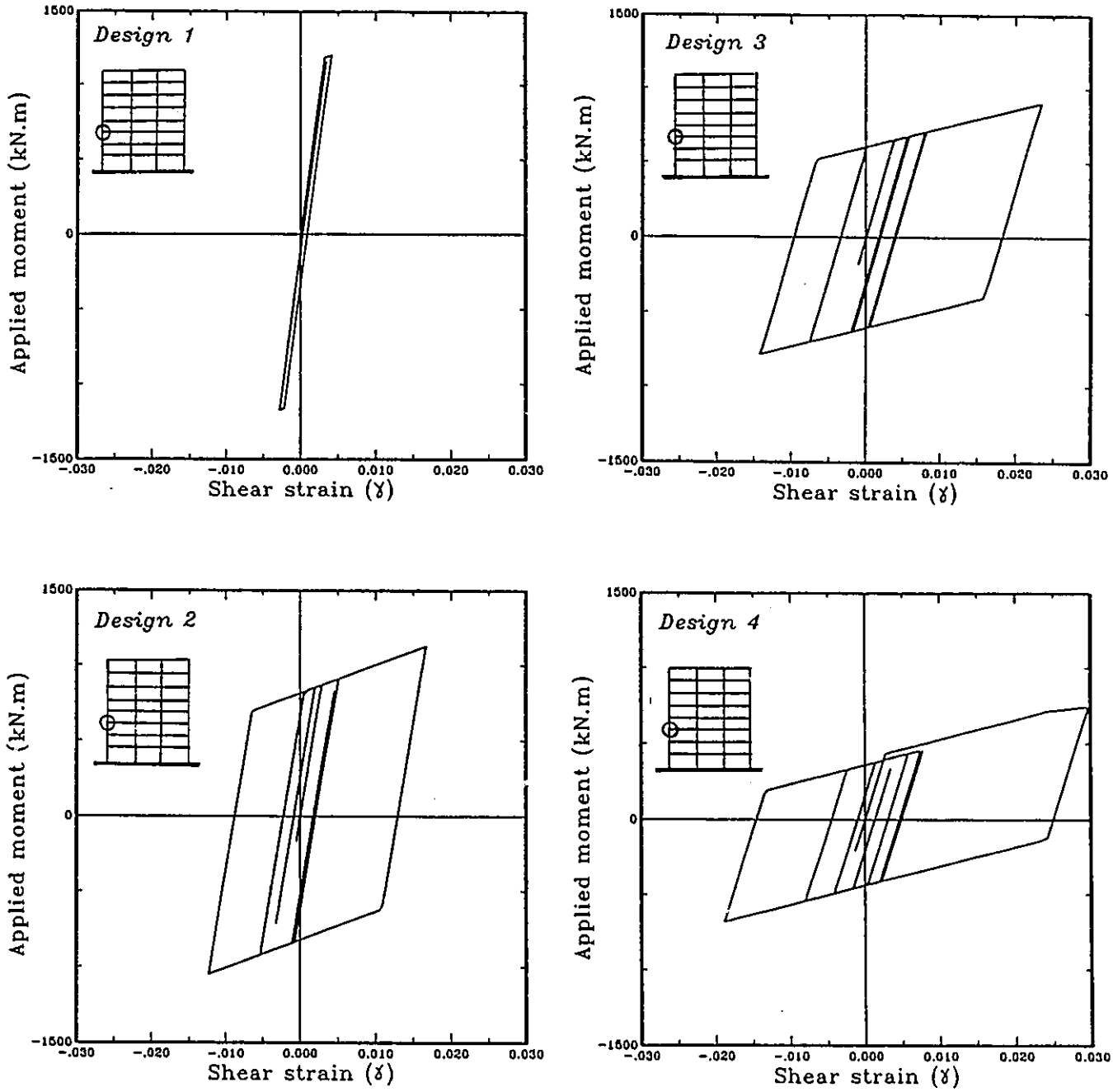

Fig. 6.28 Exterior panel zone deformation versus applied moment hysteretic loops.

Response to Mexico Earthquake.

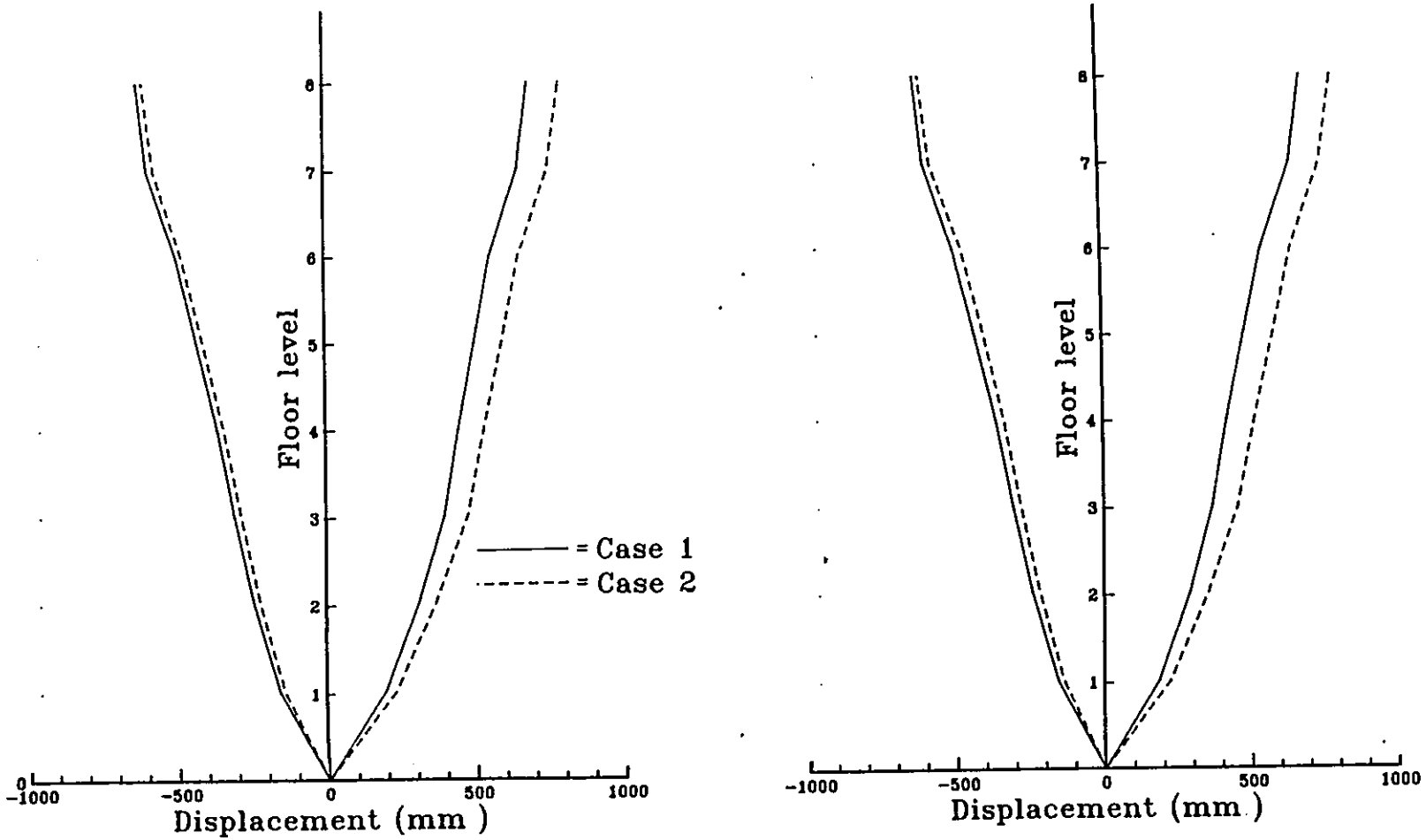

a)Maximum floor displacement. *b) Floor displacement at peak roof displacement*

Fig. 6.29 Effect of connection flexibility on the dynamic lateral displacement.

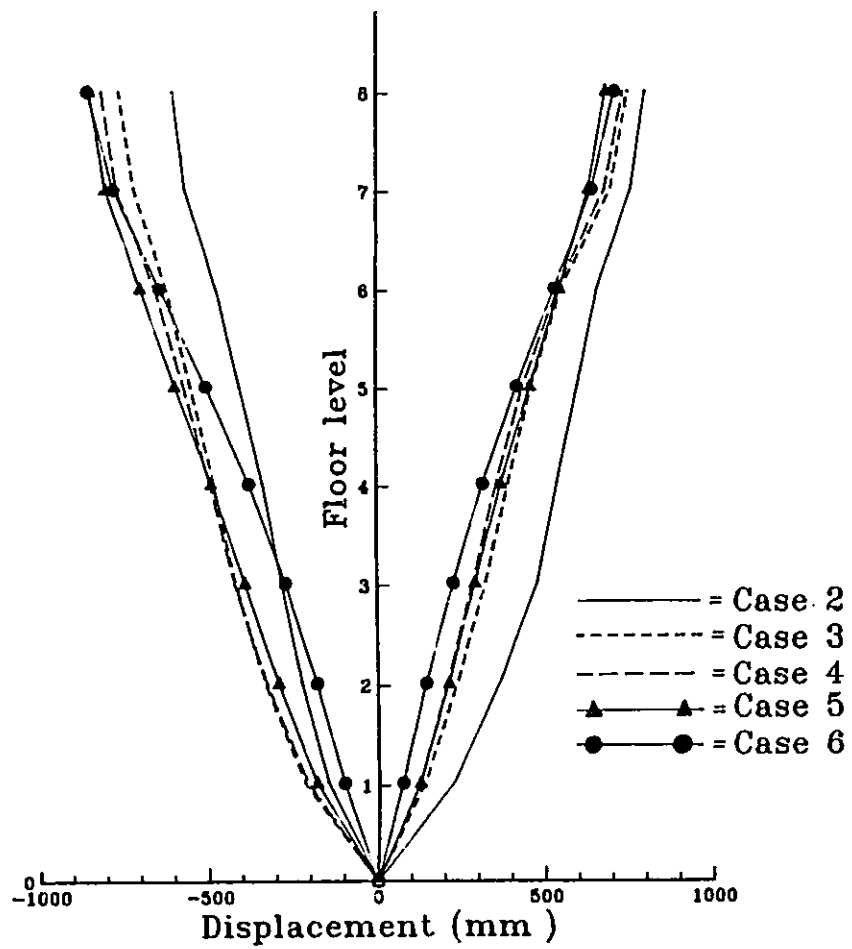

a) Maximum floor displacement.

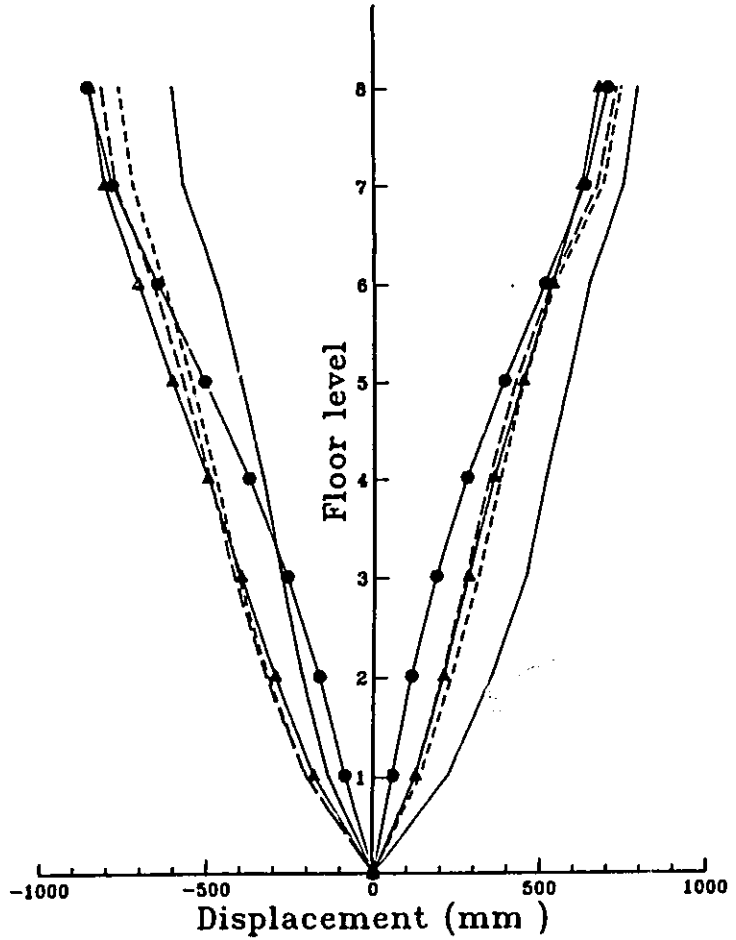

b) Floor diplacement at peak roof displacement.

Fig. 6.30 Effect of panel zone deformation on the dynamic lateral displacement.

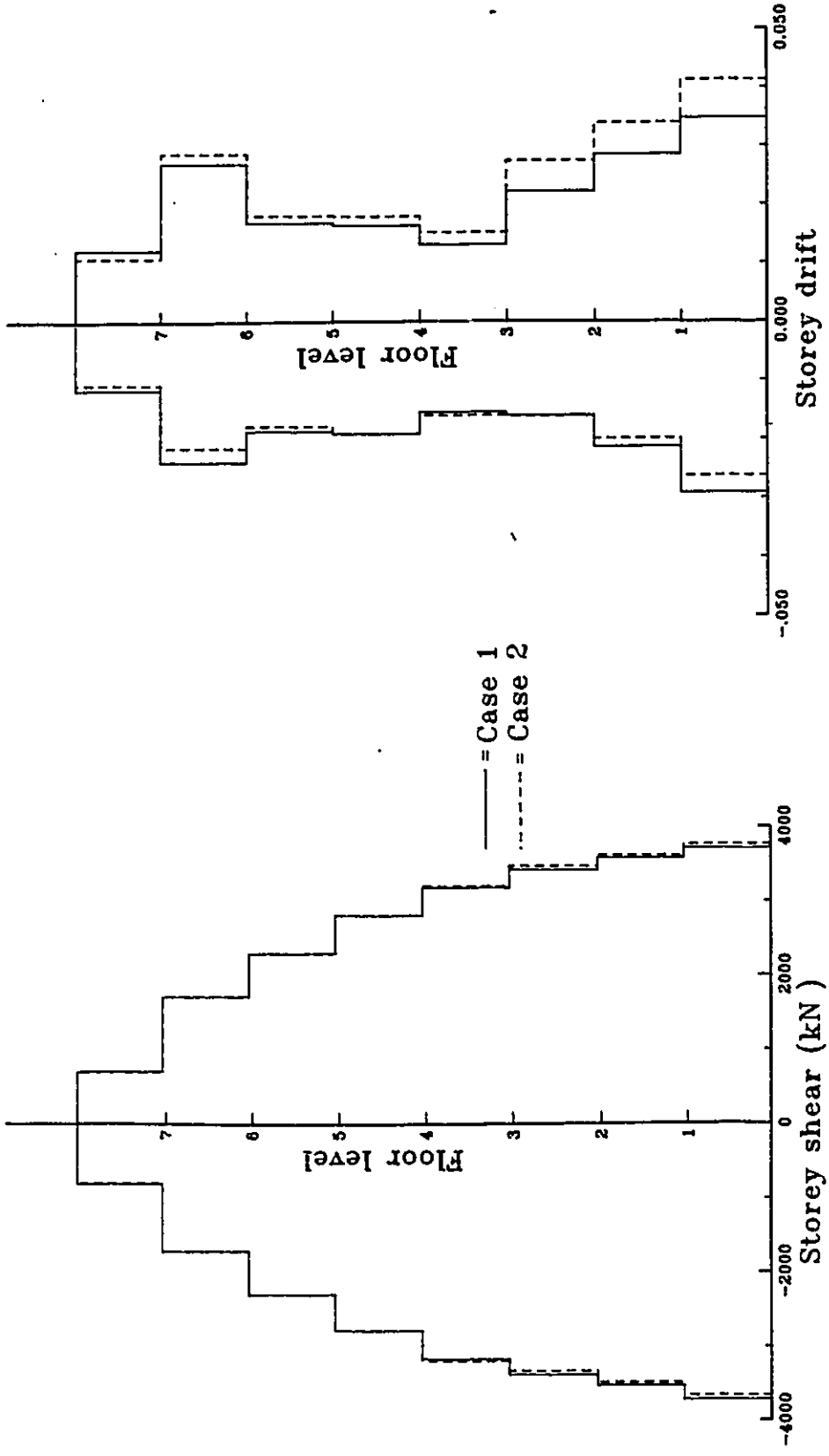

Fig. 6.31 Effect of connection flexibility on the storey shear and storey drift.

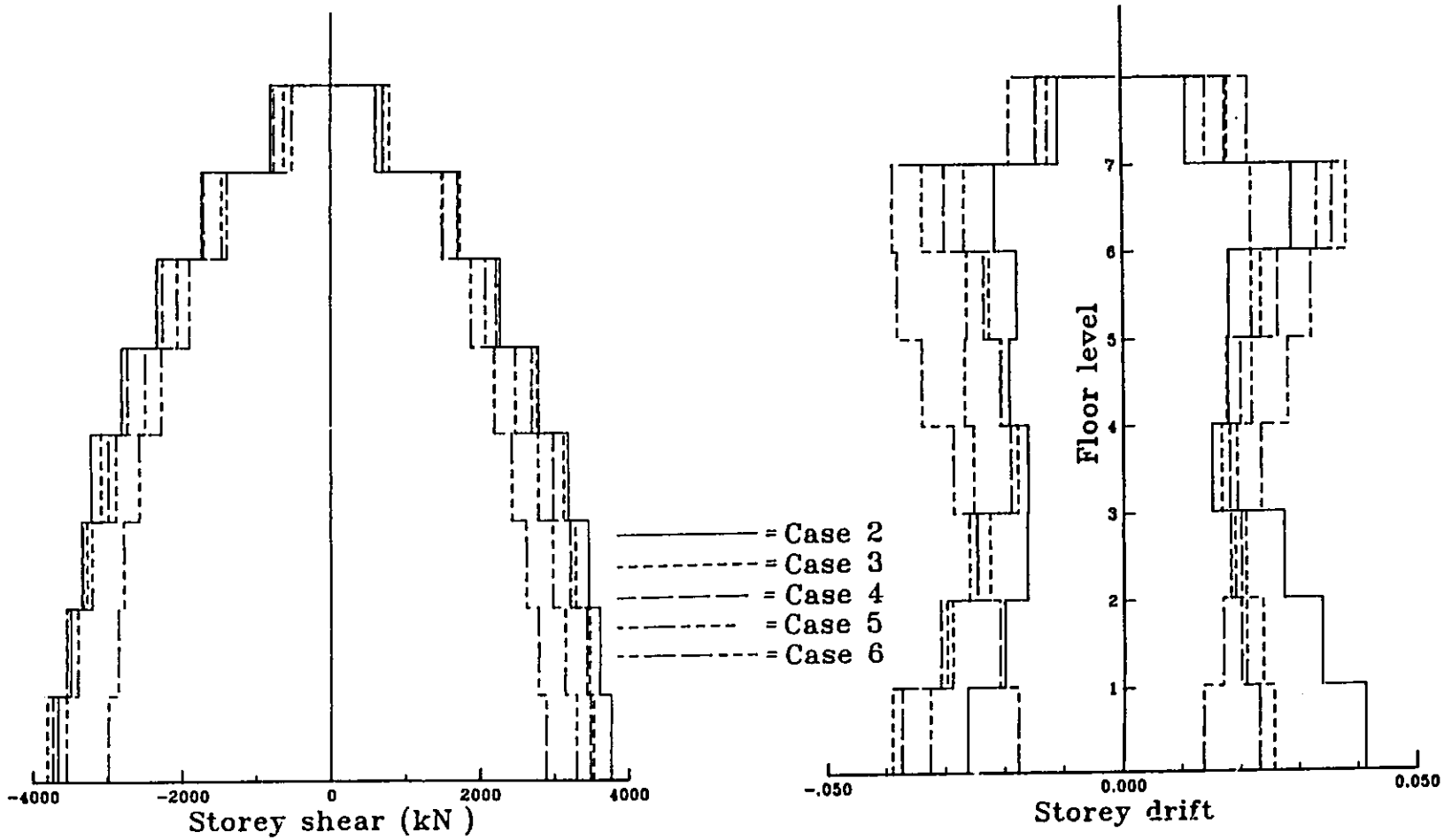

Fig. 6.32 Effect of panel zone deformation on the storey shear and storey drift.

Mexico Earthquake

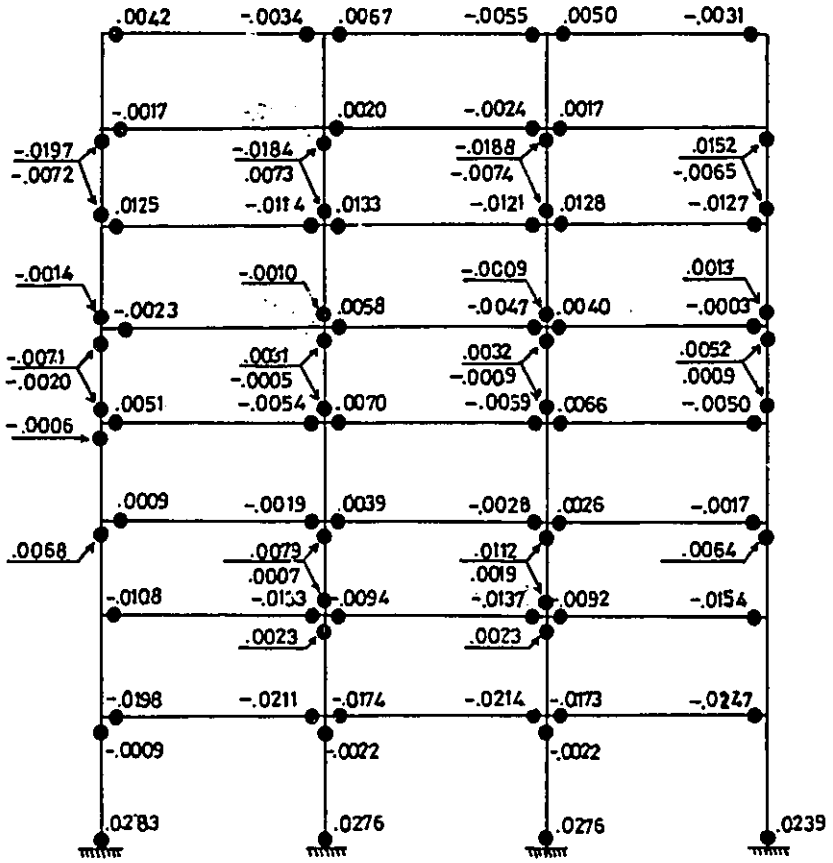

Fig. 6.33 Maximum beam and column plastic rotations for MRF case 1(in radians).

Mexico Earthquake

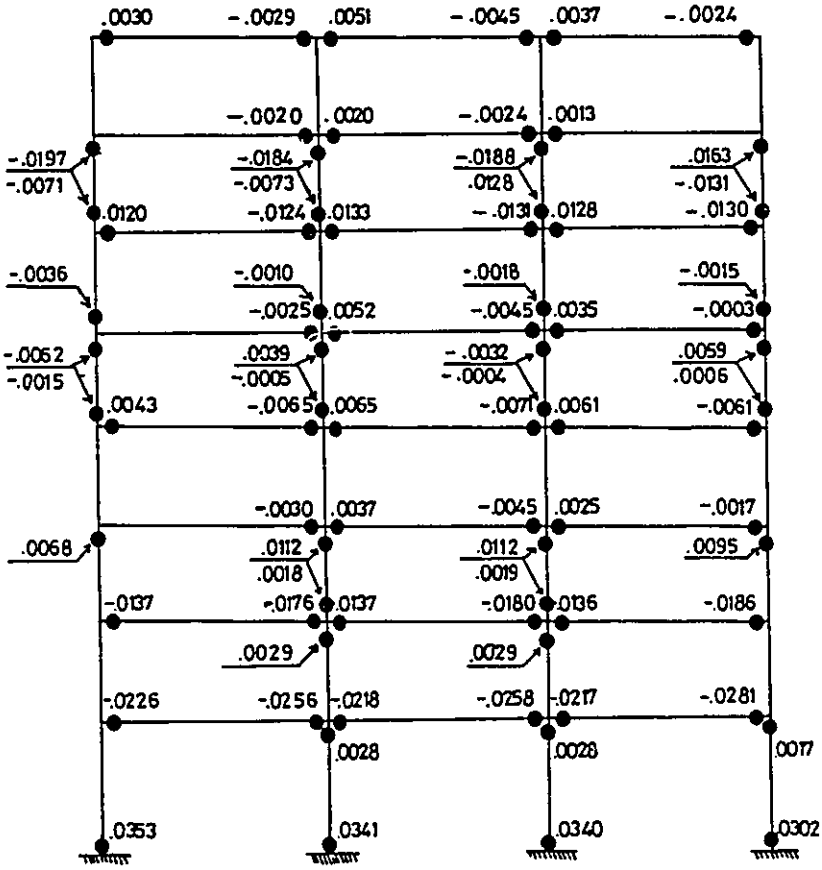

Fig. 6.34 Maximum beam and column plastic rotations for MRF case 2(in radians).

Mexico Earthquake

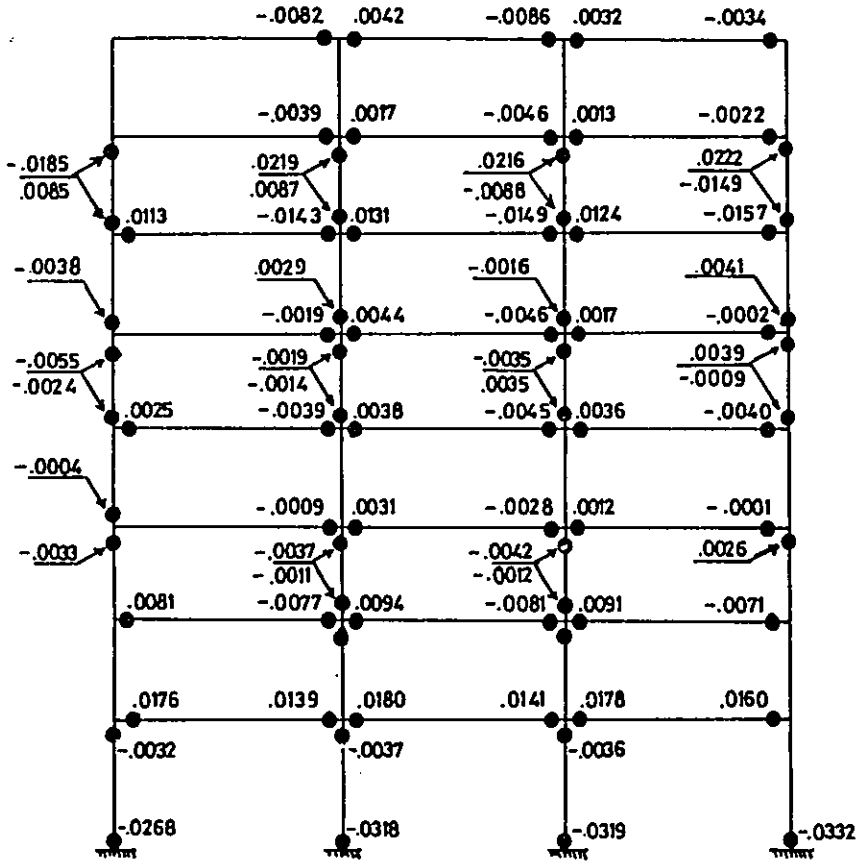

Beams and columns

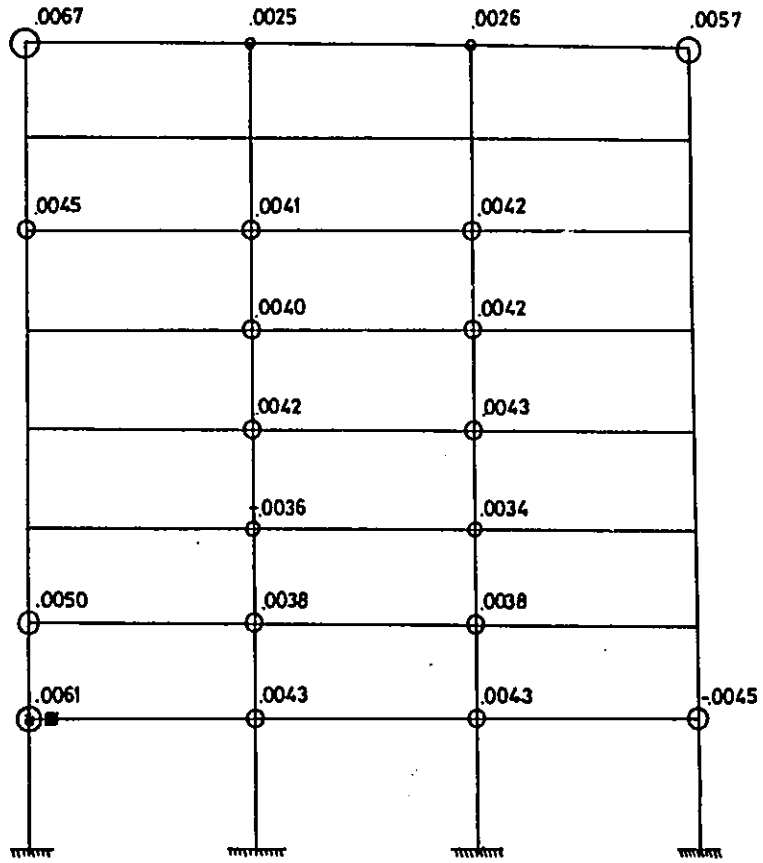

Panel zones

Fig. 6.35 Maximum beam, column and panel zone joint plastic rotations for MRF case 3. (in radians)

Mexico Earthquake

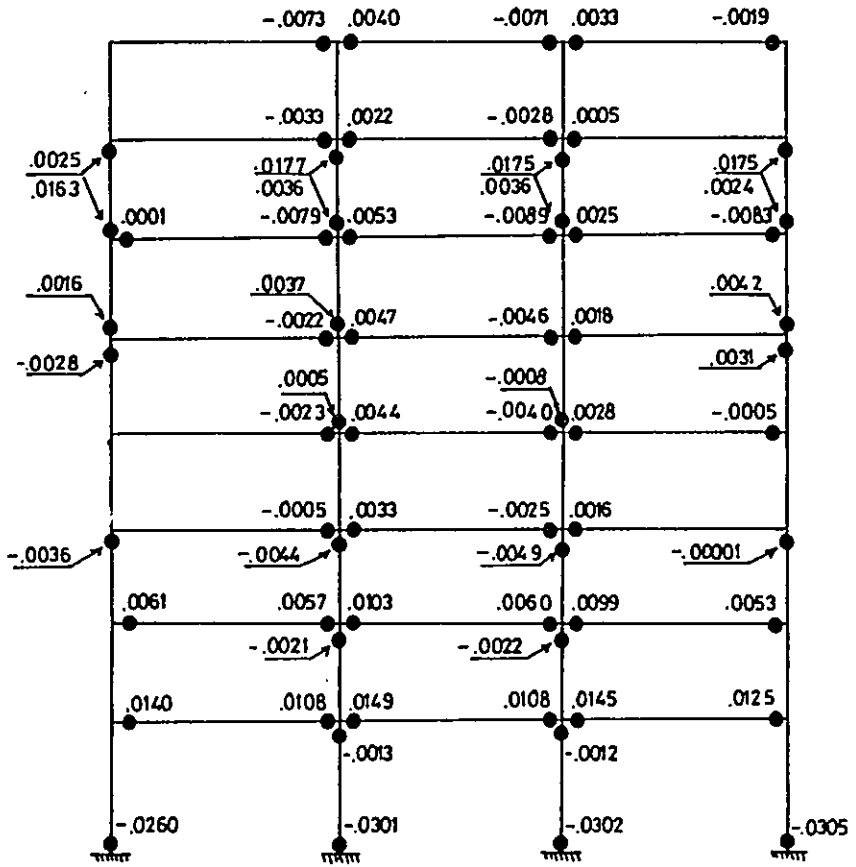

Beams and columns

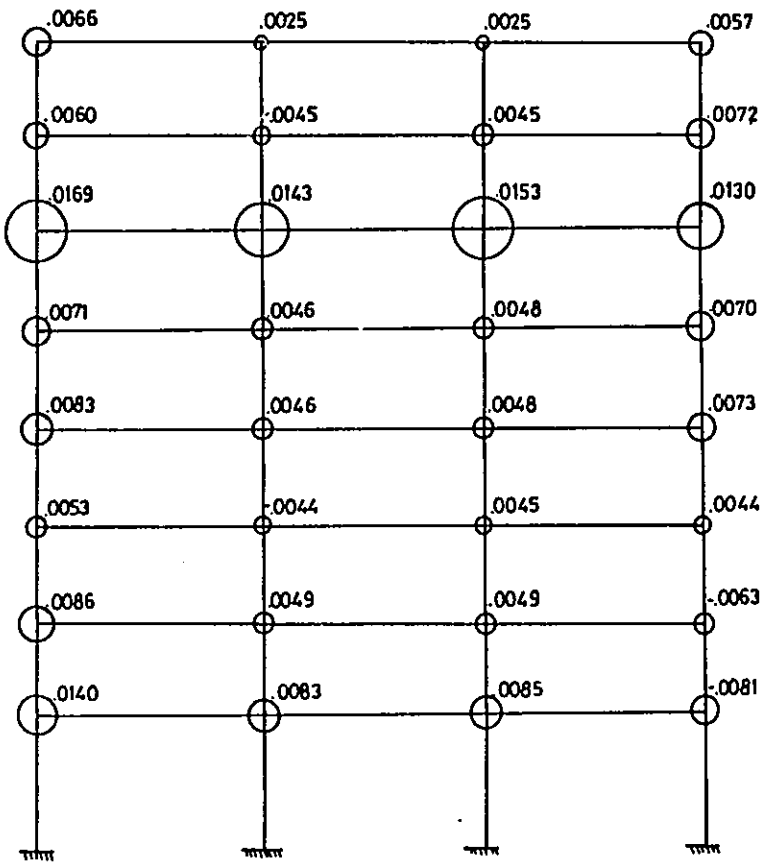

Panel zones

Fig. 6.36 Maximum beam, column and panel zone joint plastic rotations for MRF case 4. (in radians)

Mexico Earthquake

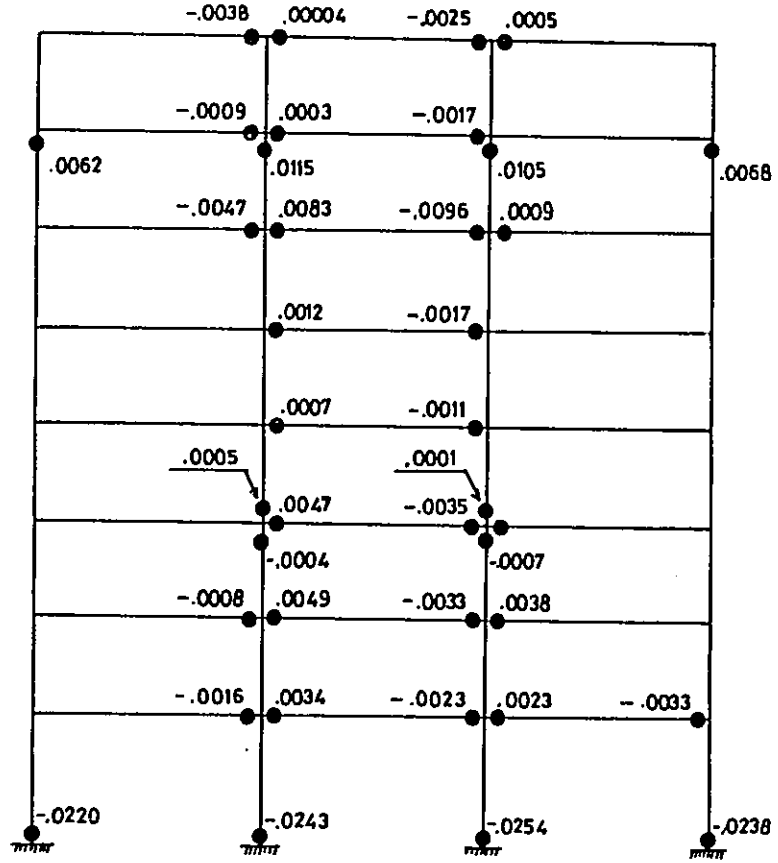

Beams and columns

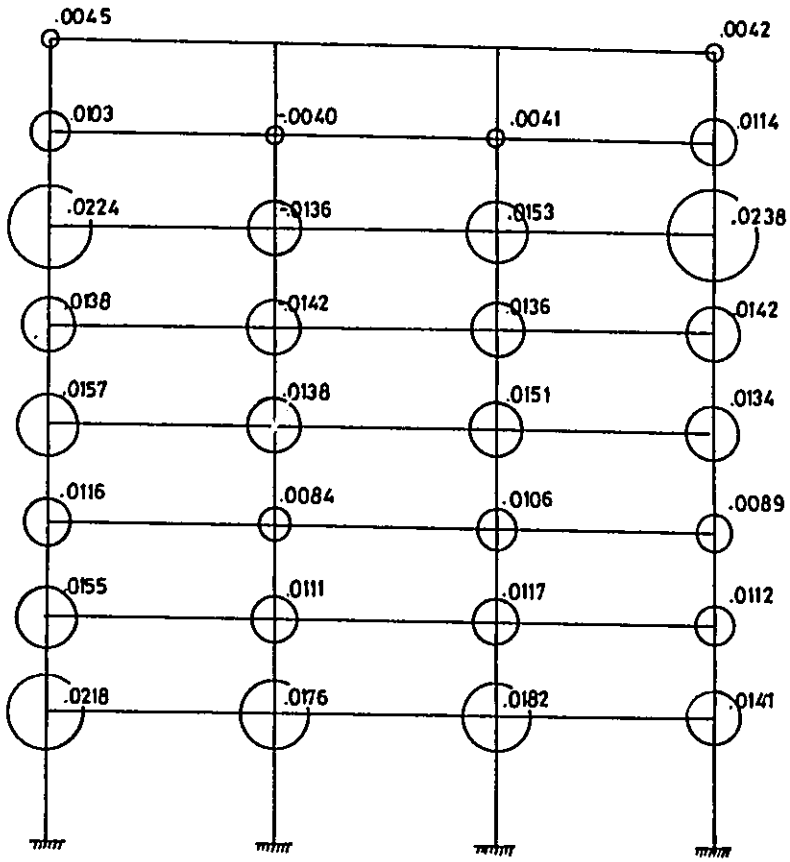

Panel zones

Fig. 6.37 Maximum beam, column and panel zone joint plastic rotations for MRF case 5. (in radians)

Mexico Earthquake

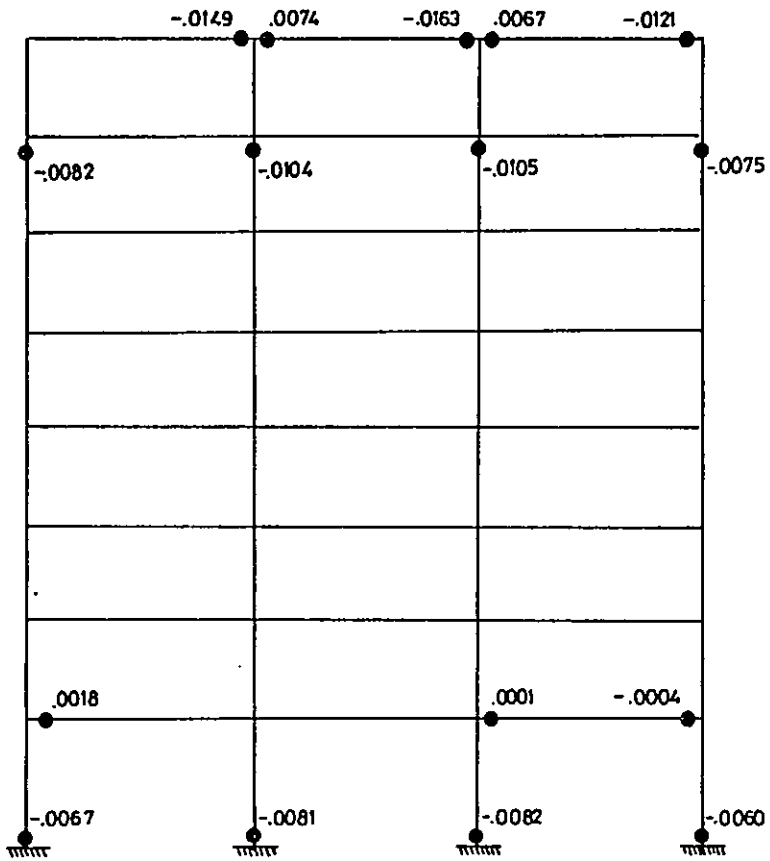

Beams and columns

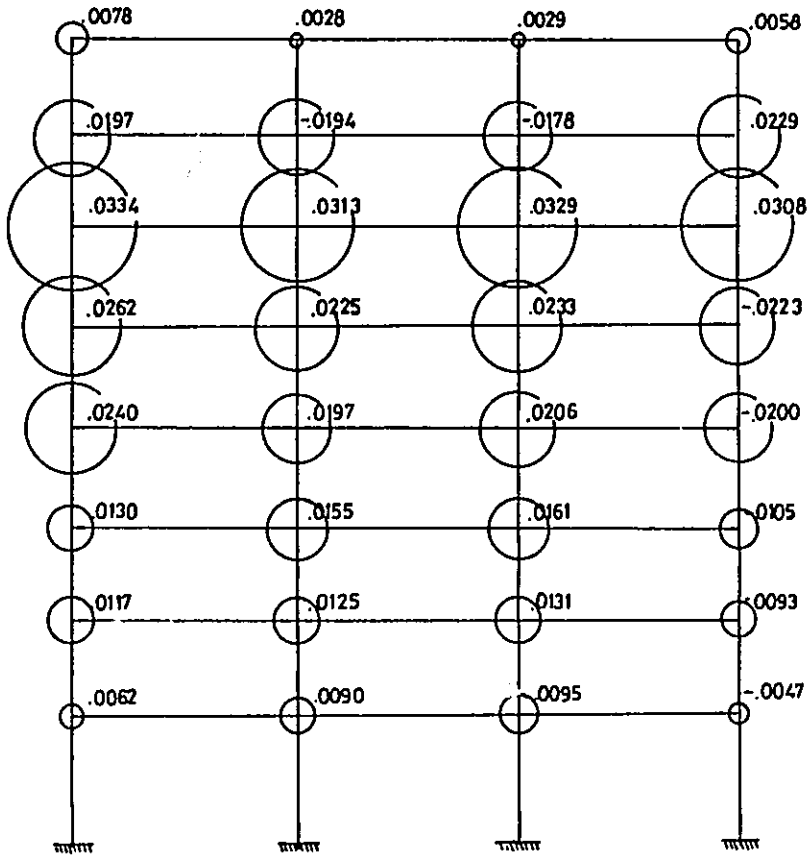

Panel zones

Fig. 6.38 Maximum beam, column and panel zone joint plastic rotations for MRF case 6. (in radians)

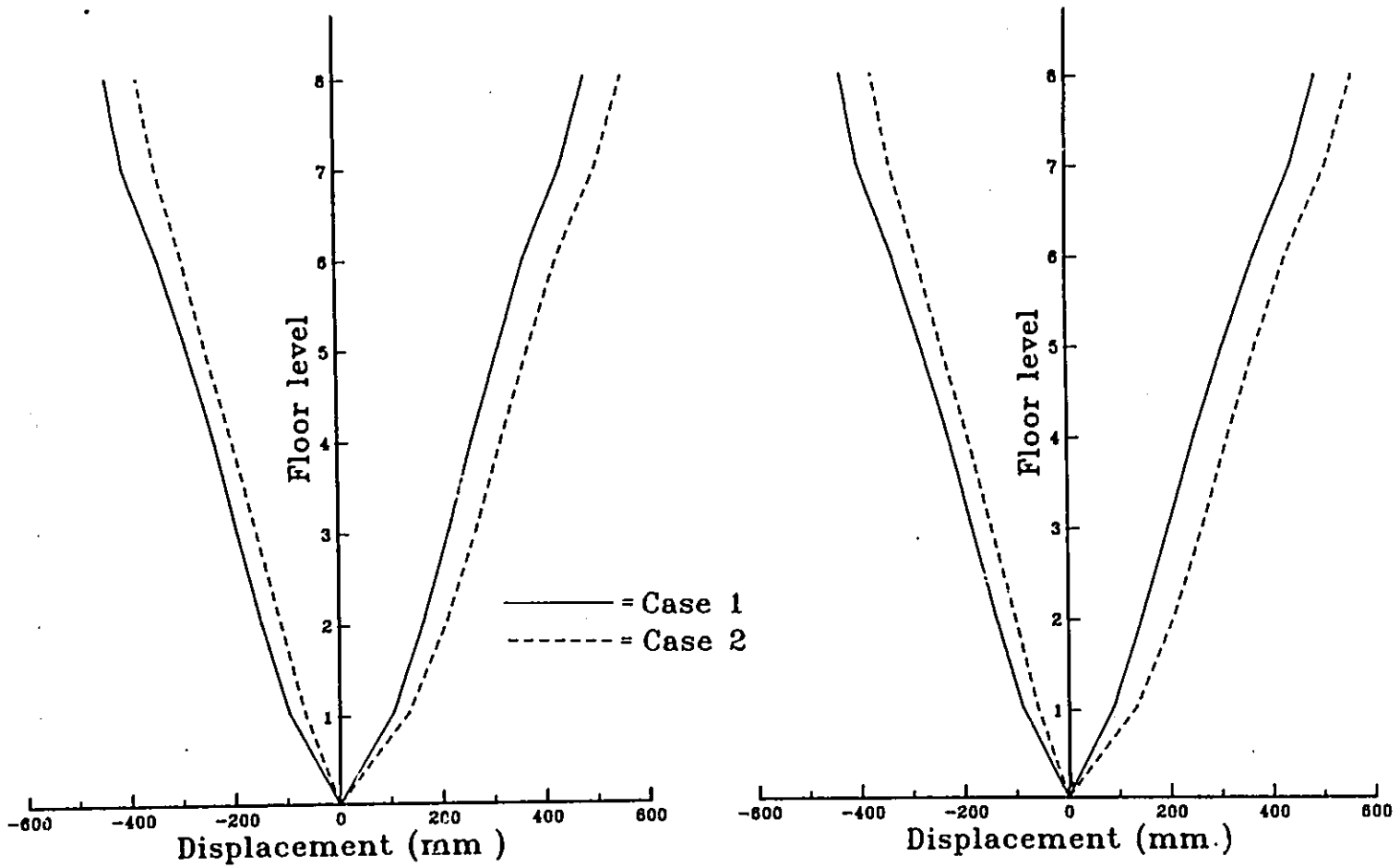

a) Maximum floor displacement. *b) Floor displacement at peak roof displacement*

Fig. 6.39 Effect of connection flexibility on the dynamic lateral displacement.

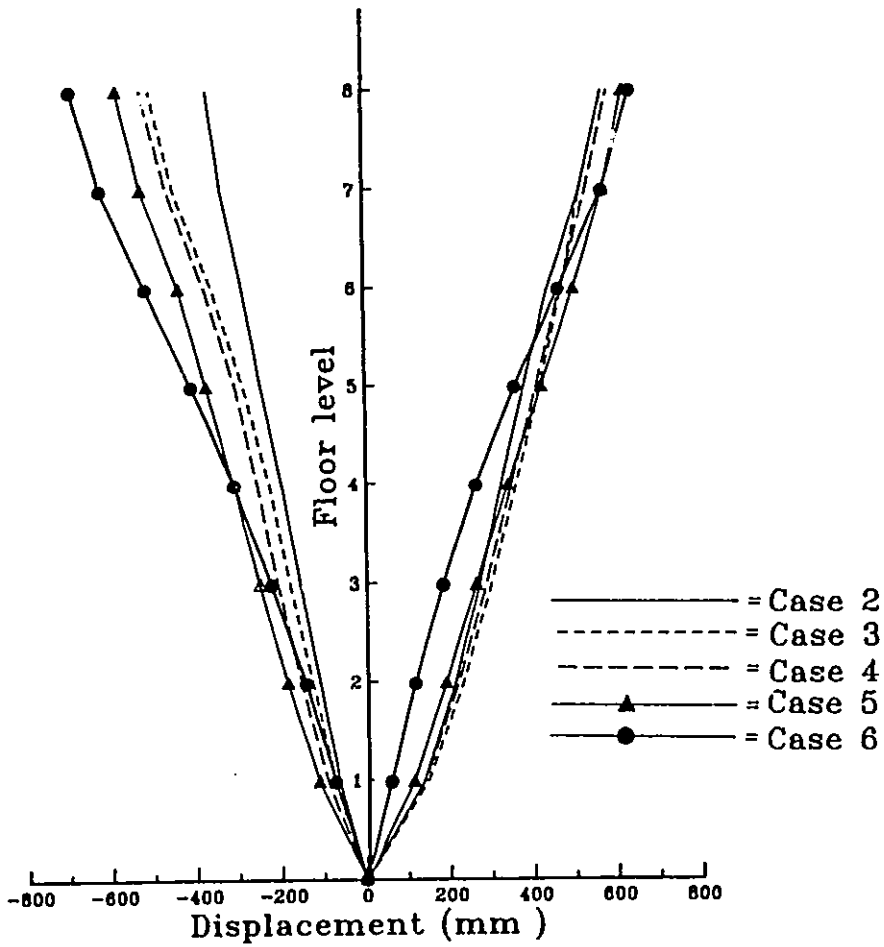

a) Maximum floor displacement.

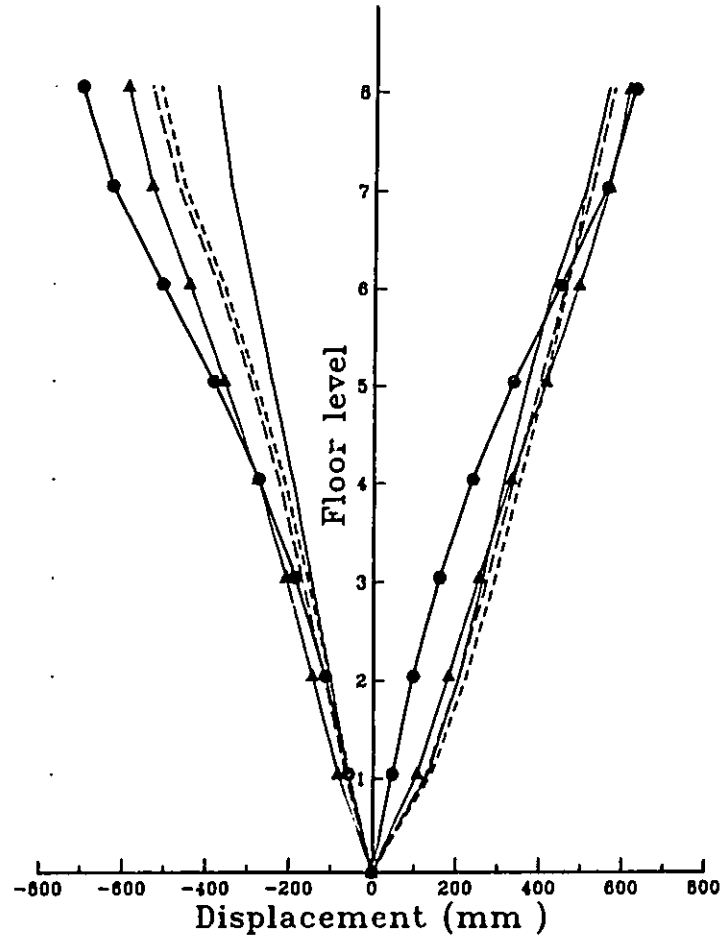

b) Floor displacement at peak roof displacement

Fig. 6.40 Effect of panel zone deformation on the dynamic lateral displacement.

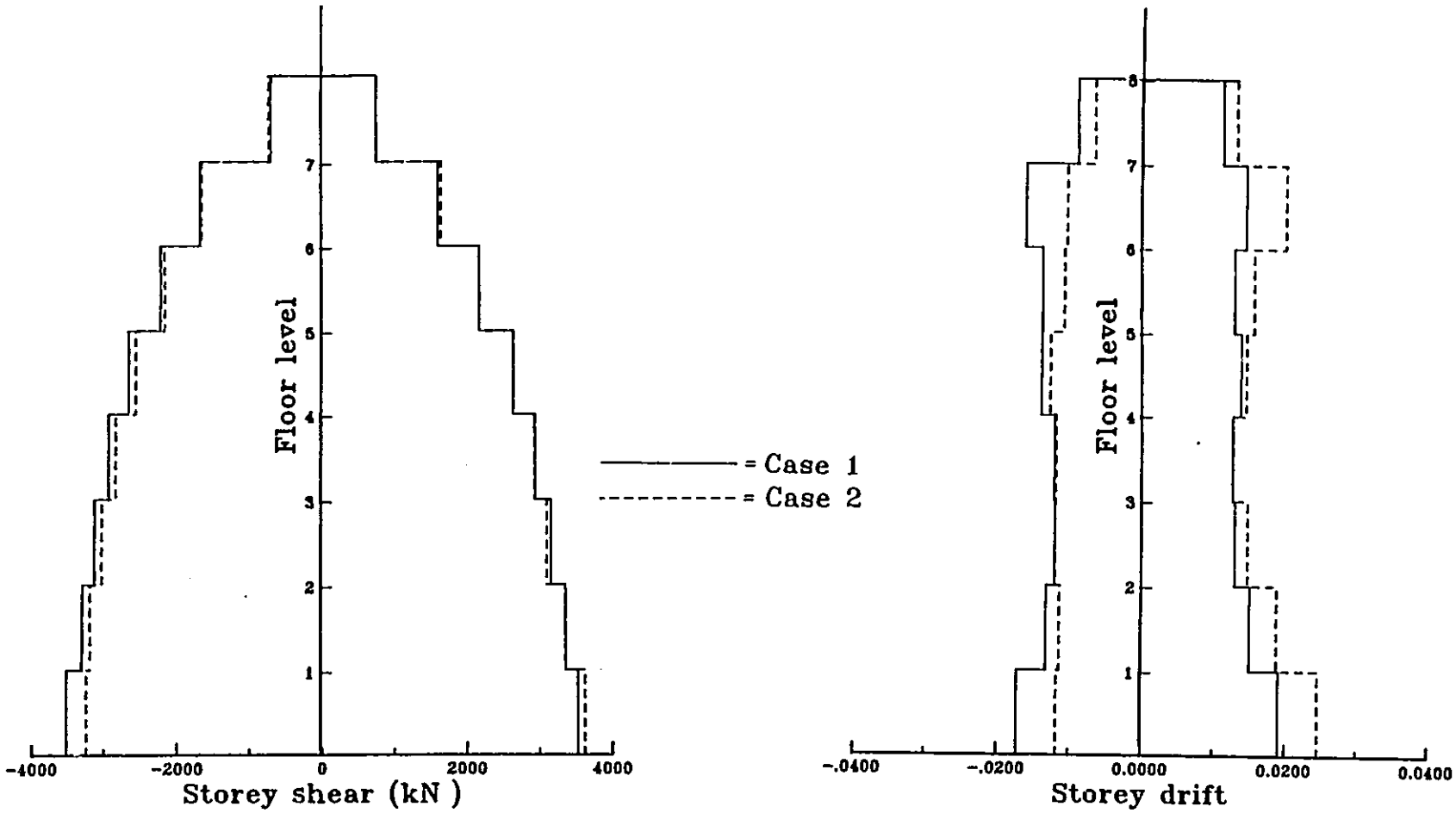

Fig. 6.41 Effect of connection flexibility on the storey shear and storey drift.

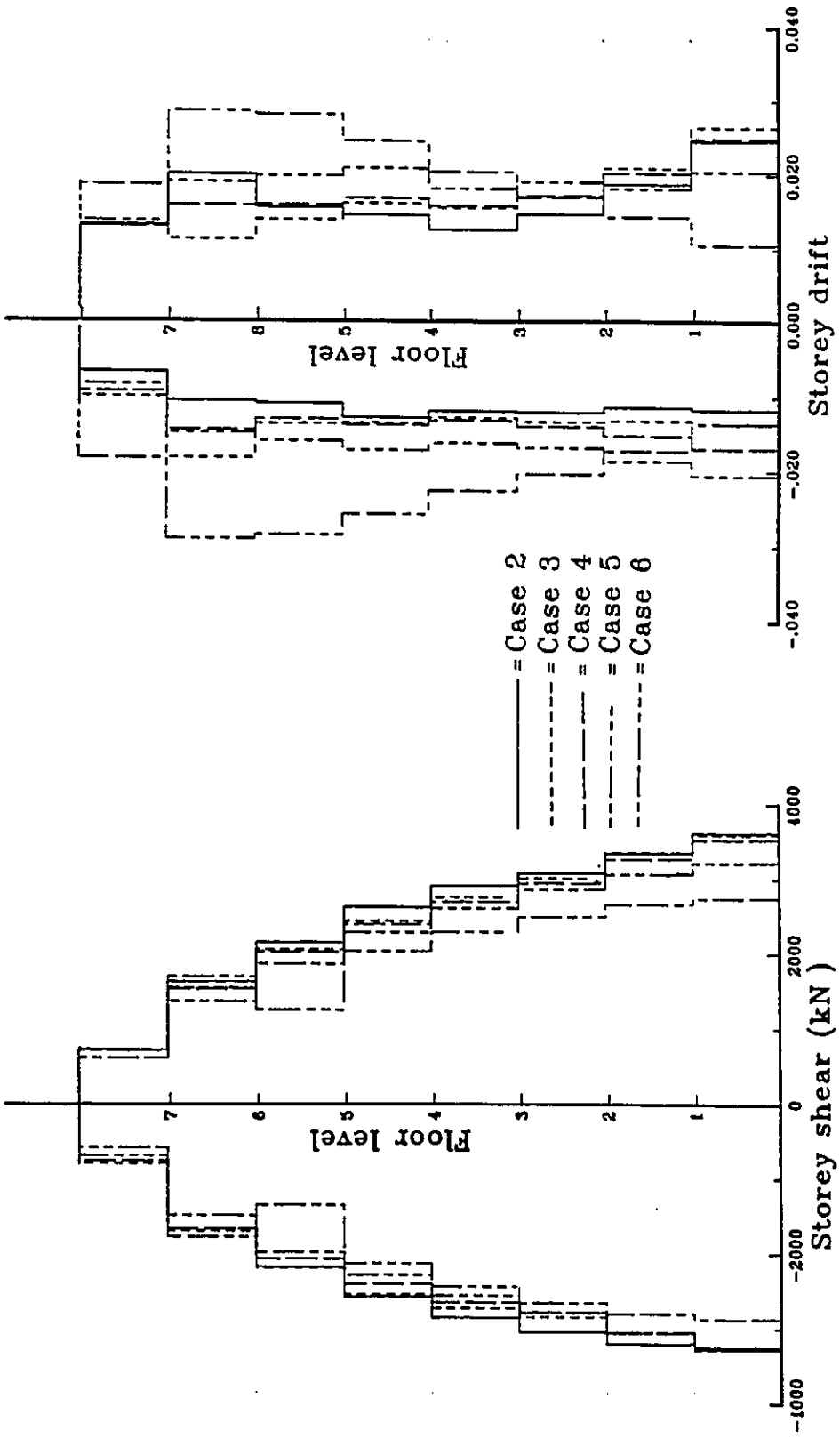

Fig. 6.42 Effect of panel zone deformation on the storey shear and storey drift.

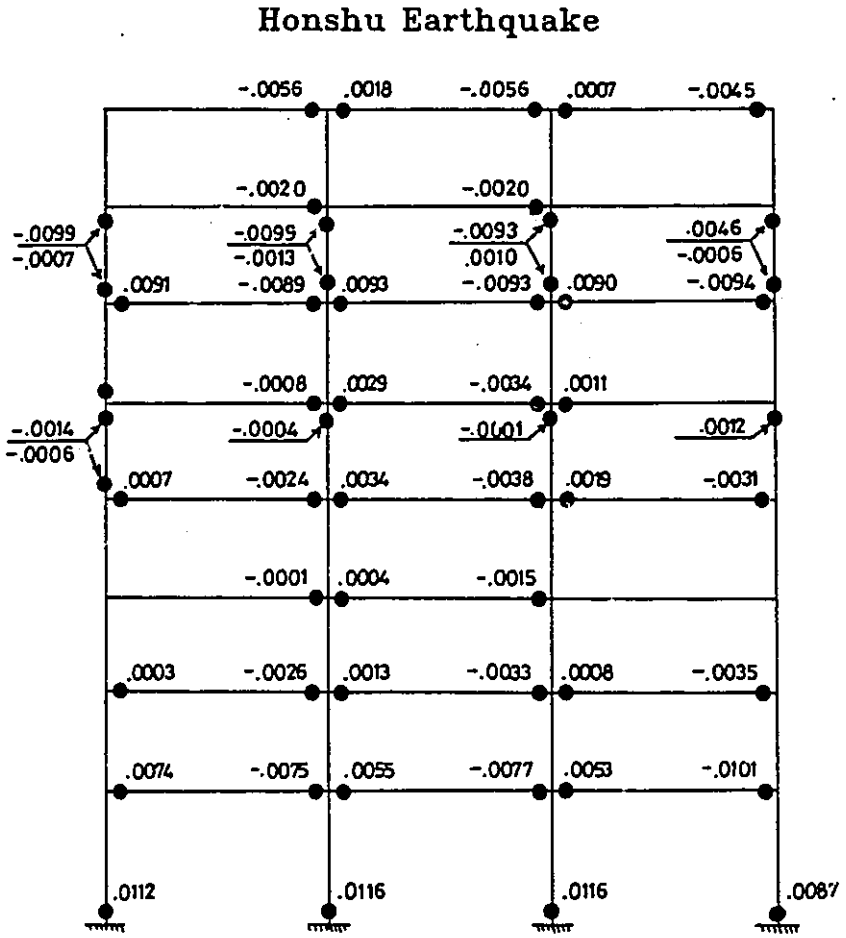

Fig. 6.43 Maximum beam and column plastic rotations for MRF case 1(in radians).

Honshu Earthquake

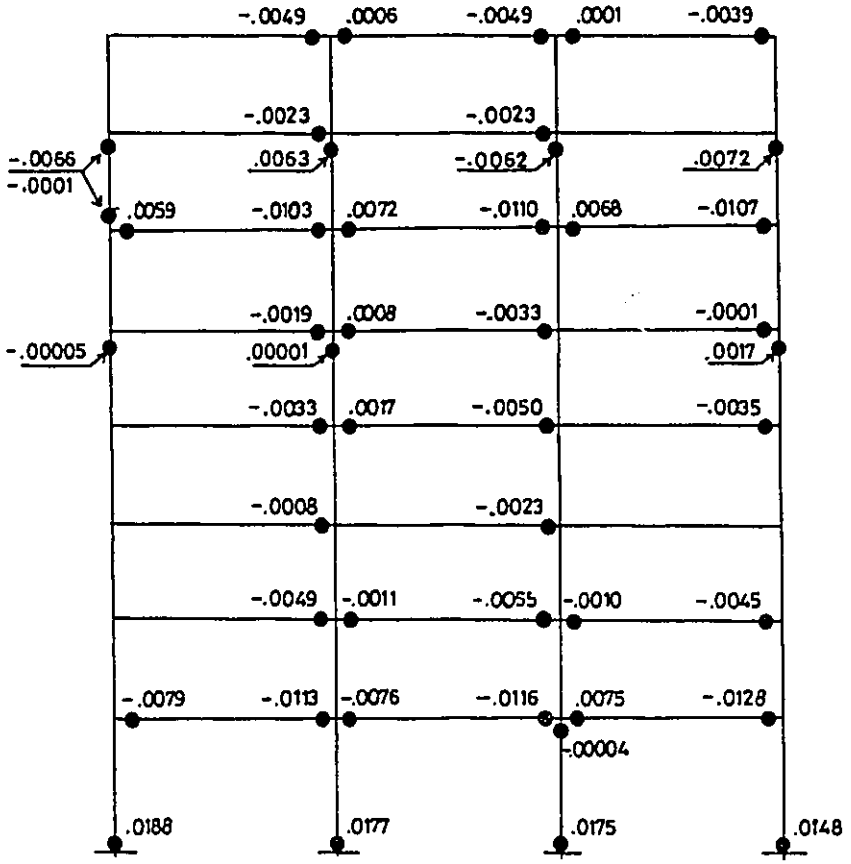

Fig. 6.44 Maximum beam and column plastic rotations for MRF case 2(in radians).

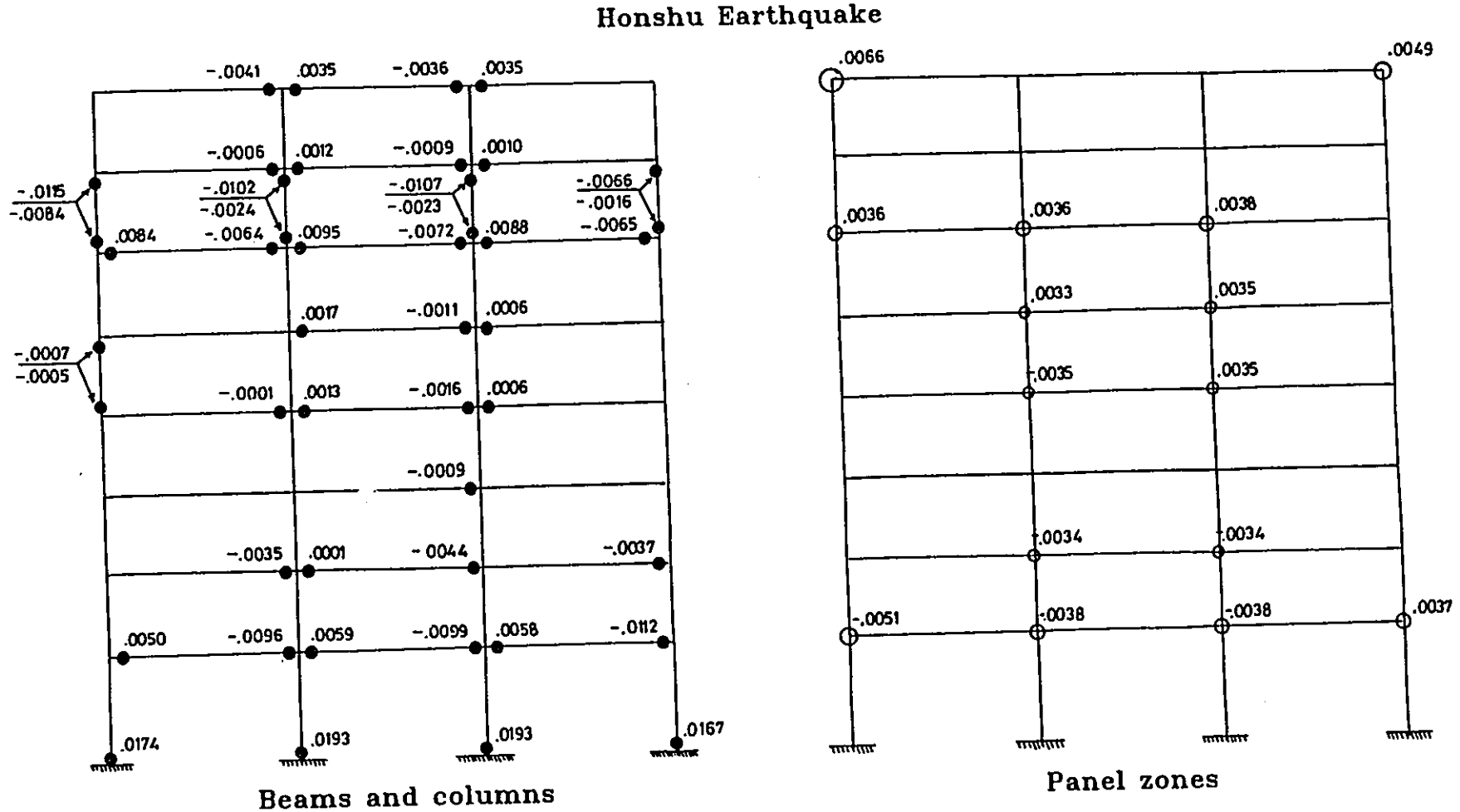

Fig. 6.45 Maximum beam, column and panel zone joint plastic rotations for MRF case 3. (in radians)

Honshu Earthquake

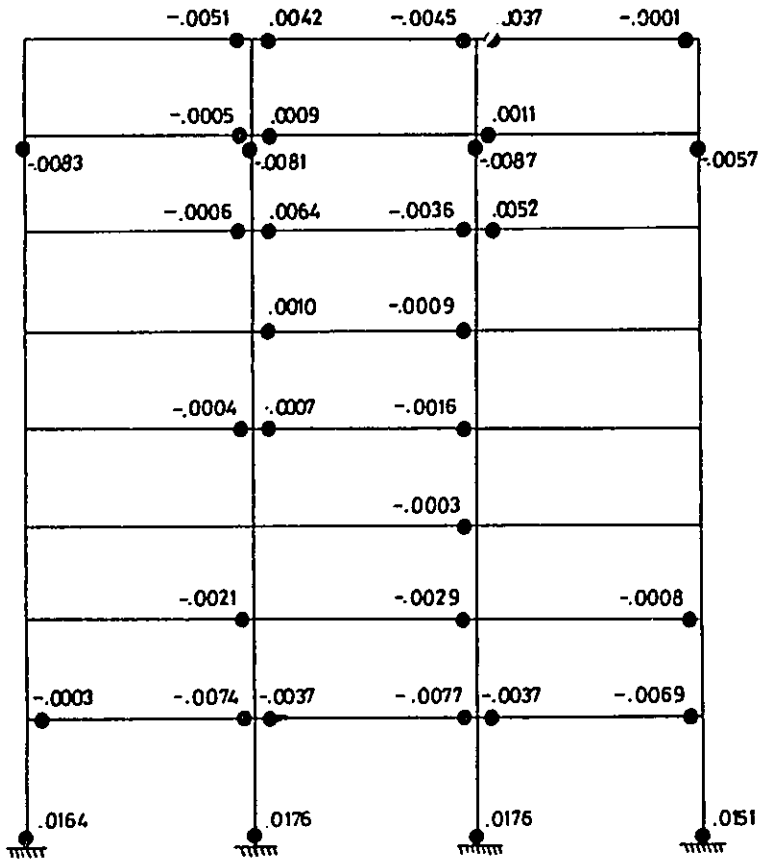

Beams and columns

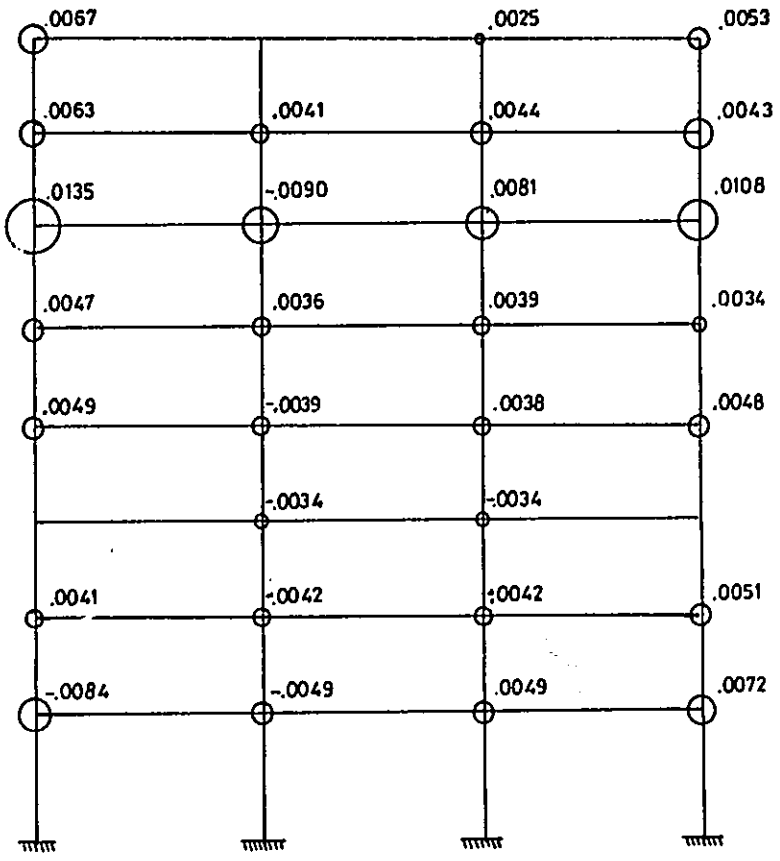

Panel zones

Fig. 6.46 Maximum beam, column and panel zone joint plastic rotations for MRF case 4. (in radians)

Honshu Earthquake

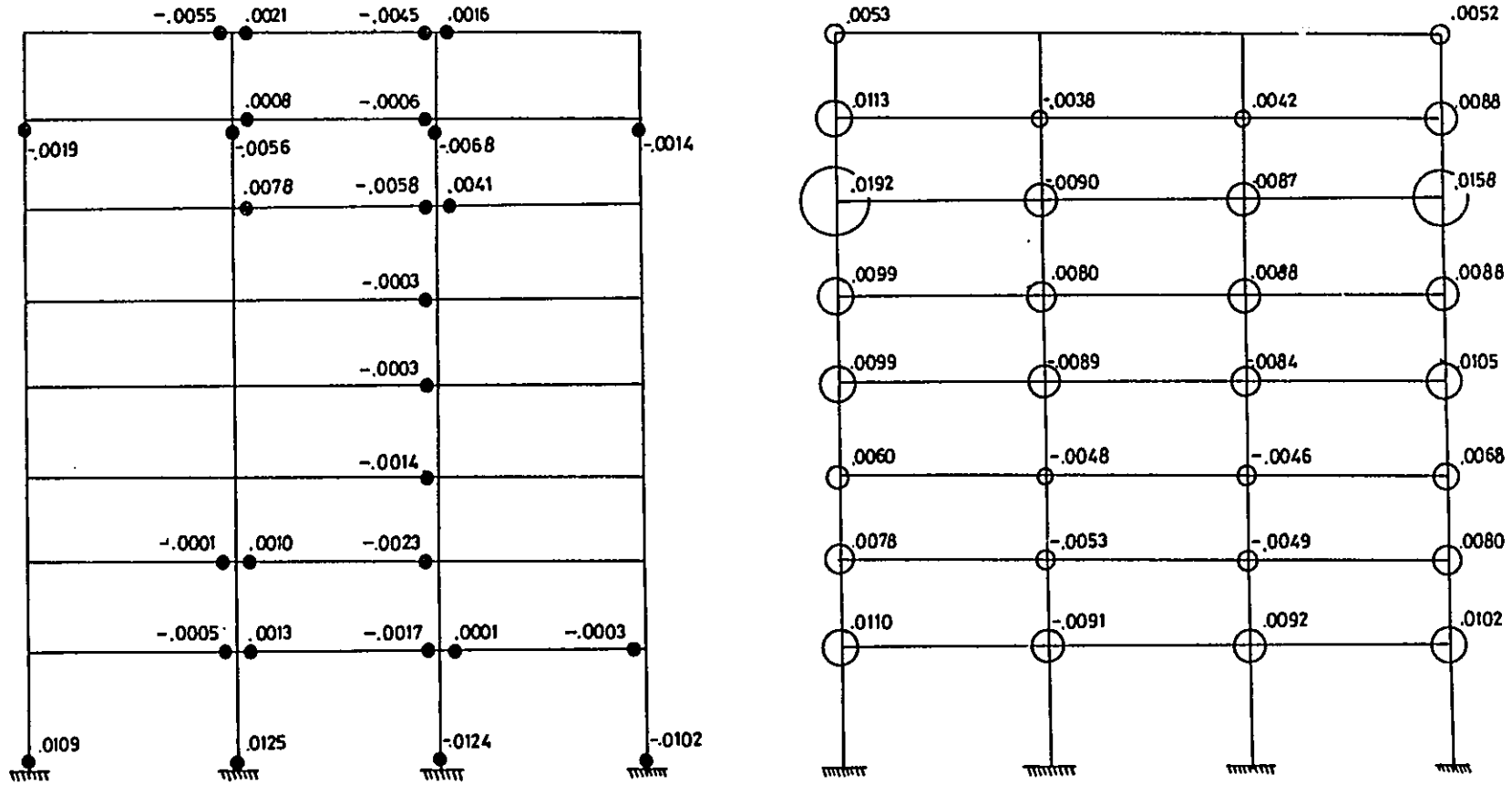

Beams and columns

Panel zones

Fig. 6.47 Maximum beam, column and panel zone joint plastic rotations for MRF case 5. (in radians)

Honshu Earthquake

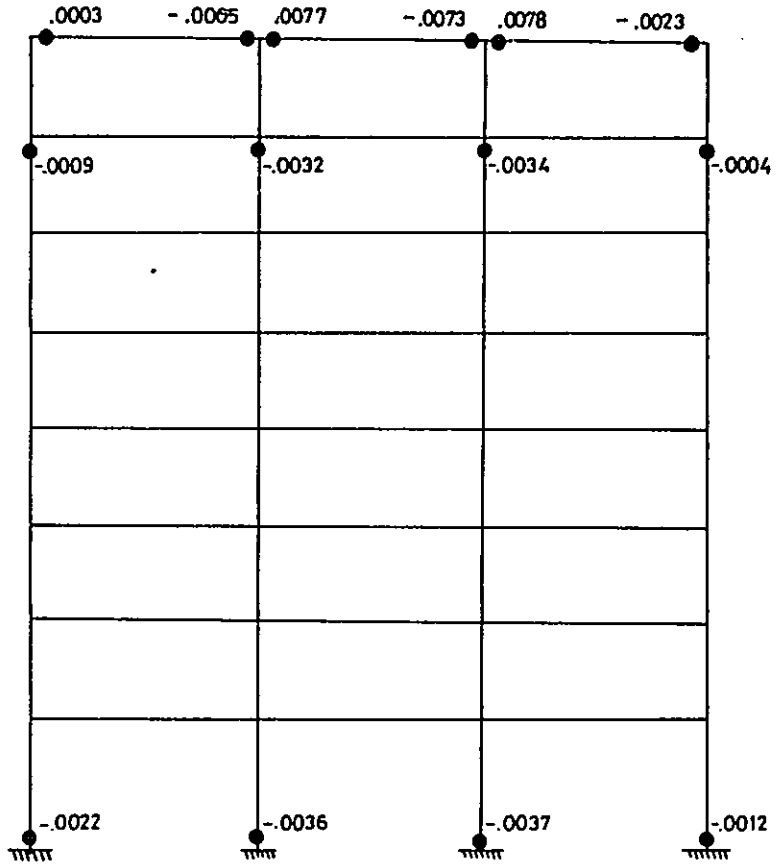

Beams and columns

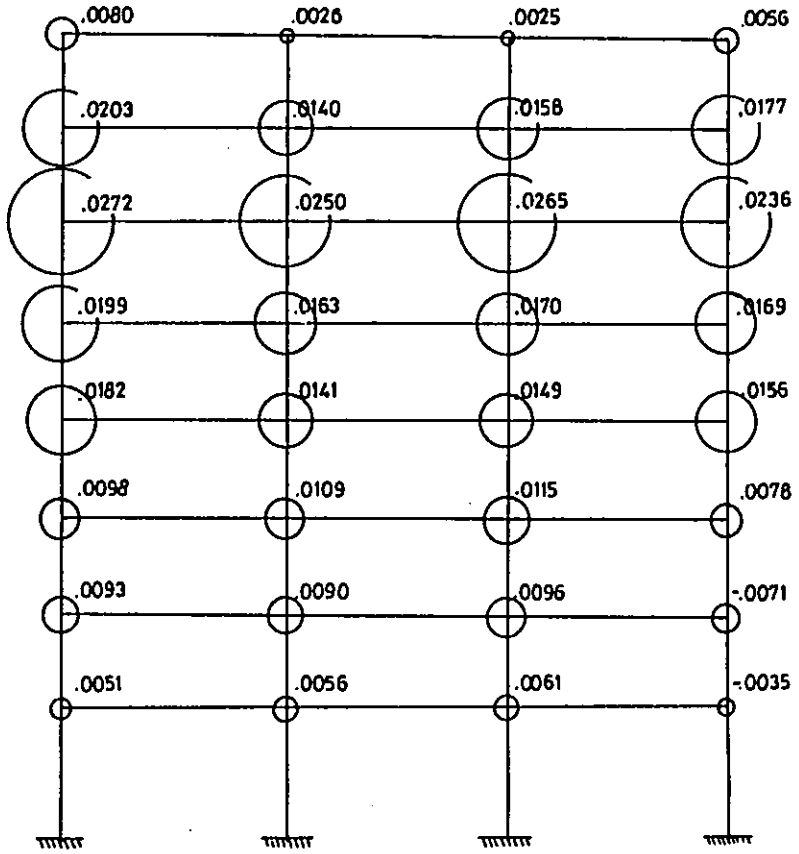

Panel zones

Fig. 6.48 Maximum beam, column and panel zone joint plastic rotations for MRF case 6. (in radians)

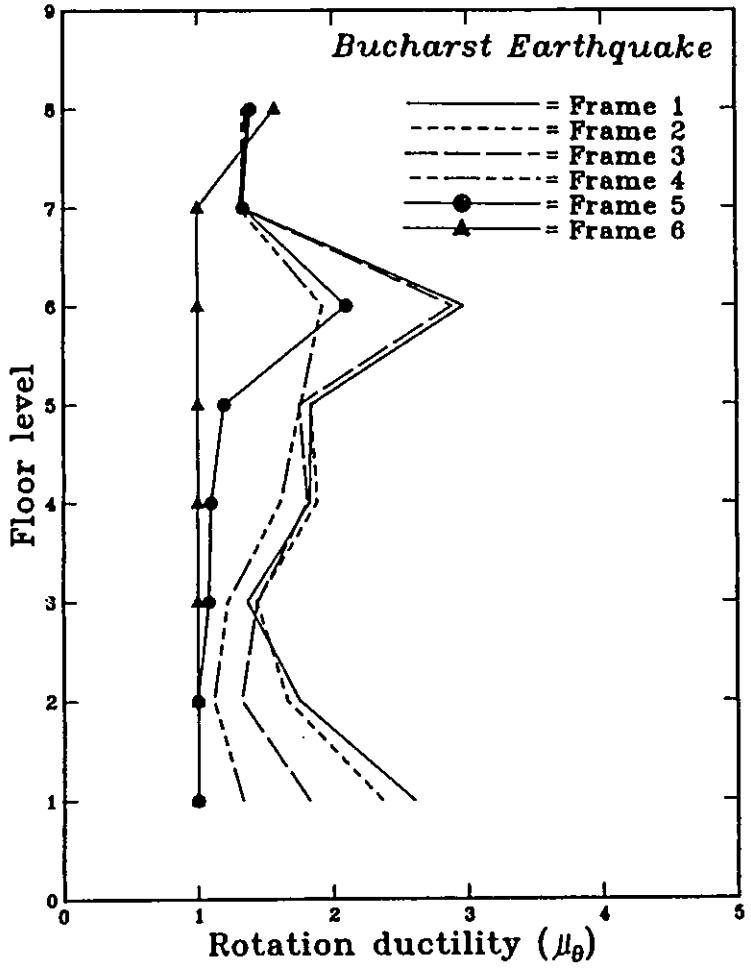

Maximum beam rotation ductilities

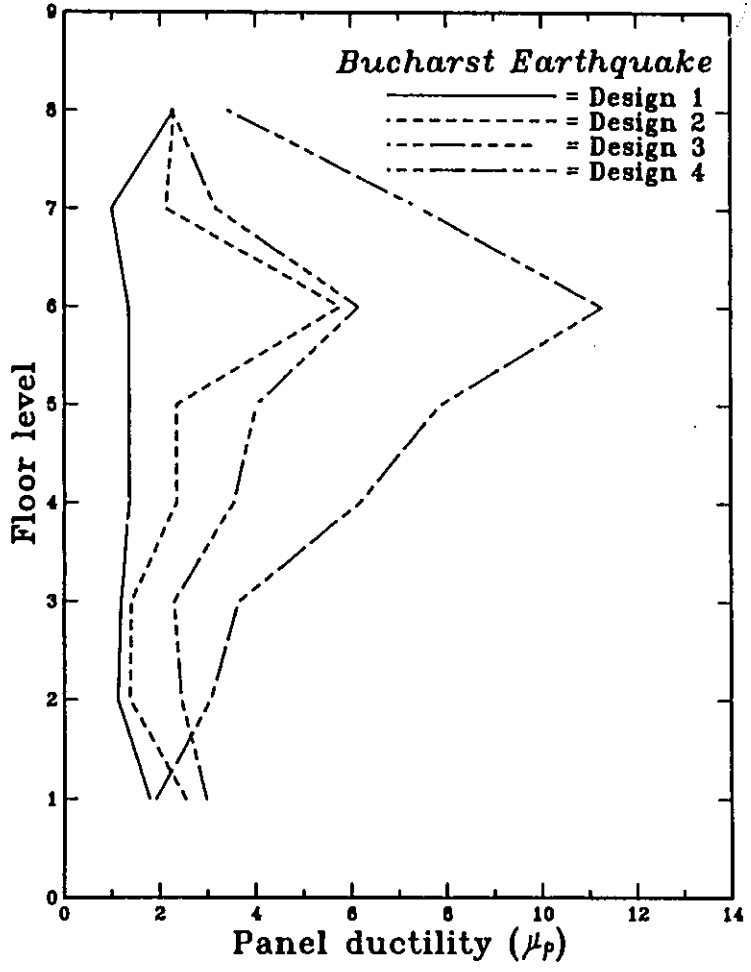

Maximum panel zone ductilities

Fig. 6.49 Ductility demands for Bucharest earthquake.

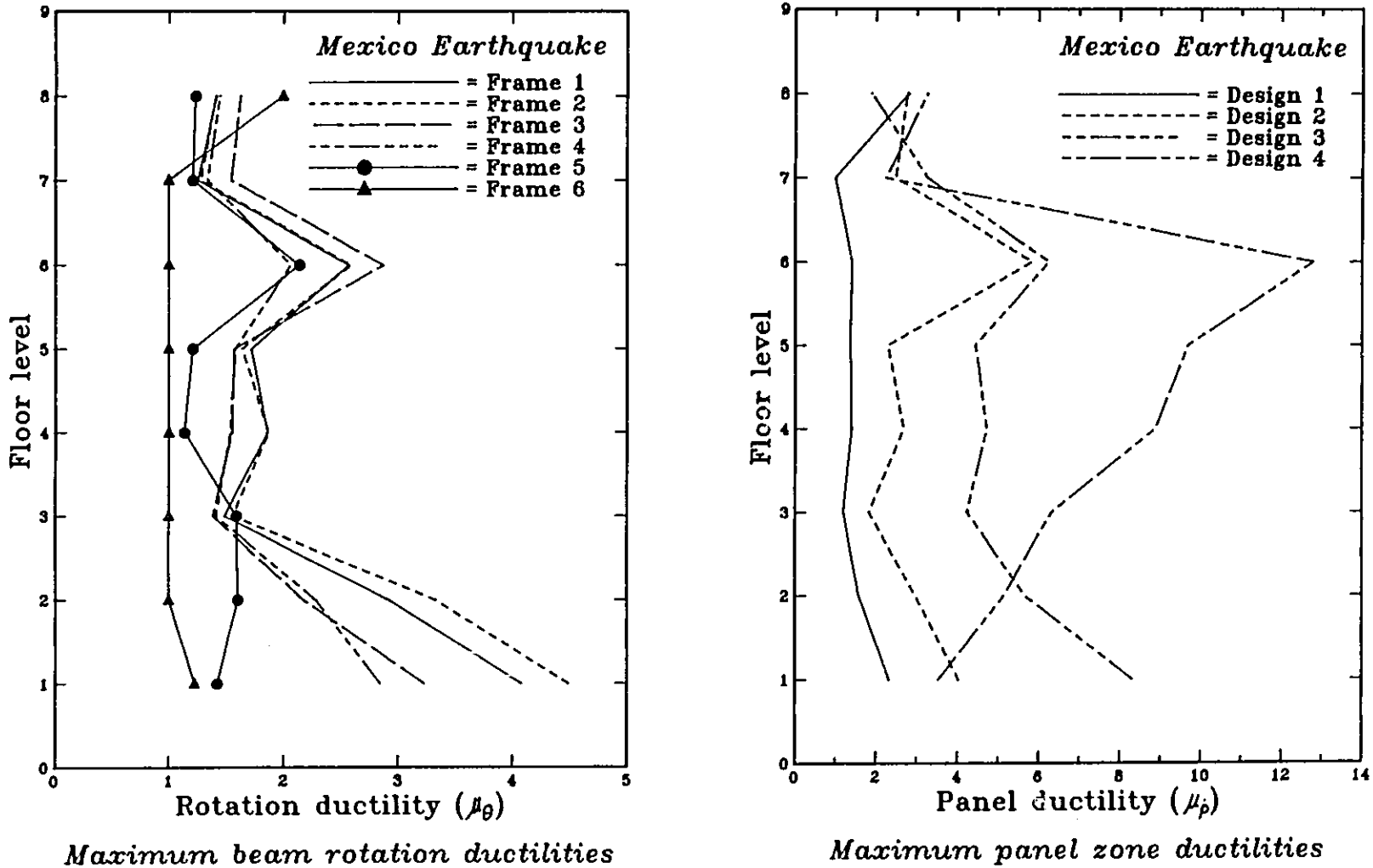

Fig. 6.50 Ductility demands for Mexico earthquake.

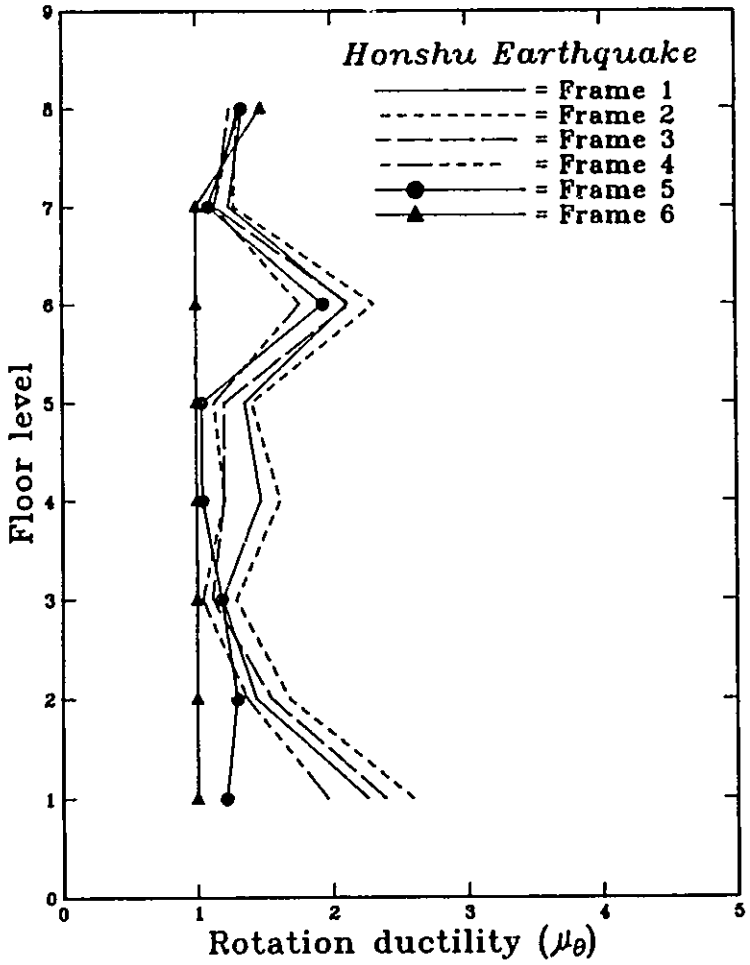

Maximum beam rotation ductilities

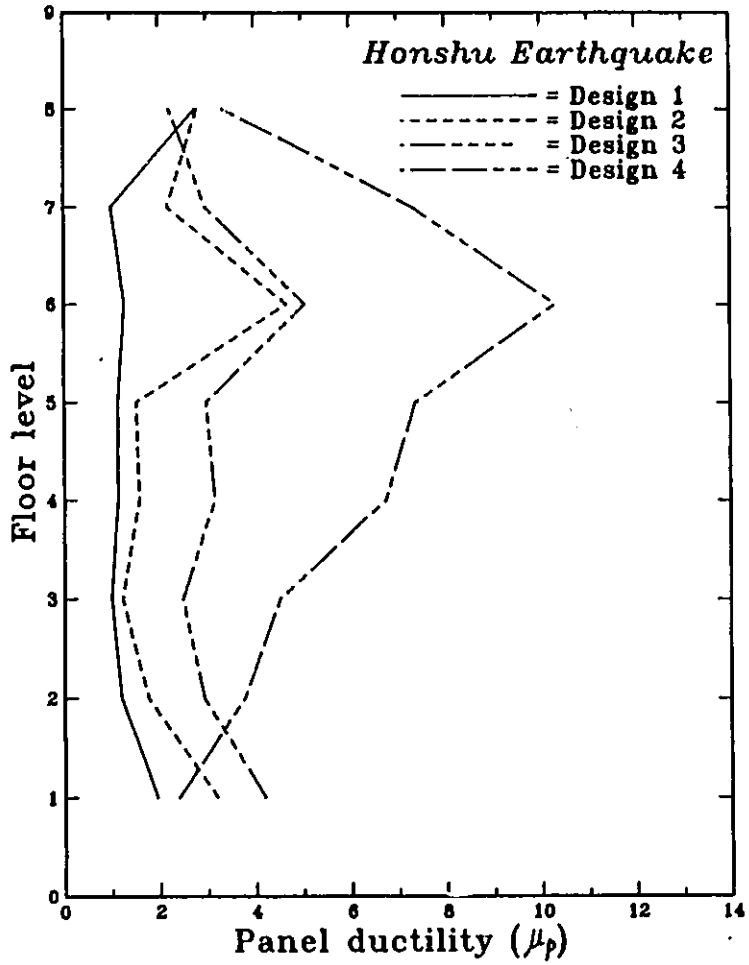

Maximum panel zone ductilities

Fig. 6.51 Ductility demands for Honshu earthquake.

CHAPTER 7

NONLINEAR STATIC AND DYNAMIC ANALYSES OF 20-STOREY BUILDING

7.1 Introduction

In Chapter 6, the static and dynamic behaviour of 8-storey MRFs were presented. The frames were designed in accordance with the current Canadian codes (CAN3-S16.1-M89, 1989 and NBCC, 1990) and utilized extended end-plate beam-to-column joints. The obtained results reflect the effect of joint flexibility on the behaviour of low-rise steel frames. Taller frames with longer vibration periods adopting the same type of joints may exhibit completely different response. To ascertain whether similar conclusions are valid for high-rise steel frames, a 20-storey steel frame building employing extended end-plate joints, was studied. The selected structure was three bay by three bay square office building located at Quebec city, Quebec. Its height is 84.7 meters while its plane area is 729 m^2 as shown in Figs. 7.1 and 7.2.

The lateral load resisting system for the building in the E-W direction consisted of four moment resisting frames, while in the N-S direction, a braced frame was used. This framing system (the use of several MRFs to resist lateral loads) which is not common in North America was selected to minimize the sizes of the frames' beams. Consequently, the diameter of the bolts used to join the end-plate to the column flange can be reduced. Using the common framing system (MRFs arranged along the perimeter of the building) usually results in large sized beams. These beams in the case of extended end-plate joints with four bolts will require large diameter bolts that cannot be tightened in the field without the need of special tools (Notch, 1986). Although this problem can be overcome by increasing the number of bolts around the beam flange (Lu, 1990), it is considered out of the focus of this study.

7.2 Design Procedure

For the purpose of this study, the frame located on axis C in the E-W direction was used. As can be observed, this frame is expected to resist 33.3% of the lateral loads and carry 33.3% of the gravity loads.

The storey heights of the building were selected to be 4 meters for typical floors, 6 meters for the ground floor, 4.5 meters for the retail floor and 5 meters for the mechanical floor.

7.2.1 Loads

a) Gravity loads and flooring system

A floor system and gravity loads similar to the ones used in the 8-storey building were adopted for all storeys in the 20-storey building, except for the retail floor where a 5 in thick slab and 4.8 KPa live loads were used.

For the roof, a 3.04 KPa intensity load was applied to account for the accumulation of snow, ice and rain. This load corresponds to 80% of the ground snow load, which would probably be exceeded once in 30 years on average at Quebec city.

b) Lateral loads

For designing against lateral loads, wind and earthquake, the equivalent static loads given by the NBCC (1990) were used. For the wind loads, the reference velocity pressure "q" used for the design of structural members for strength was taken to be equal to 0.48 KPa which corresponds to " $q_{1/30}$" in Quebec City area. In the analysis, the variation of the wind with the height was considered. The unfactored base shear due to the wind was calculated to be 1238 kN for the studied frame.

For seismic lateral forces, the structure was designed based on the equivalent lateral force procedure recommended by the NBCC (1990). The base shear was found to be 703 kN. The calculated base shear was distributed to each floor level and roof using the procedure given in the NBCC. According to this procedure a concentrated force at the top of the structure was applied to account for the effect of higher modes.

7.2.2 Design of frames members

a) Design for strength

Similar to the case of 8-storey building, the "portal frame method" was used to calculate the moments and the axial forces in beams and columns due to both gravity and lateral loads. Then, the moments and the axial forces were factored and combined for trial selection of the beams and the columns. It was found that, for beam design the load combination due to dead and live loads govern the design of beams in the top three floors. For floors below and up to the 14th floor, the loads due to dead, live and earthquake controlled the design, while for floors below the 14th floor the loads due to dead, live and wind governed the design. For the columns, wind and dead load controlled except for the top three floors where the load combination $(1.25\,D+0.7(1.5\,L+1.5\,Q))$, where Q is the wind, governed. Following the selection of preliminary sections for beams and columns, a second order elastic analysis was performed using the ETABS computer program. In this analysis, the lateral forces were applied in conjunction with the gravity loads and the members were checked for the different load combinations.

b) Drift limitations

During analysis, the building was checked for code drift requirements. It was found that the drift controlled the frame design rather than the strength requirements. The lateral deflections of the 20 storey frame due to code specified earthquake loads and wind loads are shown in Fig.7.3.As can be observed, the frame lateral deflection due to specified earthquake loads conservatively met the code requirements (h/(R/0.02)). However, under the wind loads the frame deflection exceeded the code limits (h/400). Since, the effects of nonstructural elements were neglected in formulating the building stiffness, no attempt was made to refine the frame design in order to meet the wind drift limits. In these analyses the P-Δ effect was considered.

c) Strong column-weak beam concept

In the design of the 20-storey building, the principle of strong column-weak beam was maintained. The formula given by UBC and described previously in section 6.2.2(c) was used for such purposes. Fig.7.4 shows the final sections selected for the beams and columns.

7.2.3 Design of end-plate connections

The method previously proposed in Chapter 2 for designing the extended end-plate connections, was used to detail the beam-to-column connections for the 20-storey frame. Tables 7.1 through 7.4 show the connection dimensions and their model parameters.

7.2.4 Design of panel zones

Following the design and detailing of the connections, the panel zone requirements were determined. In designing the panel zone for the 20-storey building, the design 2 criterion described in section 6.2.4 and recommended based on the analyses of 8-storey frame was adopted. As previously mentioned, applying this design criterion results in doubler plates with reasonable thicknesses and allows inelastic action to take place in the panels without causing excessive deformation. The thicknesses of the doubler plates and the parameters pertinent to the panel model are shown in Tables 7.5 and 7.6.

7.3 Computer Modelling

As with the 8-storey building, the beam-column elements were used to model the beams and the columns. Similar yield surfaces to those used in Chapter 6 for the beams and the columns were adopted. The connections were modeled as bi-linear springs while tri-linear springs were used to model the panel zones.

For the 20-storey building, a damping proportional to both the mass and the initial elastic stiffness was used. A 3% damping ratio was assigned to the first two modes. Masses of the tributary floor area and the core walls were assumed to be

lumped at the beam-column joints. These masses were associated with the horizontal displacement of the floors only. In addition, the frames were subjected to gravity loads consisting of the specified dead loads and the reduced live loads.

7.4 Cases Studied

Both types of analysis were conducted, static and dynamic. In each type, the response of three different frames were studied. The studied cases were:

Case 1

This case represents the response of frames with infinitely rigid beam-to-column joints, i.e. represents the case of a frame with joints utilizing fully welded connections with panel zones stiffened by diagonal shear stiffener or excessively thick doubler plates.

Case 2

In this case the frames' panel zones were assumed to be infinitely rigid. However, the connections were modeled using a bi-linear springs. Such frames represent the response of frames employing extended end-plate connections to join the beams to the columns with panel zones stiffened with diagonal stiffeners or excessively thick doubler plates.

Case 3

In this case the connections were modeled using bi-linear springs to simulate the moment-rotation relationships of the connections and the panel zones were modeled using tri-linear springs to simulate the applied moment- shear strain relationships for the panels. The panels of this frame were designed and detailed according to the design 2 criterion previously recommended. The frame response in this case represents, the behaviour of frames with flexible connections and panel zones.

7.5 Static Characteristics of the 20-Storey MRFs

In order to assess the effect of connections and panel zones flexibilities on the static response of MRFs, the NBCC specified earthquake loads were applied to

the frames in all three cases. The resulting lateral deflections of the frames are shown in Fig.7.5.As can be observed, the inclusion of the connection and the panel zone flexibilities tends to increase the frames lateral deflections. For example by comparing frame case 2 with frame case 1, it is evident that the inclusion of the connections tends to increase the roof lateral deflection by about 10.4%. An additional 20% increase in roof lateral deflection as a result of panel zone deformation was observed from comparing frame case 3 with frame case 2. These values are approximately the same as those previously obtained from analyzing the 8-storey MRFs.

On the other hand, the inclusion of such flexibilities also was shown to affect the distribution of the forces throughout the structures. Analysis shows that semi-rigid connections and panel zones tend to reduce the axial forces in the columns and increase the base moments.

7.6 Dynamic characteristics of the 20-storey frames

The effect of including the connections and panel zones flexibilities on the dynamic characteristics of the 20-storey MRFs was assessed. The resulting first ten vibration periods for each frame are shown in Table 7.7. As can be noted, the fundamental vibration periods of the frames were approximately two times the period given by the code equation. This is expected, since the analysis involved bare steel frames neglecting any stiffening effects from the infill walls, partition and other nonstructural elements. Also, it can be observed, the first vibration period for frame case 2 is 1.038 that of the frame case 1. For frame case 3, the corresponding period is 1.077 that of frame case 2. This supports the previous conclusion regarding the effect of connections and the panel zones in lengthening vibration periods of the frames. Regarding the mode shapes, Fig.7.6shows the vibration mode shapes for the MRFs in the three cases. Examining the figure shows that the differences are insignificant.

To form an idea about the locations where severe damage is expected when the MRFs oscillate in each mode, a relative storey drift index was computed for each

floor using the mode shape components as the floor lateral displacement. Fig.7.7 shows the resulting normalized relative storey drift indices for the first three modes. As can be seen, if the frames were excited in the first mode, large storey deformations could be expected from about the ninth to the sixteenth floors. On the other hand, if the frames were excited in the second or in the third modes, large deformations would be expected in a narrower range, from about the fourteenth floor to the nineteenth floor for the former and the ninth to twelveth and seventeenth to the nineteenth floors for the latter. The deformations of members or joints are would be expected to be more severe in these floors when the frame is excited predominately in the corresponding mode. Although these results are not directly relevant in the case of nonlinear inelastic analysis, they can give a good idea about the expected response of the MRFs.

7.7 Nonlinear dynamic analysis of the 20-storey MRFs

Each of the MRFs was subjected to three different earthquake records, in order to assess their dynamic performance. The records used are the same as those used for analyzing the 8-storey MRFs, i.e Bucharest, Mexico and Honshu earthquakes. The linear elastic response spectra for the selected earthquakes with the first three vibration periods for the frames are shown in Fig.7.8. From this figure it can be concluded that, during the Bucharest and Mexico events the second mode is expected to participate significantly to frames response. However, in the case of Honshu event, the third mode would be expected to dominate the frames behaviour.

7.7.1 Response to Bucharest earthquake

Fig.7.9 shows the effect of this earthquake record on the floor displacement envelopes and the floor displacements at the instant of the peak roof displacement for the MRFs. Examining this figure reveals that the frames, as expected, were excited in the second mode with significant participation from the third mode. Also, it shows that no significant differences among the frames' floor displacements were detected, except in the lower eleven floors, where frames cases 2 and 3 experienced

higher deformations than frame case 1. The time histories for the sixteenth floor, where the maximum damage was recorded in all frames, and the roof floor displacements are shown in Figs.7.10and 7.11. As can be seen, the frames vibrated in the same manner up to about 6 seconds, after which strong pulse caused the frames to yield, shifting the datums around which the oscillation occurred.

The maximum base shear experienced by the frames in the three cases were 3.6, 3.4 and 2.8 the design base shear, while the maximum storey drifts were 2.76%, 3.39% and 2.96%, respectively. These drift values exceeded the 2% drift limit expected by the code (NBCC, 1990) in the case of inelastic response. All these drifts occured in the seventeenth floor which was expected, based on the subsequent elastic analysis, to be severely damaged. The absolute maximum storey drift values experienced by the frame in such an event are reported in Table 7.8. As expected, from the fourteenth floor to the nineteenth floor the drifts exceeded the code limits (2%) as shown by the shaded columns,indicating severe damage to structural elements at these floors.

The maximum beam, column, and panel zone joint plastic rotations occurred during Bucharest event for the MRFs are shown in Figs. 7.12 through 7.14. Examining these figures shows that frames cases 1 and 2 having infinitely rigid panels experienced the highest beam rotational demands compared with frame case 3, that possessed flexible panels. Also, the plots show that the beams at the fifteenth, the sixteenth and the seventeenth floors experienced high rotational demands.

As a general trend, it was observed that as the frame stiffness decreased the plastic hinges tended to concentrate at the upper floors, subjecting the structural elements at those floors to higher ductiiity demands. This can be explained by referring to Fig. 7.8 which shows that once nonlinearities developed, the participation of the third mode in the response became more pronounced due to the increase of the spectral pseudo-acceleration for the lengthened third vibration period of the frames. Consequently, the frame will be subjected to more severe damage at the upper floors when the third mode is effective as previously explained (see Fig.7.6).

7.7.2 Response to Honshu earthquake

Similar to the case of the Bucharest event, the envelopes of the maximum floor displacements and the floor displacements at the peak roof displacement are shown in Fig. 7.15. As expected from the pseudo-acceleration spectra, the participation of the second and third modes of floor displacement appears to dominate the behaviour. No obvious trend for the floor displacements can be detected. The plastic hinging patterns for the frames in the three cases are shown in Figs. 7.16 through 7.18. In general, the beam hinges spread throughout the frames' beams. This attributed to the relatively high participation of the first mode to frame response. Again, the highest beam rotational demands were observed in the sixteenth floor beams. Analysis shows that, although the inclusion of the connections reduced drastically the rotational demands on the beams at lower floors(from first floor to twelveth floor), it tended to increase the rotational demands in the thirteenth to the nineteenth floors compared to the case of the frame with rigid connections. Inclusion of panel zone deformation in frame case 3 reduced the beams' rotational demands and dedicated most of the inelastic action to the panels. The maximum recorded base shear for the frames cases 1,2, and 3 are 4.189, 3.723, and 2.699 that of the design base shear, respectively.

7.7.3 Response to Mexico earthquake

The response of the frames to this event in terms of frames lateral deflections are shown in Fig. 7.19. In general, frame case 3 experienced the least lateral deflection among the analyzed frames. Frames cases 1 and 2 experienced approximately the same maximum roof lateral deflections. The maximum recorded base shears for the frames cases 1,2, and 3 are 2.835, 2.944, and 2.033 times the design base shear, respectively.

With regard to plastic hinging patterns, Figs. 7.20 through 7.22 show the size of the maximum plastic hinges formed in the beams, columns, and panel zones for the analyzed frames. As can be noted, the rotational demands of the beams for frame case 2 were less at the lower floors, up to the eleventh, compared to frame in case

1. On the contrary, for higher floors the beams in frame case 2, experienced higher rotational demands. Frame case 3, again experienced the lowest rotational demands among the analyzed frames.

7.7.4 Ductility demands

As was done for the 8-storey frames, Figs 7.23 to 7.26 show the beams' rotational ductilities and the panels' ductilities for the three analyzed frames in each event. Examining these figures shows the following:

1. From examining Fig.7.23, it is evident that the beams, especially at the sixteenth floor subjected to high ductility rotational demands. The inclusion of both the connection and the panel zone reduces these demands significantly. This also was obvious from Figs. 7.24 and 7.25.
2. In all the cases, the inclusion of the connection only tends to reduce the beams' plastic rotations below the twelveth floor, while increase them form it and up to the roof.
3. Comparing these rotational ductilities with the values obtained experimentally and reported in Table 2.3, shows that all these plastic rotations are within the rotational capacities expected from class 1 sections ($\mu_\theta < 6$). Also, it shows that for the MRFs subjected to Bucharest event their beams are expected to experience local instabilities, since the beams plastic rotation in some cases exceeded the θ_m values observed experimentally and given in Table 2.3.
4. Regarding the panel zone ductilities (Fig.7.26), Bucharest event imposed the highest rotational demands on the panel among the examined earthquakes. However, in any case, these demands were less than those expected to cause panel zone instability ($\gamma < 20\gamma_y$).

7.8 Summary

The preceding analyses, of the 20-storey MRFs, suggest that the nonlinear dynamic response of a high-rise MRF is very sensitive to both the connection and panel zone flexibilities as well as to the input ground motion characteristics.

However, the sensitivity of a frame's response to panel zones flexibilities is more pronounced than that of the connections. From analyses, the following conclusions may be drawn:

1) As in the case of 8-storey frames, the effect of the connection and the panel zone flexibilities on storey drifts under static lateral loads can be significant and therefore should be included explicitly in the analysis. Neglecting such effects may lead to nearly a 30% error in estimating the frames lateral deflections.

2) Inclusion of the panel zones flexibility reduced drastically the demands imposed on the beams and resulted in a more uniform distribution of energy dissipation throughout the structures.

3) Analyses have proven that well detailed and properly designed joints, i.e connection and panel zones, can improve the performance significantly of steel structures subjected to severe earthquake excitation.

4) Simple elastic analyses such as studing the frames vibration periods, the elastic response spectra of the input ground motion or the normalized relative storey indices give a good idea about the the frames nonlinear behaviour and the locations in the frame that expected to be severely damaged.

Table 7.1 End-plate design for 20-storey frames
(Interior connections)

Floorlevel	Dimensions (mm X mm)	End-plate thickness*	Bolts diameter	Column flange stiffener
1st	888X370	45	M36	No
2nd	888X370	45	M36	No
3rd	888X370	45	M36	No
4th	882X370	45	M36	No
5th	882X370	45	M36	No
6th	882X370	45	M36	No
7th	856X370	40	M36	Yes
8th	856X370	40	M36	Yes
9th	856X370	40	M36	Yes
10th	851X370	40	1 1/4"	Yes
11th	851X370	40	1 1/4"	Yes
12th	851X370	40	1 1/4"	Yes
13th	820X270	35	1 1/8"	Yes
14th	820X270	35	1 1/8"	Yes
15th	820X270	35	1 1/8"	Yes
16th	720X250	35	1"	Yes
17th	720X250	35	1"	Yes
18th	720X250	35	1"	Yes
19th	800X270	35	1"	Yes
20th	510X350	32	1 1/8"	Yes

All bolts are grade A490.
End-plate thicknesses in mm.

Table 7.2 Connection model parameters
(Interior connections)

Floor level	K_i (kN.m/rad)	K_p (kN.m/rad)	M_p (kN.m)
1st	3931124	196556	2443.9
2nd	3931124	196556	2443.9
3rd	3069619	153481	2443.9
4th	3069619	153481	2443.9
5th	1666668	83333	3102.0
6th	1666668	83333	3102.0
7th	1096054	164408	1810.5
8th	1096054	164408	1810.5
9th	2100482	315072	2102.8
10th	2100482	315072	2102.8
11th	1808968	271345	2102.8
12th	1808968	271345	2102.8
13th	1684937	252740	1366.0
14th	1684937	252740	1366.0
15th	1603059	240458	1366.0
16th	1536502	230475	1240.0
17th	1439997	215999	1240.0
18th	1439997	215999	1240.0
19th	1486640	222996	1282.3
20th	477619	71642	792.9

Table 7.3 End-plate design for 20-storey frames
(Exterior connections)

Floor level	Dimensions (mm X mm)	End-plate thickness*	Bolts diameter	Column flange stiffener
1st	888X370	45	M36	Yes
2nd	888X370	45	M36	Yes
3rd	888X370	45	M36	Yes
4th	882X370	45	M36	Yes
5th	882X370	45	M36	Yes
6th	882X370	45	M36	Yes
7th	856X370	40	M36	Yes
8th	856X370	40	M36	Yes
9th	856X370	40	M36	Yes
10th	851X370	40	1 1/4"	Yes
11th	851X370	40	1 1/4"	Yes
12th	851X370	40	1 1/4"	Yes
13th	820X270	35	1 1/8"	Yes
14th	820X270	35	1 1/8"	Yes
15th	820X270	35	1 1/8"	Yes
16th	720X250	35	1"	Yes
17th	720X250	35	1"	Yes
18th	720X250	35	1"	Yes
19th	800X270	35	1"	Yes
20th	510X350	32	1 1/8"	Yes

All bolts are grade A490.
End-plate thicknesses in mm.

Table 7.4 Connection model parameters
(Exterior connections)

Floor level	K_i (kN.m/rad)	K_p (kN.m/rad)	M_p (kN.m)
1st	3438946	515842	2443.9
2nd	3438946	515842	2443.9
3rd	2134399	320159	2443.9
4th	2134399	320159	2443.9
5th	1847488	277123	2443.9
6th	1847488	277123	2443.9
7th	1476966	221545	2102.8
8th	1476966	221545	2102.8
9th	1368189	205227	2102.8
10th	1368189	205227	2102.8
11th	1124894	168734	1774.0
12th	1124894	168734	1774.0
13th	1205691	180853	1366.0
14th	1205691	180853	1366.0
15th	1294564	194184	1366.0
16th	1264726	189709	1240.9
17th	1102769	165415	1240.9
18th	1102769	165415	1240.9
19th	907651	136147	1130.
20th	312903	46935	487.3

Table 7.5 Panel zone joint for 20-storey frame
(Interior columns)

Floor level	Doubler Plate thickness	M_1	M_2	k_1	k_2	k_3
1st	1PL#10	4151	5925	1714473	791901	58292
2nd	1PL#10	4151	5925	1714473	791901	58292
3rd	2PL#20	3793	5453	1557121	582796	52942
4th	2PL#20	3750	5269	1542295	541699	52438
5th	2PL#6	2453	4117	911798	800827	31001
6th	2PL#6	2453	4117	911798	800827	31001
7th	2PL#12	2530	3804	1017871	420854	34607
8th	2PL#12	2530	3804	1017871	420854	34607
9th	2PL#18	3416	4493	1267587	325073	43098
10th	2PL#10	2298	3309	930585	289642	31640
11th	2PL#12	2506	3330	1014282	263278	34485
12th	2PL#12	2506	3330	1014282	263278	34485
13th	2PL#8	2090	2703	846300	356344	28774
14th	2PL#8	2090	2703	846300	356344	28774
15th	2PL#8	1865	2544	738067	93940	25094
16th	2PL#6	1437	2014	585868	130532	19919
17th	2PL#6	1269	1798	517581	117291	17597
18th	2PL#6	1269	1798	517581	117291	17597
19th	2PL#8	1580	2144	608409	121873	20686
20th	No	784	1469	357798	356702	12165

All moments are in kN.m.
All stiffness are in kN.m/rad.

Table 7.6 Panel zone joint for 20-storey frame
(Exterior columns)

Floor level	Doubler Plate thickness	M_1	M_2	k_1	k_2	k_3
1st	-	1742	2931	687616	223713	23379
2nd	-	1742	2931	687616	223713	23379
3rd	2PL#6	1899	2747	779813	90766	26513
4th	1PL#6	1512	2308	636302	85742	21634
5th	1PL#8	1686	2441	684198	69495	23262
6th	1PL#8	1686	2441	684198	69495	23262
7th	1PL#8	1666	2338	677832	51925	23046
8th	1PL#8	1666	2338	677832	51925	23046
9th	1PL#6	1390	1988	555441	46387	18885
10th	-	1074	1613	432938	42166	14720
11th	2PL#6	1301	1854	503128	40189	17106
12th	2PL#6	1301	1854	503128	40189	17106
13th	1PL#6	1040	1362	406342	27203	13815
14th	1PL#6	1040	1362	406342	27203	13815
15th	-	672	1019	257447	25182	8753
16th	-	574	885	209488	26691	7122
17th	-	586	882	231653	21650	7876
18th	-	586	882	231653	21650	7876
19th	1PL#6	795	1155	300694	20092	10223
20th	2PL#6	488	734	207589	29387	7058

All moments are in kN.m.
All stiffness are in kN.m/rad.

Table 7.7 Vibration periods of 20-storey MRFs

Modes	vibration periods (s)		
	Case 1	Case 2	case 3
1st	3.88	4.03	4.34
2nd	1.45	1.49	1.60
3rd	0.84	0.87	0.93
4th	0.58	0.60	0.64
5th	0.44	0.46	0.48
6th	0.36	0.37	0.39
7th	0.30	0.30	0.32
8th	0.25	0.25	0.26
9th	0.21	0.21	0.22
10th	0.18	0.18	0.19

Table 7.8 Absolute maximum storey drifts
(Bucharest earthquake)

Storey level	Storey drift (%)		
	Case 1	Case 2	Case 3
1st	0.590	0.573	0.531
2nd	0.817	0.804	0.802
3rd	0.811	0.819	0.841
4th	0.820	0.842	0.887
5th	0.850	0.884	0.959
6th	0.860	0.913	1.000
7th	0.920	0.978	1.046
8th	0.980	1.023	1.062
9th	1.044	1.050	1.086
10th	1.130	1.096	1.151
11th	1.610	1.184	1.252
12th	1.300	1.184	1.268
13th	1.570	1.445	1.449
14th	1.920	1.923	1.749
15th	2.330	2.863	2.252
16th	2.741	3.397	2.805
17th	2.760	3.045	2.965
18th	2.230	2.324	2.535
19th	1.530	1.576	1.835
20th	0.900	1.196	1.163

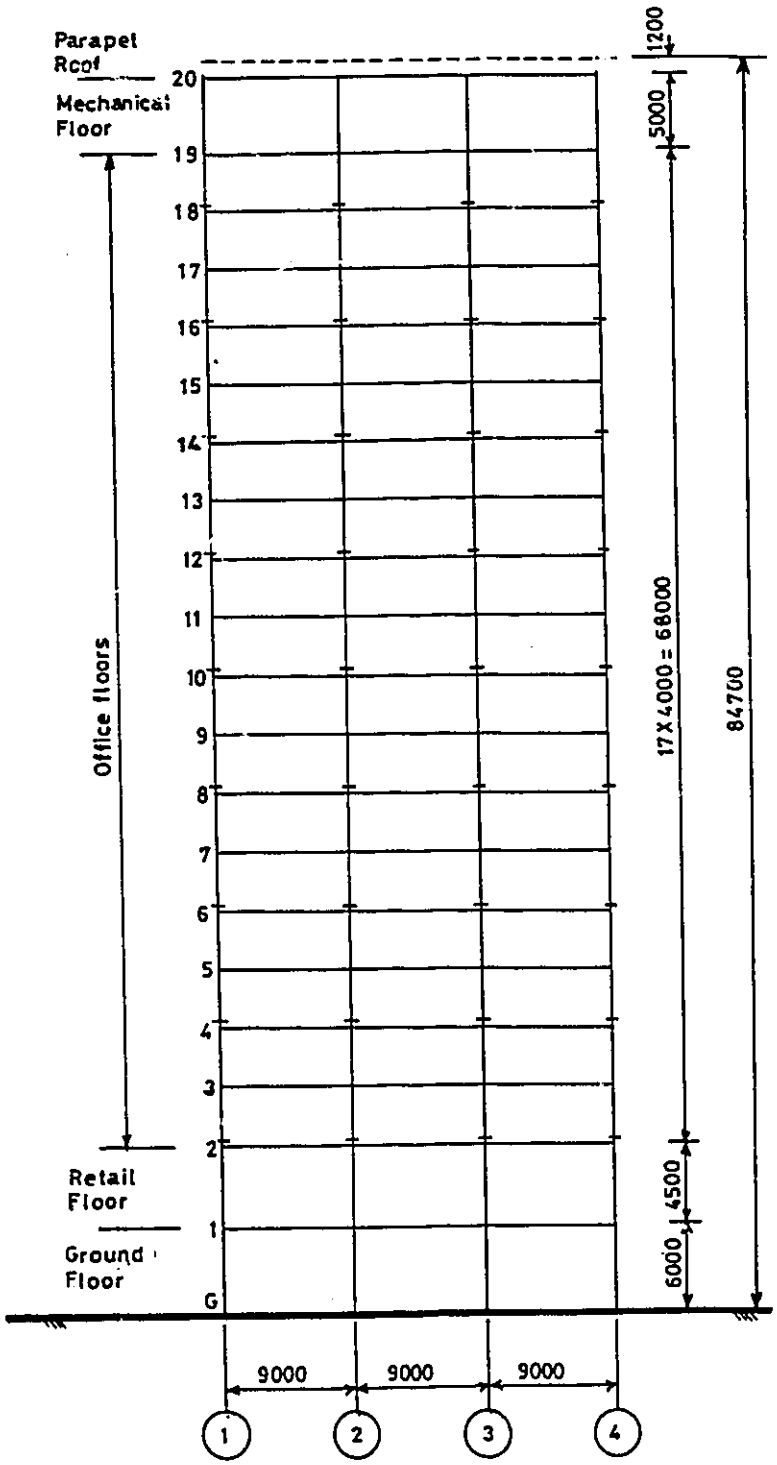

Fig. 7.1 Elevation of the 20-storey building.

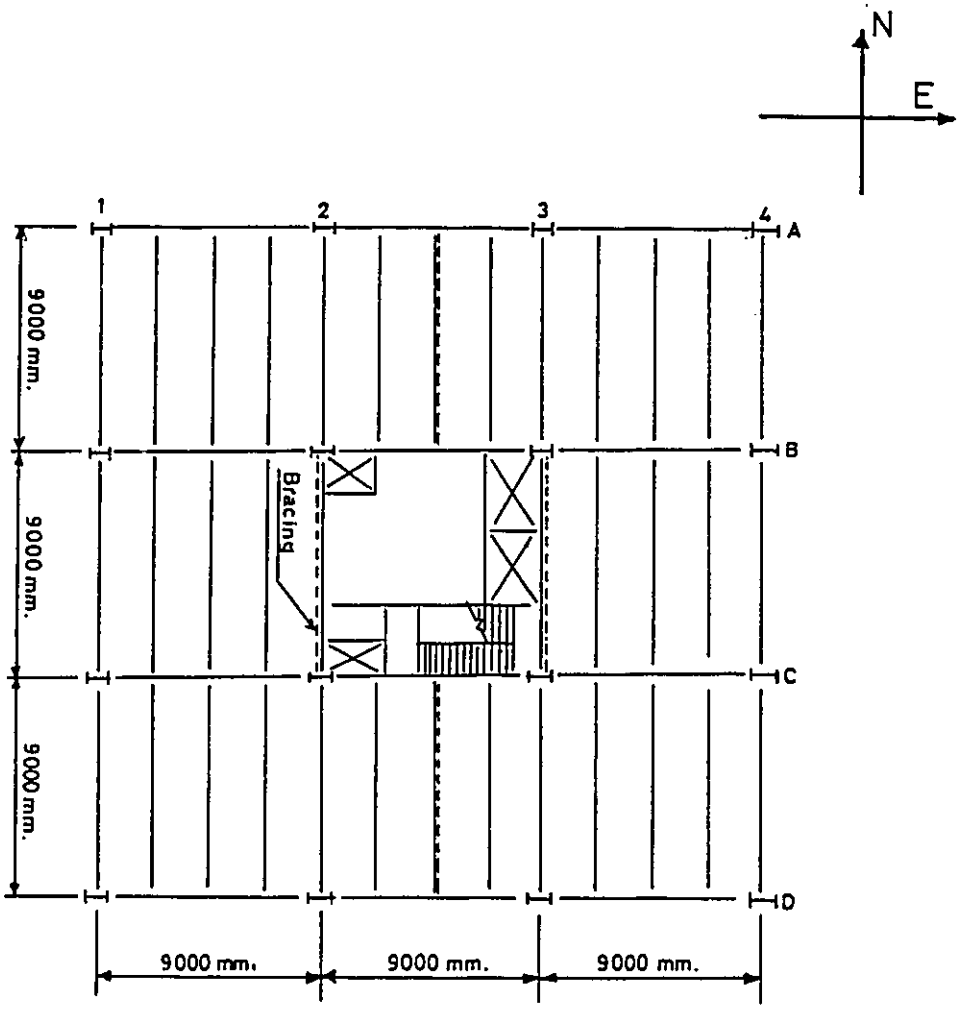

Fig. 7.2 Typical floor for the 20-storey building.

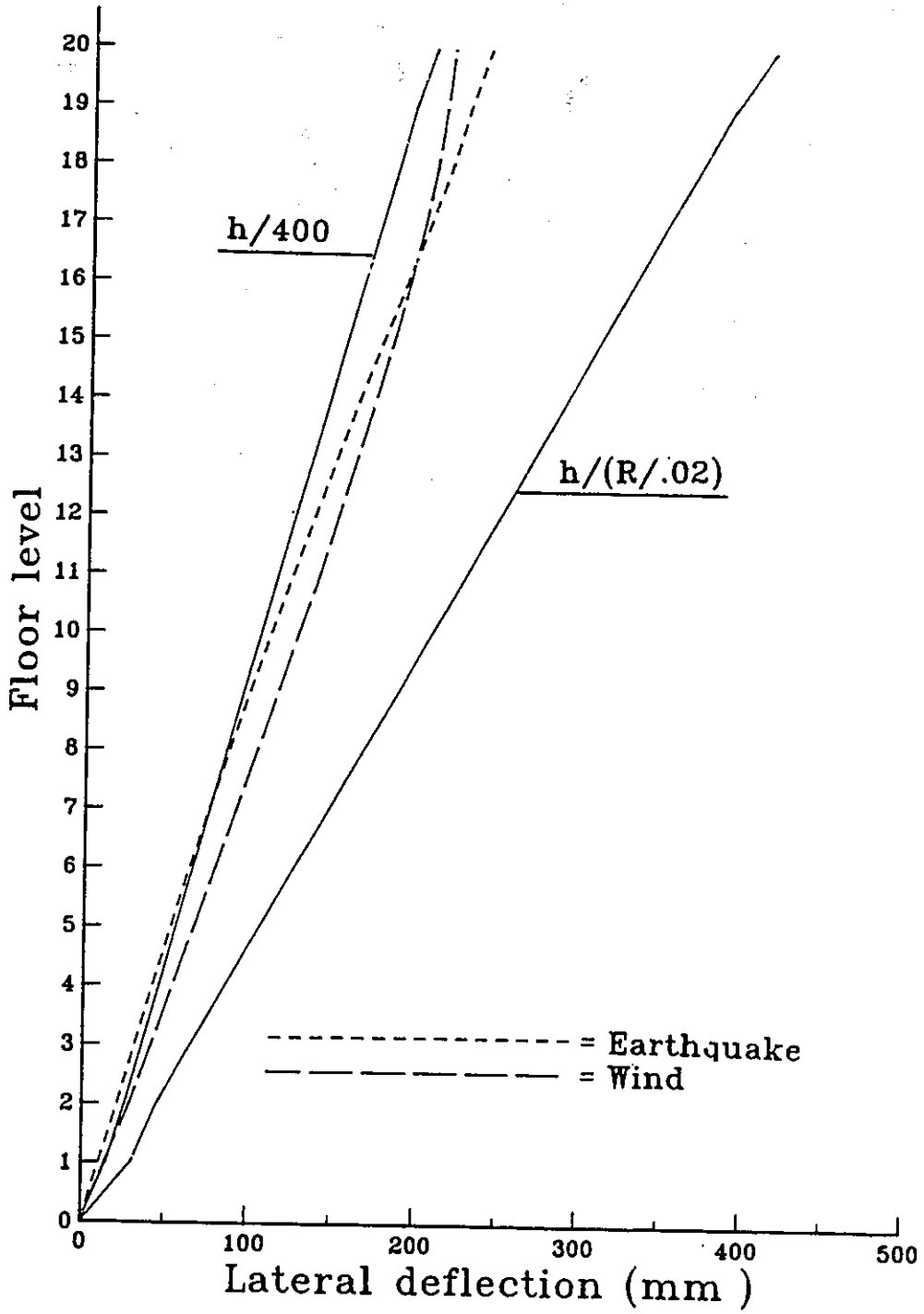

Fig. 7.3 Frame lateral deflection.

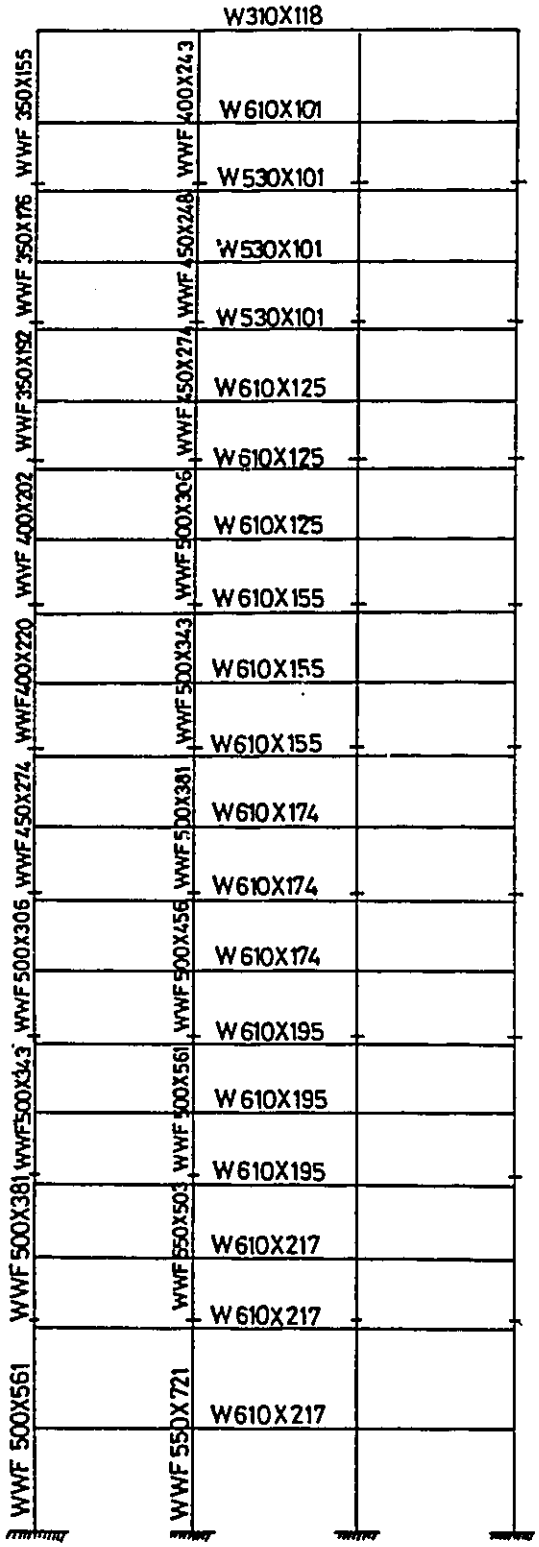

Fig. 7.4 Member sizes for the 20-storey building.

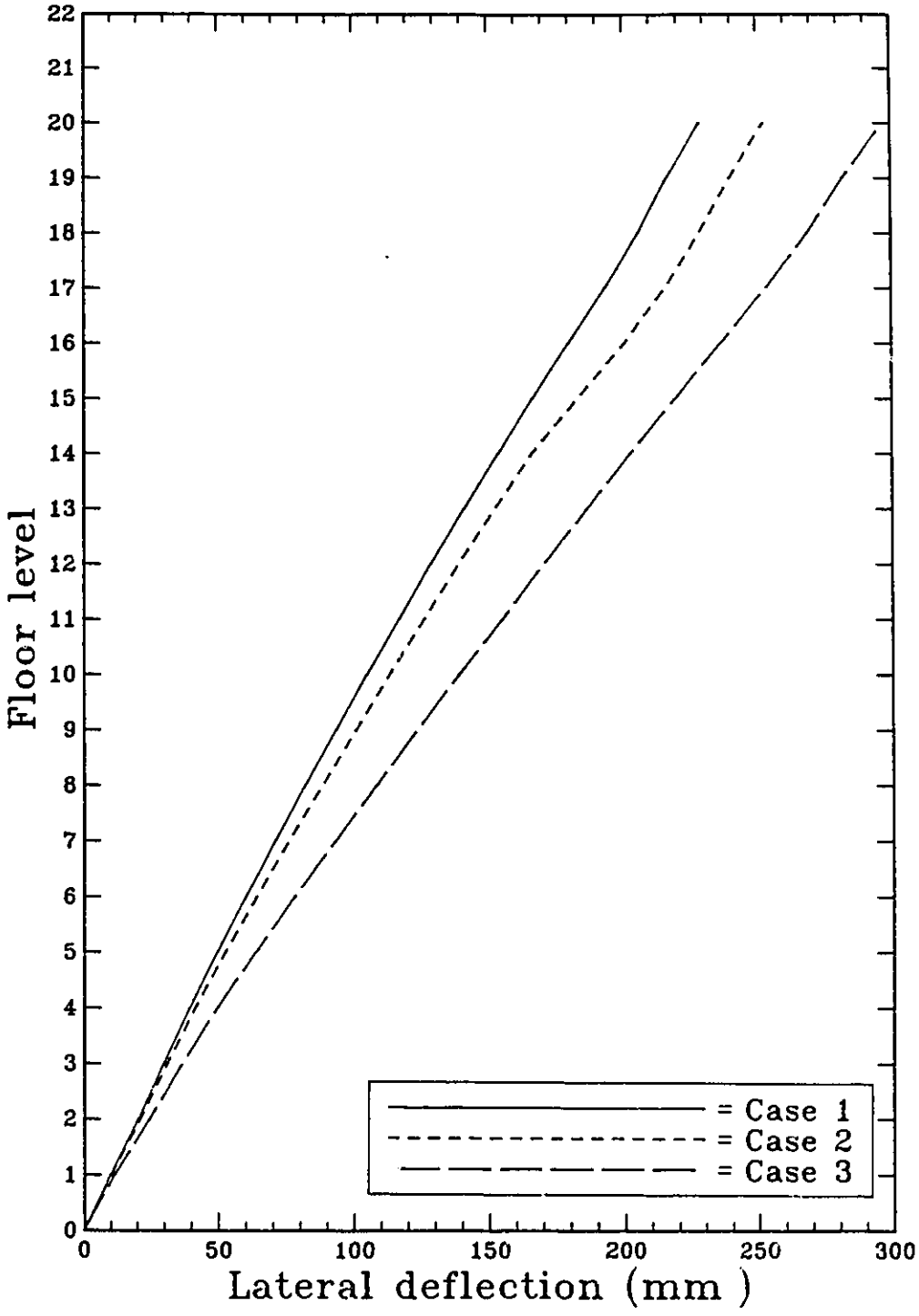

Fig. 7.5 Effect of joint flexibility on the static deflection of the 20-storey frame.

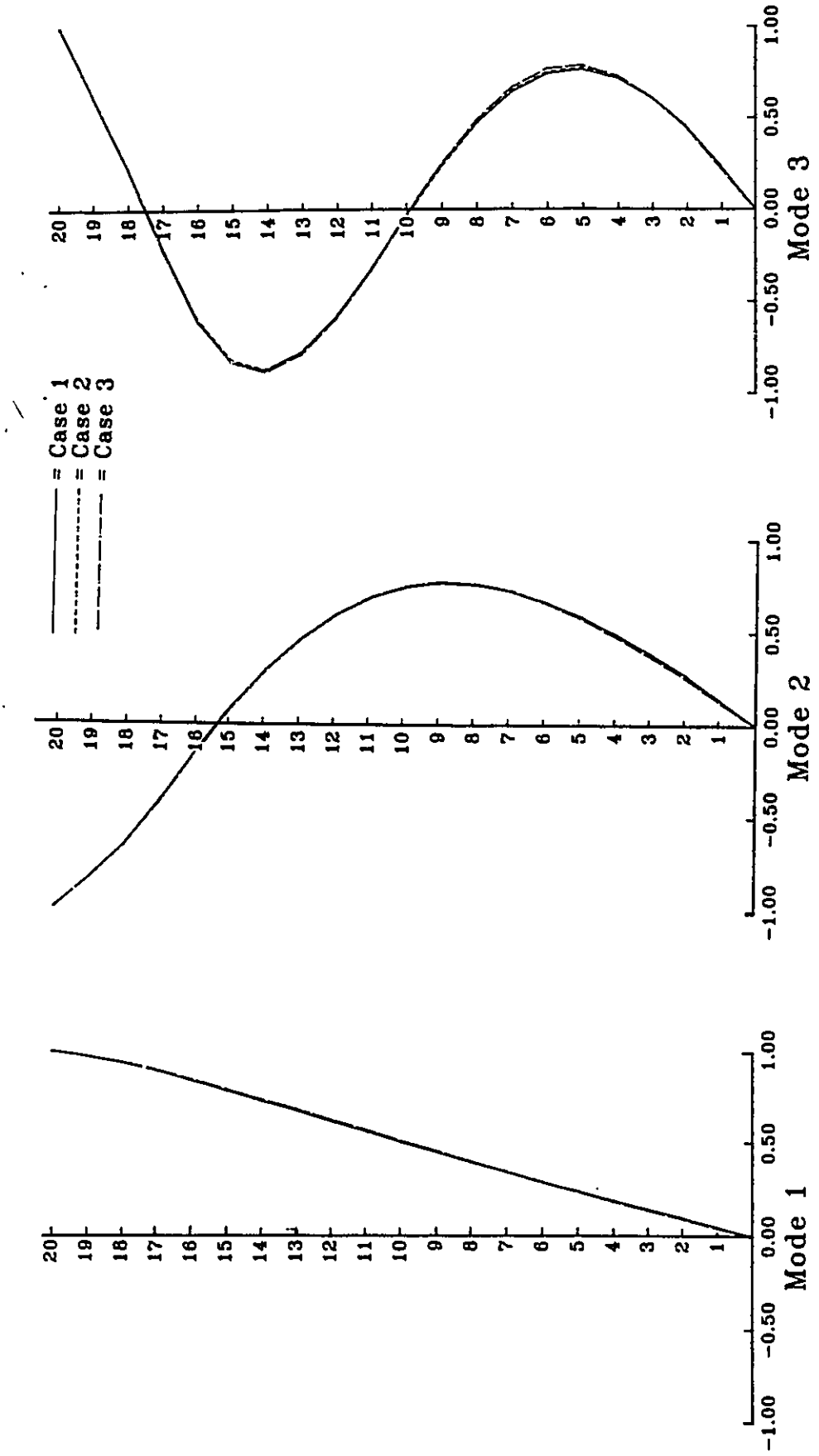

Fig. 7.6 Mode shapes

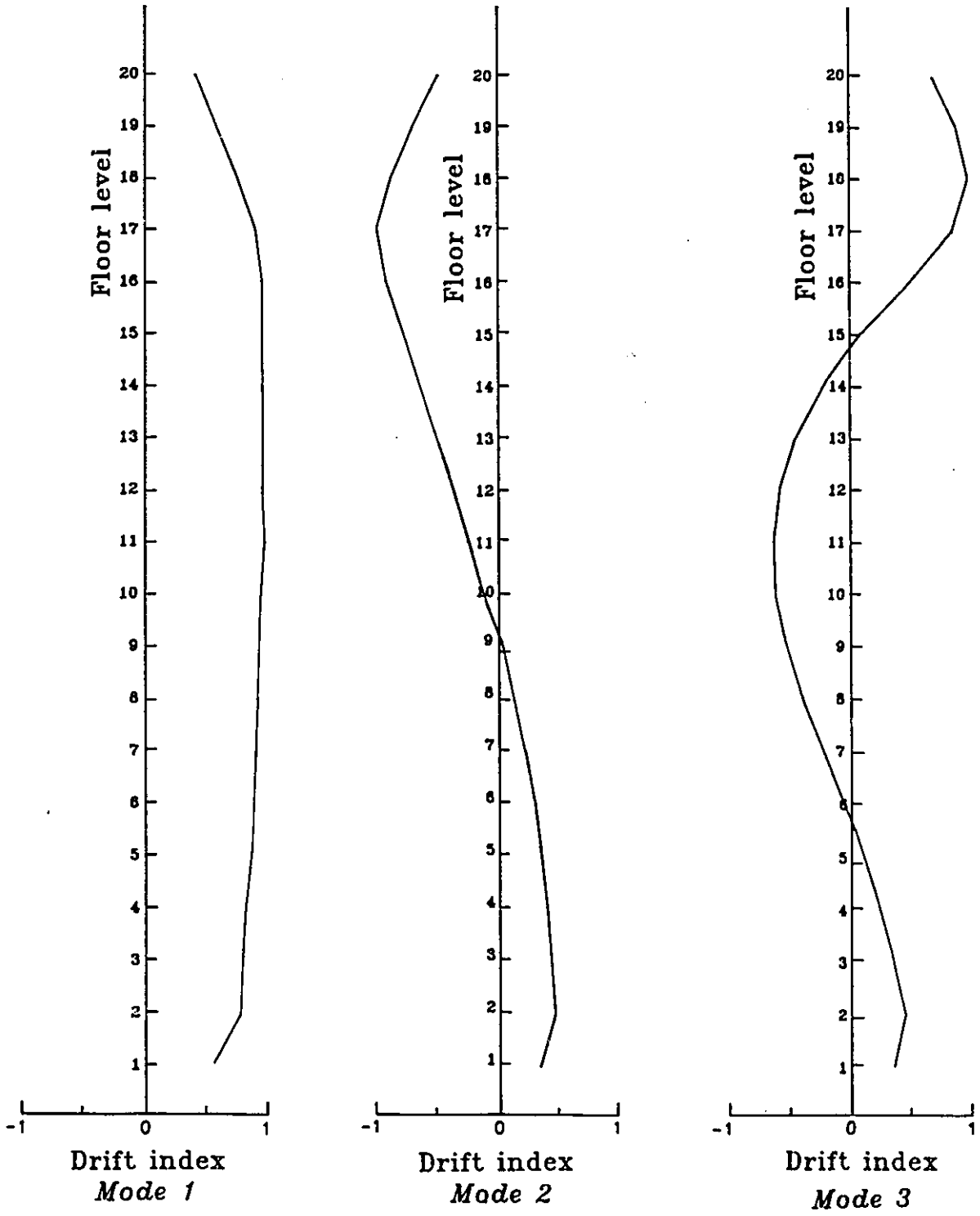

Fig.. 7.7 Normalized relative storey drift indices

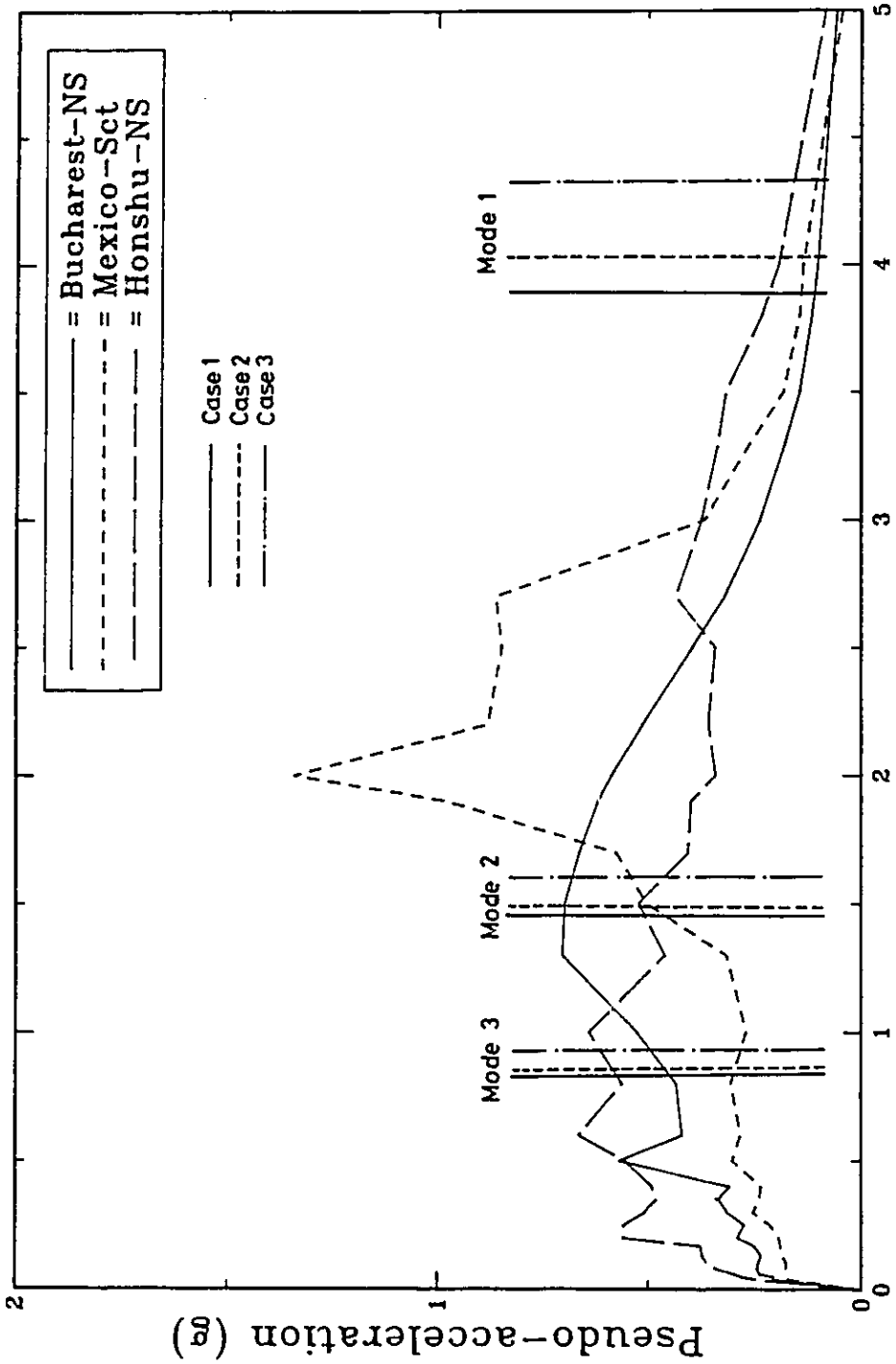

Fig. 7.8 Linear elastic pseudo-acceleration spectra for the selected ground accelerations (3% Damping).

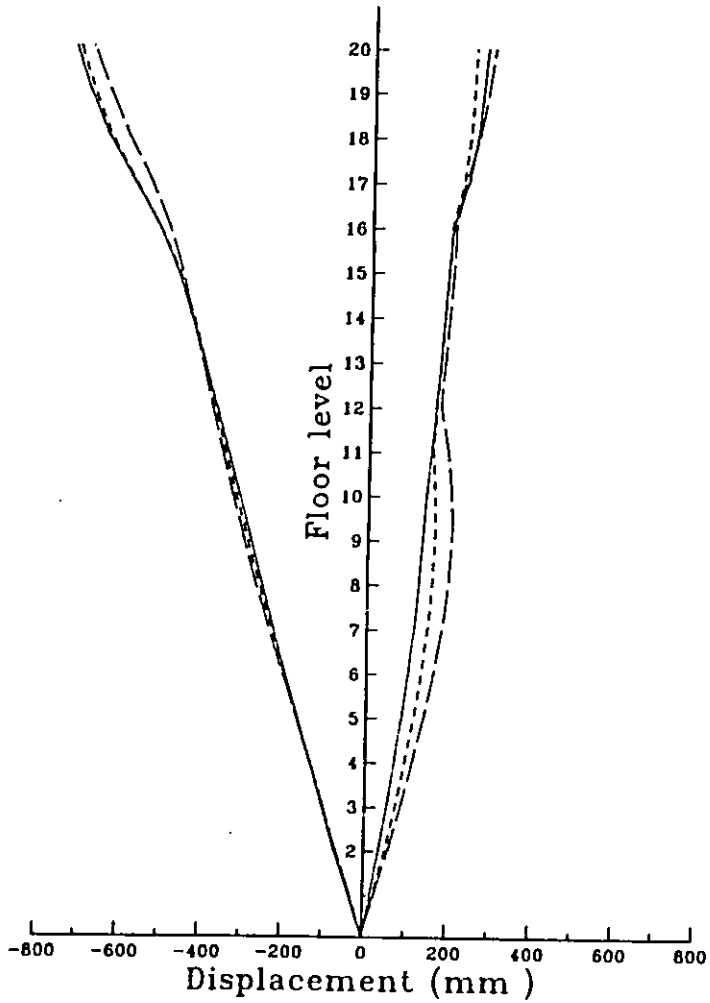

a) Maximum floor displacement

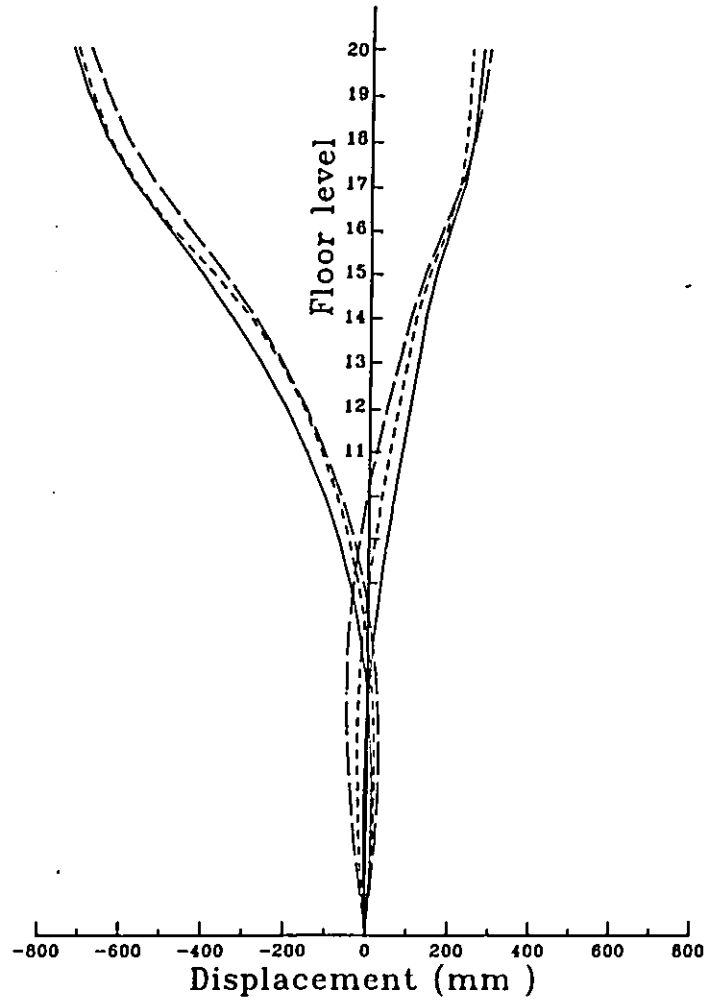

b) Floor displacement at peak roof displacement

Fig. 7.9 Effect of joint flexibility on the dynamic lateral deflection.

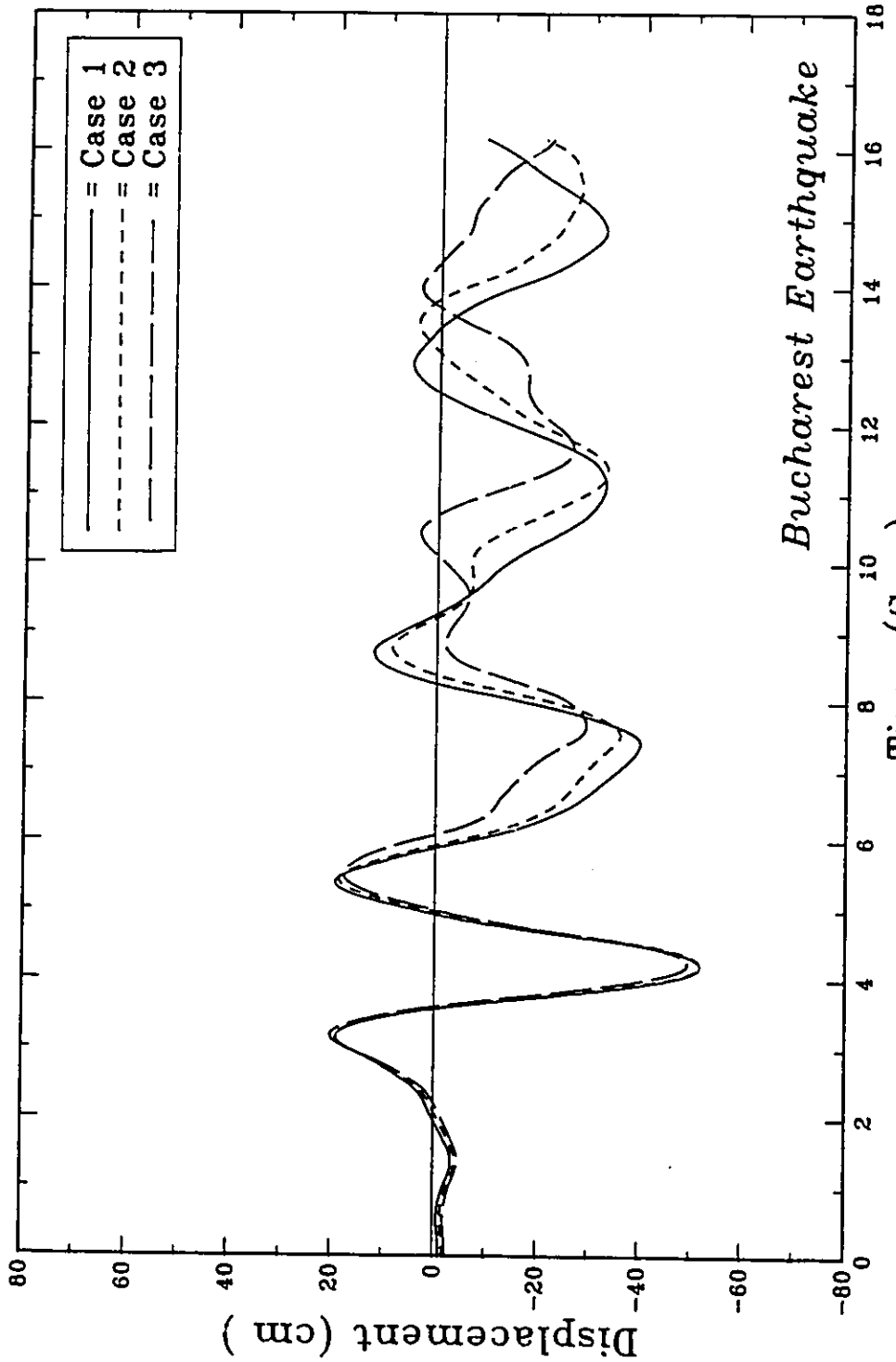

Fig. 7.10 Displacement history for the16th floor.

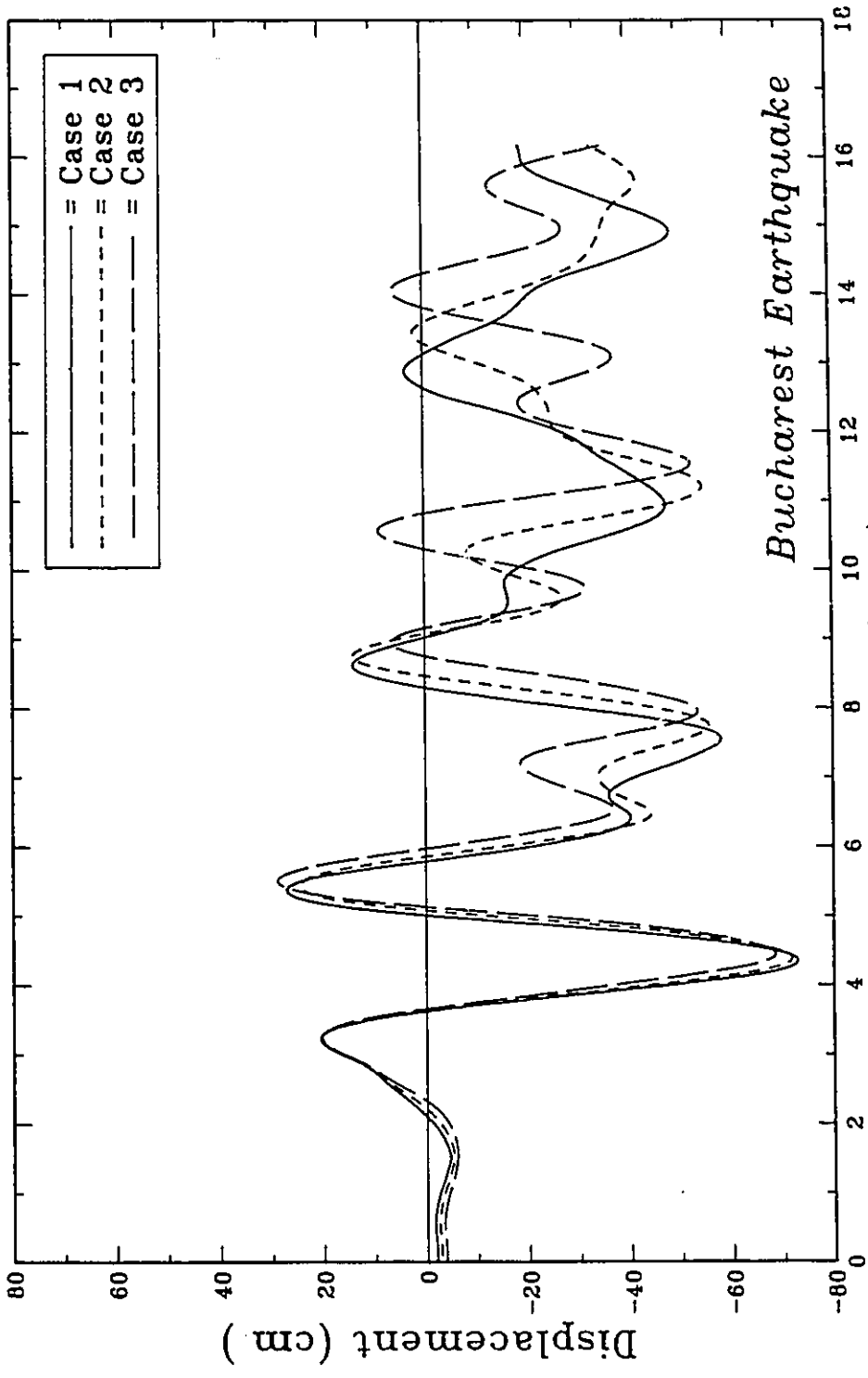

Fig. 7.11 Displacement history for the roof.

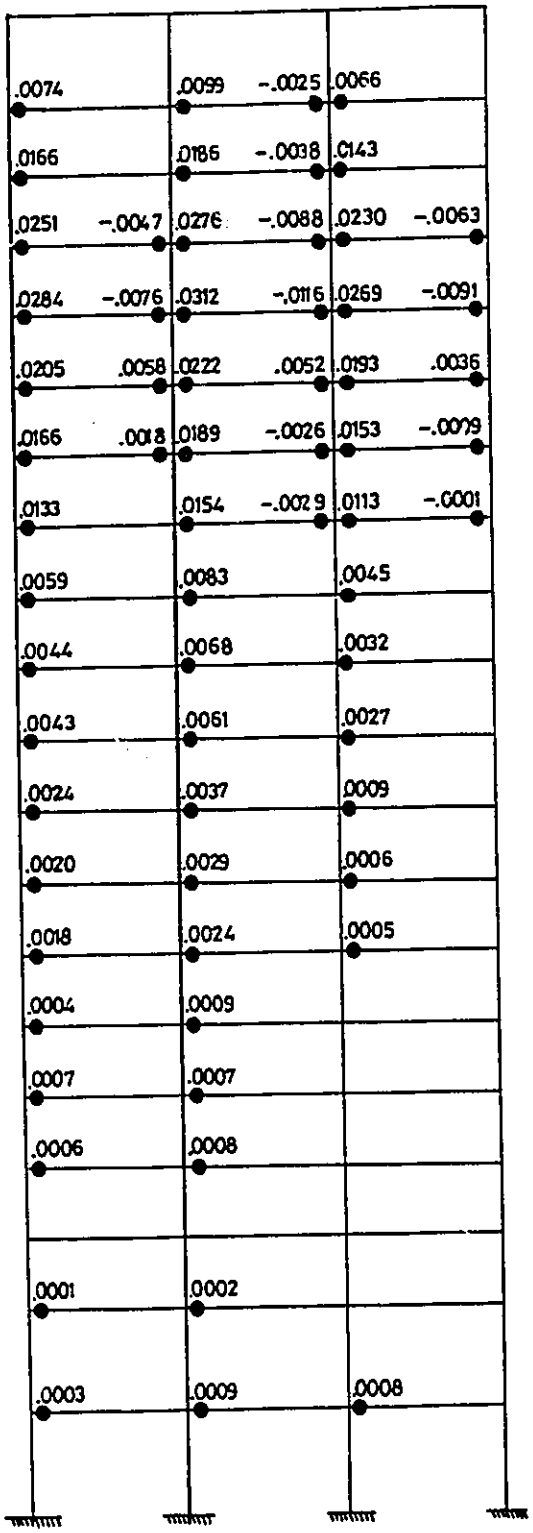

Fig. 7.12 Maximum beam and column plastic rotations for MRF case 1(in radians).

Bucharest Earthquake

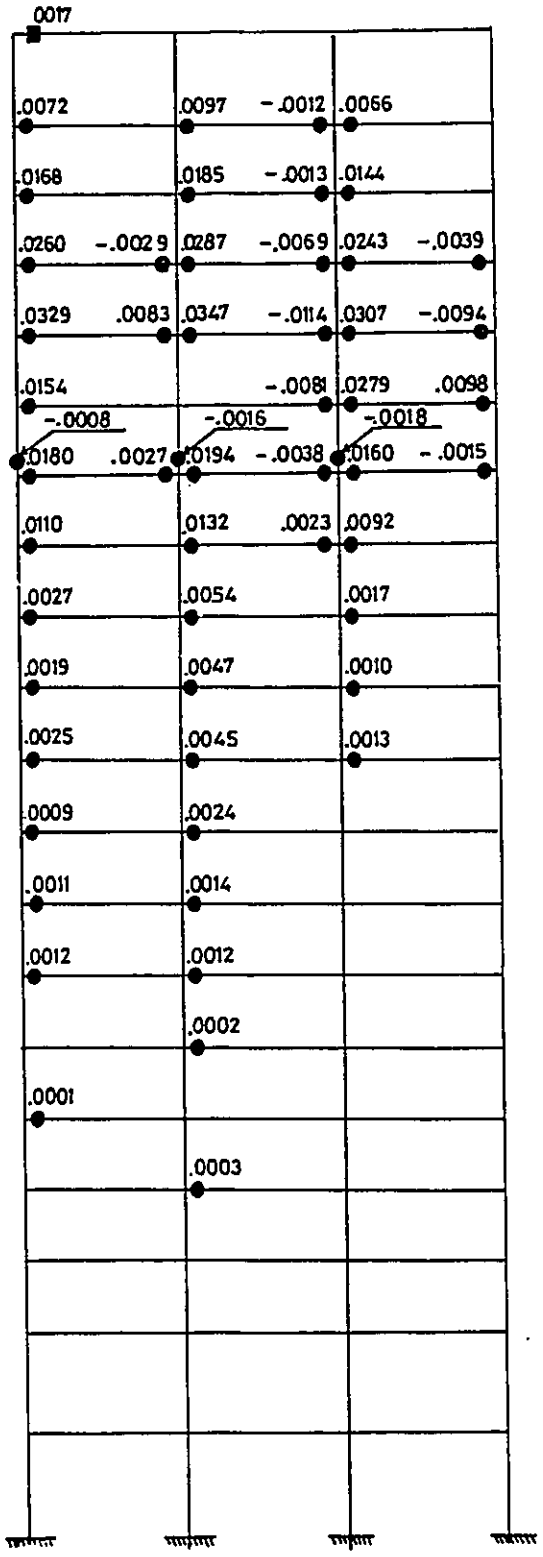

Fig. 7.13 Maximum beam and column plastic rotations for MRF case 2 (in radians).

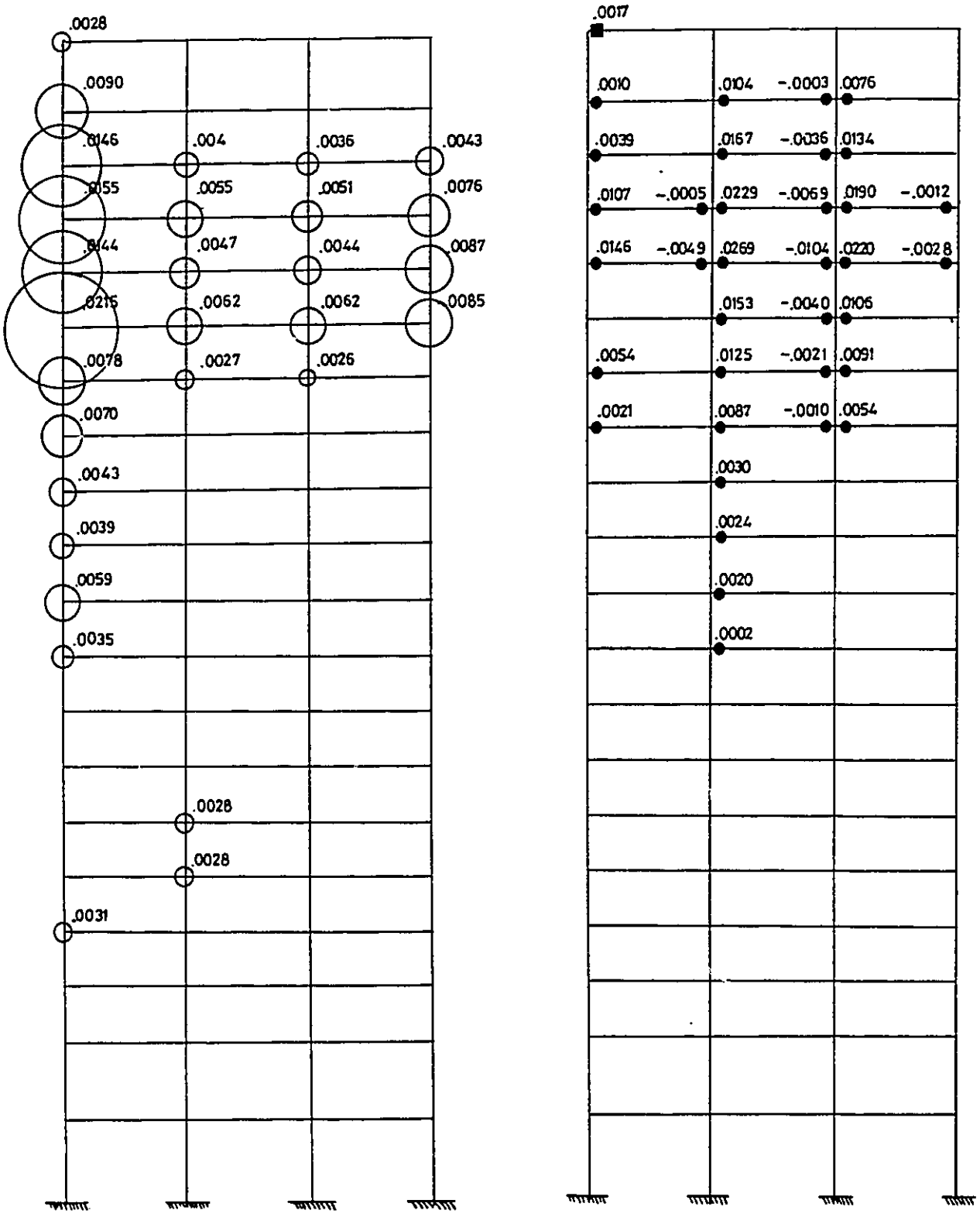

Panel zones

Beams and columns

Fig. 7.14 Maximum beam, column and panel zone joint plastic rotations for MRF case 3. (in radians)

Response to Honshu earthquake.

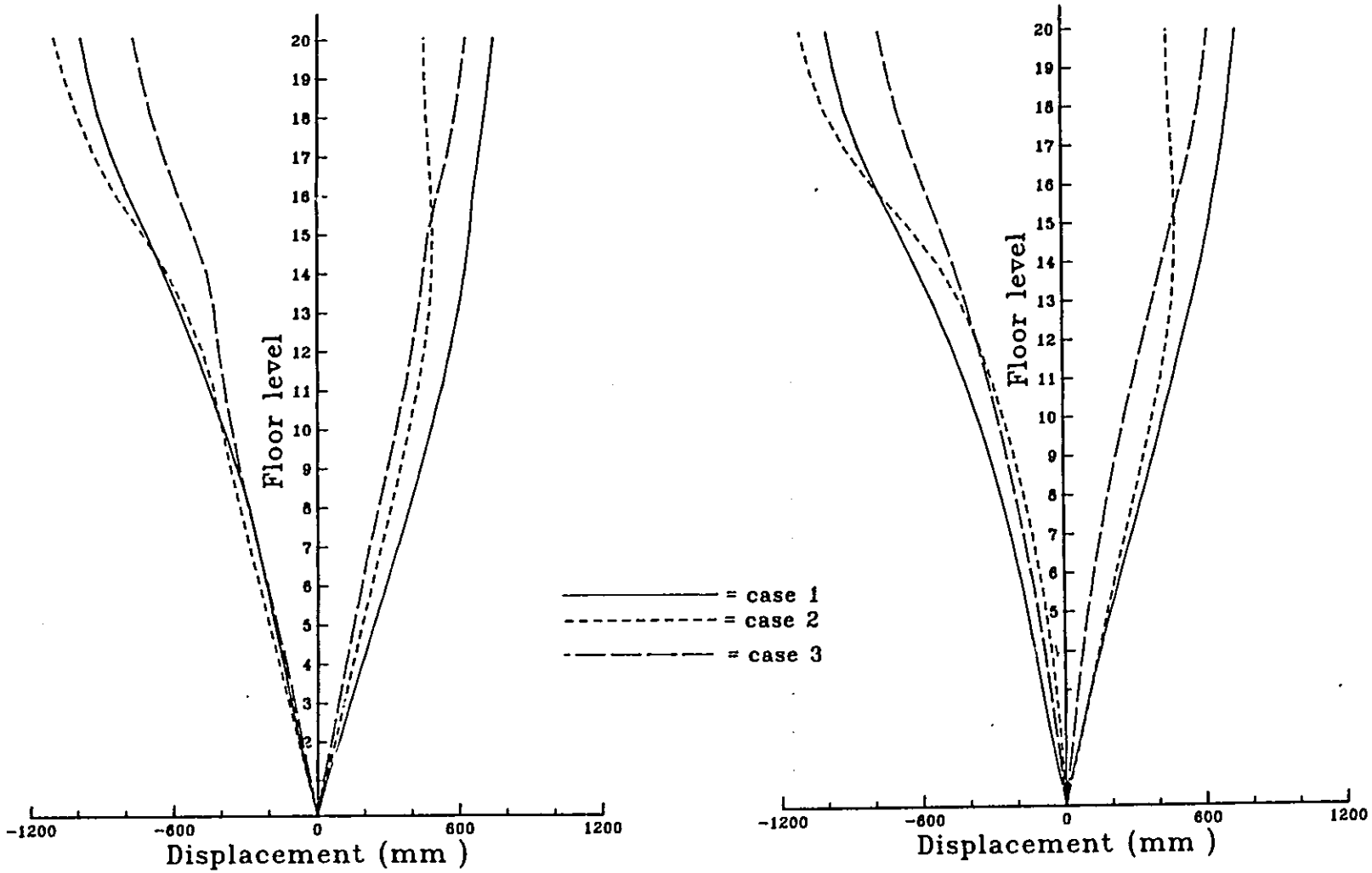

a) Maximum floor displacement. *b) Floor displacement at peak roof displacement.*

Fig. 7.15 Effect of joint flexibility on the dynamic lateral deflection.

Honshu Earthquake

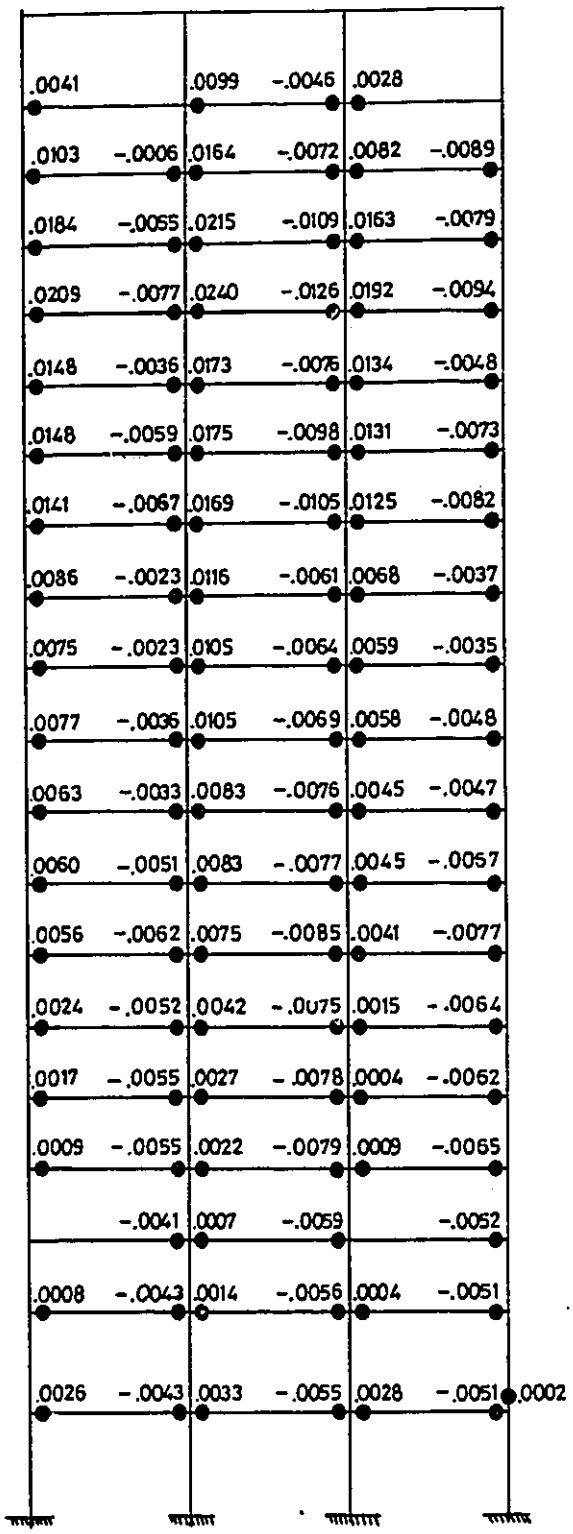

Fig. 7.16 Maximum beam and column plastic rotations for MRF case 1(in radians).

Honshu Earthquake

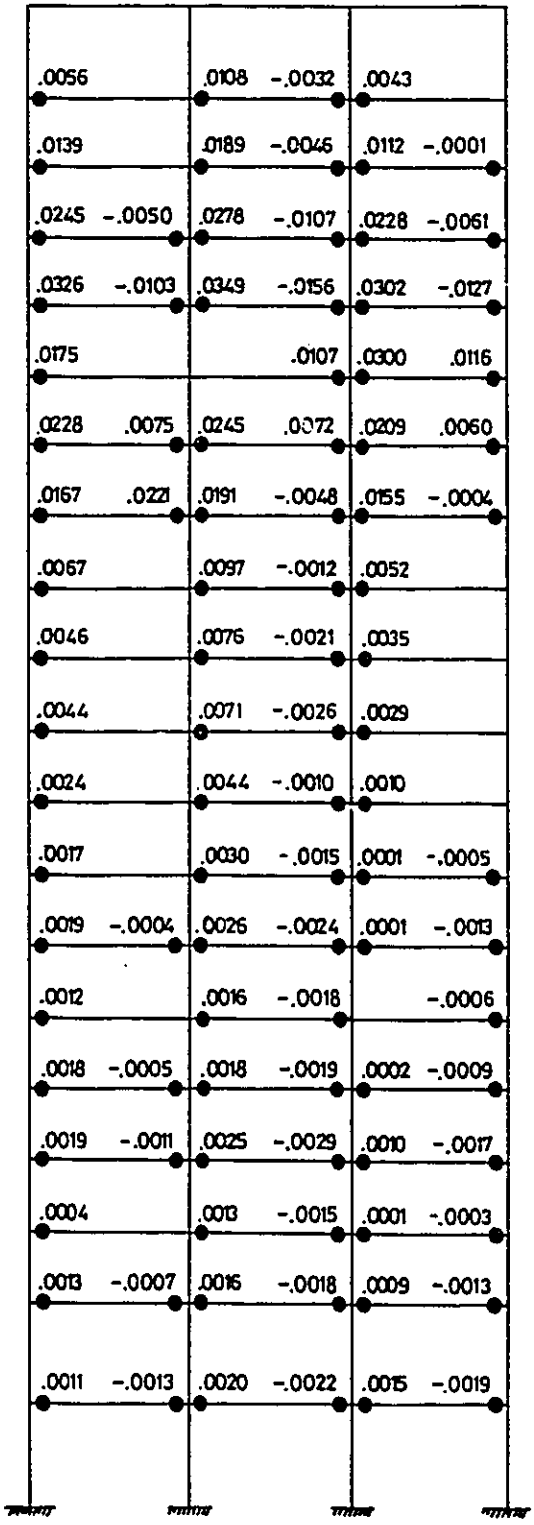

Fig. 7.17 Maximum beam and column plastic rotations for MRF case 2(in radians).

Honshu Earthquake

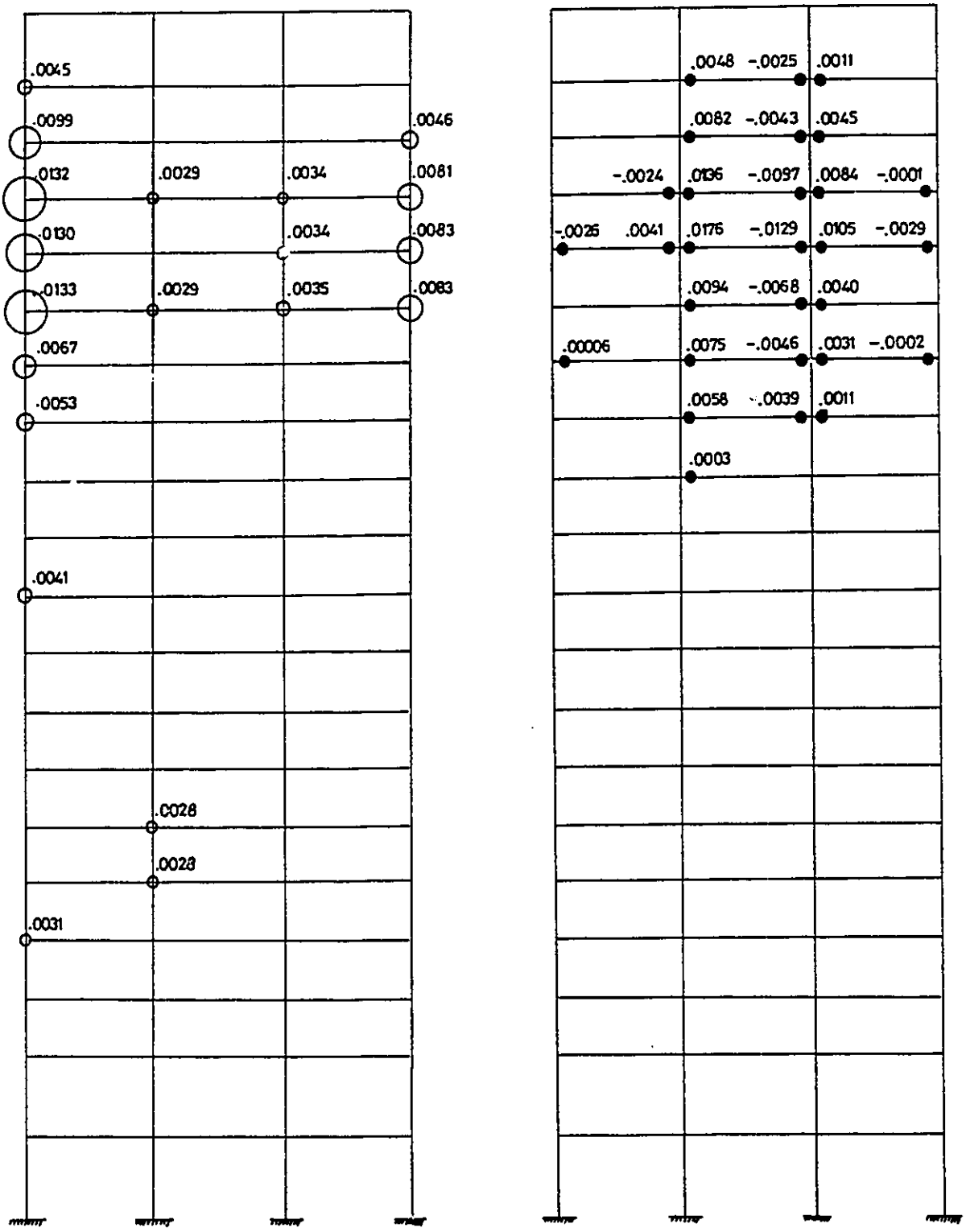

Panel zones

Beams and columns

Fig. 7.18 Maximum beam, column and panel zone joint plastic rotations for MRF case 3. (in radians)

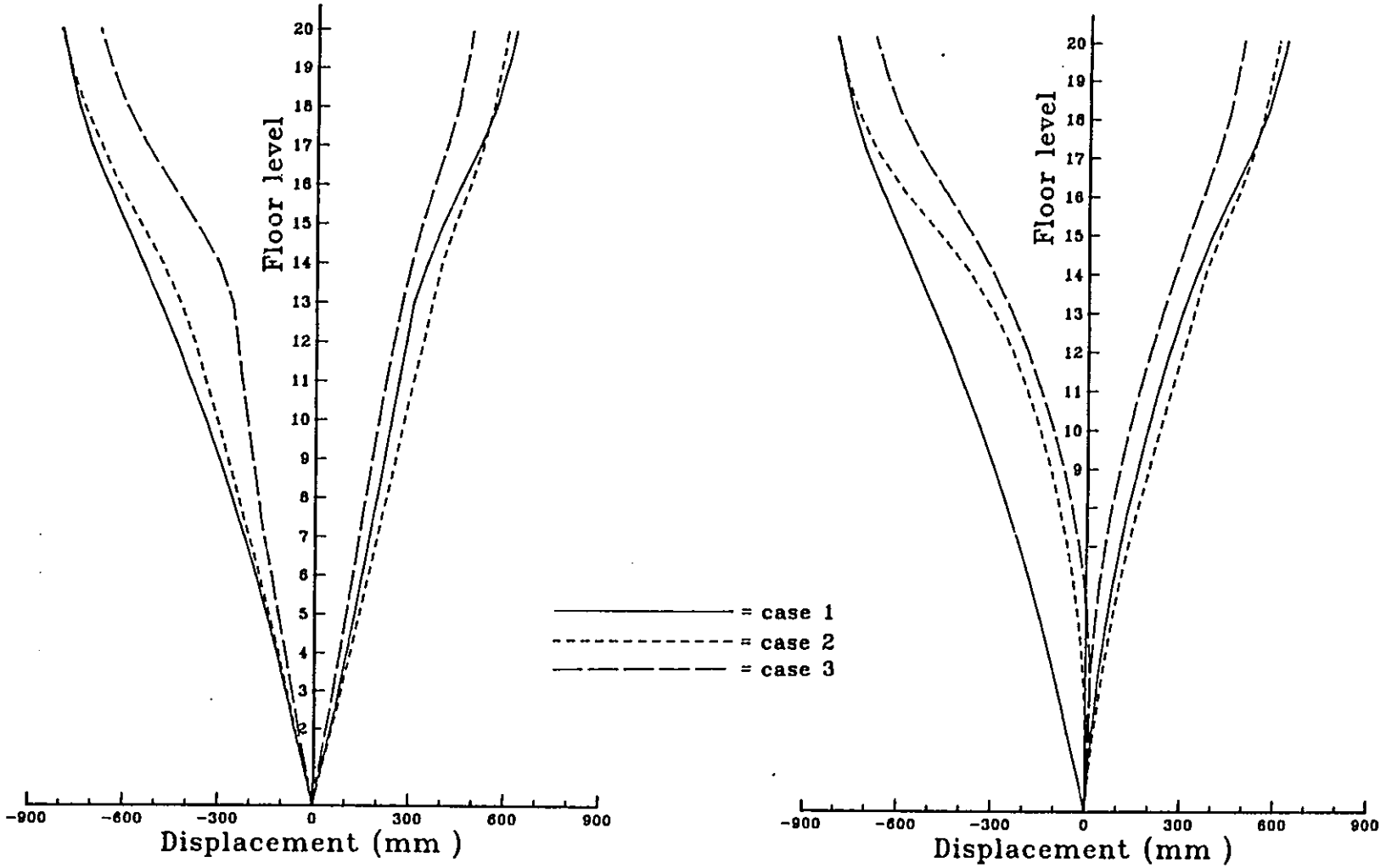

a) Maximum floor displacement.

b) Floor displacement at peak roof displacement

Fig. 7.19 Effect of joint flexibility on the dynamic lateral deflection.

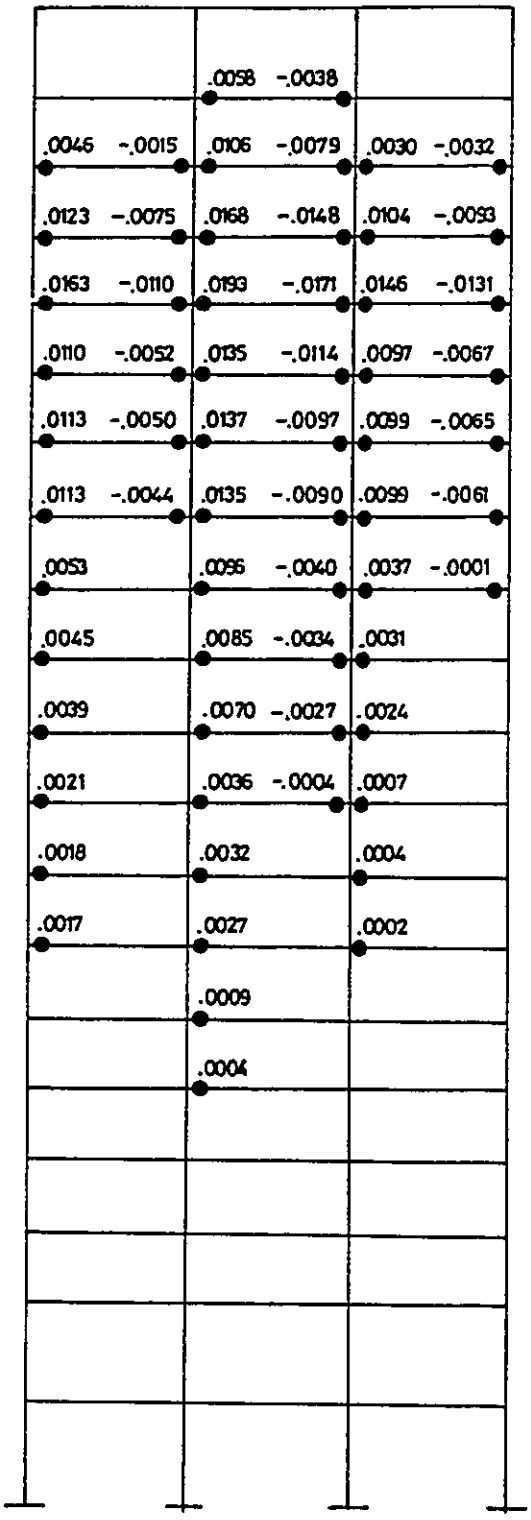

Fig. 7.20 Maximum beam and column plastic rotations for MRF case 1(in radians).

Mexico Earthquake

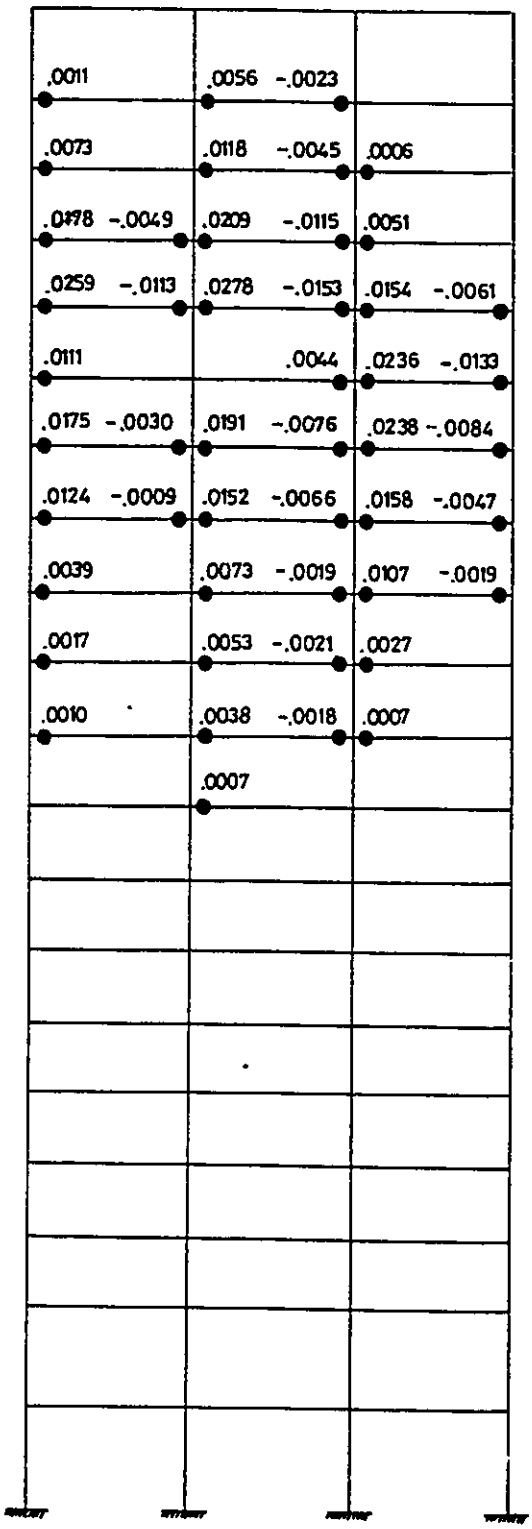

Fig. 7.21 Maximum beam and column plastic rotations for MRF case 2(in radians)

Mexico Earthquake

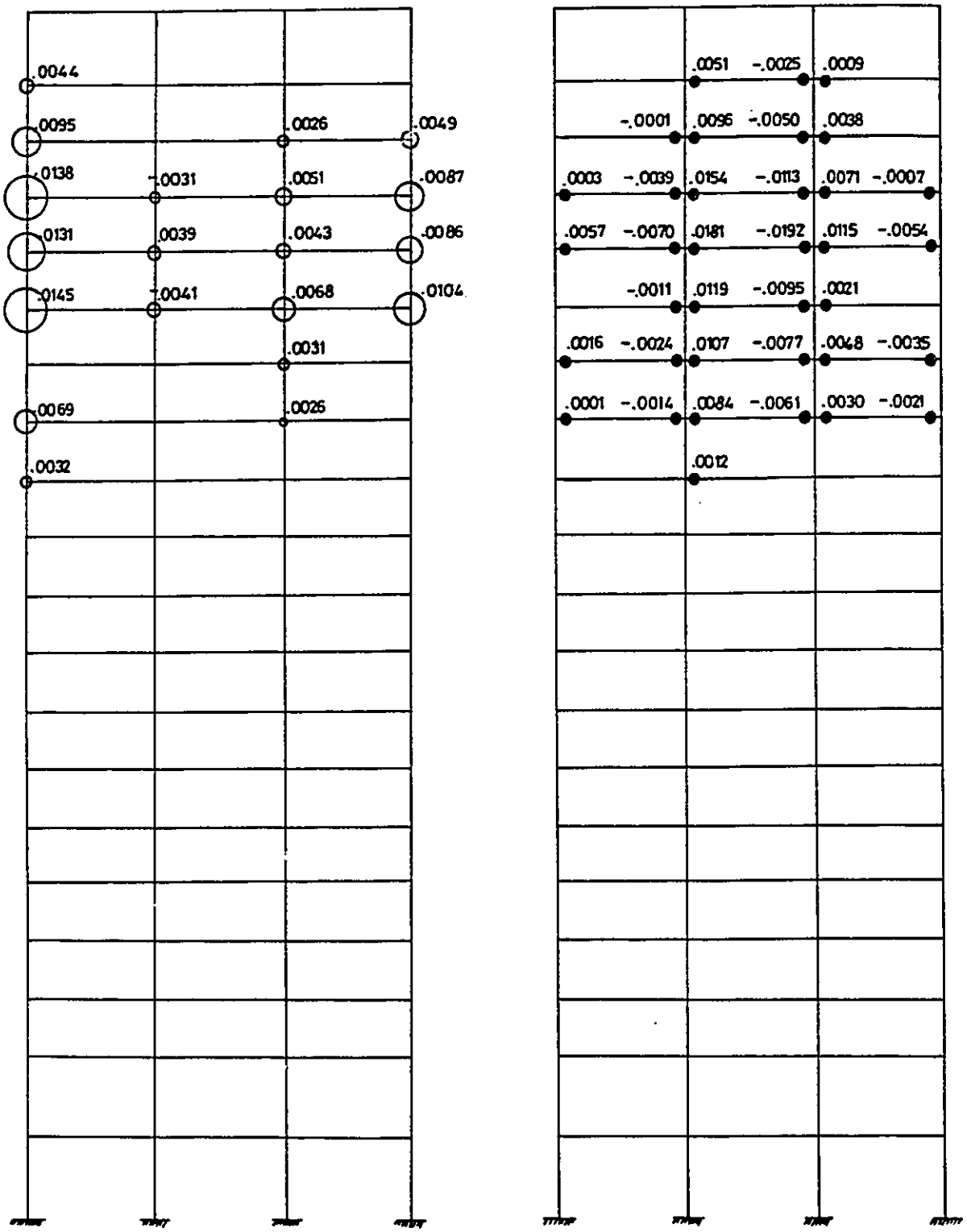

Panel zones

Beams and columns

Fig. 7.22 Maximum beam, column and panel zone joint plastic rotations for MRF case 3. (in radians)

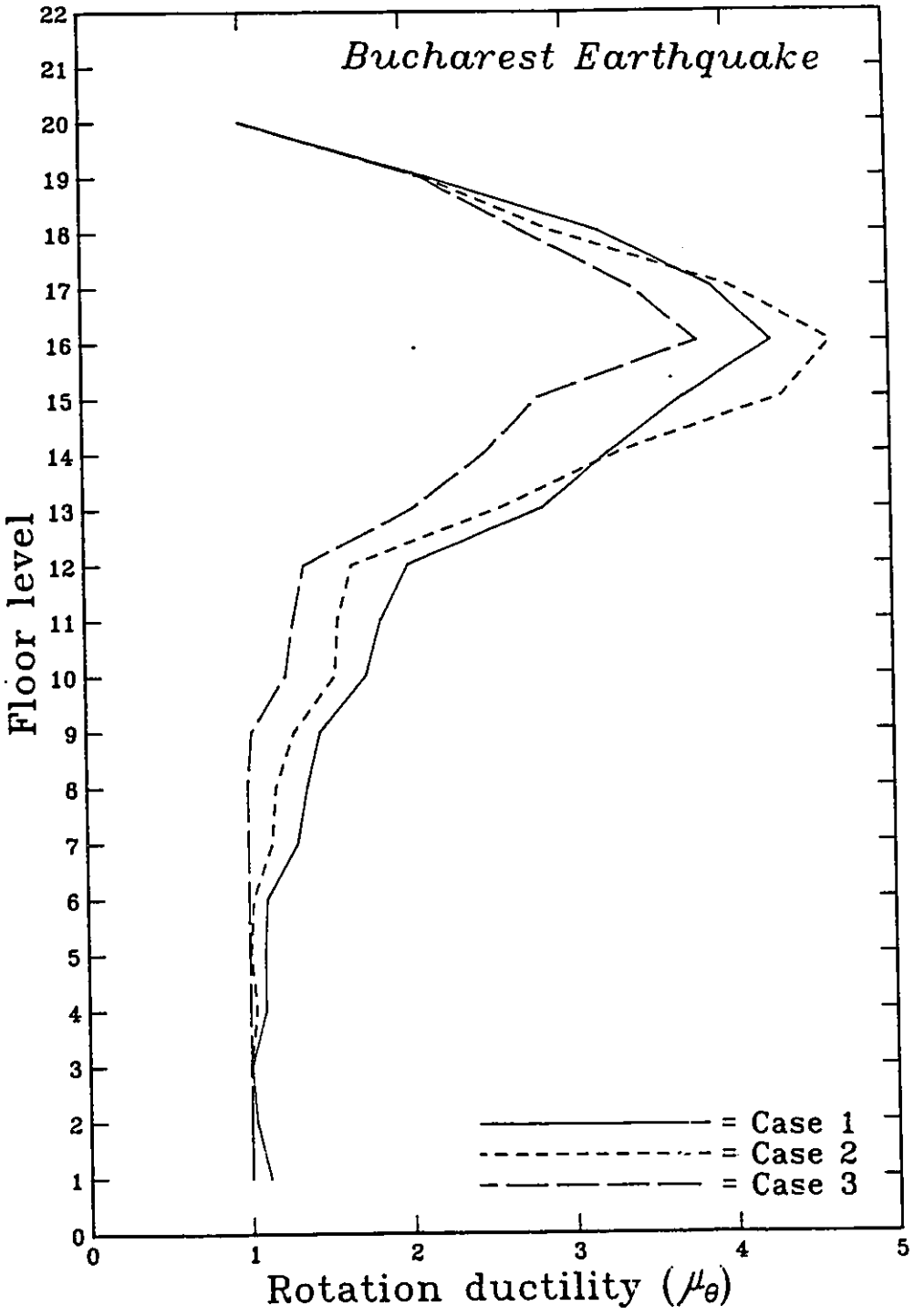

Fig. 7.23 Beams rotational demands for Bucharest earthquake.

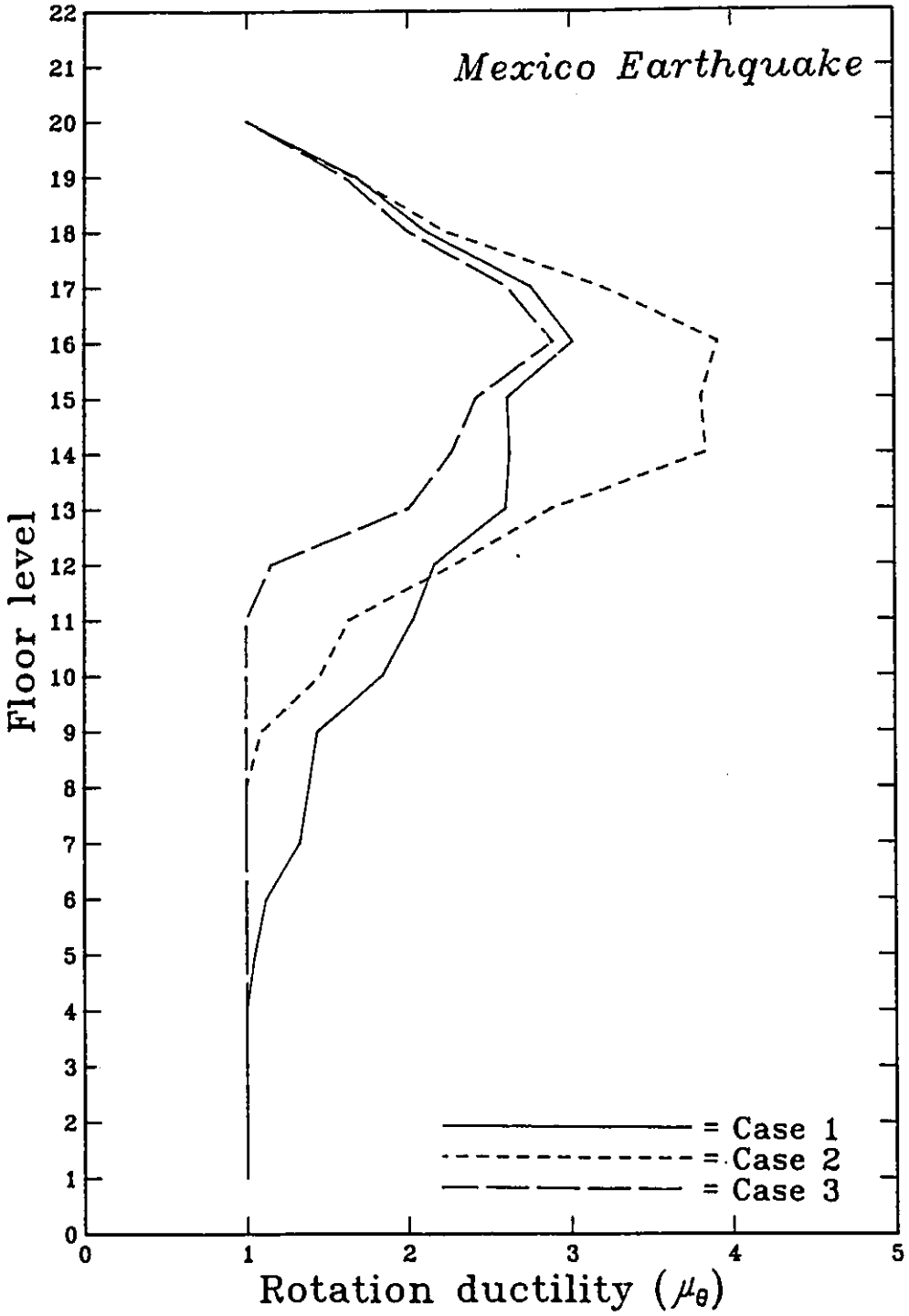

Fig. 7.24 Beams rotational demands for Mexico earthquake.

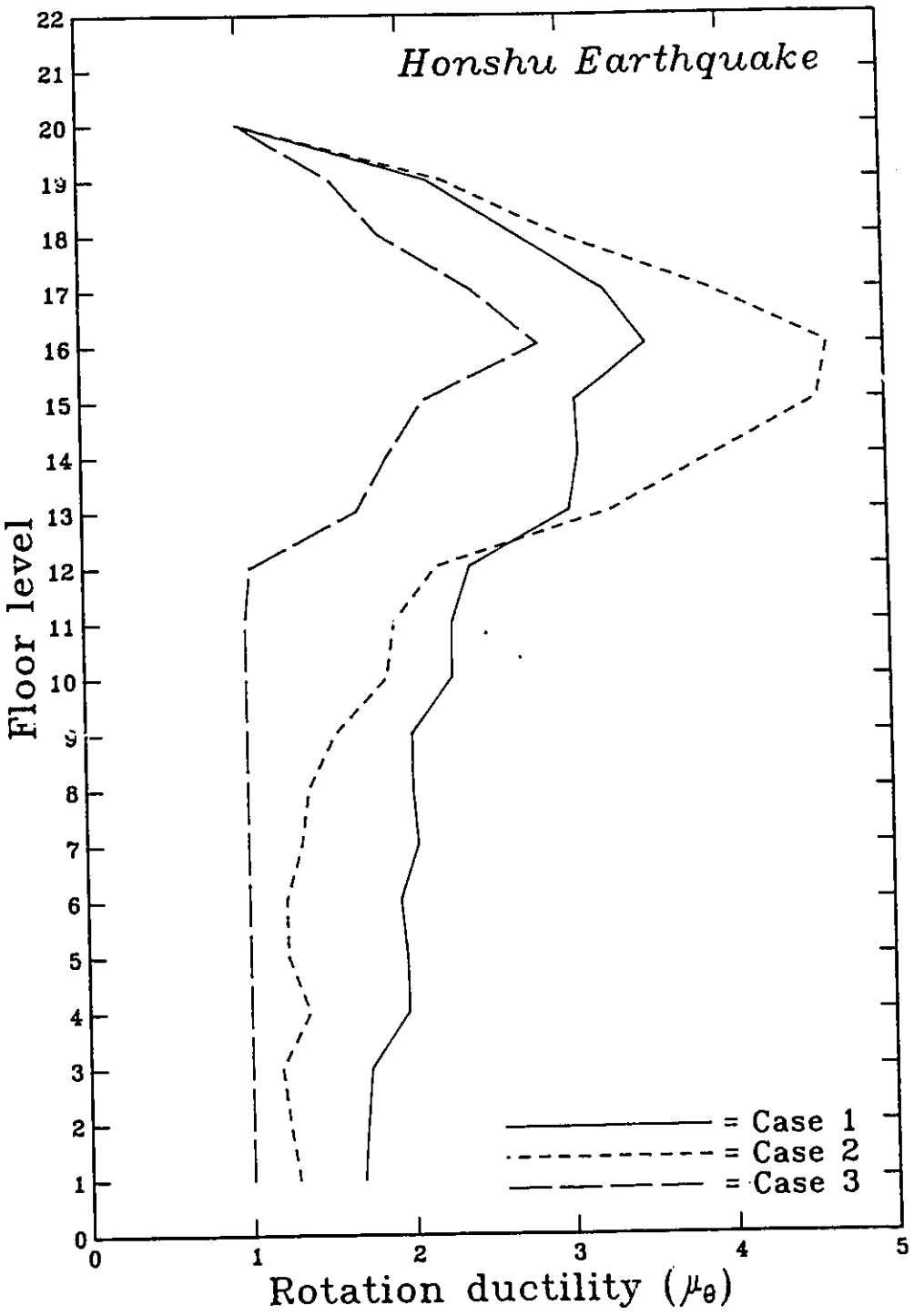

Fig. 7.25 Beam rotational demands for Honshu earthquake.

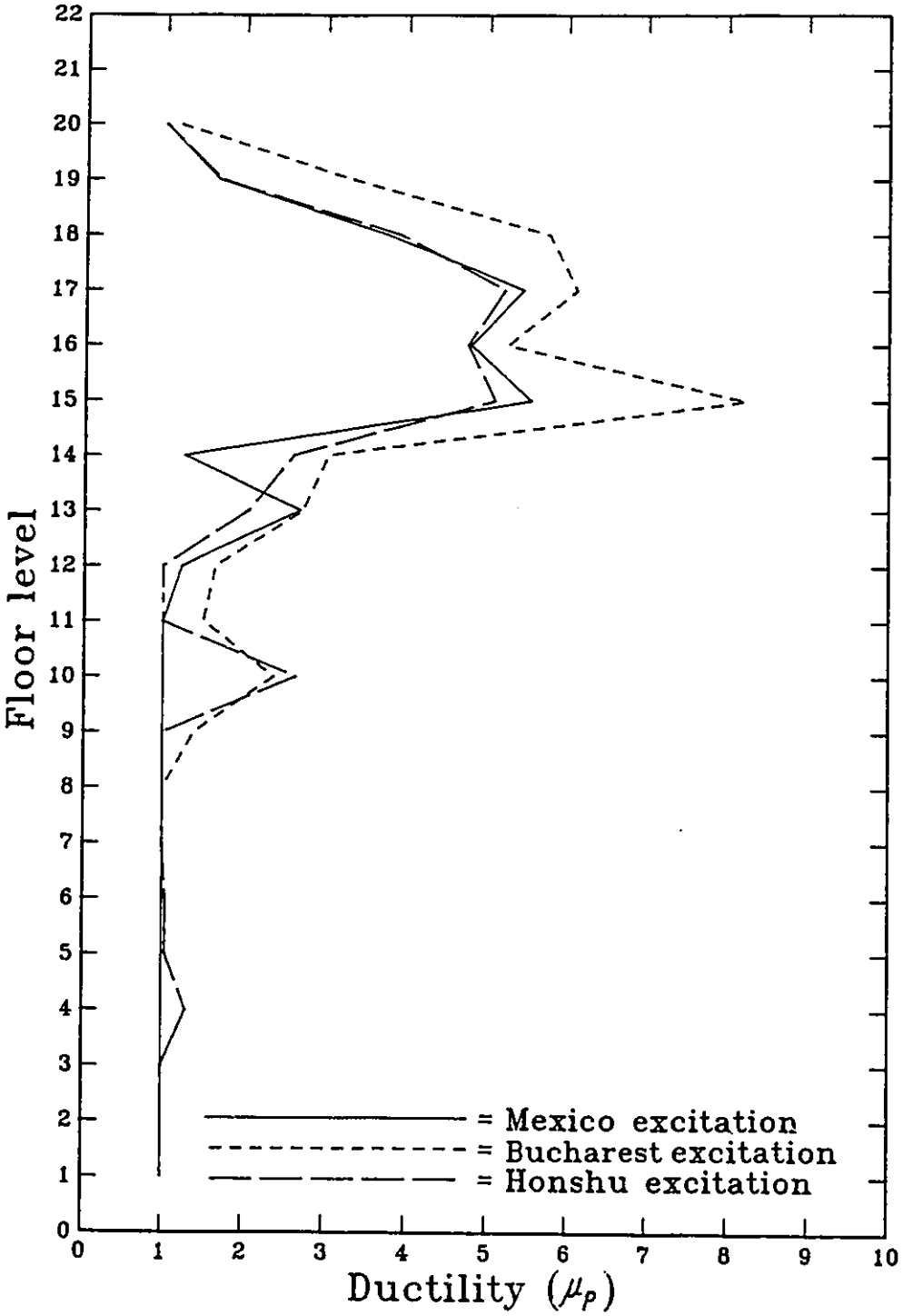

Fig. 7.26 panel zones rotational demands

CHAPTER 8

CONCLUSIONS

8.1 Summary

The principal objectives of this research program were to investigate experimentally the cyclic behaviour of extended end-plate joints and to study analytically the effect of their response on the behaviour of MRFs.

A total of seven full scale beam-to-column connections and four full scale subassemblages were subjected to quasi-static cyclic loading simulating the effects of a severe earthquake. Information about the cyclic behaviour of the connections, their individual components, and panel zone were compiled and discussed. Recommendations for proper design of this joint type were proposed.

Two models to predict the cyclic behaviour of both the connection and the panel joint were proposed. The accuracy of their predictions were compared with the experimental results obtained from the tests. Computer elements, namely a connection element and a panel zone element were introduced into in Drain-2D program to be used in analyzing MRFs taking into account the effect of joint flexibility.

An eight-storey and a twenty-storey were used to study the effects of joint flexibility on the frame response. Non-linear inelastic dynamic analyses were performed using different earthquake records. Several design criteria for detailing the panel zone in the analyzed frames were adopted. The results of these analyses provided insight into the effect of the joint flexibility on the response of frames.

8.2 Conclusions

Based on experimental observations, test results and analyses performed, the following conclusions and recommendations were formulated:

Adequacy of current design procedures

(1) The extended end-plate connections designed following the current

design requirements according to LRFD (1986), CAN3-S16.1-M89 (1989) or AISC (1980) specifications could be expected to perform poorly during severe earthquakes. In other words, the end-plate and the column flanges would likely be severely damaged. Modified design procedures as recommended in this study would result in a significant improvement in connection response.

(2) The application of current design specifications for detailing the panel zone (UBC (1988) and CAN3-S16.1-M89 (1989)) are questionable in the case of extended end-plate joints. Panels designed in accordance with these requirements are expected to be stronger than anticipated. A new procedure based on the experimental investigation has been proposed.

Cyclic performance of joints and their components

(3) In all the tests, the joints were able to sustain moments higher than the beam's nominal plastic moment capacity.

(4) All bolts in tested specimens showed degradation in their pre-tension force with loading progression. This degradation was one of the main reasons that caused the stiffness deterioration of the connection.

(5) Improved behaviour under cyclic load can be achieved by selecting the beam section with small width-to-thickness ratios for flanges and webs and by providing adequate lateral bracing of the beam flanges.

(6) The connection is an element with limited ductility. It should not be relied upon for energy dissipation.

(7) The panel zone is a very ductile element with a high ability to dissipate energy through inelastic deformation.

(8) Doubler plates directly fillet welded to the column web, proved to be fully effective in resisting the panel shear deformation.

Modelling joint behaviour

(9) Two analytical models that are capable of simulating the connection behaviour under both monotonic and cyclic loading conditions were proposed. One is a sophisticated model that can predict with adequate accuracy the connection response. The other, is less accurate but represents the principal aspects of the

connection behaviour.

(10) A model that is able to predict the monotonic and cyclic response of the panel zone in extended end-plate joints has been developed. When compared with experimental results, the model was found to approximate the panel behaviour quite closely.

Effect of joint flexibility on MRFs response

(11) The inclusion of the joint flexibility in frame analysis, significantly affects the static and dynamic characteristics of the frames. It resulted in the reduction of a frame's stiffness, an increase in its lateral deflection and the lengthening of the frame's vibration periods.

(12) Increase in MRFs lateral deflection due to joint flexibility under static loads is more pronounced as compared to that under dynamic loads.

(13) Detailing the panel zones in accordance with the proposed design method distributed the earthquake input energy more uniformly throughout the frames. As a result, the beams' ductility demands were reduced significantly reducing the possibility of their local instability.

Design philosophy

(14) A rational design philosophy for MRFs should include three major criteria: (a) The panel should yield approximately at the same time as the beam; (b) Only localized plastification is allowed to take place in the connection, i.e no formation of failure mechanisms in the connection components and (c) Panel deformation should be controlled to minimize a frame's deflections. It is believed that frames designed in accordance with these recommendations will be able to survive severe earthquakes without collapse and will perform satisfactorily under serviceability conditions.

APPENDIX I

NON-LINEAR BEAM-COLUMN ELEMENT

A two component model is used to simulate the moment-rotation relationship of the column or beam elements. In this element, yielding may take place only in concentrated plastic hinges at the element ends. Strain hardening is approximated by considering the element to consist of elastic and elasto-plastic components in parallel. The hinges in the elasto-plastic component yield under constant moment, but the moment in the elastic component may continue to increase.

With this type of strain hardening idealization, if the bending moment in the element is constant, and if the element is of uniform strength, then the moment-rotation relationship for the element will have the same shape as its moment-curvature relationship (Fig. I.1(a)). This follows because curvature and rotation in this case are directly proportional. If, however, the bending moment or strength vary, then the curvature and rotations are no longer proportional, and the moment-rotation and moment-curvature variations may be quite different(Fig. I.1(b)). With the parallel component procedure, a moment-rotation relationship is, in effect, being specified.

The yield moments may be specified to be different at the two element ends, and for positive and negative bending. The interaction between axial force and moment in producing yield may be approximately taken into account.

Yield interaction surfaces of three types may be specified, as follow:

1) Beam type (Fig. I.2(a)): This type of surface is affected by bending moment only.

2) Steel column type (Fig. I.2(b)): This type of surface is affected by both axial and bending moments and is intended to be used with steel columns.

3) Concrete column type (Fig. I.2(c)): This type of surface is affected by both axial and bending moments and is intended to be used with concrete columns.

For the analysis in this study, the first element type was used for the beams, the second type was used for the columns.

With regards to static loads applied along the lengths of the beam-column elements, they were taken into account by specifying end clamping forces.

Large displacement effects were approximated in the analysis by including simple geometric stiffness based on the element axial forces under static load.

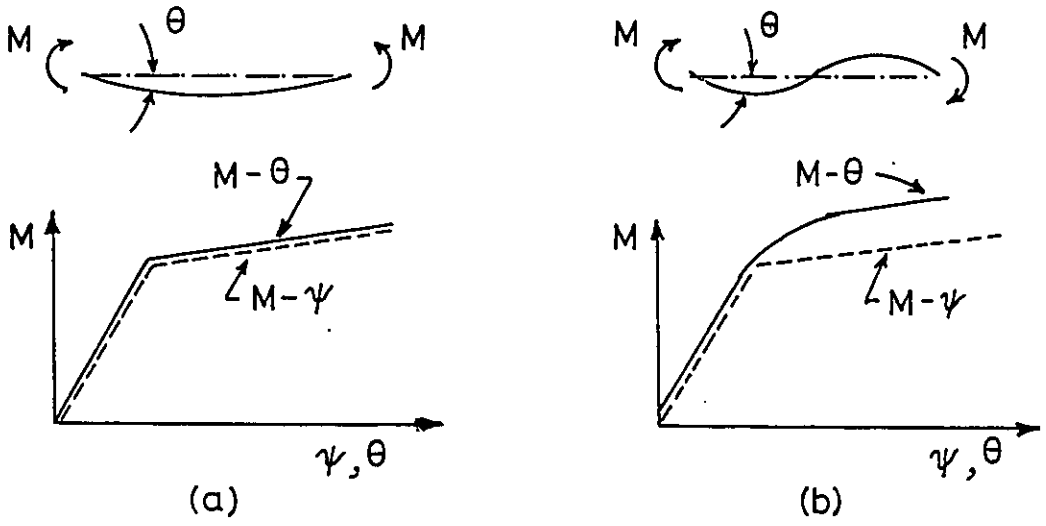

Fig. I.1 Moment–rotation and moment–curvature relationship

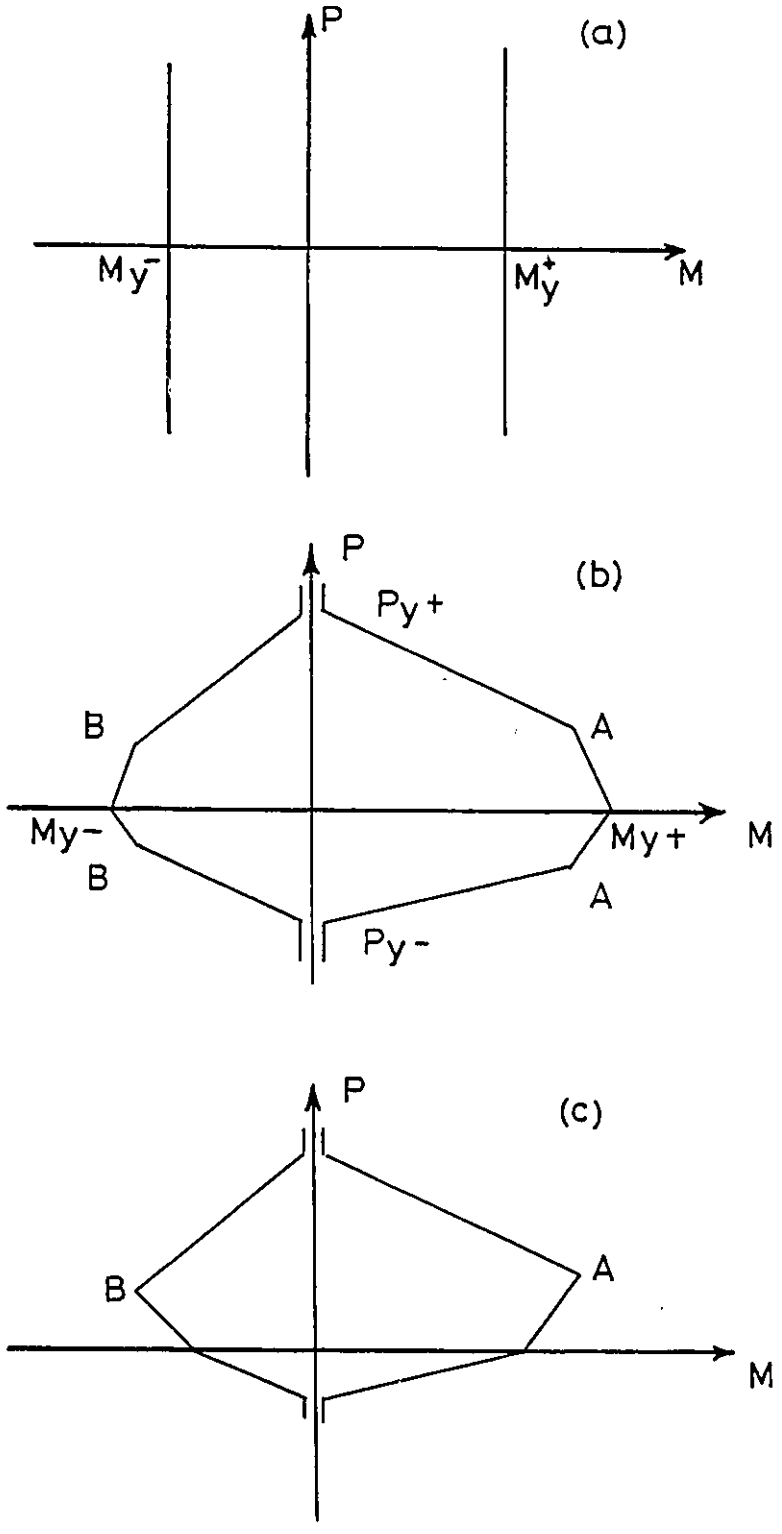

Fig. I .2 Yield surfaces

APPENDIX II

DAMPING COFFICIENTS

In Drain-2D program, the damping can be taken as mass proportional damping, tangent stiffness-dependent damping or original elastic stiffness-dependent damping, or any combination of the three damping types. Therefore, the viscous damping matrix may be specified as

$$[C_T]=\eta[M]+\zeta[K_T]+\beta_o[K_o] \qquad \text{(II.1)}$$

in which $[C_T]$ is the current viscous damping matrix, [M] is the mass matrix, $[K_T]$ is the current tangent stiffness matrix, including geometrical stiffness effects and $[K_o]$ is the original elastic stiffness matrix of the unstressed structure.

In the analysis, damping proportional only to both the mass and the tangent stiffness was used. The values of η and ζ were determined from the following equations

$$\eta=\frac{4\pi(T_j\lambda_j-T_i\lambda_i)}{T_j^2-T_i^2} \qquad \text{(II.2)}$$

$$\zeta=\frac{T_iT_j(T_j\lambda_i-T_i\lambda_j)}{\pi(T_j^2-T_i^2)} \qquad \text{(II.3)}$$

where

λ_i and λ_j = the proportional of critical damping in the ith and jth modes, respectively.

T_i and T_j = the vibration periods for the ith and the jth modes, respectively.

APPENDIX III

NUMERICAL PROCEDURE FOR NON-LINEAR DYNAMIC ANALYSIS

III.1 Incremental equation of motion

At any instant of time, the equation of dynamic equilibrium can be written as

$$[M]\{\ddot{dr}\}+[C_T]\{\dot{dr}\}+[K_T]\{dr\}=\{dP\} \qquad \text{(III.1)}$$

in which $\{\ddot{dr}\}$, $\{\dot{dr}\}$ and $\{dr\}$ are the increments of acceleration, velocity and displacement at a node, respectively; $\{dP\}$ is the increment of applied load; $[M]$ is the mass matrix and $[C_T]$ and $[K_T]$ are tangent values of the damping and stiffness matrices for the structure in its current state. For a finite time step, Δt, the following equation is approximately satisfied

$$[M]\{\Delta\ddot{r}\}+[C_T]\{\Delta\dot{r}\}+[K_T]\{\Delta r\}=\{\Delta P\} \qquad \text{(III.2)}$$

in which $\{\Delta\ddot{r}\}$, $\{\Delta\dot{r}\}$, $\{\Delta r\}$ and $\{\Delta P\}$ are finite increments of acceleration, velocity, displacement and load, respectively.

Because $[K_T]$ and $[C_T]$ represent the tangent stiffness and the tangent damping of the system at the beginning of the time step, t, Eq. III.2 will provide an accurate solution to the response only at time $t+\Delta t$, if the system maintains its stiffness equal to $[K_T]$ through the time step, Δt. In reality, yielding can occur within the step and consequently the system stiffness changes. This problem can be overcome by appropriate choice of solution strategy and time step Δt, i.e choosing Δt to be as small as possible without substantially increasing the computation time and the rounding off errors. If a change in the state of the structure occurrs during the time step as shown in Fig. III.1, corrective loads are temporarily applied in the succeeding time step to compensate for the error.

III.2 Equilibrium corrections

The error correction process is done in the Drain-2D program, by assuming that the equilibrium at the end of one time step (time t^-) be represented by

$$\{F_M\}+\{F_C\}+\{F_K\}=\{P\} \qquad \text{(III.3)}$$

where $\{F_M\}$, $\{F_C\}$ and $\{F_K\}$ are the total forces at the nodes due to inertia, damping and member forces, respectively; and $\{P\}$ is the total external load.

At the beginning of the next step (time t^+) the quantities $\{F_M\}$, $\{F_K\}$ and $\{P\}$ will be unchanged, but $\{F_C\}$ may be changed by $\{\Delta F_C\}$ to satisfy equilibrium. So, the new equilibrium equation at time t^+ is

$$\{F_M\}+\{F_C\}+\{\Delta F_C\}+\{F_K\}=\{P\}+\{\Delta F_C\} \qquad \text{(III.4)}$$

This additional external load cannot be permitted to continue to act, because it may significantly modify the resulting response of the structure. It is necessary, therefore, to eliminate this load after the interval by applying an equal and opposite load of magnitude $-\{\Delta F_C\}$. In Drain-2D program, this corrective load is applied during the next integration time step. The load $\{\Delta F_C\}$ is thus permitted to act for a short time, but the error is believed to be negligible. It should be noted that the load $\{F_C\}$ is itself approximate, because it is based on an assumed form for the damping matrix.

III.3 Solution of incremental equation of motion

In Drain-2D program, a method based on constant acceleration within the time step has been adopted (Fig.III.2). In the following the basic equations for this method will be described.

III.3.1 Constant acceleration method

In this method, the initial acceleration, $\ddot{r}_o$, at the begaining of the time step is known while the acceleration at the end of the time step, $\ddot{r}_1$, is unknown. Assuming

that the acceleration through the time step is constant and equal to the average, $\ddot{r}$ is given by

$$\ddot{r}=\frac{1}{2}(\ddot{r}_o+\ddot{r}_1) \qquad \text{(III.5)}$$

Knowing that the velocity is the integration of the acceleration, i.e

$$\dot{r}=\dot{r}_O+\int_0^t \ddot{r}dt \qquad \text{(III.6)}$$

The velocity at the end of the time step, $\dot{r}_1$, is given by

$$\dot{r}_1=\dot{r}_o+\ddot{r}_o\frac{\Delta t}{2}+\ddot{r}_1\frac{\Delta t}{2} \qquad \text{(III.7)}$$

Similarly, the displacemen at the end of the time step, r_1, is given by

$$r_1=r_o+\dot{r}_o\Delta t+\ddot{r}_o\frac{\Delta t^2}{4}+\ddot{r}_1\frac{\Delta t^2}{4} \qquad \text{(III.8)}$$

Rearrange the previous equations in terms of Δr, the following can be obtained

$$\Delta\dot{r}=-2\dot{r}_o+\Delta r\frac{2}{\Delta t} \qquad \text{(III.9)}$$

$$\Delta\ddot{r}=-2\ddot{r}_o-\dot{r}_o\frac{4}{\Delta t}+\Delta r\frac{4}{\Delta t^2} \qquad \text{(III.10)}$$

Substituting Eq.III.9 and III.10 into the the dynamic equilibrium equation (III.2) gives

$$[\frac{4}{\Delta t^2}[M]+\frac{2}{\Delta t}[C]+[K]]=\{\Delta P\}+[M]\{2\ddot{r}_o+\dot{r}_o\frac{4}{\Delta t}\}+[C]\{2\dot{r}_o\} \qquad \text{(III.11)}$$

Eq. III.11 can be written as

$$[(\frac{4}{\Delta t^2}+\frac{2\eta}{\Delta t})M+(\frac{2\zeta}{\Delta t}+1)K_T]\{\Delta r\}=\{\Delta P\}$$

$$+[M]\{2\ddot{r}_o+\frac{4}{\Delta t}\dot{r}_o+2\eta\dot{r}_o\}+\zeta[K_T]\{2\dot{r}_o\} \qquad \text{(III.12)}$$

assuming a viscous damping dependent on both mass and tangent stiffness, i.e

$$[C_T]=\eta[M]+\zeta[K_T] \qquad \text{(III.13)}$$

For avoiding the need for evaluating the term $\zeta[K_T]\{2\dot{r}_o\}$, the following transformation proposed by Wilson (1968) is introduced

$$\{\Delta x\}=\{\Delta r\}+\zeta\{\Delta\dot{r}\}=(\frac{2\zeta}{\Delta t}+1)=2\zeta\{\dot{r}_o\} \qquad \text{(III.14)}$$

Eq. III.12 can therefore be written as

$$[\omega M+K_T]\{\Delta x\}=\{\Delta P\}$$

$$+[M]\{2\ddot{r}_o+\frac{4}{\Delta t}\dot{r}_o+2\eta\dot{r}_o+2\zeta\omega\dot{r}_o\} \qquad \text{(III.15)}$$

in which

$$\omega=\frac{\frac{4}{\Delta t^2}+\frac{2\eta}{\Delta t}}{\frac{2\zeta}{\Delta t}+1}$$

When $\{\Delta x\}$ has been determined, the increment of nodal displacement follows from

$$\{\Delta r\}=\frac{1}{\frac{2\zeta}{\Delta t}+1}\{\Delta x+2\zeta\dot{r}_o\} \qquad \text{(III.16)}$$

and hence increment of velocity and displacement follow from Eqs. III.9 and III.10, respectively.

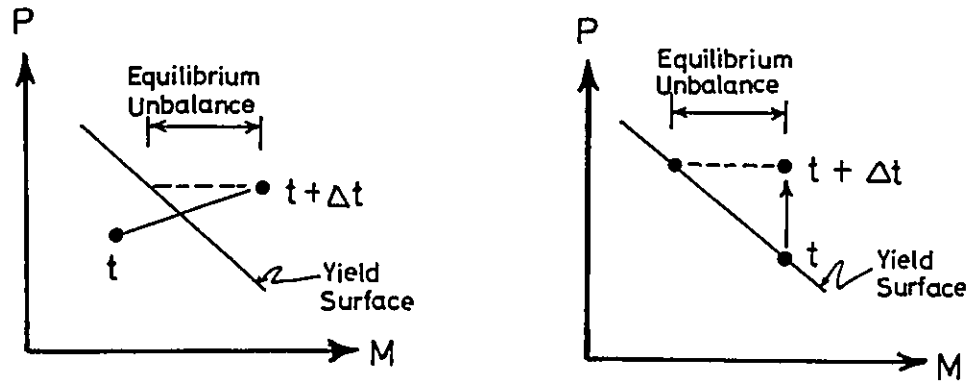

Fig. III.1 Equilibrium correction

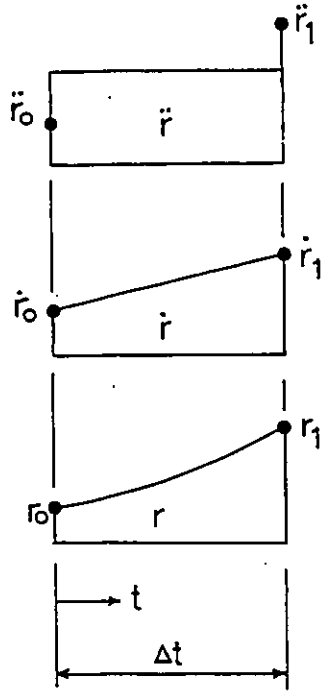

Fig. III.2 Constant acceleration method

REFERENCES

Almulti, A.M. and Hanson,R.D. 1973 ,"Static and dynamic cyclic yielding of steel beams", Jour. of Struct. Division, ASCE, Vol.99, No.ST6, pp.1273-1285.

American Institute of Steel Construction 1986 ,"LRFD,Specification for structural steel buildings", Chicago.

American Institute of Steel Construction 1980 ,"Manual of steel construction", AISC, 8th edn, Chicago.

Ang,K.M., and Morris, G.A. 1984 ,"Analysis of three dimensional frames with flexible beam-column connections", Canadian Jour. of Civil Engineering, 11, pp.245-254.

Azizinamini, A., Bradburn, J.H., and Rodziminski, J.B. 1987 ," Initial stiffness of semi-rigid steel beam-to-column connections", Jour. of Const. steel Research, 8, pp.71-80.

Ballio, G., Calado, L., DeMortino, A., Faella, C.,and Mozzolani, F.M. 1987 ,"Cyclic behaviour of steel beam-to-column joints, experimental research", Costruzioni Metalliche, No.2, pp.69-90.

Ballio, G., Calado,L., DeMartino, A., Faella, C., and Mazzolani, F.M.1986 ,"Steel beam-to-column joints under cyclic loads, experimental and analytical approach", Proc.8th European Conf. on Earthquake Eng., Lisbon, pp. 7.2/9-7.2/16.

Bertero,V.V., Krawinkler,H., and Popov,E.P. 1973 ,"Further studies on seismic behaviour of steel beam-to-column subassemblages", Report No. 73-27, Earthquake Engineering Research Center, University of California, Berkely.

Bertero,V.V., Popov,E.P., and Krawinkler,H. 1972 ," Beam-column subassemblages under repeated loading", Journal of the Structural Division, ASCE, Vol.98, No.ST5, May, pp.1137-1159.

Canadian Standards Association 1989 ,"Limit state design of steel structures", No.CAN/CSA-S16.1-M89, Canada.

De Buen,O. 1980 ,"In steel structures, Design of Earthquake Resistant Structures", ed.Emilio Rosenblueth, John wiley and Sons, New-York.

Frye, M.J., and Morris, G.A. 1976 ,"Analysis of flexibly connected steel frames", Canadian Jour. of Civil Engineering, 2, pp.280-291.

Gerstle, K.H. 1988 ,"Effect of connections on frames", Jour. of Const. Steel Research, Vol.10, pp.241-267.

Ghobarah, A., Osman, A., and Korol, R.M. 1990 ,"Behaviour of extended end-plate connections under cyclic loading", Engineering Structure, Vol.12, pp.15-22.

Griffiths, J.D. 1984 ,"End-plate moment connections-their use and misuse", Engineering Journal, AISC, 1st Quarter, pp.32-34.

Hendrick, A. , and Murray, T.M. 1984 ," Column web compression strength at end-plate connections", Engineering Journal, AISC, 3rd Quarter, pp.161-169.

Hibler, H.M., Hughes, T.J.R., and Taylor, R.l. 1977 ,"Improved numerical dissipation of time integration algorithm in structural dynamics", Earthquake Engineering and structural dynamics, Vol.5.

Jaramillo, T.J. 1950 ,"Deflections and moments due to a concentrated load on a cantilever plate of infinite length", A.S.M.E Journal of Applied Mechanics, 17, pp.67-72.

Johnstone, N.D. and Walpole, W.R. 1981 ,"Bolted end-plate beam to column connections under earthquake type loading", Report 81-7, Dept. of Civil Engineering, University of Canterbury, Christchurch, New Zealand.

Johnstone, N.D. and Walpole, W.R. 1982 ,"Behaviour of steel beam to column connections, made using bolted end-plates", Bull. New Zealand Nat. Soc. for Earthquake Eng., 15, No.2, pp.82-92.

Jones, S.W., Kirby, P.A., and Nethercot, D.A. 1982 ,"Columns with semirigid joints", Jour of struct. Division, ASCE, Vol.108, ST2, pp.361-372.

Kannan, A.E., and Powell, G.H. 1973 ,"Drain-2D, A general purpose computer program for dynamic analysis of inelastic plane structures", Report EERc-73/6, Earthquake Engineering Research Center, University of California, Berkely.(see also Sept. 1973 and Aug. 1975 revision).

Kato, B., Chen W.F., and Nakao, M. 1988 ,"Effects of joint-panel shear deformation on frames", Jour. of Const. Steel Research, Vol.10, pp.269-320.

Kato, B., Maeda, Y., and Sakae,K. 1981 ,"Behaviour of rigid frame sub-assemblages subject to horizontal force", International Conf. Joints in Structural Steelwork, Teesside, Polytechnic,pp.1.54-1.73.

Kawano, A. 1984 ,"Inelastic behaviour of low-rise steel frame based on a weak beam-

to-column connection philosophy to earthquake motion", 8th WCEE, Vol.IV, San Francisco, California, pp.519-526.

Korol, R.M., Ghobarah, A., and Osman, A. 1990 ,"Extended end-plate connection under cyclic loading: behaviour and design", Jour. of Const steel Research, Vol.16, 4. pp. 253-280.

Krawinkler, H., Bertero, V.V., and Popov, E.P. 1971 ,"Inelastic behaviour of steel beam-to-column subassemblages", Report EERC 71/7, Earthquake Engineering Research Center, University of California, Berkely.

Krawinkler, H., and Popov, E.P. 1982 ,"Seismic behaviour of moment connections and joints", Jour. of Structural Division, ASCE, 108, ST2.

Krawinkler, H., and Mohasseb, S. 1987 ,"Effects of panel zone deformation on seismic response", Jour. of Constr. Steel Research, 8, pp.233-250.

Krishnamurthy, N. 1978 ,"A fresh look at bolted end-plate behaviour and design", Engineering Journal, AISC, 2nd Quarter, pp.39-49.

Lu, W.l. 1990 ,"Behaviour and application of semi-rigid connections" ,Proc. of 4th World Congress- Tall Building: 2000 and beyond, Hongkong.

Malvern, L.E. 1968 ,"Introduction to the mechanics of a continuos medium", Prentice-Hall, Englewood Cliffs, New Jersey.

Mann, A.P., and Morris, L.J. 1979 ,"Limit design of extended end-plate connections", Jour. Struct. Div., ASCE, 105, ST3, pp.511-527.

Matsui, c., and Yoshizumi, T. 1980 ,"Influence of local and lateral buckling on inelastic behaviour of steel frames", 7th WCEE, Vol.7, Istanbul, pp.321-324.

Mitani, I., Makino, M., and Matsui, C. 1977 ,"Influence of local buckling on cyclic behaviour of steel beams", Proc. 6th WCEE, New Delhi, India, III, pp.3175-3180.

Murray, T.M. 1988 ,"Recent developements for the design of moment end-plate connections", Jour. of Constr. Steel Research, 10, pp.133-162.

Mzzalani, F.M. 1987 ,"Mathematical model for semi-rigid joints under cyclic loads", Proc. of State-of-the-art workshop on connections and the behaviour, strength and design of steel structures, Laboratorie de Mecanique et Technologie, Cachan, France.

NBCC. 1990 ,"National Building Code of Canada", Associate Committee on the National Building Research Code, National Reseach council of Canada, Ottawa.